Universidad de Concepción
Dirección de Postgrado
Facultad de Ciencias Químicas
Programa Doctorado en Ciencias Geológicas

Tsunami sources in different geologic settings: Leveraging the past to reduce future tsunami surprises

Tesis para optar al grado de Doctor en Ciencias Geológicas

MATÍAS EDUARDO CARVAJAL RAMIREZ
CONCEPCIÓN-CHILE
2022

Profesor Guía: Dr. Marco Cisternas Vega
Instituto de Geografía
Pontificia Universidad Católica de Valparaíso

Profesora co-guía: Dra. Ignacia María Calisto Burgos
Departamento de Geofísica, Facultad de Ciencias Físicas y Matemáticas
Universidad de Concepción

"It Ain't What You Don't Know That Gets You Into Trouble.
It's What You Know for Sure That Just Ain't So"[1]

[1] Usually attributed to Mark Twain but current evidence indicates that the creator remains anonymous (www.quoteinvestigator.com)

Dedication

To Lomito

Acknowledgement

My family deserves endless gratitude: Yorka, little Julián, Lomito (R.I.P.), Anita, Roberto x 2, Valentina, Pablo and Mirella. Thank you for your continuous support and understanding.

I am grateful to my supervisor, Marco Cisternas, who sparked my passion for science. Thank you for teaching me so much and making me question even the strongest evidence.

I am also grateful to Kelin Wang and to all his “team” at the Pacific Geoscience Centre and University of Victoria (Vancouver Island, Canada), especially to Tian Sun, Haipeng Luo, Matt Sypus and Yijie Zhu. Thank you for teaching me so many interesting things about the solid earth and for being extremely nice. I am so glad I received the “Canada-Chile Leadership Exchange Scholarships Program” award that allowed me to learn and continue learning (via weekly zoom meetings) from you. Also, I would like to thank my “Canadian Family” who made me feel like at home during my visit to Canada. Thank you Suzanne, Rob, Sonal, Shahin and Nilou.

This thesis was only possible thanks to many people. Thank you, Patricio Winckler, Alejandra Gubler, Manuel Contreras-López, Ignacio Sepúlveda, Daniel Melnick, Cristián Araya-Cornejo, Ignacia Calisto (my co-supervisor), Patricio Catalán, Marcos Moreno, René Garreaud and so many other colleagues and friends.

Finally, I would like to thank different scientists around the world who, although have personally met very little or have not met at all, have inspired me through their work. Among them are Kenji Satake, Hiroo Kanamori, Eric Geist, Emile Okal, Costas Synolakis, George Plafker, Brian Atwater, Seth Stein, Rob Wesson, Sergio Barrientos, Yuichiro Tanioka and many others.

This thesis was funded by the Millennium Nucleus the Seismic Cycle along Subduction Zones (CYCLO), with support of Chile’s Fondo Nacional de Desarrollo Científico y Tecnológico, FONDECYT Projects N°1190258 (Marco Cisternas) and N°1181479 (Marcos Moreno), and benefited from valuable suggestions and comments made by Rob Wesson (external reviewer).

Abstract

Damaging tsunami events have often taken the scientific and/or public community by surprise, as demonstrated by the systematic failure of risk mitigation strategies during 21st century tsunami events alone. By studying recent and historical tsunami events in diverse geologic settings across the world, this thesis seeks to demonstrate the hypothesis that the underlying reason is that the actual generation mechanisms of tsunamis are much more complex and diverse than those usually assumed. The thesis is built from five published and as yet unpublished articles that, individually and all together, contribute to the hypothesis testing. Although the data and methods vary from article to article, for the source investigation we mainly use publicly available evidence of diverse type and simple numerical models. The cases studied in the articles include tsunami events of different origin (earthquakes, submarine landslides, volcanic processes and atmospheric phenomena) and in diverse geologic settings (oceanic-continental subduction zone, oceanic-oceanic subduction zone, strike slip fault and intraoceanic volcanic island). The results demonstrate that the source mechanisms that generate tsunamis are more complex and diverse than what is usually assumed and this explains why the scientific and/or public community is often taken by surprise. This conclusion has important implications for future decision-making efforts aimed at mitigating tsunami risk in different geologic setting.

Resumen

Eventos dañinos de tsunamis han a menudo tomado por sorpresa a la comunidad científica y/o pública, como ha sido demostrado por la falla sistemática de estrategias de mitigación de riesgos durante eventos de tsunami del siglo XXI. Mediante el estudio de eventos de tsunamis recientes e históricos en diversos contextos geológicos de todo el mundo, esta tesis pretende demostrar la hipótesis de que la razón subyacente es que los mecanismos de generación de tsunamis reales son mucho más complejos y diversos de lo que se suele asumir. La tesis se construye a partir de cinco artículos publicados y aún no publicados que, individualmente y en conjunto, contribuyen a la comprobación de la hipótesis. Aunque los datos y los métodos varían de un artículo a otro, para la investigación de las fuentes utilizamos principalmente evidencia públicamente disponible de diverso tipo y modelos numéricos sencillos. Los casos estudiados en los artículos incluyen eventos de tsunami de distinto origen (terremotos, movimientos en masa submarinos, procesos volcánicos y fenómenos atmosféricos) y en diversos contextos geológicos (zona de subducción oceánica-continental, zona de subducción oceánica-oceánica, falla transcurrente e isla volcánica intraoceánica). Los resultados apoyan la hipótesis de que los mecanismos que generan tsunamis son más complejos y diversos de lo que se suele asumir y esto explica por qué la comunidad científica y/o el público a menudo son tomados por sorpresa. Esta conclusión tiene importantes implicancias para los futuros esfuerzos de toma de decisiones destinados a mitigar el riesgo de tsunamis en distintos contextos geológicos.

Table of Contents

CHAPTER 1: Introduction **8**

1.1. Background, motivation, and scientific problem 8

1.2. Research hypothesis, goals and method 9

1.2. Structure of the thesis 11

CHAPTER 2: Identifying submarine landslides as the sources of the 2018 Palu tsunami from social media videos **12**

2.1. Article information 12

2.2. Article: Nearly Instantaneous Tsunamis Following the Mw 7.5 2018 Palu Earthquake 12

CHAPTER 3: Tide gauge records reveal global fast-propagating tsunamis caused by air pressure waves originated in the 2022 Tonga volcanic blast **28**

3.1. Article information 28

3.2. Article: Worldwide Signature of the 2022 Tonga Volcanic Tsunami 28

CHAPTER 4: Previously unrecognized meteotsunamis contribute to the frequent extreme sea levels at Rapa Nui (Chile) 34

4.1. Article information 34

4.2. Article: Extreme Sea Levels at Rapa Nui (Easter Island) During Intense Atmospheric Rivers 34

CHAPTER 5: The depth of megathrust slip is a weaker predictor of tsunami size than usually thought **58**

5.1. Manuscript information 58

5.2. Manuscript under review: Evaluating the Tsunamigenic Potential of Trench-Breaching Versus Buried Megathrust Slip 58

CHAPTER 6: Leveraging the past to reduce future tsunami surprises in Central Chile 89

6.1. Manuscript information 89

6.2. Manuscript under review: Depth variation in megathrust rupture explains the tsunami gap in metropolitan Chile 89

CHAPTER 7: Discussion and final remarks 98

7.1. Complexities and diversity of actual tsunami sources 98

7.2. Historical evidence provides fundamental insights into Earth science 100

7.3. The pitfalls of sophisticated modeling approaches for hazard assessments 100

7.4. Lessons from the past to reduce tsunami surprises in the future 102

REFERENCES **104**

APPENDIX A **118**

APPENDIX B **124**

Chapter 1

Introduction

1.1. Background, motivation, and scientific problem

Tsunamis are water gravity waves generated by diverse geological and atmospheric impulsive processes with the potential to grow to hazardous heights (Kânoğlu et al. 2015). They have historically caused tremendous loss of life and property damage and have the potential to cause more in the future as coastal population increases (Huppert and Sparks 2006). Mitigating tsunami risk in coastal communities has therefore become a global effort (Bernard et al. 2006).

Understanding the hazard posed by tsunamis is key to mitigate risk. However, recent tsunami surprises[2] in different geologic settings around the world have tragically demonstrated that our knowledge of tsunami hazards is incomplete (Satake and Atwater, 2007; Tappin 2021). The reason is the short observation period of past tsunami events together with our poor understanding of the complex and diverse source mechanisms that generate tsunamis (Grezio et al. 2017). An emblematic example of a tsunami surprise was the tsunami generated by the 2004 Sumatra-Andaman earthquake, which killed about a quarter of million people of a dozen countries in part because its source (i.e., earthquake rupture) was ten times larger than expected from historical earthquakes (Satake and Atwater, 2007). Although the tragic aftermath of the 2004 tsunami led to an unprecedented increase in tsunami research and improvement of mitigation strategies[3] (Chagué-Goff et al. 2017), it was not enough to prevent tsunami surprises along other subduction zones. The scientific community failed again in anticipating the great tsunamigenic potential of the subduction fault where the 2011 Tohoku-oki earthquake occurred (Stein et al. 2012). But in 2011 the surprise was not entirely due to the unanticipated size of the earthquake rupture as in

[2] In thesis, "tsunami surprises" refer to hazardous tsunamis that were generated by source mechanisms that were not anticipated by scientific knowledge or that were not considered by mitigation countermeasures such as early warning systems

[3] According to Day and Fearnley (2015), "mitigation strategies" are policies or procedures that lead to more or less pre-planned actions that operate before or during a tsunami event to reduce its impact on vulnerable populations.

2004, but it was due to the unanticipated large slip extending all the way to the trench (Fujiwara et al. 2011; Kodaira et al. 2012), i.e., along a fault area that was supposed to stop seismic rupture (Scholz 1998). The scientific community was again surprised by the large and deadly tsunami that followed the 2018 Palu strike-slip earthquake in the Indonesian island of Sulawesi because strike-slip earthquakes were not supposed to produces tsunamis that large (Elbanna et al. 2021), and then again in 2022 by the planetary-scale, fast-travelling tsunami triggered by the explosive eruption of the Tonga volcano (Titov et al. 2022). The societal impact of these 21st century tsunami examples alone highlight the need to rethink the tsunami source assumptions for hazard assessments and mitigation strategies.

By studying recent and historical tsunami events in diverse geologic settings across the world, this thesis seeks to improve our understanding of the complexities and variety of mechanisms that trigger tsunamis. The novelty of this thesis stems not only from the results, but also from the approach underlying the investigations of the source processes leading to these tsunamis. Specifically, how publicly available observations and evidence are analyzed to extract key information about the complex sources of past tsunamis. Hopefully, these results will help reduce future tsunami surprises in different geological settings on our planet.

1.2. Research hypothesis, goals and method

The thesis is built from five standalone articles that are either published (3), under review (1) or in preparation (1) (Figure 1.1). Although they have their own, specific hypothesis, they all together aim to address the following broad hypothesis:

The actual generation mechanisms of tsunamis are much more complex and diverse than those usually assumed in mitigation strategies such as early warning systems, and this is why we have been often taken by surprise

Testing the hypothesis requires facing real-world tsunami events. Therefore, the main objective of this thesis is to compare the source mechanisms between past tsunami events and those usually assumed in mitigation strategies.

To accomplish this goal, we studied tsunami events in four different geologic settings (Figure 1.1). The source investigation was mostly guided by publicly available evidence of diverse types and varying accuracy and precision, including both instrumental (e.g., tide gauge records) and non-instrumental (e.g., amateur videos) observations. The source investigation approach also included dedicated numerical modeling experiments that varied from case to case and usually served as secondary tools for the interrogation or "squeezing" process of the observational evidence. However, in none of these cases was the use of sophisticated numerical models required.

The specific hypotheses, goals, methods, and type of data used for the source investigation of each tsunami event are detailed in the respective articles.

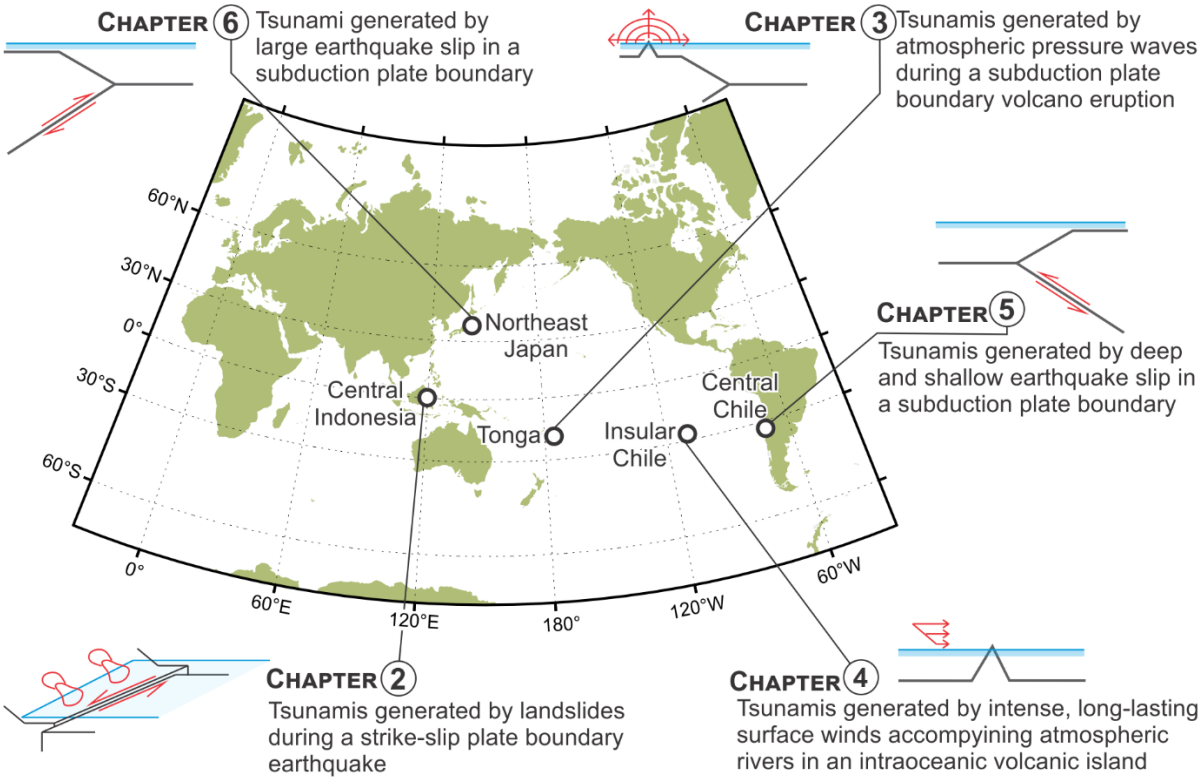

Figure 1.1 Geological settings and tsunami source mechanisms addressed in the five standalone scientific articles comprising this thesis

1.3. Structure of the thesis

Besides the current Chapter 1, which introduces the research problem, main hypothesis, goals, and methods, this thesis consists of six additional chapters that individually and all together contribute to the hypothesis testing. In Chapters 2 to 6, five standalone scientific articles are presented, in which the author of this thesis is the lead author.

The article of Chapter 2, published in *Geophysical Research Letters* in 2019, shows how a collection of amateur videos published in social media contains key evidence of the role of tsunamigenic submarine landslides in the deadly tsunami that affected the bay of Palu (Indonesia) in 2018. The article in Chapter 3, published in *Geophysical Research Letters* in 2022, shows how publicly available records from the global network of tide gauge stations reveal the complex source of the 2022 Hunga Tonga volcanic tsunami, including a previously poorly known mechanism associated with a fast-moving air pressure wave generated in the volcanic blast. In the article of Chapter 4, published in *Natural Hazards* in 2021, instrumental and non-instrumental datasets are combined to show that the extreme sea levels that frequently affect Rapa Nui (Chile) partially result from the complex generation of previously unrecognized meteotsunamis that grow in height during specific wind conditions. The manuscript presented in Chapter 5, which is currently under review in *Journal of Geophysical Research (Solid Earth)*, describes a numerical study that combines seafloor deformation and tsunami modeling to question the popular notion that shallow megathrust slip is more tsunamigenic than deeper megathrust slip, with a dedicated application to the 2011 Tohoku-oki earthquake. The as yet unpublished manuscript presented in Chapter 6 shows how eyewitnesses' descriptions of historical earthquakes in central Chile together with knowledge gained from other tsunami events in other regions of the world provide key geologic information to reduce future tsunami surprises in Chile's most populated coast. Finally, Chapter 7 presents an integrative discussion and the conclusions of this thesis.

Chapter 2

Identifying submarine landslides as the sources of the 2018 Palu tsunami from social media videos

This chapter consists of a published paper (Carvajal et al., 2019) that used social media videos to identify the sources of the deadly tsunami that affected the bay of Palu (Indonesia) in 2018. This paper was highlighted by the News and Views of Nature (Marshall 2019) with an article titled “Mystery of deadly Indonesian tsunami cracked using social-media videos” and was featured as an “Editor’s Highlight” in the Eos magazine of the American Geophysical Union (Hayes 2019) with the title “Modeling Tsunamis with Social Media”.

The article information is provided in Section 2.1. and the article itself is presented in Section 2.2.

2.1. Article information

The article title, coauthors, DOI, and journal where it was published are included in the article reference below:

Carvajal, M., Araya-Cornejo, C., Sepúlveda, I., Melnick, D., & Haase, J. S. (2019). Nearly instantaneous tsunamis following the Mw 7.5 2018 Palu earthquake. Geophysical Research Letters, 46(10), 5117-5126. DOI:10.1029/2019GL082578

Publisher link: https://agupubs.onlinelibrary.wiley.com/doi/full/10.1029/2019GL082578

The supplementary material and acknowledgments are available in the link above.

2.2. Article: Nearly Instantaneous Tsunamis Following the Mw 7.5 2018 Palu Earthquake

2.2.1. Abstract

The tsunami observations produced by the 2018 magnitude 7.5 Palu strike-slip earthquake challenged the traditional basis underlying tsunami hazard assessments and early warning systems. We analyzed an extraordinary collection of 38 amateur and closed-circuit television videos to show that the Palu tsunamis devastated widely

separated coastal areas around Palu Bay within a few minutes after the mainshock and included wave periods shorter than 100 s missed by the local tide station. Although rupture models based on teleseismic and geodetic data predict up to 5-m tsunami runups, they cannot explain neither the higher surveyed runups nor the tsunami waveforms reconstructed from video footage, suggesting that either these underestimate actual seafloor deformation and/or that non-tectonic sources were involved. Post-tsunami coastline surveys combined with video evidence and modeled tsunami travel times suggest that submarine landslides contributed to tsunami generation. The video-based observations have broad implications for tsunami hazard assessments, early warning systems, and risk-reduction planning.

2.2.2. Introduction

Sulawesi Island in the central part of Indonesia is located in a complex tectonic setting where the Australian, Sunda, and Philippine plates meet in a triple junction (Socquet et al., 2006; Walpersdorf et al., 1998). This region is characterized by distributed deformation over a broad region, which can be explained by block rotations along active faults with variable kinematics. Earthquake and tsunami events have repeatedly affected this region in the recorded history (Katili, 1970). The most recent tsunami occurred on the evening of 28 September 2018, at 18:02:45, local time (UTC+8), when a moment magnitude (Mw) 7.5 earthquake ruptured a ~200-km-long segment of the Palu-Koro strike-slip fault, which bisects Sulawesi and connects with the Minahassa Trench in the north (Bellier et al., 2001; Socquet et al., 2006; Walpersdorf et al., 1998; Watkinson et al., 2012; Watkinson & Hall, 2017; Figure 1a). In this region, three tsunamigenic earthquakes were reported in the past century (1927, 1968, and 1996) with accompanying tsunamis of up to 10 m (Soloviev & Go, 1974), most of them presumably associated with vertical motions caused by either thrust or normal faulting (Prasetya et al., 2001). In contrast, the Palu earthquake was associated with horizontal motion caused by strike-slip faulting. Rupture models based on distant teleseismic waveforms (U.S. Geological Survey, USGS, 2018) and onshore space geodesy data (Socquet et al., 2019) consistently indicate up to ~7 m

of horizontal slip confined above 10-km depth with local dip-slip motion of up to only 2 m (Socquet et al., 2019).

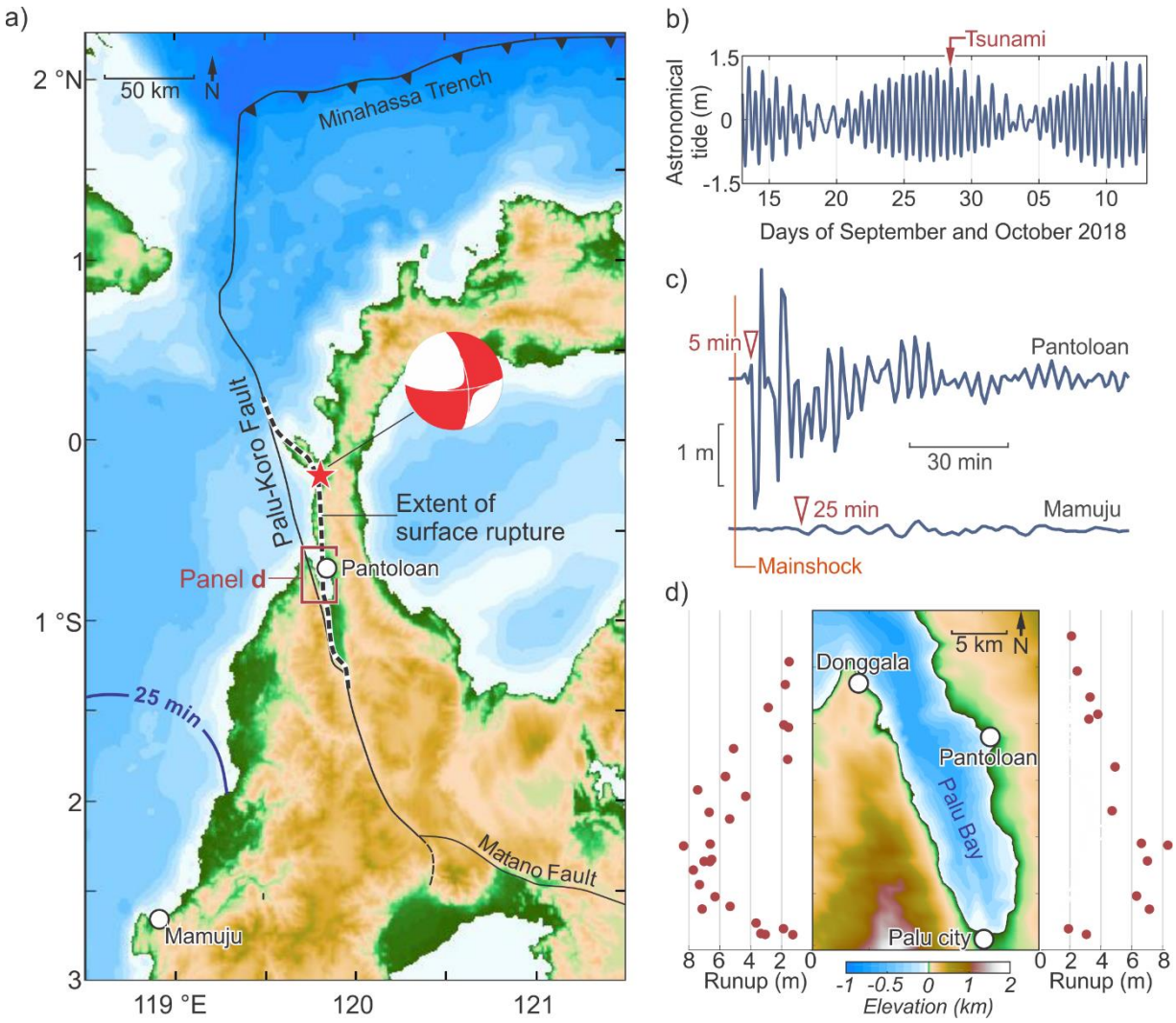

Figure 2.1. Seismotectonic setting and tsunami observations. (a) Tectonic setting and proposed earthquake rupture of the Mw 7.5 strike-slip Palu earthquake (Socquet et al., 2019). Black dashed line indicates the surface rupture proposed by Socquet et al. (2019); red star denotes the epicenter and focal mechanism from USGS (2018). Blue isoline indicates 25-min travel time for a point source tsunami originating at Mamuju. If the clock at Mamuju is correct, by reciprocity, the source of the waves recorded at Mamuju should be somewhere between this isoline and Mamuju. (b) Timing of the tsunami relative to 30 days of predicted astronomical tides for Palu Bay. Note that the tsunami occurred during a high tide of ~1 m above mean sea level. (c) De-tided records of the Palu tsunamis at Pantoloan and Mamuju. The arrival times of the first evident perturbations are indicated in reddish triangles. (d) Topobathymetric map of Palu Bay (Informasi Geospasial, 2018a) and surveyed tsunami runup heights (Fritz et al., 2018).

Large tsunamis following the Palu earthquake rapidly attracted the attention of the scientific community. Although strike-slip earthquakes have caused historical (Imamura et al., 1995) and recent tsunamis (Hornbach et al., 2010), their amplitudes were much smaller than those observed around Palu Bay, where runups over 8 m were measured in field surveys (Figure 2.1d; Fritz et al., 2018; Muhari et al., 2018; Omira et al., 2019). This suggests that (i) despite its predominant strike-slip mechanism, the earthquake was capable of producing significant, coseismic vertical deformation beneath the bay, (ii) that tsunami waves were largely amplified by the unusual bathymetric features of the long and narrow bay (Figure 2.1d), and/or (iii) that additional non-tectonic sources contributed to tsunami generation. To gain insight into this problem, Heidarzadeh et al. (2019) compared tsunami waveforms predicted by numerical modeling with the two closest tide gauge records available for this event (Pantoloan and Mamuju, Figure 2.1c). They suggested that additional tsunami sources were required and that submarine landslides were the most reasonable candidates. However, these results were likely biased by the use of GEBCO bathymetry for tsunami modeling, which in some locations shows water depths 3 times smaller than those reported on higher-resolution charts (Informasi Geospasial, 2018a). Moreover, their analysis relied only on the Pantoloan tide gauge record (Figure 2.1c), which is relatively far (15 km) from the area affected by the largest waves (Figure 2.1d).

Here, we complement the Pantoloan tide gauge data with non-conventional evidence inferred from a novel approach that combines the analysis of video footage and satellite imagery. We used an extraordinary collection of video images that captured different phases of the tsunami event (i.e., formation, propagation, and inundation) to derive quantitative estimates of their amplitudes, periods and timing around Palu Bay. Our analysis provides temporal data that is not possible to recover in field surveys (Fritz et al., 2018; Muhari et al., 2018; Omira et al., 2019). By tracking sea level changes from image pixels in subsequent frames, we constructed accurately timed tsunami waveforms from the quantitative interpretation of video footage (e.g., Fritz et al., 2006, 2012; Koshimura & Hayashi, 2012). In addition to providing valuable observations to constrain further source studies, we show that hazardous, short-

period tsunamis struck nearly instantaneously with the seismic shaking at several locations around the bay and that these short-period waves were not recorded by the Pantoloan tide gauge station due to its longer sampling interval.

2.2.3. Video-Based Characterization of the Palu Tsunamis

Our extensive search on social media platforms resulted in 38 videos showing tsunami behavior at 14 sites around Palu Bay (white and magenta circles on Figure 2.2a; Table S1 and Data Set S1 in the supporting information), from which 23 provide relevant spatiotemporal information at six sites that can be used to reconstruct tsunami waveforms (Table S2 and Text S1). All videos were further used to support the satellite imagery analysis conducted to derive inundation distances around Palu Bay. We will refer to these videos by the names shown in Figure 2.2a and Table S1. The richness of tsunami information depends on the quantity and quality of the videos, which differ substantially among locations. While tsunamis at some places were observed by a single amateur video, others were precisely captured by several closed circuit television (CCTV) cameras.

In Figure 2.2b, the waveforms derived from video footage show the tsunami amplitude and timing at six locations (see Data Set S2 for waveform data). For reference we show the simulated tsunami waveforms predicted from the Socquet et al. (2019; blue) and USGS (2018; tan) earthquake rupture models. The tsunami occurred at high tide, corresponding to ~1 m above mean sea level (MSL). The vertical coseismic seafloor deformation generated by the source model at each location added to the tidal value gives the initial sea surface elevation above MSL shown in the figure. For example, at Dupa, the Socquet et al. (2019) model, which concentrates slip beneath the center of the bay, predicts negligible vertical coseismic deformation and therefore the initial value is nearly the tidal level (i.e., 1 m above MSL). On the other hand, the USGS (2018) model predicts significant coseismic subsidence of the seafloor at Dupa; therefore, the water drops with the land instantaneously in our simulations, producing an initial sea level of approximately 0.5 m above MSL. See Text S1 for the details of the waveform reconstruction procedure.

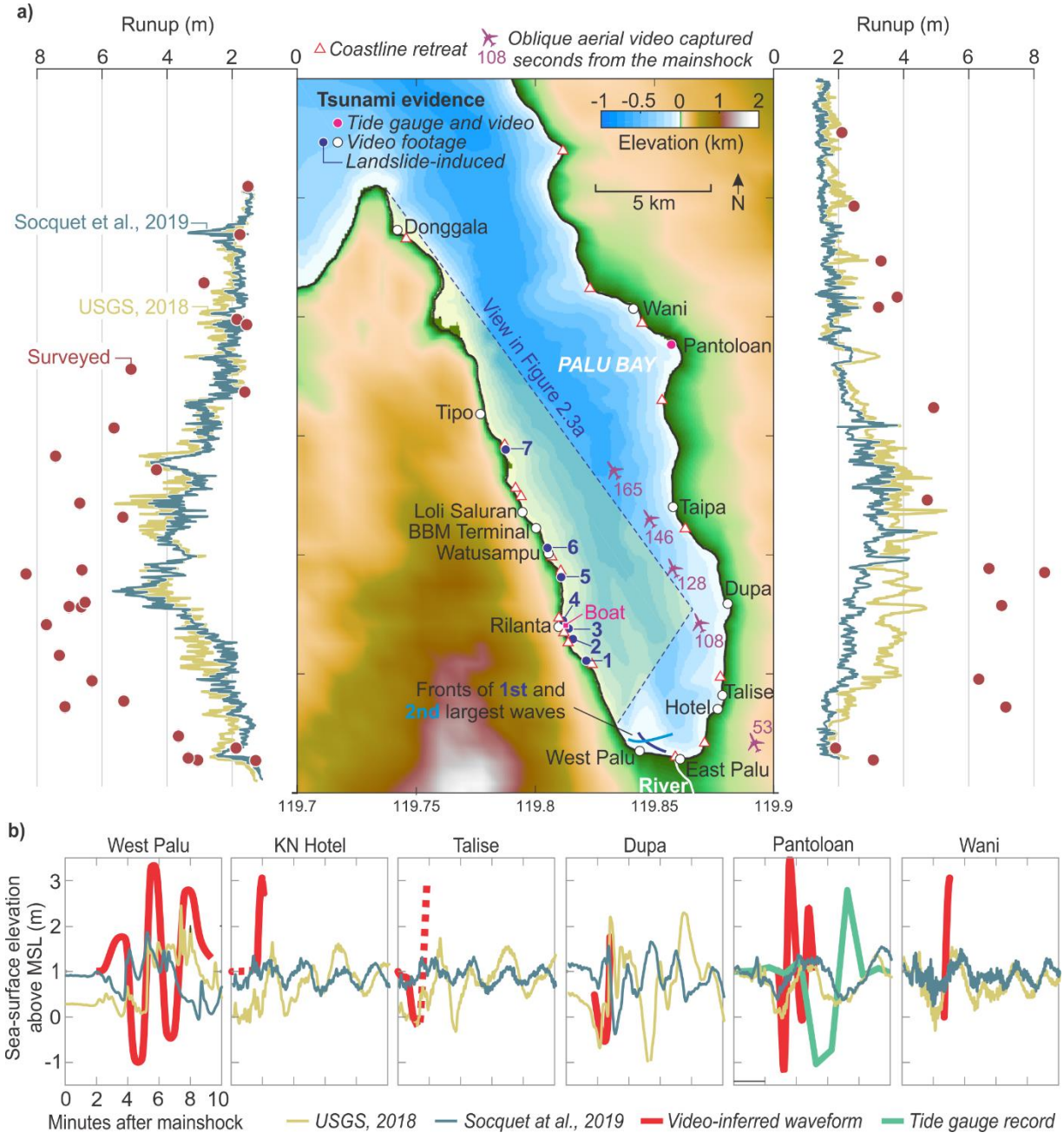

Figure 2.2. Observations and modeling results. (a) Map showing tsunami video location names (white and magenta circles), location of coastline retreat identified from satellite imagery (triangles), and flight path and timing (in seconds after the mainshock) of the aircraft pilot who recorded the point-source tsunamis shown in Figure 2.3a (video 38). The left and right panels show a comparison of tsunami runups measured by field surveys (Fritz et al., 2018) with those simulated based on existing coseismic slip models (Socquet et al., 2019; USGS, 2018). (b) Tsunami waveforms reconstructed from video footage (red) and predicted by the Socquet et al. (2019; blue) and USGS

(2018; tan) coseismic slip models. The red dashed lines represent the waveform segments interpreted from videos with lower confidence (see text). Tsunami waveforms (available in Data Set S2) were inferred using videos 15–21 at Palu west (see video compilation 43), videos 1–3 at the KN Hotel (see video compilation 42), video 13 at Talise, video 14 at Dupa, video 11 at Pantoloan, and videos 7 and 8 at Wani (Table S2). Note the longer period waveform of the Pantoloan tide gauge record (green) with respect to the waveform reconstructed from closed circuit television footage (red). Tsunami simulations (runups in a and waveforms in b) and the video-inferred tsunami waveforms (b) are plotted as sea surface elevation including the high tide level of ~1 m above mean sea level at the time of the earthquake (Figure 2.1b).

Probably the most remarkable features of the tsunamis that devastated Palu were the very short, nearly instantaneous arrival times. Usually, it is assumed that the time lag between an earthquake and its associated tsunami spans from tens of minutes to several hours (Cienfuegos et al., 2018; Mori et al., 2011), depending on the distance to the source region. However, CCTV footage from the Kampung Nelayan Hotel (KN Hotel), on the southeast coast of Palu Bay, recorded devastating tsunamis arriving 100 s after the seismic shaking (videos 1–6 and compiled video 42, Text S2, and Figure S1). This extremely short arrival time is robustly estimated by the difference in the timing between seismic shaking and water inundation using three cameras that had a clear view of the coastline (videos 1–3). Another array of CCTV cameras at Wani, located 20 km north of KN Hotel, showed tsunami inundation 3.5 min after the seismic shaking, which include the time needed for the tsunami to reach the site located 150 m inland (videos 7 and 8, Text S3, and Figure S2). If we assume a typical 5-m/s inundation rate, a positive-polarity wave (water level rise) should have reached the coast of Wani about 3 min after the mainshock (Figure 2.2b). Such an inference is consistent with reports from crewmembers of a passenger ship that was stranded on the adjacent coast (Figure S2 and video 9), who unanimously reported that immediately after the earthquake the sea level retreated significantly and was followed 3–5 min later by a large wave (Associated Press, 2018; Chicago Tribune, 2018; Text S3). This sea level pattern is consistent with the vertical movements of a container ship berthed at the Pantoloan port, 2.5 km south of Wani. There, a CCTV camera recorded more than ~2 m of water drawdown ~3 min after the end of seismic shaking followed by a rapid sea level rise of at least ~4 m (Figure 2.2b, video 11, Text

S4, and Figure S3). In summary, videos collected at the KN Hotel, Wani, and Pantoloan (~20-km maximum separation) indicate rapid widespread tsunami inundation following the earthquake and provide valuable reconstructions of tsunami sea level waveforms at these locations (Figure 2.2b).

Negative-polarity waves (water level drawdown) occurring immediately after the earthquake followed by tsunami inundation were observed at some sites but were not ubiquitous around the bay. For example, at Talise, an evident water retreat occurred almost instantaneously with seismic shaking (continuous red line in the Talise waveform of Figure 2.2b), which then appeared to be followed by a large wave that spurred people to run landward (dashed red line in the Talise waveform of Figure 2.2b; video 13). A very similar spatiotemporal behavior of sea level appeared to occur ~4 km north at Dupa, where a tsunami bore rapidly formed after an evident water drawdown (Figure 2.2b and video 14). However, negative-polarity leading waves followed by bore fronts, if existed, were not evident in the CCTV videos at the KN Hotel (see video 3), which is located 5 km south of Dupa and only 1 km from Talise. Instead, we infer an initial positive inundation from a rapid sea level increase of at least 2 m (Figure 2.2b and video 3).

Bore-type tsunamis followed by water retreat characterized the tsunamis that devastated the western parts of Palu city. Here, the tsunamis were captured by seven amateur videos collected within the Palu Grand Mall (videos 15–21 and compiled video 43 and Figure S4). The videos complement each other, in terms of view angles and temporal windows, and we were thus able to construct a quantitative composite estimate of arrival time, amplitudes and wave periods (Figure 2.2b). The video analysis shows that most of the destruction throughout Palu city was caused by two large tsunami waves arriving after smaller, but still significant, leading waves (Figures 2.2b and S4). Both of the largest waves featured evident bore fronts and impacted the coast from significantly different directions; first from the northeast and then from the northwest (Figures 2.2a and S4). Although no CCTV cameras recorded the exact tsunami arrival time at Palu city, the panic on the scene observed at the beginning of videos 15 and 16 strongly suggests that the leading, smaller waves likely arrived less

than 2 min after the earthquake. Because the first and second large trailing waves impacted 2 and 4 min after these initial inundations, respectively, the western sector of Palu city was likely devastated within 4–6 min of the mainshock, which is consistent with precise video observations at KN Hotel, Wani, and Pantoloan. Interestingly, if a single tsunami source is considered, the time span between waves at Palu city is consistent with a wave train period of ~2 min, which is unusually short for typical tectonic tsunamis (eg., Ward, 2011). Alternatively, the tsunamis that hit Palu city may have been caused by different sources, as suggested by their contrasting incoming directions.

Tsunami wavefronts impacting the local coastline with different orientations were apparently a hallmark of the Palu event, possibly produced by refraction in the shoaling of the waves due to the coastal bathymetry and/or by non-tectonic sources occurring close to the coast where observations were made. For instance, westward, coast-parallel inundation was captured by amateur videos in the eastern sectors of Palu city (videos 22 and 23). The KN Hotel CCTV footage simultaneously captured both eastward (videos 3 and 6) and westward (videos 1 and 2) inundations (Figure S1 and video 42). Unfortunately, the inundation at KN Hotel was nearly perpendicular to the evacuation road (video 6). This, combined with the nearly instantaneous arrivals (~100 s), prevented a successful evacuation (Figure S1). In contrast, the fortunate orientation of the road perpendicular to the coastline near the Wani house allowed timely self-evacuations even from rapid tsunami arrivals (see Text S3). Vertical evacuation proved to be critical in areas where there was insufficient time available to evacuate horizontally, as revealed by video footage at the KN Hotel (video 4), eastern (videos 23 and 25–27), and western Palu (videos 1 and 5). The video analysis highlights the importance of addressing the possible directions of tsunami inundation in hazard assessments and their mitigation in planning evacuation routes, including vertical platforms if necessary, to reduce loss of life.

Overall, our video-based observations are consistent with high-amplitude tsunamis with sources near the coast (short arrival times), with unusually short periods (~2 min) and consequently short wavelengths. These tsunami characteristics resulted in rather

high destructive capacity very close to the coast but limited capacity to inundate far inland (Satake et al., 2013). These characteristics are consistent with inland inundation distances inferred from satellite imagery (Figure S5), which provide a regional-scale assessment. Our interpretation of high-resolution satellite images collected 3 to 4 days after the event (Digital Globe, 2018) suggests that severe devastation was confined to at most ~400 m inland (Figure S5). These characteristics are also consistent with the time-frequency signature of the Pantoloan tide gauge record, which shows that most of the initial energy was limited to 2- to 6-min periods (Figure S6). However, we note that the 1-min sampling interval of the Pantoloan record, which would usually be sufficient for characterizing subduction zone tsunamis, may be too coarse to capture the tsunami patterns inferred from CCTV footage collected in the vicinity of the tide gauge station (video 11 and Figure S3)[4]. The vertical movements of the berthed container ship at Pantoloan port observed in video 11 are best explained by two tsunami waves (two troughs and two crests) occurring within less than 5 min after seismic shaking stopped (Figure S3). Interestingly, these waves were not captured by the local tide gauge station, which recorded longer-period fluctuations (~6 min) beginning with a leading drawdown at ~5 min following the mainshock (Figures 1c, 2.2b, and S6). Hence, our observations suggest that the Palu tsunamis included wave periods too short (~1–2 min) to be well captured by tide gauge running at the typical sampling intervals of 1 min.

2.2.4 The Role of Coastal Landslides in the Palu Tsunamis

Our simulated tsunamis based on initial conditions from the fault slip models published to date (ie., Socquet et al., 2019; USGS, 2018) fail to fully explain the surveyed runups (Fritz et al., 2018) and cannot predict the tsunami waveforms inferred from our analysis of video footage (Figure 2.2; see methods for tsunami modeling). Aside from Dupa, where both slip models predict the video observations reasonably well, the inferred phases and amplitudes at the other five sites cannot be reproduced from these slip models (Figure 2.2b). This may be explained by three

[4] Also, after this paper was published, we learned that the Pantoloan tide gauge record resulted by averaging 30 measurements per minute, so the record could represent a low pass filtered version of the actual sea level oscillations.

possible scenarios: (1) Slip models fail to predict the actual seafloor displacements beneath Palu Bay, which is possible owing to data limitations and uncertainties in both offshore fault geometry and seafloor mechanical properties; (2) our tsunami models fail to reproduce particular aspects of unusually short-period waves; and/or (3) additional nontectonic sources, such as submarine landslides triggered by strong seismic shaking (Bao et al., 2019), contributed to tsunami generation.

Widespread onshore landslides were triggered by the Palu earthquake (Petley, 2018; Sassa & Takagawa, 2019), and submarine slope failures may be a plausible mechanism to explain the additional sources required by the reconstructed tsunami waveforms. Indeed, the tsunamis observed in the tide gauge record at Mamuju, located ~200 km south of the Palu Bay (Figures 2.1a and 2.1c), may have been very likely triggered by landslides outside the bay. There, the local tide gauge station recorded tsunami amplitudes of up to 6 cm arriving only 25 min after the mainshock. Based on simulated tsunami travel times, the source must be within 100 km of Mamuju, and thus is incompatible with the timing of a source near Palu Bay and the fault rupture (Figure 2.1a). Heidarzadeh et al. (2019) ascribed the Mamuju tsunami to the earthquake by proposing a 45-min delay on the tide gauge station clock to fit modeled and predicted waveforms; however, this assessment seems unlikely for two reasons. First, the official cancellation of the tsunami alert, 34 min after the earthquake, was decided based on the 6-cm small tsunamis recorded by the Mamuju tide gauge station (Hoffmann et al., 2018). And second, such a clock error would also imply a delay between the tides of Mamuju and Pantoloan (Figure S7), which does not seem to be the case (Informasi Geospasial, 2018b). Therefore, shaking-triggered landslides are the most reasonable source for the tsunamis observed at Mamuju, which is interesting since seismic shaking in this area (enclosed by the 25-min isoline in Figure 2.1a) is expected to be significantly less intense than in the area surrounding the fault zone, especially within Palu Bay.

To explore the possible role of submarine landslides as tsunami sources within Palu Bay, we analyzed video footage and satellite images to determine likely source regions. A detailed comparison of pre-and post-earthquake satellite imagery revealed

evidence of shoreline retreat at 18 sites around Palu Bay of distances from 10 to 120 m (Figures 2.2 and S8). Interestingly, all cases occurred along coastal plains adjacent to fluvial and alluvial fan deltas (Figure S8) and, therefore, may be interpreted as the surface expressions of submarine failures of these landforms. Deltas, formed from unconsolidated material, are very sensitive to failure by an external trigger such as seismic shaking (Girardclos et al., 2007; Hasiotis et al., 2006; Hilbe & Anselmetti, 2014; Leithold et al., 2018). Furthermore, the potential for delta failures to generate significant tsunamis during strong shaking events (Vanneste et al., 2018) has been documented at sites with diverse climatic conditions, such as Alaska (USA; Field et al., 1982; Parsons et al., 2014) and Haiti (Hornbach et al., 2010).

Evidence for tsunamis induced by delta failures during the Palu event is supported by video footage. Four extraordinary amateur videos, taken from a plane, a moored boat and from high ground captured the initiation and/or early formation of 7 tsunamis along the west coast of the bay (Figure 2.3 and videos 38–41). Strikingly, all of these came from areas where delta landforms failed during the Palu earthquake (Figures 2.2a and S8). However, based on their small sizes and late timing, they seem unlikely to be the complementary sources required to explain all the tsunami observations around Palu Bay. In order to explore whether similar sources occurred elsewhere in the bay, we interviewed Ricoseta Mafella, the aircraft pilot who collected video 38. Although he noticed that these sea level phenomena were only present along the western coast of the bay, he only had a clear view of the eastern flank about 3 min after the mainshock when he turned “left” (west). This time, however, may be too late given the nearly instantaneous occurrence of the Palu tsunamis and therefore, tsunamis triggered by submarine landslides along the eastern shore of the bay cannot be ruled out. Indeed, a video recorded at Taipa (Figure 2.2a) captured a large tsunami wave coming from the northeast coast of the bay (video 31 and Figures 2.3e and 2.3h). Although not as evident as the landslide tsunamis originating along the west coast, the steepness and seaward traveling direction of the wave seen in the video seem more consistent with a localized source near the coastline than one

produced by the earthquake faulting beneath the bay.

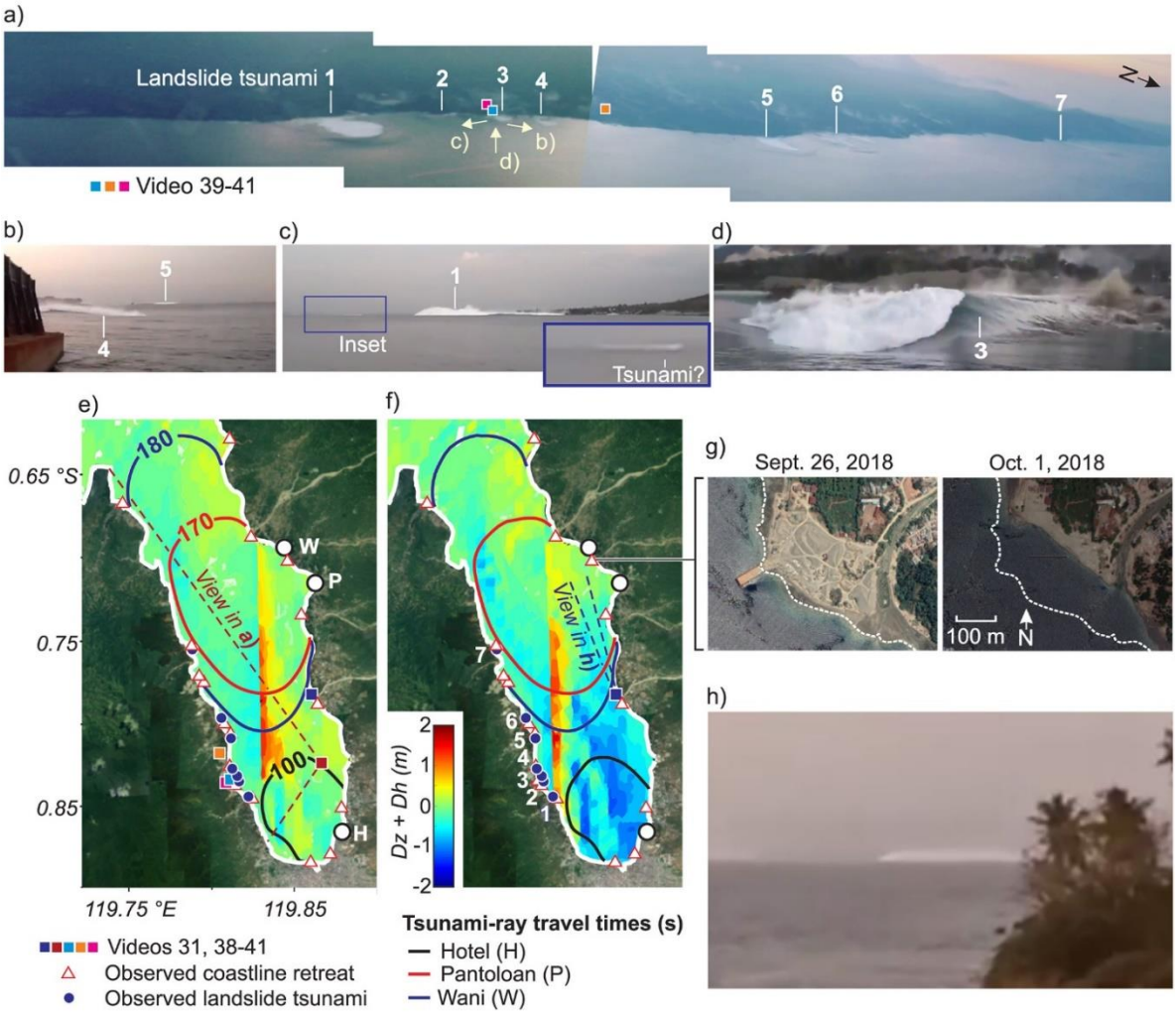

Figure 2.3. Examples of tsunamis interpreted to have been associated with submarine landslides and probable landslide locations inferred from a combined analysis of pre- and post earthquake satellite imagery and video footage. (a) Seven point-source sea level perturbations along the western coast of Palu Bay captured at ~1,000-m elevation by aircraft pilot Ricosseta Mafella (video 38). In the vicinity of landslide tsunami 3, a boat captured the tsunamis shown in (b)–(d) (video 39). Inset in (c) shows an additional sea level perturbation which could have been the first large wave to hit Palu (see text). (e) and (f) Tsunami-ray travel times (in seconds) from Wani, Pantoloan, and KN Hotel superimposed on vertical displacements of the sea surface due to vertical coseismic deformation (Dz) and the bathymetry effect (Dh; Tanioka & Satake, 1996), predicted by the fault slip models (Socquet et al., 2019; USGS, 2018, respectively). (g) Pre-and post-earthquake satellite images showing the shoreline between Pantoloan and Wani. Note pronounced retreat of the deltaic coastal plain. (h) Snapshot of video 31 when filming toward the north of the bay where a tsunami wave propagates seaward (see video 31).

The precise arrival times estimated at Wani, Pantoloan, and the KN Hotel can be used to locate probable individual landslides sources. Figures 2.3e and 2.3f show the possible source regions predicted from backward tsunami-ray tracing from the video-inferred arrival times (methods), superimposed on the seafloor displacement patterns predicted by rupture models (Socquet et al., 2019; USGS, 2018) and coastline retreats inferred by satellite imagery (Figure S8). These isolines cross the areas of largest seafloor displacement and include multiple locations of coastline retreat, suggesting that the rapid arrival times at these three locations can be explained either by fault slip or by delta failures associated with such coastline retreats. However, the tsunami amplitudes reconstructed at these locations are 3 times greater than those predicted by tsunami simulations based on seafloor displacements (Figure 2.2b), and therefore, fault slip alone fails to fully explain the video-observed tsunamis at Wani, Pantoloan, and KN Hotel. Although bathymetric surveys are needed to address the occurrence of delta failures near the locations of coastline retreat, they are plausible candidates for localized, complementary tsunami sources. Particularly intriguing is the region between Pantoloan and Wani (Figure 2.3g), where we mapped the largest coastline retreat in Palu Bay (up to ~120 m). Failure of a delta front there would produce an immediate sea level drawdown followed by rapid tsunami inundation, as has been predicted by numerical simulations of other tsunamis (Watts et al., 2005) and reported by eyewitnesses to the tsunamis produced by delta failures triggered by the 2010 Haiti earthquake (Hornbach et al., 2010). Interestingly, such a sea level response was inferred from video footage and eyewitness reports immediately north (Wani) and south (Pantoloan) of this pronounced coastline retreat (Text S2 and S3 and video 11). Although plausible, whether or not this was the source for the large wave propagating seaward from this part of the bay (Figures 2.3e and 2.3h), as seen in video 31, cannot be confirmed with the available data.

2.2.5 Concluding Remarks and Future Work

Our video-based analysis indicates that although the Palu earthquake was produced by predominantly horizontal fault slip, it generated devastating tsunamis reaching widespread coastal areas of Palu Bay nearly instantaneously, within tens of seconds

after the end of seismic shaking. Shallow slip extending to the surface combined with the steep bathymetry of the long and narrow Palu Bay likely contributed to the large runups observed around the bay, which were further enhanced by the high tide (~1 m above MSL) at the time of the tsunami (Figure 2.1b). However, we note that tsunami simulations from existing fault slip models are not sufficient to reproduce the runup heights measured in field surveys, and cannot explain the spatial and temporal patterns inferred from the video-derived tsunami waveforms and local tide gauges. Unless these fault models underestimate the actual dip-slip component beneath Palu Bay, additional non-tectonic tsunami sources are likely to have contributed to tsunami generation. In this case, submarine landslides triggered by delta failures along the bay are plausible candidates for such supplementary sources, as suggested by locations of observed coastline retreat, video footage and tsunami-ray travel time simulations.

Our results provide valuable data and guidance for future efforts aimed at understanding the sources of the Palu tsunamis. Our inferred tsunami waveforms (available in the supporting information) may be used to test future fault slip models with improved offshore resolution and guide dedicated modeling experiments of tsunamis generated by a combination of submarine landslides and coseismic seafloor deformation. Additionally, our satellite imagery results can guide detailed bathymetric surveys where delta failures, potentially acting as tsunami sources, may have occurred. Based on our video analysis, we emphasize that future studies should use tsunami modeling strategies capable of simulating the generation, propagation and runup of unusually short-period tsunamis such as those observed. Finally, we highlight that the 1-min sampling interval of the Pantoloan tide gauge record did not reliably capture the damaging short-period features of the Palu tsunamis inferred from our analysis of CCTV footage captured in the vicinity of the station. This instrumental limitation, revealed by our analysis of video footage, has critical implications for tsunami early warning systems based on real-time sea level observations along coasts adjacent to diverse tectonic settings.

The apparently early arrival of the tsunami wave at Mamuju remains a bit of a puzzle. If the clock there is correct, then that wave was likely triggerer by submarine landslides off the coast near the 25-min isoline shown in Figure 2.1. However, how submarine landslides could be triggered by shaking that far from the inferred rupture surface is puzzling.

The tragic Palu story highlights several important lessons to be considered in areas with similar geomorphic and tectonic settings potentially exposed to tsunami hazards. The main lesson is that tsunami risk needs to be assessed locally; hazard assessments must consider all reasonable sources of tsunami generation based on the local tectonic setting and including areas of potential landslides. Also, because inundation and damage caused by short period waves can be quite different than those caused by longer period waves in a limited coastal inundation zone, a locally defined spectrum of wave periods must be considered, and according modeling strategies and bathymetric data must be used. Local infrastructure and urban design should consider this and other local aspects of tsunami hazards. The Palu tsunamis demonstrated that damaging waves may arrive within a few minutes after the seismic shaking, and therefore, escape routes must be appropriately located and oriented to allow timely self-evacuations, and if not possible, vertical evacuation shelters must be implemented.

Our waveform reconstructions from video footage complement previous video-based approaches (e.g., Fritz et al., 2006, 2012; Koshimura & Hayashi, 2012) aimed to better understand tsunami phenomena. We encourage the increased scientific use of tsunami videos shared on social media platforms that provide valuable constraints for scientific studies and help guide tsunami hazard mitigation efforts and focused post-tsunami surveys.

Chapter 3

Tide gauge records reveal global fast-propagating tsunamis caused by air pressure waves originated in the 2022 Tonga volcanic blast

This chapter consists of a published paper (Carvajal et al., 2022) that presents decisive tide gauge evidence for atmospheric pressure waves as the cause of the worldwide tsunami following the explosive eruption of the *Hunga Tonga-Hunga Ha'apai* volcano in January 2022.

The article information is provided in Section 3.1. and the article itself is presented in Section 3.2.

3.1. Article information

The article title, coauthors, DOI, and journal where it was published are included in the article reference below:

Carvajal, M., Sepúlveda, I., Gubler, A., & Garreaud, R. (2022). Worldwide signature of the 2022 Tonga volcanic tsunami. Geophysical Research Letters, 49, e2022GL098153. https://doi.org/10.1029/2022GL098153.

Publisher link: https://agupubs.onlinelibrary.wiley.com/doi/10.1029/2022GL098153

The supplementary material and acknowledgments are available in the link above.

3.3. Article: Worldwide Signature of the 2022 Tonga Volcanic Tsunami

3.3.1. Abstract

The eruption of the Hunga Tonga-Hunga Ha'apai Volcano in January 2022 in the southwest Pacific islands of Tonga triggered a tsunami that was detected beyond the Pacific basin. Here we show its spatiotemporal signature as revealed by hundreds of publicly available coastal tide gauge records from around the world. The Tonga tsunami was characterized by a uniformly small leading wave that arrived earlier than theoretically expected for a tsunami wave freely propagating away from the volcano. In contrast, the largest waves, of up to +3 m high, were concentrated in the Pacific and their timing agrees well with tsunami propagation times from the volcano. While

the leading waves were caused by a previously reported fast-moving atmospheric pressure pulse generated in the volcanic explosion, the large waves observed later in the Pacific were likely originated in the vicinity of the volcano although its generation mechanism(s) cannot be identified by the tide gauge data alone.

3.3.2. Tide Gauge Observations of the Tonga Tsunami

On 15 January 2022, at 4:14:45 UTC (17:14:45 local time), an explosive eruption of the Hunga Tonga-Hunga Ha'apai Volcano (U.S. Geological Survey, 2022), in the Islands of Tonga in the southwest Pacific Ocean, triggered a tsunami that prompted the issuance of tsunami alerts around the world (Titov et al., 2022). The Tonga tsunami was widely recorded by a global network of coastal tide gauge stations, which detected conspicuous tsunami waves not only in the Pacific Ocean, but also in the Atlantic and Indian oceans, and in the Caribbean and Mediterranean seas (Fountain, 2022). The rare origin and far-reaching nature of this tsunami compared to those frequently triggered by subduction zone earthquakes highlight the scientific and societal need for a better understanding of this event.

In this paper we present the worldwide signature of the Tonga tsunami as revealed by coastal tide gauge data. The purpose is to show the spatiotemporal characteristics of a volcanic tsunami on the world coasts and to provide valuable evidence to be used in dedicated tsunami source studies. We analyzed 831 tide gauge records publicly available via the Intergovernmental Oceanographic Commission of UNESCO (http://www.ioc-sealevelmonitoring.org/). Specifically, we (a) downloaded the time series, (b) selected those with reliable data (589 out of 831) from a supervised algorithm that identifies and assess data quality parameters (e.g., size and location of gaps), (c) extracted the tsunami signal by bandpass filtering in the tsunami frequency band (provided in digital format in Dataset S1, and (d) calculated the arrival time and crest-to-trough height of both the leading and largest tsunami waves by combining an automatic algorithm based on signal-to-noise ratio with a visual inspection. The procedure is described in Text S1 and Figure S1 in Supporting Information S1, and the main results are presented in Figure 3.1.

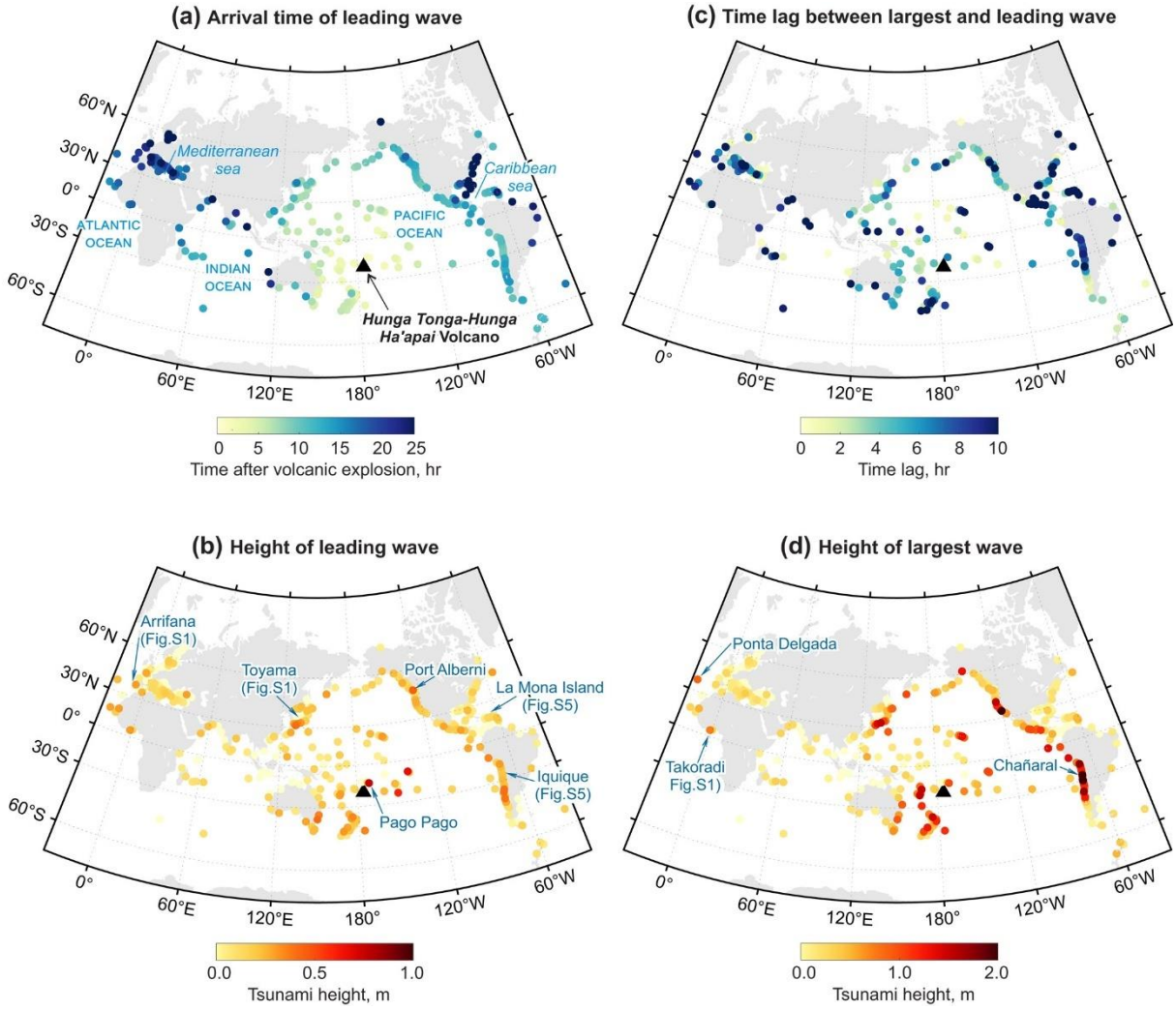

Figure 3.1. The spatiotemporal signature of the January 2022 Tonga tsunami as derived by coastal tide gauge measurements around the world. (a) Arrival time of the leading wave at each station relative to the time of the explosion of the Hunga Tonga-Hunga Ha'apai Volcano reported by the U.S. Geological survey (4:14:45 UTC). (b) Crest-to-trough height of the leading wave. (c) Time of occurrence of the largest wave relative to the arrival time of the leading wave. (d) Crest-to-trough height of the largest wave. The black triangle indicates the location of the Hunga Tonga-Hunga Ha'apai Volcano, and the blue arrows in (b) and (d) indicate the locations of stations mentioned in the text and/or figures. The source data for this figure is available in Table S1 in Supporting Information S1.

With a few exceptions, the arrival time of the leading tsunami wave gradually increased with distance to Tonga (Figure 3.1a). Their heights were usually smaller than half a meter and rather uniform among stations regardless of their distance to Tonga (Figure 3.1b). However, higher than average leading waves were estimated at

some places. While higher leading waves near Tonga (e.g., Pago Pago; Figure S2 in Supporting Information S1) are likely real, those at distant locations (e.g., Port Alberni; Figure S2 in Supporting Information S1) may be not but instead represent subsequent waves because the leading waves were not conspicuous enough to be reliably identified by our method.

The spatiotemporal signature of the largest waves differs from that of the leading waves. First, in most stations, the temporal occurrence of the largest waves was generally independent on the arrival of the leading waves, with time lags ranging from 0 to +10 hr (Figure 3.1c). Second, the height of the largest waves varied significantly among stations, with the largest waves concentrated in the Pacific (Figure 3.1d). Although not as big as the largest tsunami heights observed in the Pacific (reaching up to 3.4 m at Chañaral, Chile; Figure S2 in Supporting Information S1), tsunami waves as high as a meter were observed in the Atlantic Ocean such as in Takoradi, Ghana (0.9 m; Figure S2 in Supporting Information S1), and Ponta Delgada, Portugal (1.1 m; Figure S2 in Supporting Information S1), both located near the antipode of Tonga.

3.3.3. Complex Source of the Tonga Tsunami

The tide gauge evidence confirms the previously recognized atmospheric source mechanism for the leading waves observed across the world and sheds some light on the possible complex sources of the larger waves occurring later in the Pacific coasts.

A remarkable feature of the Tonga tsunami is the generally small and uniform height of the leading wave across the world oceans and seas, a signature that earthquake-triggered tsunamis usually lack. As previously recognized, their arrival times at most stations are much shorter than theoretically expected for a tsunami wave freely propagating away from Tonga (Figure S3 in Supporting Information S1) and instead coincide with the passing of a fast-moving atmospheric pressure wave generated in the volcanic explosion (Adam, 2022) for which we estimated a speed of 307 m/s (Figure S4 in Supporting Information S1). The travel time correspondence between the atmospheric pulse and leading tsunami wave clearly seen in Figure 3.2 confirms the atmospheric origin of the leading waves observed in most of the stations

worldwide. A similar atmospheric mechanism was invoked to explain sea-surface perturbations recorded at different oceans following the 1883 Krakatoa Explosion in Indonesia (Press & Harkrider, 1966).

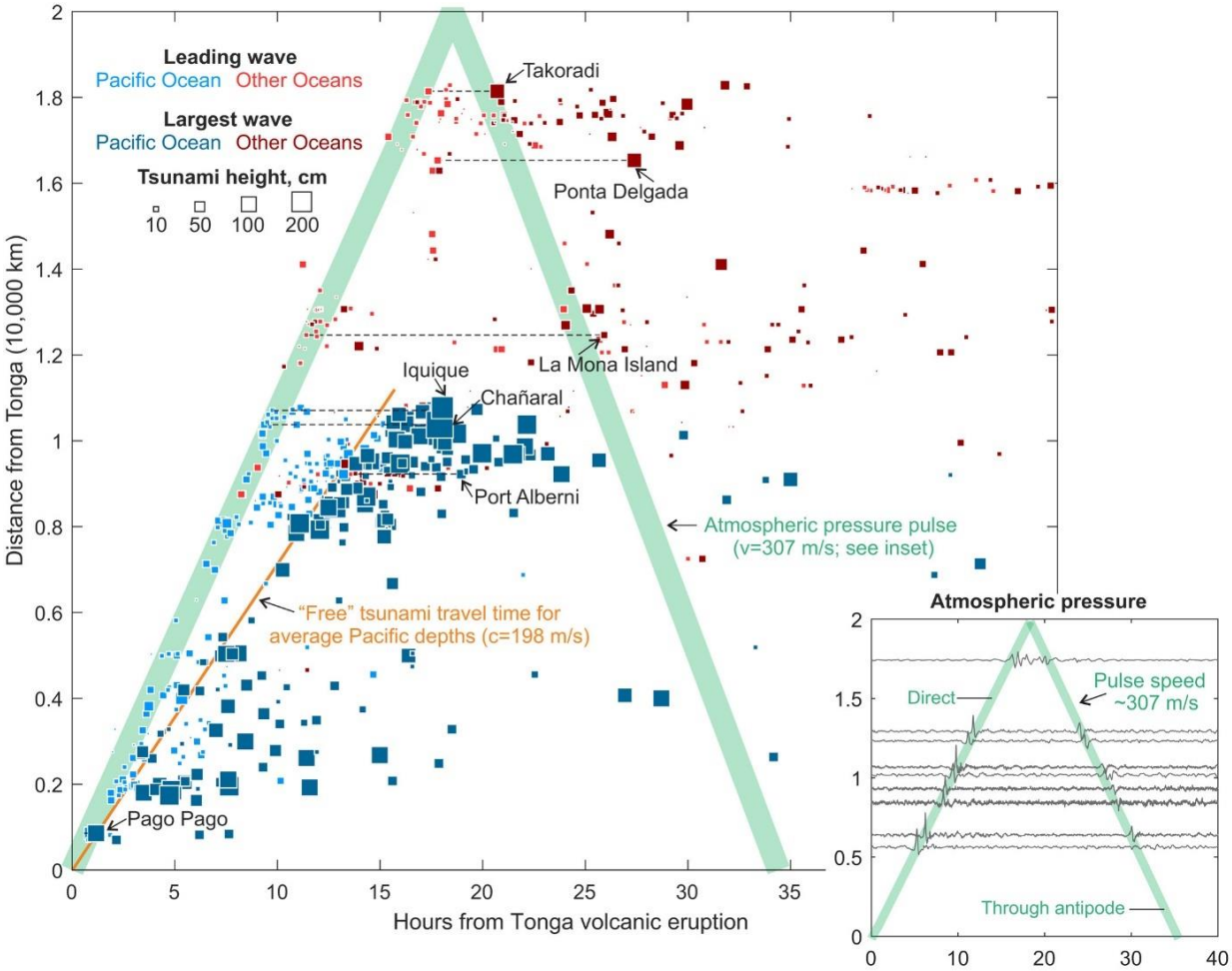

Figure 3.2. Aggregated results of tsunami arrival times in comparison with the estimated passing time of an atmospheric pressure pulse generated in the volcanic explosion (green band) and the theoretical arrivals to the Pacific coasts of a tsunami originated in Tonga (orange line). The estimated average speed of the passing atmospheric pressure pulse, of ~307 m/s, was inferred from the 9 atmospheric pressure records shown in the inset, with details in Figure S4 in Supporting Information S1. The orange line indicates the propagation times of a tsunami (free long wave) traveling over the average Pacific water depths (i.e., 4,000 m) and is shown for reference (see Figure S3 in Supporting Information S1 for more precise numerical calculations of arrival times from Tonga to the continental borders assuming realistic bathymetry). The horizontal dashed lines connect the arrival times of the leading (left end) and largest (right end) waves for stations mentioned in the text and/or figures.

However, the tide gauge evidence alone cannot conclusively determine whether the moving atmospheric pressure pulse was also the main source of the larger waves

occurring later in the Pacific or additional generation mechanisms were involved. There are two main arguments that seem to favor the contribution of a generation mechanism localized in the vicinity of the volcano. The first are the distinct global signatures of the leading and largest waves. While the leading wave heights were generally uniform across the world oceans and seas (Figure 3.1b and Figure S5 in Supporting Information S1), the largest waves were systematically larger in the Pacific basin (Figure 3.1d). Unless the particular geomorphology of the Pacific basin played a role, the global patterns of leading and largest waves should not have been as different if the moving atmospheric pulse was the main source since its amplitude was similar everywhere (Figure S4 in Supporting Information S1). The second is the temporal agreement of the largest waves occurring later in the Pacific coasts with the theoretical travel times of a free tsunami wave originated in the vicinity of the volcano at the eruption time, which for the average Pacific water depths can be approximated using a mean wave speed of 198 m/s (orange line in Figure 3.2). Specifically, unlike the leading waves, the largest waves observed in the Pacific coincided with or occurred systematically after the theoretical travel times of a tsunami freely propagating away from the volcano via the oceanic path (Figure 3.2). This temporal correspondence is not seen as clearly at stations outside the Pacific, where the largest waves generally occurred before the theoretical travel times from Tonga (Figure S3 in Supporting Information S1) and usually coincided with or occurred after the first or second passing of the atmospheric pressure pulse (Figure 3.2 and Figure S5 in Supporting Information S1). While the above suggests that the largest waves were originated in the vicinity of the volcano, the tide gauge evidence alone can neither identify their dominant generation mechanisms nor rule out additional contributions from atmospheric forcing processes.

The unusual signature of the Tonga tsunami around the world reflects the complexities of the volcanic, atmospheric and oceanic processes that generated it and demonstrate the potentially global-scale impact of volcanic tsunami hazards. We believe that the results presented here will provide valuable data to improve their understanding.

Chapter 4

Previously unrecognized meteotsunamis contribute to the frequent extreme sea levels at Rapa Nui (Chile)

This chapter consists of a published paper (Carvajal et al., 2021) in which datasets of diverse type are combined to show that extreme sea levels at Rapa Nui (Easter Island) result from a complex combination of processes including previously unrecognized tsunami-like waves that grow in height during specific wind conditions.

The article information is provided in Section 4.1. and the article itself is presented in Section 4.2.

4.1. Article information

The article title, coauthors, DOI, and journal where it was published are included in the article reference below:

Carvajal, M., Winckler, P., Garreaud, R., Igualt, F., Contreras-López, M., Averil, P., Cisternas, M., Gubler, A. & Breuer, W. A. (2021). Extreme sea levels at Rapa Nui (Easter Island) during intense atmospheric rivers. Natural Hazards, 106(2), 1619-1637. DOI: 10.1007/s11069-020-04462-2

Publisher link: https://link.springer.com/article/10.1007/s11069-020-04462-2

The acknowledgments are available in the link above. There is no supplementary material associated with this article**.**

4.2. Article: Extreme Sea Levels at Rapa Nui (Easter Island) During Intense Atmospheric Rivers

4.2.1. Abstract

In addition to the tsunami hazard posed by distant great earthquakes, Rapa Nui (Easter Island), in the Southeast Pacific Ocean, is exposed to frequent and intense coastal storms. Here, we use sea-level records and field surveys guided by video and photographic footage to show that extreme sea levels at Rapa Nui occur much more

frequent than previously thought and thus constitute an unrecognized hazard to the island's maritime supply chain. We found that extreme sea-level events, including the two most extreme (March 5th and May 5th, 2020) in the 17-month-long period analyzed (from January 1st, 2019, to May 31st, 2020), resulted from constructive superpositions of seiches on the shelf, storm surges and high tides. By further analyzing time series of atmospheric and wind-generated wave data, we conclude that these extreme sea levels are ultimately driven by the breaking of large waves near the coastline (i.e., wave setup), with lesser contribution of barometric setup and even less of wind setup. We also propose that these large waves were mainly generated from strong, long-lasting, NW winds associated with intense atmospheric rivers (long, narrow regions in the atmosphere that transport abundant water vapor) passing over Rapa Nui. Given that the intensity of atmospheric rivers and sea level are thought to increase as climate changes, a deeper understanding of the relation between meteorological and oceanographic processes at Rapa Nui is strongly needed.

4.2.2. Motivation

Isolated in the southeast Pacific Ocean, Rapa Nui, also known as Easter Island (Chile; 27,1°S–109,4°W), is the most remote inhabited place in the world (Figure 4.1a). Its triangular-shaped surface of ~ 164 km2 is home to about 7750 people, most of them living in the village of Hanga Roa (Rangel-Buitrago et al. 2018), on the western coast of the island (Figure 4.1b). The island's main port infrastructure is at Hanga Piko Harbor, located 1 km south of Hanga Roa (Figure 4.1b). All maritime cargo arriving on the island is unloaded there with the aid of self-propelled barges that transfer goods from ships anchored offshore. This harbor also hosts the island's only tide gauge station.

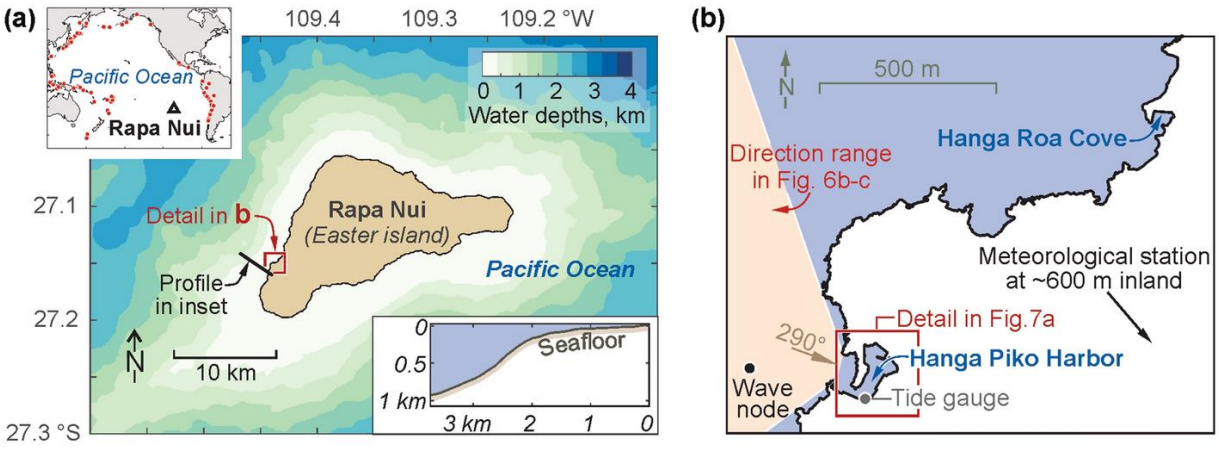

Figure 4.1. Index maps. (a) Bathymetry around Rapa Nui (Easter Island). Upper left inset shows the location of Rapa Nui relative to the epicenters (red dots) of global earthquakes greater than magnitude 8 since 1900 (Bilek and Lay 2018). Lower right inset shows a bathymetric profile off Hanga Piko along the track indicated by the black line. (b) Study area showing the Hanga Roa Cove and Hanga Piko Harbor. The pink area represents the direction range (240–340°) in which winds and waves impact directly to the Harbor, with 290° as the pure cross-shore direction. The black dot represents the node where the wave hindcast is obtained, the gray dot shows the tide gauge location, and the black southeastward arrow points to Mataveri Airport, where the meteorological stations is located.

The location of Rapa Nui makes it particularly exposed to large tsunamis generated in the far field and to intense coastal storms produced by diverse weather phenomena. Flooding of low-lying areas due to far-field tsunamis has been identified as a greater risk than that from storms (Quillam et al. 2014). This is not surprising since the island is surrounded by the Ring of Fire, where subduction zones trigger the world's greatest megathrust earthquakes (Bilek and Lay 2018) (Figure 4.1a). However, coastal storms are much more frequent than far-field tsunamis and can also cause inundation in low-lying areas. Indeed, photographic and video footage published in social media evidence recent flooding episodes at Hanga Roa and Hanga Piko during intense weather conditions. These episodes have attracted the attention of locals and authorities as also causing major impacts on harbor operations and therefore constitute a previously unrecognized hazard to the supply of the island.

Here, we show that extreme sea levels at Rapa Nui occur much more frequently than previously thought and result from constructive superpositions of seiches, storm surges and high tides.

4.2.3. Setting

Rapa Nui is the largest emerged part of the Easter Seamount Chain, an E-W trending alignment of volcanic seamounts extending eastward of the East Pacific Rise for about 3000 km (Baker et al. 1974; Rappaport et al. 1997). Due to its volcanic origin, the island of Rapa Nui rises abruptly from abyssal plain depths of ~ 3000 m to typical altitudes of ~ 150 m above sea level (Figure 4.1a). As for most volcanic islands, Rapa Nui's shelf is very narrow, with water depths of hundreds to thousands of meters within a few to several kilometers from the coast (Figure 4.1a). Near Hanga Piko, the shelf is about 2 km wide with the seaward edge at about 100 m below sea level (inset in Figure 4.1a). Inside the harbor, water depths are of ~ 2 m.

The island is located at the western flank of the southeast Pacific subtropical anticyclone (Figure 4.2a) which is maintained by the descending branch of the Hadley cell (e.g., Rahn and Garreaud 2014). During summer–fall, this results in predominant trade (easterly) winds passing over the island as shown in the polar diagram in Figure 4.2b, in which each point represents zonal (EW) and meridional (NS) wind components at 10 m above MSL for a given day (12:00 UTC), along with the long-term mean wind vector that is nearly 5 m/s from the east. The weather at Rapa Nui, however, is frequently disrupted by transient systems of both tropical and extratropical origin. The South Pacific Convergence Zone (SPCZ), with copious rainfall and unsettled weather, is rooted in the tropical central Pacific and extends southeastward not far from Rapa Nui (Figure 4.2a). Farther south, there is an incessant transit of midlatitude cyclones embedded in the southern hemisphere westerly wind belt (40-55ºS).

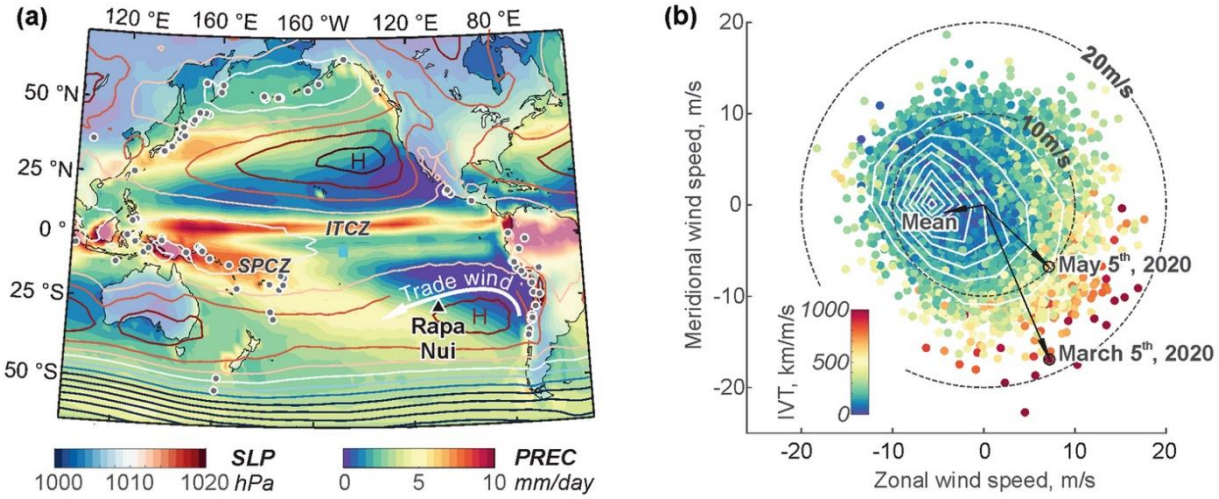

Figure 4.2. Climate background of Rapa Nui. (a) The background shading indicates long-term March-April-May mean (1980–2010) rainfall rate (PREC, in mm per day). The Intertropical Convergence Zone (ITCZ) and South Pacific Convergence Zone (SPCZ) are indicated. The overlay contours are the long-term seasonal mean sea-level pressure (SLP, in hPa). The letter H indicates the centers of the subtropical high-pressure cells over the SE and NE Pacific. The anticyclonic flow around these cells contributes to the trade winds along their equatorward side as indicated by the white arrow passing over Rapa Nui (black triangle). Shading grey dots indicate the epicenters of global earthquakes shown in Figure 4.1a. (b) Bivariate distribution of the daily (12:00 UTC) zonal (EW) and meridional (SN) components of the wind at 10 m above sea level for a point at 27 ºS, 109.1 ºW. Data from ERA-5 reanalysis covering the period January 1, 2000–October 7, 2020. White contours indicate density of data points. In this polar plot, each circle can be interpreted as the head of a wind vector. The circles are colored according to the integrated water vapor transport (IVT, scale at bottom) of that day. Also included is the long-term mean wind vector (blowing from the ENE), as well as the wind vectors for March 5th and May 5th, 2020 (blowing from the NNW).

Cold fronts, anchored in extratropical cyclones, contribute to the formation of atmospheric rivers (ARs), long filaments of high water vapor transport (e.g., Ralph et al. 2018) that can reach Rapa Nui and transfer vast amounts of moisture from the tropical Pacific into midlatitudes. Indeed, global surveys indicate a local maximum of AR frequency over the subtropical SE Pacific accounting for over 30% of the rainfall accumulation and connected with nearly half of the extreme wind events (Guan and Waliser 2015). ARs often extend for a few thousand kilometers, and they can last 1–3 days over Rapa Nui. During that period, strong low-level winds blowing from the NW (i.e., opposed to the more prevalent trade winds) account for most of the water vapor

transport (IVT). Footnote 1 These events stand out in the polar wind diagram (Figure 4.2b) by their warm-colored circles (indicating high IVT) in the lower-right quadrant, with speeds typically above 10 m/s. While ARs can produce local precipitation, most of the vapor continues its travel until they make landfall in south-central Chile (Viale et al. 2018).

Ocean tides are characterized by a mixed regime with a maximum range of ~ 0.8 m during spring tides and ~ 0.3 m during neap tides. Mean wave climate is controlled by swells emerging from extratropical cyclones moving on a latitudinal belt between 40°S and 60°S. The associated winds transfer energy to waves, which propagate from the South Pacific Ocean, reaching the island with mean significant wave heights of 2.6 m, mean periods of 9.0 s and mean directions of 211° (Beyá et al. 2017). However, these statistical parameters overshadow the multimodal nature of wave climate in the western coast of the island, where northwestern swells occasionally arrive during summer and locally-generated wind waves regularly arrive in winter.

4.2.4. Data and methods

4.2.4.1. Recorded and modeled data sets

We examined both atmospheric and sea-level data for a 17-month period from January 1st, 2019, to May 31st, 2020 (Figure 4.3). The former includes 1-min resolution times series of wind speed, wind direction and atmospheric pressure at sea level, recorded by the meteorological station of the Mataveri Airport, located about 600 m inland of Hanga Piko (Figure 4.1b). The sea-level data, also with 1-min resolution obtained by averaging 120 data points per minute (personal communication with former tide gauge chief operator Juan Fierro), was recorded by a tide gauge located in the southeast corner of the Hanga Piko Harbor (Figure 4.1b).

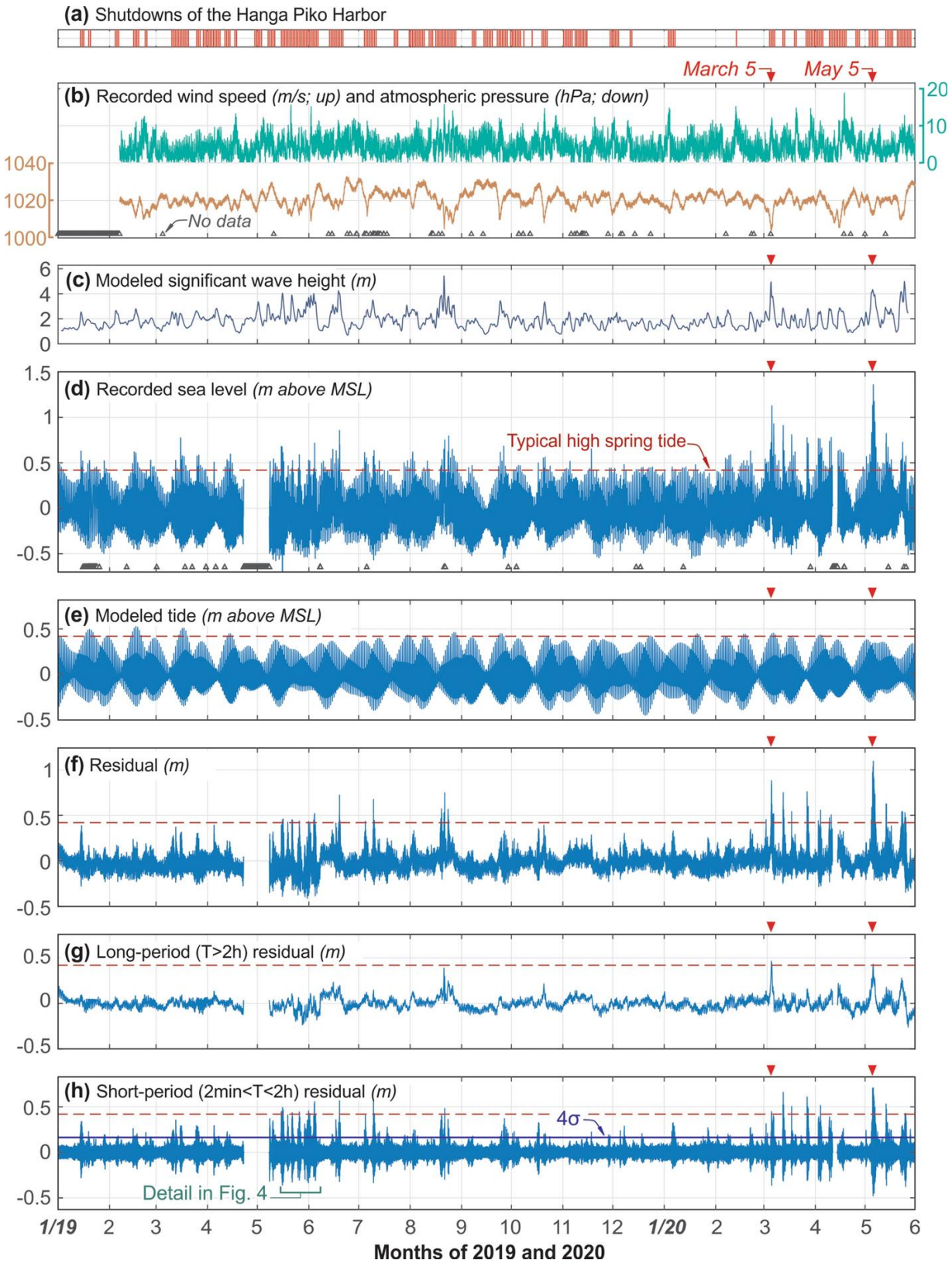

Figure 4.3. Main datasets time series used in this study. (a) Shutdowns of the Hanga Piko Harbor (red lines). (b) Recorded wind speed (green) and atmospheric pressure

(orange) at Mataveri Airport (See Figure 4.1b for station location). (c) Modeled significant wave height at a node located 300 m off Hanga Piko at 20 m water depths (see Figure 4.1b for node location). (d) Recorded sea level at Hanga Piko's tide gauge. (e) Modeled astronomical tide. (f) Residual sea level. (g–h) Long- and short-period component of the residual sea level, respectively. Blue horizontal line in (h) indicates four standard deviations (4σ) from the mean, used as a threshold for meteotsunamis identification (Monserrat et al. 2006). All time series span from January 1st, 2019, to May 31st, 2020 (17 months). Red downward triangles indicate the March 5th and May 5th, 2020, extreme sea-level events analyzed in this study. The upward black triangles in (b) and (d) indicate positions of data gaps

Synoptic-scale meteorological conditions were described using hourly fields of sea-level pressure (SLP), winds (zonal and meridional components) at selected levels and integrated water vapor transport (IVT) from the European Center for Weather Forecast reanalysis (ERA5) available from 1979 onwards on a 0.5° × 0.5° latitude–longitude grid (Hersbach et al. 2018). The data providers and accessibility are detailed in the Acknowledgement section.

Given the absence of local observations of wind-generated waves, we modeled wave climate in a node located 300 m off Hanga Piko at a depth of 20 m (see node location in Figure 4.1b). To this end, we used Wavewatch III (Tolman, 2014) with parametrizations adjusted for Rapa Nui (Beyá et al., 2017) and wind fields from NOAA's Global Forecast System GFS database. In the wave node, we retrieved statistical wave parameters of significant wave heights, mean directions and mean periods.

4.2.4.2. Time series analyses

Each recorded data set was first subjected to careful quality control, in which outliers were removed, gaps were identified and data offsets were adjusted. Tidal oscillations in the sea-level data were modeled (Figure 4.3e) using the T_tide software package based on harmonic analysis (Pawlowicz et al., 2002) and then removed from the recorded sea level to obtain the residual sea level (Figure 4.3f).

We decomposed the atmospheric and residual sea-level time series into long-period signals with periods longer than 2 h (Figure 4.3g) and short-period signals with periods between 2 min (Nyquist period) and 2 h (Figure 4.3h). This decomposition yields sea-

level signals that reflect different meteorological and oceanographic processes: While the long-period signal includes the storm surge and other lower-frequency anomalies, the short-period signal is expected to comprise different classes of oscillations in the tsunami frequency band (i.e., ~ 2 min to 2 h). The spectral separation was made using the wavelet method described by Torrence and Compo (1998) with the bias corrections introduced by Liu et al. (2007). In particular, we first obtained the long-period signals by applying a low-pass wavelet filter with a cutoff period of 2 h to the recorded atmospheric and residual sea-level time series. The short-period signals were then obtained by subtracting these resulting long-period signals from the parent time series. We remark that the resulting short-period signal of the sea level may contain infragravity (IG) waves with periods over 2 min, as well as aliased IG waves with shorter periods, but excludes waves with typical periods between 2 and 30 s.

4.2.4.3. Field survey guided by visual records

To gain insights on the effects of extreme sea-level events at the coast, we conducted both remote and in situ field surveys guided by both video and photographic footage obtained from eyewitnesses during the March 5th and May 5th (2020) events, when the recorded sea level reached the highest values in our analyzed period (Figure 4.3d). Our survey, conducted fourteen and six weeks after these events, respectively, focused on measuring water levels and inundation extents at Hanga Piko and Hanga Roa. All measured levels were confirmed by eyewitnesses and were referenced to MSL by using official harbor drawings provided by the local authority. These drawings include the levels of structures that were captured in the photographs and videos (e.g., gravity quay walls) and therefore served as reference to determine water levels during the events.

4.2.4.4. Sea-level variability at Rapa Nui

The diverse weather phenomena affecting Rapa Nui often induce large sea-level fluctuations at the coast. These are evident in the 17-month-long sea-level time series at Hanga Piko, which shows frequent high-amplitude oscillations that often far exceed the typical high spring tide (Figure 4.3d). Together with the wind (Figure 4.3b) and

waves (Figure 4.3c), these high-amplitude oscillations are very likely the main reason behind the frequent harbor shutdowns at Hanga Piko (Figure 4.3a).

The spectral separation of the residual sea level shows that both the long- and short-period components contributed significantly to the observed variability (Figure 4.3g-h). The contribution of each signal alone is occasionally comparable to, and sometimes even larger than, the maximum high spring tide. This is especially true for the short-period oscillations, whose amplitudes frequently exceed the high spring tide (Figure 4.3h). The long-period signal, instead, generally exhibited lower amplitudes but reached significant levels of a few decimeters in late August 2019 and in early March and May 2020 (Figure 4.3e). There is a 3-h-data gap in the former event that prevents us from knowing the true sea level reached on that occasion.

A closer examination of the short-period signal reveals the occurrence of continuous seiching off Hanga Piko. This is well illustrated in Figure 4.4b which shows the time series and wavelet spectrum between May 14th and June 7th, 2019 (other time windows show similar features). The wavelet spectrum shows that most of the signal variability occurs within a narrow period band centered around ~ 5 min. The reason to believe that these oscillations mainly reflect local seiches instead of other classes of waves (e.g., IG waves) is their roughly constant frequency and persistence, which together strongly suggest that they are controlled by the local submarine and coastal morphology rather than by the properties of the external forcing. Unfortunately, the lack of observations at other sites prevents us from understanding the spatial domain where these seiches occur, but they are very likely occurring on the shelf rather than inside the Hanga Piko Harbor. Indeed, according to the Merian's formula (e.g., Rabinovich, 2009), the fundamental or Helmholtz mode of a simplified cross section scaled to the profile shown in the inset of Figure 4.1b is 5.5 min, while that for the harbor basin in Hanga Piko is only from a few to several tens of seconds.

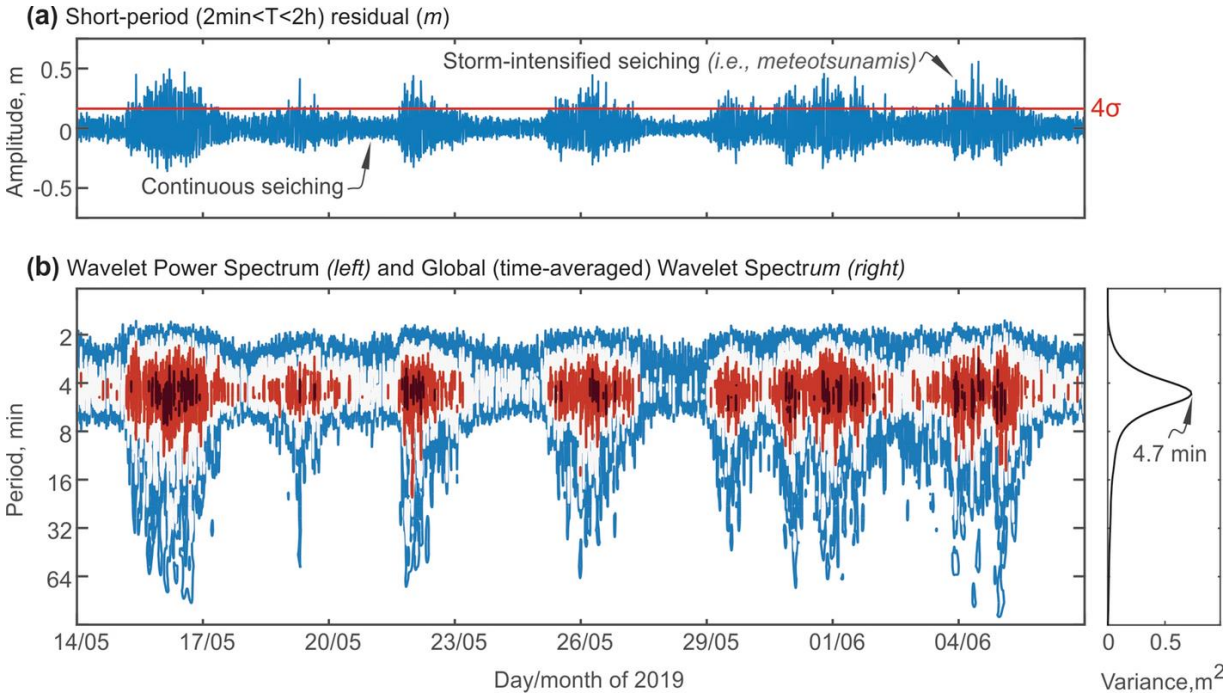

Figure 4.4. Continuous and intensified seiching. (a) A 24-day-long segment of the short-period component of residual sea level, between May 14 and June 7, 2019. Red horizontal line indicates four standard deviations (4σ) from the long-term mean shown in Figure 4.3h. According to Monserrat et al. (2006), amplitudes exceeding this threshold are defined as meteotsunamis. (b) Wavelet power spectrum (left) and normalized global wavelet spectrum (right) for the time series in (a). Reddish colors indicate large energy levels, and bluish colors indicate lower energy levels

Another evident feature of the short-period signal is the frequent intensification of the seiches. This can be seen in Figure 4.4, which shows recurrent intensification of the energy around the ~ 5 min period. This pattern clearly resembles the meteotsunami description of Defant (1961), who wrote that “The Meteorologic tsunami are nothing but seiches of bays and of the shelf, but they exceed in intensity the normally smaller amplitudes of the seiches …” If we set an amplitude threshold of four standard deviations (4σ), as suggested by Monserrat et al. (2006) to define meteotsunamis, we count dozens of seiches that meet this criterion in our 17-month-long analyzed window (Figure 4.3h) and therefore fall in the meteotsunami definition of Defant (1961) and others (e.g., Rabinovich 2020). Nonetheless, because we do not clearly understand the external forcing and resonant processes underlying their intensification, we hereafter simply call them intense seiches.

Furthermore, when these intense seiches are accompanied with significant storm surges, the residual sea level increases drastically, and when they both coincide with high tides the water level inside the harbor reaches hazardous levels. During the analyzed period, these hazardous combinations of seiches, storm surges and tides were most extreme during the events of March 5th and May 5th, 2020 (and possibly on the 21 August event). On both occasions, the sea level recorded in the harbor tripled the high spring tide. In the following section, we focus on these two events.

4.2.5. The coastal storms of March and May 2020

4.2.5.1. Synoptic and local weather conditions

Figure 4.5 shows the IVT magnitude (background colors) and the wind velocity (arrows) at 10 m above MSL at 12 UTC for March 5th and May 5th, 2020. A salient feature in these maps is a swath of strong NW flow near the surface and high IVT extending for more than 2000 km from the tropical Pacific to midlatitudes, the fingerprint of an AR in this area. The band of strong NW winds extends from the surface to the upper troposphere (not shown) transporting moist air sourced in the tropical central Pacific toward the southeast Pacific. In both snapshots, Rapa Nui was near the major axis of the ARs and we verified that the AR conditions prevailed over the island in a window of about 24 h around those times. The AR of the March event was stronger, wider and longer than that of May, although both reached Category 4 with IVT > 800 kg/m/s, the second strongest according to Ralph et al. (2017). The ARs were ultimately driven by the large-scale pressure gradient between midlatitude cyclones drifting toward southern Chile and the subtropical anticyclone (identified in Figure 4.5 as L1 and H, respectively).

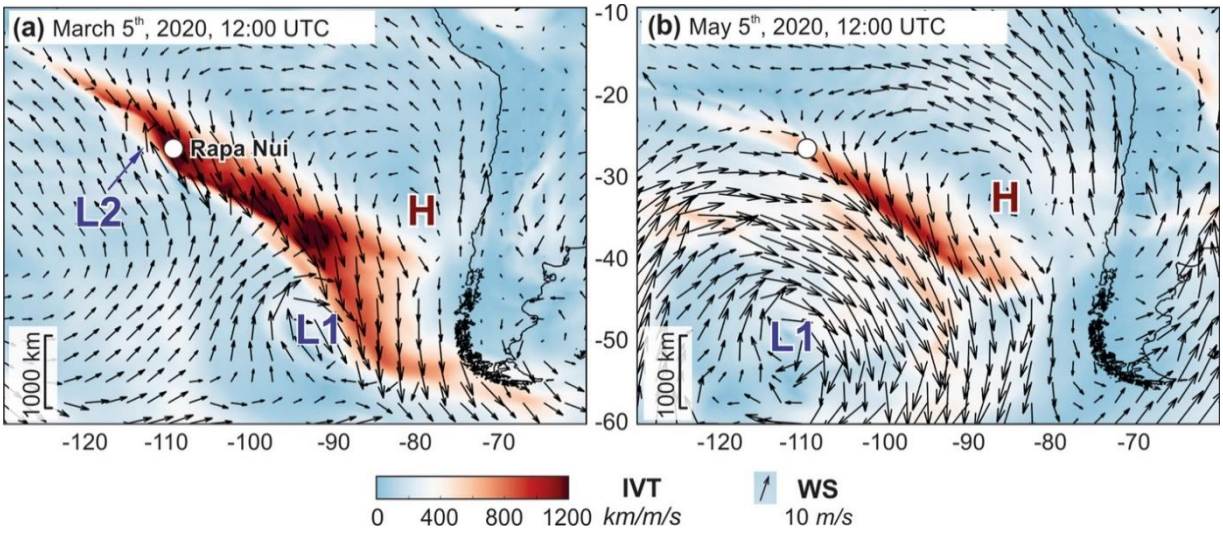

Figure 4.5. Synoptic weather conditions during the extreme sea-level events. The arrows represent the wind velocities at 10 m above MSL (see scale at the bottom). Letters H, L1 and L2 indicate the center of the subtropical anticyclone, the midlatitude cyclone and the secondary cyclogenesis, respectively. The white circle is the location of Rapa Nui. The magnitude of the integrated water vapor transport (IVT) is shown in shades (scale at the bottom). (a) is for 12 UTC March 5th, 2020, and (b) for 12 UTC May 5th, 2020

To place the two storms in context, the polar diagram of the daily (12 UTC) wind at 27ºS, 109.1ºW (Figure 4.2b) includes the wind vector and IVT for March 5th and May 5th, 2020. The March storm stands out for its large IVT value and strong NNW wind, among the largest of the record (~ 20 m/s). The wind during the May storm was from the NW and accompanied by a large value of IVT. The wind speed was large but not extreme, reaching ~ 10 m/s on May 5th and ~ 15 m/s the day before.

The local conditions, recorded at Mataveri airport, indicate some differences between the two storms (Figure 4.6a, b). In the first case, the surface wind changed rapidly from near calm on March 3rd to ~ 10 m/s northerly winds on March 5th (Figure 4.6b). In that 36-h period, the atmospheric pressure dropped by ~10 hPa, influenced by the passage of the main cyclone (L1) at midlatitudes and a secondary cyclogenesis within the AR and very close to Rapa Nui (L2 in Figure 4.5a). The absolute atmospheric pressure, however, remained above 1005 hPa, which is not a particularly low value. The atmospheric pressure drop was even weaker for the May event (8 hPa in 48 h), and the wind remained below 8 m/s (except for a brief period on May 5th), but the NNW

direction prevailed at least for the 72 h before the highest sea levels were recorded at the tide gauge.

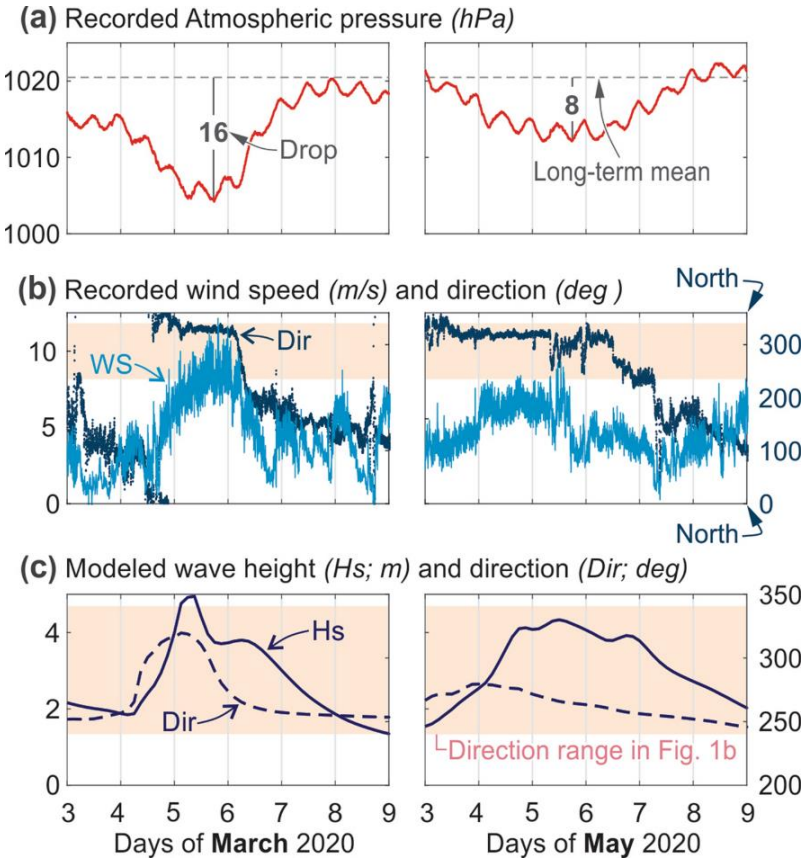

Figure 4.6. Local weather and wave conditions during the March 5th (left) and May 5th (right), 2020, extreme sea-level events. Time series of atmospheric pressure (a) and wind speed and direction (b) recorded at the Mataveri Airport (600 m east of Hanga Piko). (c) Time series of significant wave heights and mean directions modeled at a node located 300 m off Hanga Piko at 20 m water depths (location of the node in Figure 4.1b)

4.2.5.2. Wind–wave climate

Our modeled results show large waves with significant heights of up to 5 m and 4.2 m during the March 5th and May 5th events, respectively (Figure 4.6c). The March 5th event peaked with NW waves, lasting for about 2 days with wave heights above 4 m (left panel in Figure 4.6c). Those during the May 5th event had a roughly constant W direction, remaining with relatively high wave heights for nearly 3 days (right panel in Figure 4.6c).

4.2.5.3. Visual records and field survey

The effects of both events were partially captured by visual records obtained from eyewitnesses at different locations of the island. These, however, are more abundant for the May event at Hanga Piko. Because the tide gauge is located at this harbor, here we mainly focus on the sea-level fluctuations captured therein.

The May 5th, 2020, event was well captured by one video and two photographs, taken shortly after 23:00 UTC (17:00 local time Footnote 2), only tens of meters away from the tide gauge (Figure 4.7). This visual evidence provides lower bound estimates of the peak water levels and flooding extents around the harbor, revealing oscillations that complement the tide gauge record. A striking feature is the clear augmented water level lasting for at least 1 min (length of video), as shown in the left photographs of Figure 4.7b-d. By comparing these with photographs taken at the same sites during calm conditions and similar tide levels (~ 20 cm in both cases), the storm-induced sea levels can be visually inferred. The video also captures intense wave breaking outside the harbor, strong wave agitation induced by waves within the harbor (Figure 4.7b) and ubiquitous overtopping around the harbor quay walls (Figure 4.7b-d).

In the eastern sector of the harbor, the water level exceeded the quay wall at + 1.4 m above MSL and reached the base of the retaining wall on the other side of the road, which is at + 1.5 m above MSL (Figure 4.7b, d). The water level in the southern sector exceeded an even higher quay wall whose crest is at + 1.7 m above MSL (Figure 4.7c). We therefore consider + 1.7 m as a lower bound estimate of the maximum runup in this event. Following a similar approach for the March 5th event, we measured water levels of up to + 1.4 m above MSL at both Hanga Piko and Hanga Roa. Although we did not find footage at Hanga Roa for this event, competent witnesses informed that the effects were like those typically produced by regular storms.

Figure 4.7. Field survey results and visual effects of the May 5th, 2020, extreme sea-level event at Hanga Piko. (a) Aerial view of the Hanga Piko Harbor and water levels and inundation extents, as derived from video and photographic footage. (b–d) Comparisons of photographs taken at the same site with similar tide levels (0.2 m above MSL) during this event and calm conditions. The left panel of (b) is a video frame.

4.2.5.4. Time series analysis

Tide gauge records for both events show high-amplitude sea-level oscillations that remained visible for about 3 days (Figure 4.8a). Peak levels during the March 5th event occurred at 20:52 UTC (15:52 local time), when the sea level rose up to + 1.1 m above MSL (left panel in Figure 4.8a). Although the tide was at its highest level at that moment, its amplitude was only + 0.4 m. In the May 5th event, the highest sea level of + 1.35 m was recorded at 22:51 UTC during a tide of + 0.2 m (right panel in Figure 4.8a). Therefore, in both cases, the recorded sea levels were a few decimeters lower than those derived from visual records (Figure 4.8a). The difference is likely associated with the complex phenomena of wave agitation, harbor resonance and the presence of IG waves which are not captured by the tide gauge due to its relatively low, 1-min sampling interval.

The long-period signal reveals significant storm surges that increased the sea level for 2 days in March and 3 days in May, reaching maximum levels of + 0.5 above MSL in both occasions (Figure 4.8b). These, were the highest recorded during the analyzed window, leaving the August 21st (2019) event aside due to the data gap (see Figure 4.3g).

The short-period signal reveals intense seiches occurring in both events (blue curve in Figure 4.8d). The temporal intensification of these seiches agrees well with the concurring storm surges, with maximum amplitudes of ~ 0.4 m (March 5th, 14:58 UTC) and ~ 0.7 m (May 5th, 22:51 UTC). Therefore, in both events, the extreme water levels inside the harbor are explained by constructive superpositions of high tides, storm surges and intensified seiches, besides shorter-period phenomena captured by the video (Figure 4.8a) but missed by the tide gauge.

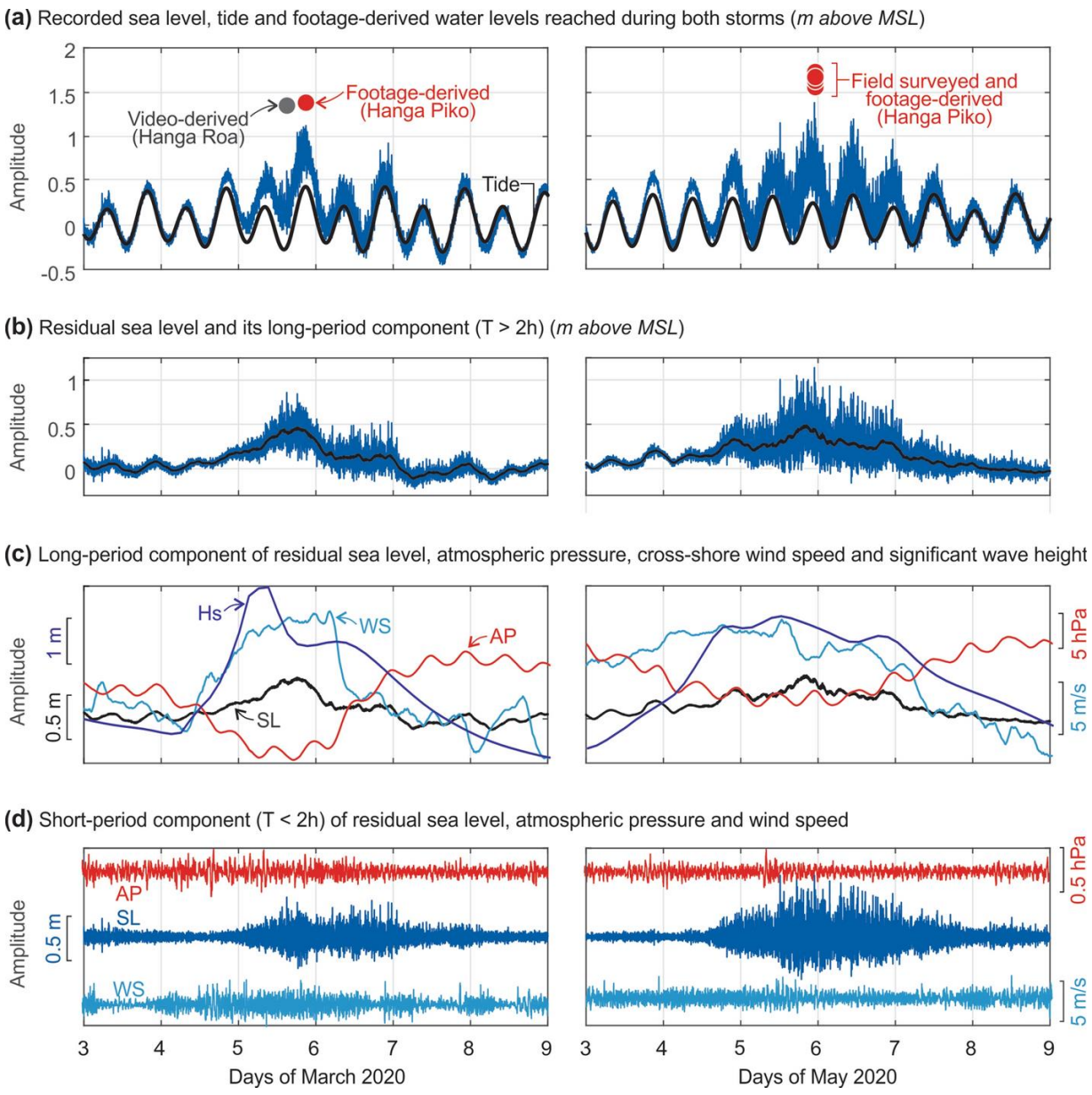

Figure 4.8. Time series analysis of the recorded sea level at Hanga Piko during the March 5th and May 5th, 2020, extreme sea-level events. (a) Sea level at Hanga Piko recorded by the tide gauge and inferred from video and photographic footage. (b) Residual sea level (blue) and its long-period component with periods longer than 2 h (black). (c) Comparison of the long-period components of the residual sea level (SL), atmospheric pressure (AP) and cross-shore wind speed (WS), and the modeled significant wave height (Hs). For absolute values, refer to (b) and Figure 4.4.6. (d) Short-period components of the residual sea level (SL), atmospheric pressure (AP) and wind speed (WS). Note that no relevant perturbations occurred in the atmospheric pressure or wind records, which rules out the occurrence of meteotsunamis formed by high-frequency atmospheric perturbations (e.g., Monserrat et al. 2006)

4.2.6. Inferred mechanisms behind the extreme sea levels observed at Rapa Nui

To elucidate the physical processes behind extreme sea-level events, as those observed in March and May, 2020, we performed simple correlation analysis between the sea-level signals and the atmospheric and wind–wave datasets. For this, we considered the time series shown in Figure 4.9a, which are modified versions of those in Figure 4.3. In particular, we only considered segments with no gaps in all the time series. For the wind speed, we considered the cross-shore components taking 290° as the pure cross-shore direction (Figure 4.1b). Also, instead of using the seiche amplitudes, which include both positive and negative values, we used their crest-to-trough heights calculated with the zero-up crossing method. Finally, given that the modeled significant wave heights have 1 data point every 3 h, we smoothed all the time series using a 3-h boxcar window.

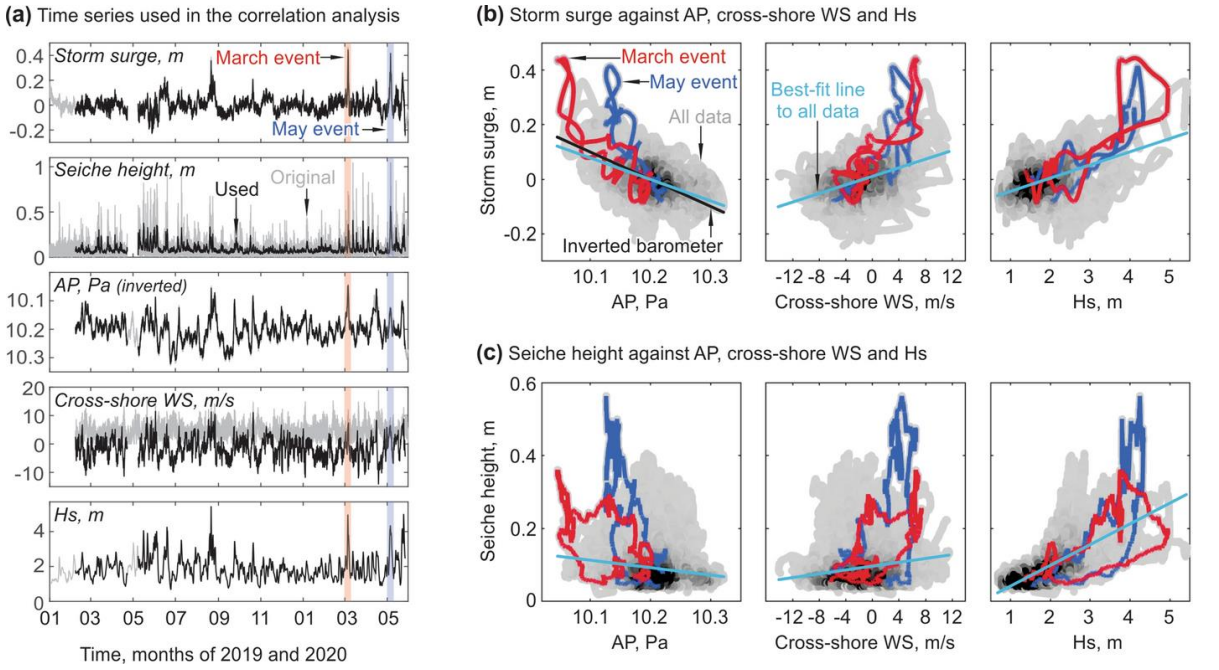

Figure 4.9. Correlation analysis between the sea-level signals and the atmospheric and wave datasets. (a) The time series in black are the ones used in the analysis, which are modified versions of the time series in grey presented in Figure 4.3 (see text for details) (in the second upper panel, the grey curve is the crest-to-trough heights of the short-period signal of Figure 4.3h). (b) Correlation plots between the long-period sea-level residual (storm surge), the atmospheric pressure (AP), cross-shore wind speed (WS) and significant wave height (Hs). For reference, the inverted barometer effect in the left panel is shown by the black line. (c) Same as (b), but the dependent variable is now the crest-to-trough seiche height, calculated by applying the zero-up crossing method to the short-period sea-level residual shown in Figs. 4.3h and 4.8d

4.2.6.1. Statistical correlation results

The results for all data show good correlation between the storm surge and the atmospheric and wave data (Figure 4.9b). In particular, the storm surge amplitude increases as the atmospheric pressure decreases (i.e., barometric setup) and as both the cross-shore wind speed (i.e., wind setup) and significant wave height increase, which we assume is scaled with the static component of the wave setup. The results also show that the storm surge increase with decreasing atmospheric pressure (represented by the best-fit line to all data) is slightly smaller than what is expected from the inverted barometer effect (compare slopes of the cyan and black lines).

The correlation results for the seiche heights (Figure 4.9c) are somewhat different. No clear correlation is observed between this variable and the atmospheric pressure and cross-shore wind speed. A positive correlation, however, is found with the significant wave height, which could be linked to the dynamic component of the wave setup and IG waves generated off the coast of Hanga Piko. As the significant wave heights become larger, the seiche heights increase.

Focusing on the two extreme events of March and May (red and blue lines in Figure 4.9), the correlation deviates from the general trend, especially for the seiche height. In particular, regressions feature a greater, and seemingly nonlinear, increase in both the storm surge amplitude and seiche heights when the atmospheric and wave parameters reach extreme values. Although not shown here, this pattern is observed in other extreme events throughout the data. The deviation from the trend in relatively large values, remain to be unexplained in light of the limited sampling frequency of the tide gauge and relatively coarse wave model which does not capture IG waves nor wave agitation in the nearshore.

4.2.6.2. Storm surge controlled by both wave and barometric setup

We interpret the correlation results of Figure 4.9b as either direct or indirect causal relationships. The increase in the sea level with decreasing atmospheric pressure, or barometric setup, is well known and has been observed in different settings (Wunsch and Stammer 1997), including other volcanic islands (e.g., Kennedy et al. 2012). For

the analyzed period, the barometric setup is evident in both the correlation results of Figure 4.9b and in the time series of Figs. 8c and 9a, with a good agreement of storm surge peaks and atmospheric pressure drops.

The positive correlation between the storm surge and the significant wave heights can be explained by the static component of wave setup, which results from the transfer of wave-related momentum to the water column during wave breaking (Pugh and Woodworth 2014). Wave setup has been reported to contribute significantly to elevated water levels especially during severe storms (e.g., Dean and Bender 2006) and can be even larger in regions where the shelf is extremely narrow or inexistent (Kennedy et al. 2012), as it is the case for steep volcanic islands. In the case of Hanga Piko, and according to satellite imagery (e.g., Google Earth), video footage and reports of local dockworkers, waves break a few to several tens of meters from the harbor entrance. Because the tide gauge is located only 50 m from the entrance (Figs. 1b, 7a), it is therefore unusually exposed to wave setup, in contrast to most other tide gauges located in sheltered areas.

The contribution of wind setup to the recorded sea levels is expected to be rather small, in spite of the relatively strong wind speeds and good correlation shown in Figure 4.9b. To a first-order approximation, the wind setup scales with the square of the wind speed, it is linearly dependent on the fetch and inversely proportional to the water depth. Despite the large fetch during both events (Figure 4.5), the energy transfer from wind to the sea surface occurred over very deep waters. This, plus the very narrow shelf off Hanga Piko, supports a relatively small contribution of wind setup, as previously reported for Rapa Nui (Quillam et al. 2011, 2014) and other volcanic islands (Kennedy et al. 2012).

In summary, from the analysis of meteorological and wave conditions, we posit that extreme storm surges in the March 5th and May 5th, 2020, events were dominated by wave setup, followed by barometric setup, and with little if any contributions of wind setup.

4.2.6.3. Seiches on the shelf modulated by wind–wave-related IG waves

Wind-driven phenomena are also the main candidate to explain the short-period sea-level signal. First, given the absence of relevant high-frequency perturbations of atmospheric pressure and wind speed preceding or during the high-amplitude seiches recorded in March 5th and May 5th, 2020 (Figure 4.5d), we rule out the atmosphere as the ultimate triggering mechanism of these oscillations (e.g., Monserrat et al. 2006). However, as mentioned in Chapter 4, the seiches with larger than usual amplitudes still fall into the general meteotsunami definition (e.g., Defant 1961), specifically as “bad weather” meteotsunamis (Rabonivoch 2020). Second, given the continuous seiching with a roughly constant period, of ~ 5 min, observed throughout the 17-month-long record, we rule out the continuous occurrence of IG waves, which are expected to have a wider frequency spectrum. Instead, we explain the 5-min oscillations by seiches on the shelf. Given the good correlation with significant wave heights, the amplitude of such seiches is likely controlled, or at least influenced, by the energy transferred from IG waves released during wave breaking to the shelf sea. Whether the seiches are propagating across the shelf or along it as progressive or standing edge waves is not known and needs further investigation.

4.2.6.4. The role of atmospheric rivers

Even if the wind did not contribute directly to the enhanced water levels through wind setup, it seemed to play a very important role at least during the March 5th and May 5th extreme events. Indeed, both events occurred during long-lasting (24–48 h) periods of strong NW winds, a condition that contrasts with the local wind climatology characterized by much weaker easterlies (see Figure 4.2b). The local wind conditions were, in turn, associated with strong ARs in which a swath of NW flow and high water vapor transport extended for several hundred kilometers upstream (and downstream) of the island. Thus, we hypothesize that ARs passing over Rapa Nui favor the generation of large NW swells that directly impact the NW facing Hanga Piko Harbor (i.e., little diffraction and refraction). As discussed above, these large waves were the main responsible for augmenting the sea level in both the short- and long-period bands. Although a few studies have reported relations between ARs and high water levels in

continental coastlines (Khouakhi and Villarini 2016; Shinoda et al. 2019) via wind setup, what we report here is somewhat different because the phenomena occur on a steep volcanic island surrounded by deep waters where the mechanism is wave setup rather than wind setup. Many issues regarding the connection between ARs and extreme sea levels at Rapa Nui are still unclear for us, but their scientific and societal importance revealed by the observations presented herein motivates their investigation.

4.2.7. Concluding remarks

From the analyses of the sea-level record at the main harbor of Rapa Nui (Hanga Piko), located on its western coast, we conclude the following:

1. Beyond the small tidal oscillations, the local sea level is highly variable, with multiple episodes of extreme sea levels. These extreme episodes usually result from the combination of high tides, storm surges and intense seiches on the shelf.

2. Storm surge is dominated by wave setup, followed by barometric setup, and with little if any contribution of wind setup. Seiching is continuous in the records and is very often intensified during intense weather conditions.

3. The two most extreme events during our analyzed period (between January 1st, 2019, and May 31st , 2020) occurred in March 5th and May 5th, 2020, when the sea level in the harbor tripled the high spring tide. Peak levels recorded by the tide gauge were + 1.1 m and + 1.3 m above MSL, respectively, although, according to video footage, real water levels in the harbor were a few decimeters higher.

4. In both cases, Rapa Nui was near the major axis of well-defined atmospheric rivers with a NW–SE direction. We hypothesize that the strong, long-lasting synoptic-scale winds that accompanied both atmospheric rivers favored the generation of large NW swells that directly impacted the NW facing Hanga Piko Harbor, which in turn were the main responsible for increasing the sea level through significant storm surges and intense seiches.

5. Given that the sea level and the strength of atmospheric rivers in the South Pacific Ocean are thought to increase as climate changes (e.g., Espinoza et al. 2018;

Dangendorf et al. 2019), a deeper understanding of the meteorological and oceanographic processes affecting the operational efficiency of Rapa Nui's main harbor (and thus its maritime supply chain) is strongly needed.

Chapter 5

The depth of megathrust slip is a weaker predictor of tsunami size than usually thought

This chapter consists of a manuscript under review in Journal of Geophysical Research (Solid Earth) in which seafloor deformation models and tsunami propagation models are combined to explore the role of the depth of megathrust slip in tsunami generation in generic subduction zone earthquakes and in the 2011 Tohoku-oki earthquake.

The manuscript information is provided in Section 5.1 and the manuscript itself in Section 5.2.

5.1. Manuscript information

Title: Evaluating the Tsunamigenic Potential of Trench-Breaching Versus Buried Megathrust Slip

Authors: Carvajal, M., Sun, T., Wang, K., Luo, H., and Zhu, Y.

The supplementary material is available in the Appendix A.

5.2. Manuscript: Evaluating the Tsunamigenic Potential of Trench-Breaching Versus Buried Megathrust Slip

5.2.1. Abstract

Subduction megathrust ruptures that breach the surface at the trench, such as in the 2011 M=9 Tohoku-oki earthquake, are commonly thought to be the most tsunamigenic. However, despite its important hazard implications, the validity of this notion has never been rigorously tested. Here, we conduct this test by studying the mechanics of seafloor deformation and the resultant tsunami runup elevation. With a trench-breaching rupture, deformation is dominated by the rigid-body translation of the frontal upper plate, and seafloor uplift is enhanced by the horizontal motion of the sloping seafloor. With a buried rupture, the rigid-body motion is reduced, but the shortening of the upper plate due to seaward slip termination causes elastic

thickening to enhance tsunamigenic seafloor uplift. By combining a finite-element deformation model and a shallow-water equation tsunami model, we systematically test various subduction zone geometrical and slip parameters to study how the trade-off between rigid-body translation and elastic thickening affects the tsunamigenic potential of trench-breaching versus buried ruptures. We find that very shallow ruptures, including those breaching the trench, are generally less tsunamigenic than deeper ruptures with the same peak slip magnitude. Given peak slip, tsunamigenic potential is maximized if the rupture is not too shallow or too deep but is buried to moderate depths. Our re-examination of the 2011 Tohoku-oki earthquake suggests that the large tsunami runup along the coast facing the main rupture zone resulted primarily from the very large magnitude of the fault slip, rather than by its shallow depth.

5.2.2. Introduction

Earthquakes that rupture the very shallow part of subduction megathrusts are commonly believed to be the most tsunamigenic, especially those that breach the trench. This notion appears to be supported by the large tsunamis associated with tsunami earthquakes that rupture the shallowest part of subduction megathrusts (Kanamori, 1972; Satake et al., 1994; Hill et al. 2012) and by the widely held belief that the trench-breaching nature of the 2011 M=9 Tohoku-oki earthquake was primarily responsible for the ensuing devastating tsunami (Kodaira et al., 2021). This notion has led to an intense focus on the shallow megathrust in the study of subduction earthquakes and tsunamis by the scientific community (e.g., Gulick et al., 2011; Lay and Rhode, 2019; Hubbard et al. 2015). Intuitively, it seems that trench-breaching slip can displace large(r)??? volumes of water to cause a large tsunami because of the seaward motion of the sloping seafloor (Tanioka and Satake, 1996; Hooper et al. 2013; Sun et al., 2017) and because of the large water depths around the trench (Geist et al. 2006; Polet and Kanamori, 2000). However, the theoretical validity of this notion has never been rigorously examined. In this study, we assess its validity from the perspective of the mechanics of tsunamigenic seafloor deformation.

If large coseismic slip of the megathrust occurs at the trench, seafloor deformation is dominated by the rigid-body translation of the frontal wedge of the upper plate, and seafloor uplift is indeed enhanced by the horizontal motion of the sloping seafloor (Figure 5.1a). However, if the slip is buried and tapers toward the trench (Figure 5.1b), seafloor uplift is not necessarily smaller. In this situation, the frontal part of the overlying upper plate is horizontally shortened, and consequent elastic thickening can lead to large seafloor uplift (Figure 5.1b). How these two deformation components, namely rigid-body translation and elastic thickening, contribute to tsunamigenic seafloor uplift in different rupture scenarios is the focus of this study.

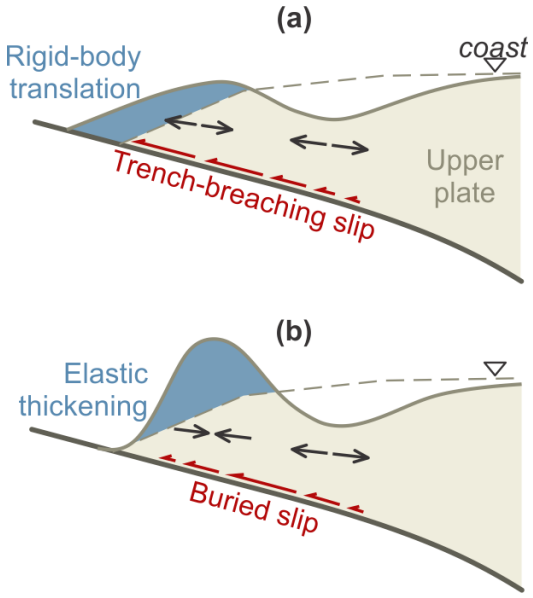

Figure 5.1. Cartoon illustrating the trade-off between the two mechanisms that control tsunamigenic seafloor deformation in trench-breaching and buried ruptures. (a) Dominance of rigid-body translation in trench-breaching rupture. The blue shaded area illustrates the enhanced near-trench seafloor uplift due mainly to the horizontal motion of the sloping seafloor. (b) Dominance of elastic thickening in buried rupture. The blue shaded area illustrates the enhanced seafloor uplift due mainly to the horizontal contraction and resultant thickening of the upper plate. Dashed line indicates pre-earthquake seafloor geometry.

The vast majority of published subduction zone tsunami source models are derived using an Earth model with a flat top surface (e.g., half space). Model predicted surface deformation is then combined with actual bathymetry for computing tsunami

propagation and inundation. These flat-surface models yield reasonable deformation results if the megathrust rupture is sufficiently deep. However, because of the absence of seafloor slope and/or incorrect thickness of the wedge-shaped crustal material overlying the megathrust, these models are rather inadequate if the rupture is shallow, particularly if it breaches the trench (Wang et al., 2018). To explore the deformation mechanisms illustrated in Figure 5.1, in this work we employ finite element models of elastic deformation that include long-wavelength surface geometry appropriate for subduction zones. Using seafloor deformation predicted by these models as tsunami sources, we simulate tsunami wave propagation and runup at the model coast.

With the combination of seafloor deformation modeling and tsunami modeling, we are able to examine how seafloor geometry, fault geometry, and slip distribution affect the relative contribution of the two deformation components illustrated in Figure 5.1 to influence the main tsunami wave parameters that determine runup. To isolate the effect of slip depth, we compare rupture scenarios with different depths but the same maximum slip. We show that the enhanced uplift due to the rigid-body translation of the sloping seafloor is at the price of much reduced elastic thickening, and vice versa, and we explore how this trade-off is modulated by geometrical and slip parameters. By applying the theory to the 2011 Tohoku-oki earthquake, we reassess the role of the trench-breaching slip in controlling the observed tsunami runups.

5.2.3. Methods of deformation and tsunami modeling

5.2.3.1. Finite element modeling of tsunamigenic seafloor deformation

5.2.3.1.1. The subduction zone deformation model

We employ a simple subduction zone geometry that reflects the main characteristics of many real subduction zones (Figure 5.2a). To focus on the main physical process, we ignore along-strike variations in most of our test models. In our modeling, the trench-coast distance is fixed at 150 km, and the trench depth varies in the range 3,300-10,300 m. The megathrust geometry shown in Figure 5.2a is typical of most

subduction zones, but we will also vary the average dip of the fault in some models for testing purpose.

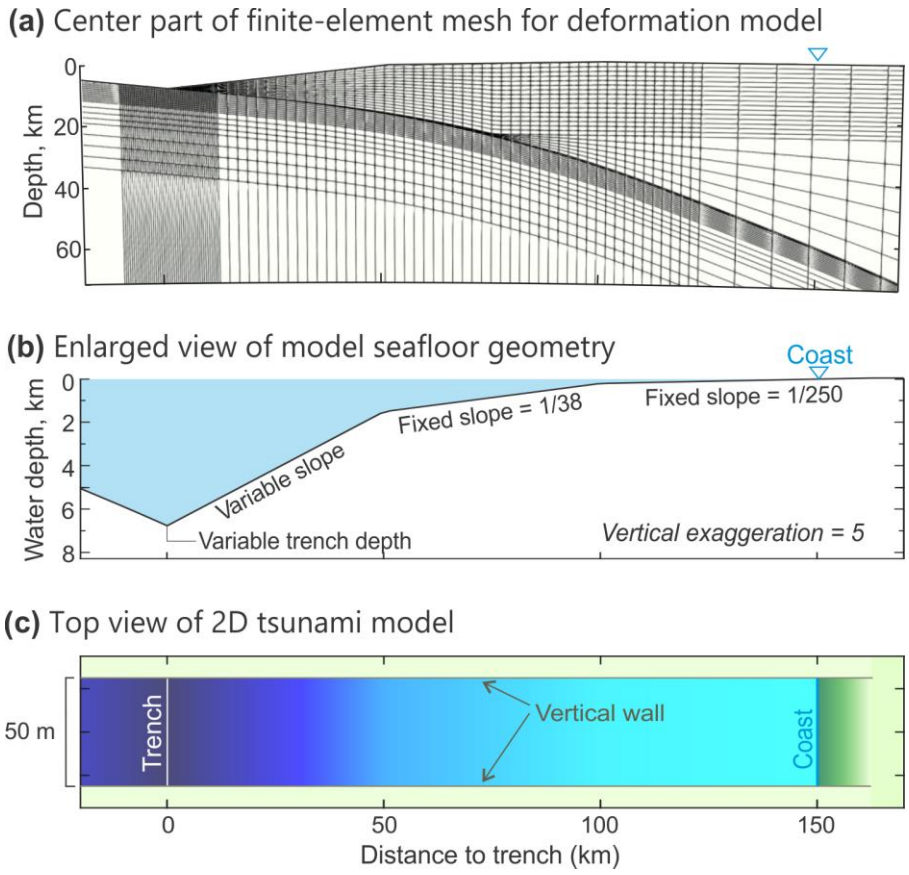

Figure 5.2. Illustration of the 2-D models used for surface deformation and tsunami modeling. (a) Center part of the finite-element mesh for subduction zone deformation models. The model is run in a spherical-Earth coordinate system, so that the depth axis and radial mesh lines are not strictly vertical in this display. (b) Vertically exaggerated seafloor geometry consisting of linear segments of different slopes. The shallowest segment extends landward of the coast to allow inundation and runup calculation. (c) 2-D channel used for tsunami modeling (width exaggerated 500 times). The model grid consists of 50 × 50 m2 square cells, but only one row is needed in the strike-normal direction.

The model seafloor, from the coast to the trench axis, consists of three linear segments (Figure 5.2b). All segments are 50 km long and together represent the general shape of real active continental margins. The shallowest segment, with its seaward limit at ~200 m below sea level and a slope of 1/250 (~0.2°), represents the

continental shelf and extends landward of the coast to allow tsunami inundation on land (see section 2.2). The middle segment, with a slope of 1/38 (~1.5°), extends 100 km offshore to a depth of ~1,500 m below sea level. The deepest and most seaward segment represents the lower continental slope and defines the upper surface of the frontal wedge. Because we are particularly interested in the impact of the sloping seafloor on tsunami generation (Figure 5.1a), we vary the slope angle of this segment over a range of 1/10 to 1/5.8 (2° to 10°) in different models to cover the observed range at subduction margins. With the slope break fixed at 1,500 m below sea level, the variations in the lower slope lead to the variations in trench depth mentioned above. Seaward of the trench, we allow the seafloor to slope toward the trench as in real subduction zones (Figure 5.2a and 5.2b).

We use the finite-element code PGCviscl-3D, which has been extensively benchmarked against analytical solutions and used in our earlier subduction zone earthquake cycle models (Hu et al., 2004; Wang et al., 2012; Sun et al., 2014, 2018; Luo and Wang, 2021), to simulate the tsunamigenic seafloor deformation. The models considered in this work are purely elastic with prescribed coseismic fault slip (see section 2.1.2). Potential permanent deformation of parts of the upper plate in the form of localized faulting or distributed plastic yielding adds further complications in real earthquakes (e.g., Tsuji et al., 2013; Hananto et al., 2020) but are ignored in our modeling because of the focus of this study. For simplicity, we assume a uniform model domain with Poisson's ratio 0.25, except for special tests. Because megathrust slip distribution is kinematically prescribed, rigidity plays little role in controlling model deformation, as graphically illustrated in Figures S1 and S2. For a uniform model neglecting gravity, different rigidity values yield identical deformation results. Our models include the effect of gravity except for the illustrations in Figure S2, but the effect is negligibly small. The presence of low-rigidity materials in the frontal wedge or shallow crust (e.g., Sallarès and Ranero 2019) only slightly affects predicted seafloor deformation (Figure S2).

We set the lateral boundaries more than 1,000 km away from the model rupture area and the bottom boundary at 600 km depth. The boundaries are adequately distant so

that they do not affect model results in our region of interest. Our code models deformation in a spherical Earth, but a Cartesian system will yield nearly identical results for this spatial scale. There is no strictly 2-D model in a spherical Earth, but we still call our models with no along-strike variations 2-D models.

The deformation models yield three-component coseismic surface displacements. To obtain the added seafloor uplift due to the horizontal motion of the sloping seafloor (Figure 5.1a), we use the method of Sun et al. (2017) to derive the bathymetry difference before and after the rupture. For the smooth seafloor in our synthetic models (sections 3 and 4), the approximate method of Tanioka and Satake (1996) will yield the same results. Because the main objective of this study is to investigate the trade-off between the two deformation components illustrated in Figure 5.1, it suffices to use a static model of instantaneous deformation. Potential contributions from realistic rise time and rupture propagation are of minor importance for this objective and are thus neglected.

5.2.3.1.2. Fault slip assignment

To focus on the main objective, we only consider megathrust ruptures that are completely offshore. In the suite of trench-breaching and buried rupture models that we use to investigate the aforementioned trade-off, the peak slip is 10 m, and the horizontal projection of the downdip rupture width is 100 km, both being representative of observed fault slip in Mw 8-8.5 megathrust earthquakes (Allen & Hayes, 2017). Although seafloor deformation scales linearly with slip magnitude, the resultant tsunami runups do not, because of the nonlinear nature of tsunami propagation and runup. Therefore, we do not normalize any of our model results using the peak slip value. Nonetheless, the knowledge learned from the 10 m slip models is qualitatively applicable to models of other slip values.

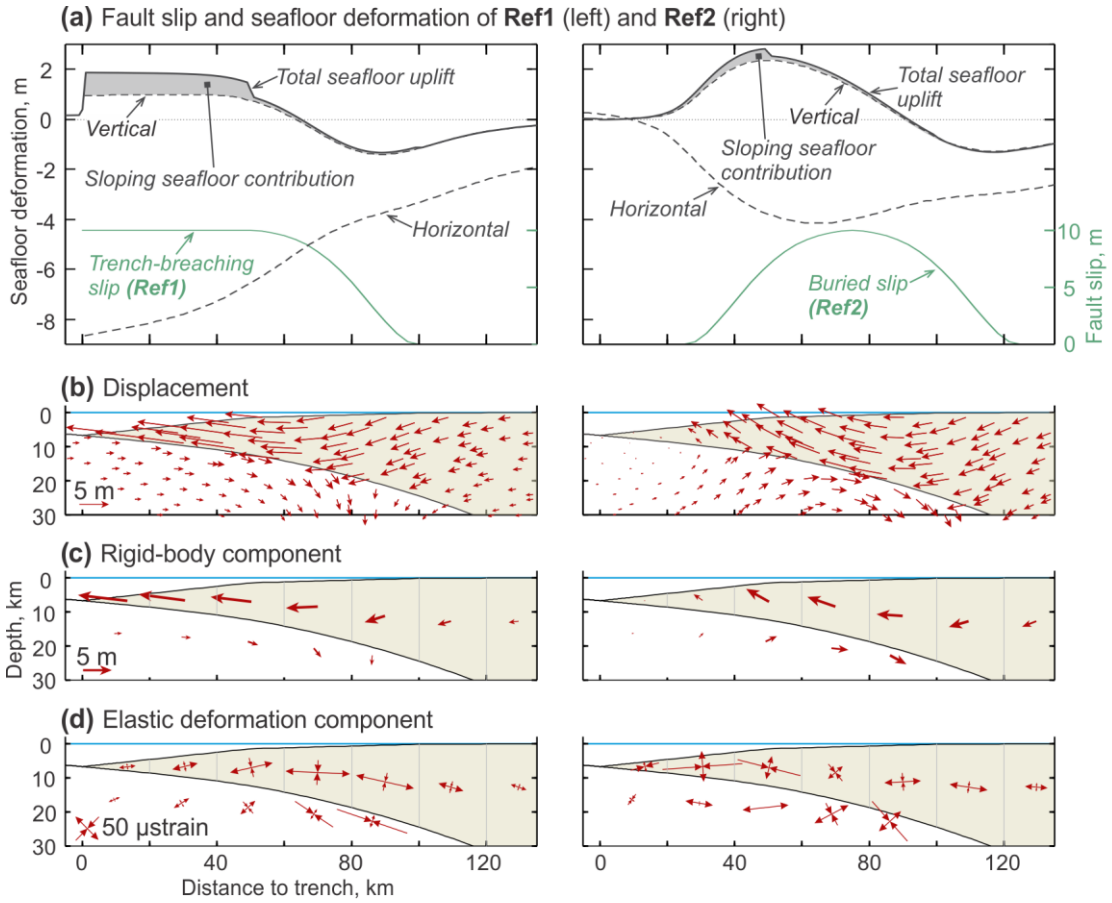

Figure 5.3. The two reference models Ref1 (left) and Ref2 (right). (a) Fault slip distribution (axis to the right) and seafloor deformation (axis to the left). "Sloping seafloor contribution" is the contribution to total seafloor uplift from the seaward horizontal translation of the sloping seafloor. (b) Displacement field. Displayed displacement vectors are randomly selected. The horizontal and vertical components along the top surface are shown in (a) using dashed lines. (c) Rigid-body component of the upper plate shown with translation vectors. (d) Elastic deformation component shown with principal strains. In (c) and (d), the deformation components are averaged over 20-km-wide blocks of the upper plate (block boundaries indicated by grey vertical lines) and shown at the center of each block.

Figure 5.3a (green curves) shows the slip distribution in typical trench-breaching and buried rupture scenarios used in our models. Deformation and tsunami results for these models will be discussed in section 3.1. The slip in the buried rupture follows a modified version of the bell-shape function of Freund and Barnett (1976) proposed by Wang and He (2008) with typographic errors fixed in Wang et al. (2013). This function depicts slip that tapers smoothly both updip and downdip. It also allows the bell-

shaped slip distribution to be skewed updip or downdip, which will be dealt with in section 4.4. Trench-breaching slip is modeled by replacing the updip limb of the bell-shape function with part of a sinusoidal function that allows the slip to decrease smoothly toward the trench (Gao et al., 2018). Different degrees of trench-breaching are represented by the amount of slip at the trench expressed as percentage of the peak slip at the apex of the bell-shape slip function. For 100% trench-breaching, the peak slip is sustained all the way to the trench (Figure 5.3a).

5.2.3.2. Tsunami Modeling

The seafloor deformation predicted by the deformation model described above is the tsunami source for our runup modeling. However, the size of the runup is determined not only by the tsunami source but also by the tsunami propagation path from the source area to the coast (e.g., Geist 1998). Specifically, since tsunami wavelength is comparable with the trench-coast distance, the back portion of the leading wave is in greater water depths than the front portion and hence travels faster. This situation leads to progressive shortening of the wavelength and shoaling of the leading wave. Given coastal topography, runup is determined by the size and shape of the incident leading wave. All our source models except for a few in section 5.2 produce a trough-leading wave because the megathrust rupture is sufficiently far offshore, such that the runup increases with the characteristic wavelength, trough amplitude, and frontal steepness of the leading wave (e.g., Tadepalli & Synolakis 1994; Geist 1998; Satake et al. 2013).

To isolate the effect of the tsunami source on runup, we try to minimize the effect of the propagation path in causing differences between different models. Therefore, we use identical seafloor geometry for distances > 50 km from the trench in all our models (Figure 5.2b). However, we must vary the near-trench seafloor slope because it is an important parameter in our source study, but the effect on runup is very small. Therefore, we are confident that the runup differences between different models predominantly reflect differences in the source, not in the propagation path. We have also run models in which the seafloor geometry at > 50 km distance from the trench is slightly different from that shown in Figure 5.2b, such as with a steeper or flatter slope

for the middle segment or around the coast, but still identical between different models. The results (not displayed) verify that what we learn about the source effect from the models in sections 3 and 4 is not fundamentally changed.

We use the widely adopted Kajiura transfer function (Kajiura, 1963) to convert the static seafloor deformation to sea surface deformation, which provides the initial condition for tsunami propagation. The 2-D Kajiura function approximates the attenuation of the short-wavelength components through the water column, leading to a smoother sea surface elevation. The effect is particularly obvious in trench-breaching rupture scenarios in which the displacement discontinuity at the trench richly produces short-wavelength components (Felix et al., 2021). For simplicity, we use a constant water depth – the trench depth – in the function, despite the presence of seafloor slope. We have verified that using different reference water depths makes only slight differences to the tsunami model results and does not affect our conclusions.

We use modeling software COMCOT (Cornell Multi-grid Coupled Tsunami model; Wang and Power, 2011) to compute sea-surface elevations during tsunami propagation and inundation from the source area to the farthest point inland where runup is calculated. COMCOT adopts explicit staggered leap-frog finite difference schemes to solve the two-dimensional Linear and Nonlinear nondispersive Shallow Water Equations in either spherical (section 5.2) or Cartesian (sections 3, 4 and 5.1) coordinates. Because a few of our tsunami source models produce relatively short tsunami waves compared to the local water depth and thus push the theoretical performance limits of COMCOT which does not include the effect of frequency dispersion, we also tested a more sophisticated code NEOWAVE (Yamazaki et al., 2011). NEOWAVE includes a vertical velocity term to handle dispersive tsunami waves and a shock capturing scheme to handle very steep wave front in runup calculation, both at the cost of computing time. With a comprehensive comparison of the performance of COMCOT against NEOWAVE (see Supporting Text S1), we found that for our source models and the relatively short trench-coast distance, the

two codes yield very similar results (Figure S3). We therefore decided to use COMCOT for efficiency and convenience.

A subduction zone deformation model without along-strike variations is called a 2-D model. However, because of the absence of depth dimension in the mathematical formulation of depth-averaged shallow-water equation models, a tsunami wave model based on such a 2-D deformation source is commonly referred to as a one-dimensional (1-D or 1-DH) tsunami model. Nonetheless, in this paper we refer to this type of tsunami model also as 2-D, to be compatible with its 2-D deformation source. Similarly, a tsunami model based on a 3-D deformation source such as for any real earthquake is therefore called a 3-D tsunami model in this paper, despite the fact that it is strictly a 2-D or 2-DH model.

Our 3-D tsunami modeling follows a standard procedure (e.g., Wang and Power, 2011; Carvajal et al., 2016, 2017a). Our 2-D tsunami models, in which the tsunami propagates only in the strike-normal direction, use a special design to enhance computing efficiency, so that we can readily run hundreds of 2-D models using a laptop computer to investigate the physical process. Only a distilled set of models are shown in this paper. For these 2-D models, we use a 228-km-long channel discretized into squared grid cells of 50 × 50 m2, with 4,559 grid cells in the strike direction and only 1 in the strike-normal direction (Figure 5.2c). We apply an absorbing boundary condition to the open ocean end of the model and use the moving boundary scheme (implemented in COMCOT) at the landward wet-dry boundary to track the moving shoreline and simulate inundation and runup. We use the Nonlinear Shallow Water Equations and incorporate the effects of bottom friction along the channel using a Manning's roughness coefficient of 0.025 s m−1/3 (Kotani et al., 1998). The computation time step is set to satisfy the Courant-Friedrichs-Lewy stability condition of the finite difference method and varies from 0.07 to 0.14 s. All simulations are run for 1 h tsunami propagation time, which is more than adequate to capture the maximum model runup (associated with the leading wave).

5.2.4. Tsunami generation by trench-breaching and buried ruptures

5.2.4.1. Trade-off between rigid-body translation and elastic thickening

The two reference models shown in Figure 5.3, namely Ref1 and Ref2, accentuate the trade-off between the two deformation components illustrated in Figure 5.1. Figure 5.3a shows their slip distribution (green) and resultant surface deformation (black), and Figure 5.3b shows the displacement field in cross-section view. In Figure 5.3a, the vertical and horizontal components of the seafloor displacement (Figure 5.3b) are illustrated using dashed lines. The total tsunamigenic seafloor uplift, which includes the contribution from the horizontal motion of the sloping seafloor (shaded area), is illustrated using a solid line.

In understanding the results in Figure 5.3, we need to consider the horizontal and vertical components of the rigid-body translation separately. The presence of the vertical component is because of the dip of the fault. The vertical (upward) translation contributes to both Ref1 and Ref2, but the difference in tsunamigenic seafloor deformation between these two models primarily reflects the trade-off between the horizontal rigid-body translation and elastic thickening. In Ref1, the horizontal motion of the sloping seafloor contributes to about 50% of the total uplift but there is no contribution from elastic thickening. On the other hand, in Ref2, thickening due to elastic shortening causes large seafloor uplift, but the sloping-seafloor contribution is greatly diminished.

To better explain this trade-off, we separately illustrate the rigid-body translation component (Figure 5.3c) and the elastic deformation component (Figure 5.3d) averaged over 20-km-wide blocks of the upper plate, with the translation vector and the principal strains shown at the center of each block. The translation vector is simply the average of a dense grid of displacement vectors within each block. The strain tensor is derived by fitting a model of constant strain to all these displacement vectors; averaging strain tensors of individual finite elements in the block will yield nearly identical results. The domination of one of the two deformation components in each model is clear. Rigid-body translation near the trench approaches the value of fault slip in Ref1 but is zero in Ref2 (Figure 5.3c). This causes the large near-trench seafloor uplift in Ref1 but not in Ref2 (Figure 5.3a). In Ref1, the trenchward decrease in the stiffness of the wedge-shaped frontal upper plate causes the horizontal

displacement to increase trenchward despite the uniform fault slip in this area (Figure 5.3a). The consequent horizontal extension causes slight thinning of the upper plate (Figure 5.3d), so that the contribution of elastic thickening to seafloor uplift is actually negative. In Ref2, the updip tapering of the fault slip (Figure 5.3a) leads to horizontal shortening, and the resultant thickening (Figure 5.3d) gives rise to large seafloor uplift peaking at the location where the slip gradient is the highest (Figure 5.3a).

5.2.4.2. The mechanism of elastic thickening

The horizontal motion of the sloping seafloor in the trench-breaching model is straightforward to understand, but the mechanism of elastic thickening in the buried rupture model requires further explanation. To illustrate the mechanism, we show the deformation due to bell-shape slip along a hypothetical horizontal fault in an elastic half space (Figure 5.4). The use of a horizontal fault eliminates any uplift due to the upward rigid-body translation of the hanging wall. The model-predicted surface uplift (and subsidence) is therefore purely a consequence of elastic deformation. Drawing an analogy to our 2-D megathrust models (Figure 5.3), we call the portion of the slip zone to the left of the peak slip the “updip” segment of the rupture, and the portion to the right the “downdip” segment. In Figure 5.4, all distances are normalized using Wu, the width of the updip segment. For simplicity, we assume a symmetric slip distribution (Figure 5.4a), such that the deformation is antisymmetric with respect to the location of the peak slip, but a skewed slip distribution would demonstrate the same mechanical principles.

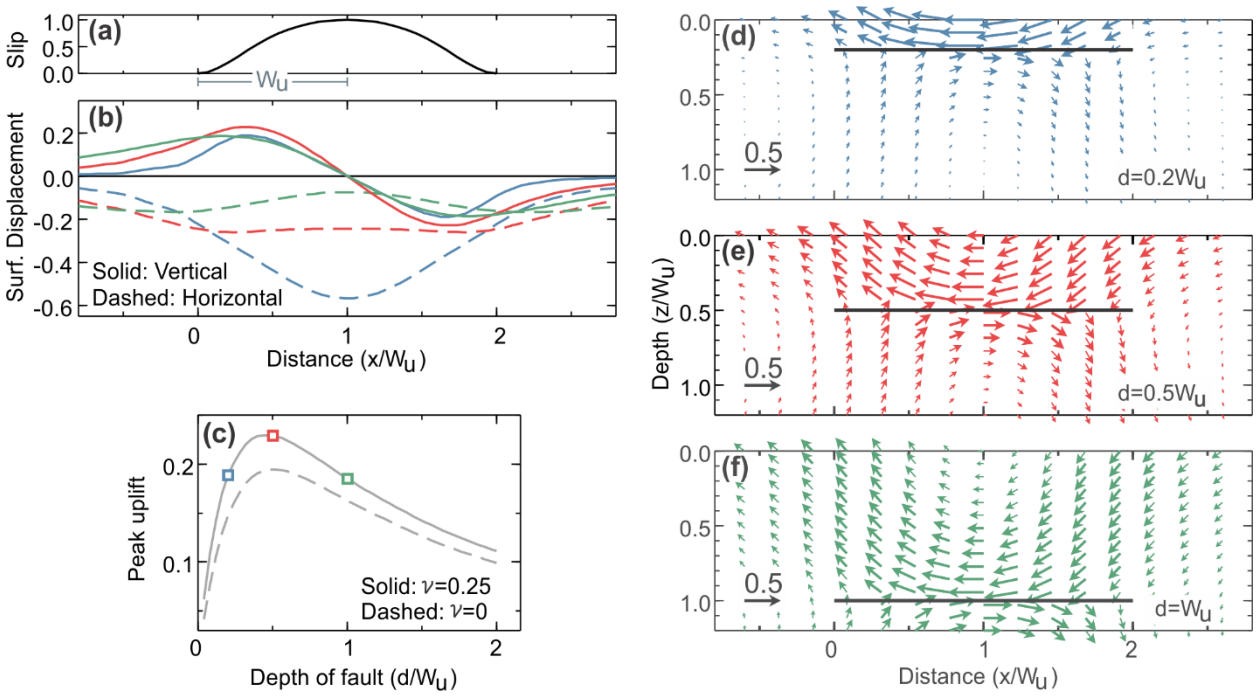

Figure 5.4. Model deformation due to buried rupture on a hypothetical horizontal fault to illustrate the mechanism of elastic thickening. (a) Slip distribution normalized by peak slip. Hanging wall moves to the left. W_u is the width of the "updip" segment of the slip zone. (b) Surface displacements of the three color-coded models shown in (d-f). (c) Peak surface uplift (normalized by peak slip) as a function of fault depth d (normalized by W_u) for two Poisson's ratio values (ν), showing that the highest peak uplift occurs when fault depth $d = 0.5W_u$. Results for the three models in (d–f) are shown with color-coded squares. (d-f) Cross section view of displacement vectors for three models with different fault depths.

The model displacement field around the center of the rupture zone exhibits opposite horizontal motion of the hanging wall and footwall (Figures 4d – 4f). While their relative motion is determined by the assigned slip magnitude, the absolute motion of each side (i.e., relative to its pre-rupture position) is governed by their stiffness contrast. For a shallowly buried fault, the thin hanging wall is much less stiff than the footwall, resulting in much greater leftward motion of the former than the rightward motion of the latter (Figures 4d – 4f). Consequently, the part of the hanging wall overlying the updip segment of a shallowly buried rupture suffers greater shortening than for a more deeply buried rupture. If the rupture were extremely deeply buried, such as to a depth ten times the rupture width, the opposite displacements of the hanging wall and footwall would be similar in size.

The effect of the slip gradient does not require explanation and illustration. It is self-evident that a sharper tapering of the slip causes greater shortening and hence more uplift. An extreme example commonly seen in the literature is the uplift spike caused by a sudden updip termination of fault slip (infinite slip gradient), an artefact in numerous tsunami source models, especially those that use uniform-slip rectangular fault segments with their updip edges buried at small depths.

In these models, the amount of surface uplift caused by the horizontal shortening of the hanging wall depends on the slip gradient, the depth of the fault, and the Poisson's ratio.

The effect of fault depth is more complex. As discussed above, given slip distribution, there is greater shortening if the fault is shallower. However, surface uplift is an integrated effect of vertical strain over a depth range. If the fault is too shallow, despite the large shortening, the integrated effect of thickening over the small depth range it too small to cause large uplift (Figure 5.4d). Conversely, if the fault is too deep, although the effect of thickening is integrated over a greater depth range, the horizontal shortening is too small to cause much thickening (Figure 5.4f). Therefore, there is an optimal depth that maximizes surface uplift. Our systematic model tests show the optimal depth to be 0.5Wu (Figure 5.4c). The scaling between Wu and the optimal fault depth for elastic thickening is fundamental to tsunamigenic seafloor uplift. Although it cannot be directly applied to a curved dipping fault, the physics behind this scaling dictates that a rupture buried at moderate depths has a greater tsunamigenic potential than very deeply or very shallowly buried ruptures. In a theoretical study of tsunami energy, Ward (1980) found an optimal depth of 5 km for a hypothetical point source. Our optimal depth for a finite fault is only for elastic thickening, and the maximization of tsunami energy will require additional factors. Nonetheless, in addition to maximizing the amplitude of the uplift, our optimal depth also appears to result in surface deformation with a steeper land-facing slope (Figure 5.4b) which, as discussed in section 2.2., enhances tsunami runup.

The effect of the Poisson's ratio is minor. If we assume zero Poisson's ratio, the predicted uplift will only be slightly reduced (Figure 5.4c). Likewise (not displayed), if

we assume a Poisson's ratio 0.5 (incompressible), the uplift will only be slightly enhanced. However, the demonstrated small role of the Poisson's ratio helps to clarify the mechanics that governs the uplift. It shows that the elastic thickening here is not a simple matter of compressing an elastic object in one direction causing it to expand in the other direction. Instead, it is the result of complex deformation. In simple words, as the hanging wall moves updip and encounters resistance due to the decrease and termination of fault slip, materials elastically "pile up" mostly by shear deformation to cause the surface to bulge. As reflected by the displacement vectors near the fault in Figures 4d – 4f, the originally horizontal fault also endures some geometrical distortion in this process.

5.2.4.3. Tsunami runup due to trench-breaching and buried ruptures with the same peak slip

Having explained the mechanics of seafloor uplift due to trench-breaching and buried ruptures, here we use the same examples Ref1 and Ref2 to calculate tsunami runup. The results shown in Figure 5.5 serve two purposes. First, by comparison with 3-D results, they demonstrate the effectiveness of 2-D tsunami runup models in representing the primary physical process. Such a demonstration is important, because the exploration of the physical process in section 4 will be carried out using 2-D models. Second, they demonstrate that a rupture buried to a moderate depth generates greater tsunami runup than does a trench-breaching rupture with the same peak slip. Besides, this is a convenient occasion to show how the Kajiura transfer function (section 2.2) modifies seafloor uplift to yield sea surface uplift (Figure 5.5d).

In the two 3-D examples in Figure 5.5, fault slip in the dip direction is identical to the 2-D Ref1 and Ref2 models, but the along-strike rupture length is 300 km with slip smoothly terminating at the side edges. Figures 5a and 5b show their slip distribution and the resultant seafloor uplift in map view. Figure 5.5d shows that the seafloor uplift along the line of symmetry of the 3-D model (dashed) is very similar to what is predicted by the corresponding 2-D model (solid). Similarly, Figure 5.5c shows that the 3-D model tsunami runup within 50 km of the line of symmetry (dashed) is very

similar to what is predicted by the corresponding 2-D model (solid). By systematically comparing 2-D runup models with 3-D models of different along-strike lengths (results not displayed), we find that the 2-D runup results rather accurately approximate 3-D results derived along the line of symmetry if the rupture lengths in the 3-D models are longer than the trench-coast distance.

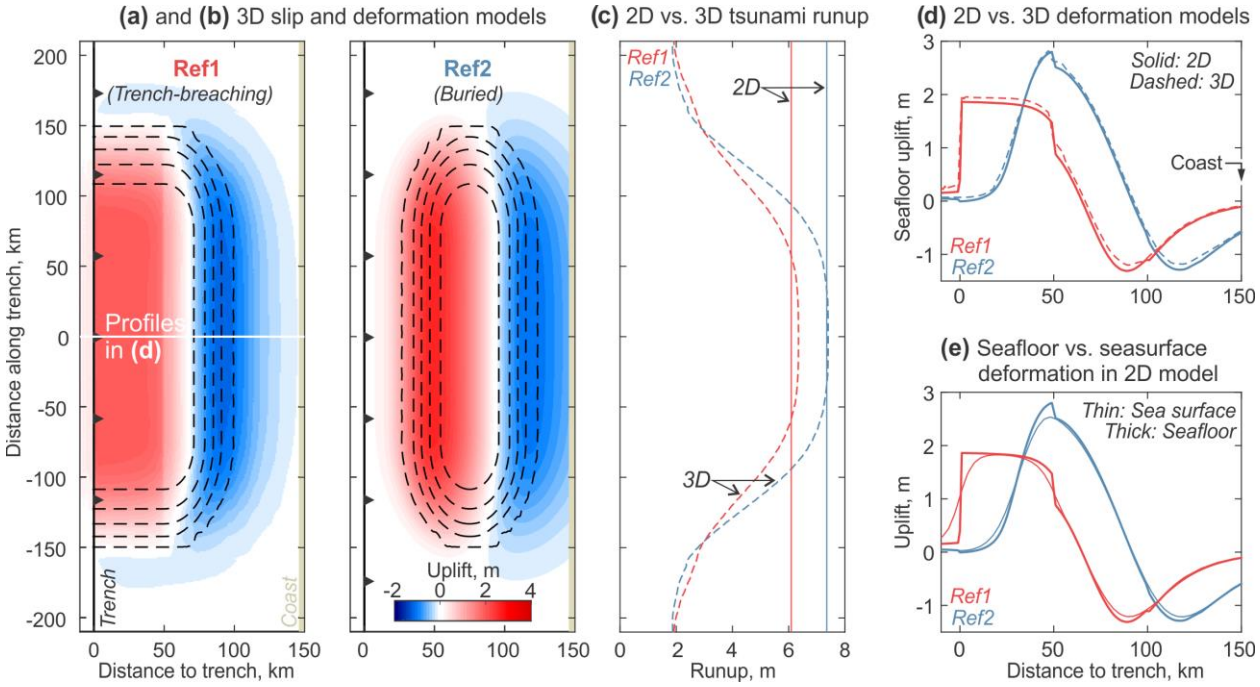

Figure 5.5. Tsunami source and corresponding runup for the two reference models and their 3-D variations. (a) Fault slip distribution (dashed contours at 2 m interval from 0 m to 8 m) for a 3-D variation of Ref1 and its consequent seafloor deformation. The 3-D model is modified from Ref1 by limiting rupture length along strike as shown. (b) Similar to (a) but for Ref2. (c) Comparison of tsunami runup between the two reference models and between each model and its 3-D variation. (d) Comparison of seafloor uplift between the two reference models and between each model and uplift along the line of symmetry of its 3-D variation. (e) Comparison between seafloor and sea-surface deformation for both reference models. The smoother sea-surface deformation here and in (a) and (b) is obtained by applying the Kajiura (1963) transfer function to the seafloor deformation (see section 2.2).

Of greater importance to the theme of the present study is the impact of the trade-off between the two deformation components discussed above on tsunami runups. Contrary to what one may intuitively expect without doing the modeling, the buried rupture Ref2 causes a larger runup than the trench-breaching rupture Ref1. In terms

of producing tsunamigenic seafloor uplift, the effect of the horizontal translation of the sloping seafloor in Ref1 fails to compete against the effect of the elastic thickening in Ref2. If the peak slip value in Ref1 did not sustain for 50 km but occurred only at the trench, it would produce even less runup. The peak slip in Ref2 occurs near the optimal depth 0.5Wu to maximize elastic thickening. It is worth reiterating (see section 2.2) that runup is controlled not only by peak seafloor uplift, but also by the seafloor geometry (thus water depth) along the tsunami propagation path which modifies the shape of the leading wave. Nonetheless, there is no doubt that the much larger seafloor bulge in Ref2 due to enhanced elastic thickening plays a dominant role in causing the larger runup, despite the shallower average water depth above the source and hence different propagation path compared to Ref1.

5.2.5. Factors that influence the relative importance of the two deformation components

In Section 3.3 (Figure 5.5), we showed that the trench-breaching model Ref1 is less tsunamigenic than the buried-rupture model Ref2. In this section we further investigate the competition of the two deformation components in a broader parameter space. The model tests summarized in Figures 6 and 7 show how geometrical factors may enhance or hinder tsunami runup caused by a trench-breaching rupture. Tests summarized in Figure 5.8 show how the downdip distribution of slip affects tsunami runup caused by a buried rupture. We again fix the peak slip at 10 m. We use the same width of the horizontal projection of the rupture for all the slip models in these tests to simplify parameter analyses, such that the buried ruptures shown in Figures 6–8 differ from Ref2 for being shallower. Therefore, unlike Ref2 (Figure 5.3a), the buried-rupture models in Figures 6–8 feature significant seaward translation of the sloping seafloor, although not as much as in trench-breaching models because of the diminishing fault slip toward the trench (Figure 5.6a). The models in Figures 6–8 illustrate how this effect is further strengthened or weakened at the cost or to the benefit, respectively, of elastic thickening.

5.2.5.1. Unimportance of increasing the degree of trench breaching given peak slip

For demonstrating the trade-off between the two deformation components, the most illuminating is the stunningly small effect of increasing the degree of trench breaching in affecting tsunami runup shown by the many models summarized in Figures 6 and 7. Because the rigid-body translation of the sloping seafloor causes large near-trench uplift below deep water (Figure 5.1a), one might expect that a greater degree of trench breaching such as 100% (red curves in Figures 6a, 6b, and 7a) would produce much larger runup. But quantitative modeling shows the effect to be very small. The results in Figures 6c and 7b show that the runup due to 100% trench slip is only slightly larger than 0% trench slip or in some situations even less.

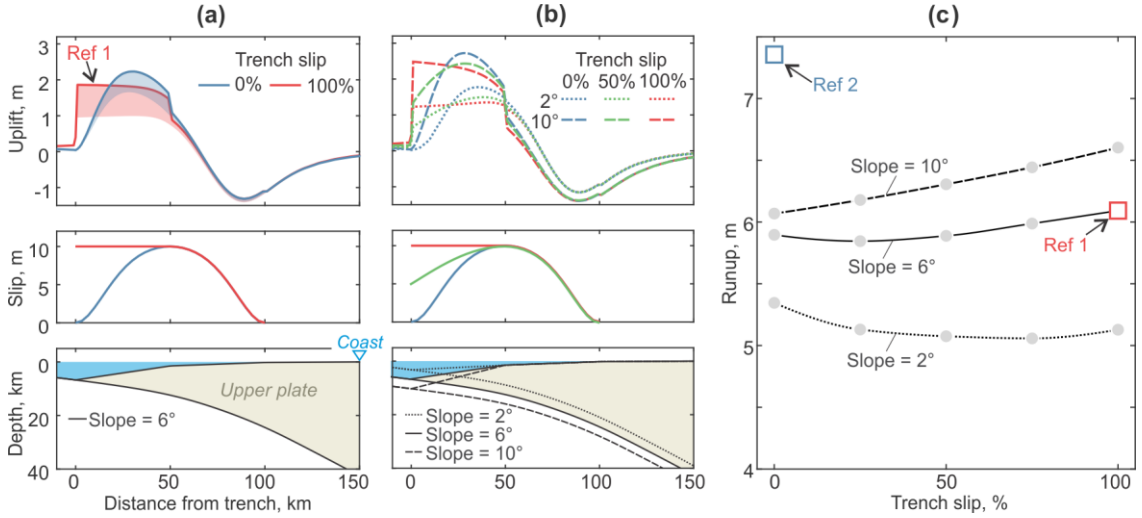

Figure 5.6. Test models to illustrate how tsunami runup due to trench-breaching rupture is affected by near-trench seafloor slope. (a) From bottom to top: model geometry, slip distribution, and seafloor uplift, coded by line color and style. Shaded areas in top panel show contributions to uplift from the horizontal motion of the sloping seafloor. (b) Similar to (a) but for a lower (2º) and higher (10º) near-trench seafloor slope. (c) Runup as a function of trench slip for the three different slopes shown in (a) and (b). Each circle represents a model test. The runup values produced by the two reference models are shown for comparison.

The mechanical reason for the unimportance of increasing the degree of trench breaching in these models is explained in section 3: an increase in the effect of rigid-body translation is always at the cost of elastic thickening. In Figure 5.6a, given seafloor slope, a larger trench slip leads to greater rigid-body translation and hence

greater uplift near the trench, but at the same time the smaller elastic thickening leads to reduced uplift farther landward. Consequently, tsunami runup stays at a similar level regardless of the degree of trench breaching (the slope = 6º curve in Figure 5.6c). The fact that most of the curves in Figures 6c and 7b have a concave upward shape indicates that there usually is some “optimal” amount of trench slip that produces runup smaller than either 0% or 100% trench slip.

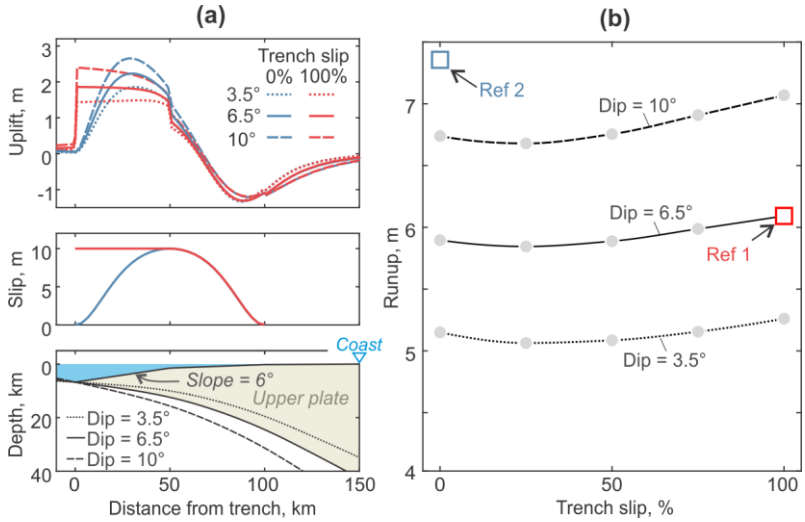

Figure 5.7. Test models to illustrate how tsunami runup due to trench-breaching rupture is affected by fault dip. (a) Similar to Figure 5.6b but for different values of fault dip averaged over the 0–50 km distance and for only the two end-member degrees of trench breaching (i.e., 0% and 100%). The value 6.5° has been used for all the models in Figures 3, 5, and 6. (b) Similar to Figure 5.6c but for the three fault dips shown in (a). The dip = 6.5° curve is identical to the slope = 6° curve in Figure 5.6c.

5.2.5.2. Effects of near-trench seafloor slope

Although the trade-off between the two deformation components tends to be balanced regardless of the degree of trench breaching, geometrical factors can slightly tip the balance. Steepening or flattening the near-trench seafloor slope will amplify or reduce, respectively, the contribution of the horizontal seafloor motion (Figure 5.6). This effect is most pronounced in trench-breaching ruptures with 100% trench slip which produce the largest horizontal motion of the sloping seafloor. As discussed above, even for 0% trench slip, there is still significant horizontal motion of

the sloping seafloor, although diminishing trenchward. Its contribution to seafloor uplift is larger if the seafloor slope is higher, as exemplified by runup values for the three models with 0% trench slip in Figure 5.6c. In this model setting, a greater seafloor slope also means a greater thickness of the upper plate, but the increase in the effect of elastic thickening on seafloor uplift is much less than that of the rigid-body translation. For example, for 100% trench slip, the effect of elastic thickening is negative (i.e., thinning) as shown in Figure 5.3c, which implies that in the high-slope examples in Figures 6b and 6c, the rigid-body translation effect overcompensates for the diminished elastic thickening effect to generate greater runup than in the lower-slope examples.

In the models shown in Figure 5.6b, a higher slope angle is accompanied with a greater water depth at the trench. Given the dominance of the trade-off effect between the two deformation components in this process (Figure 5.1), we do not deem it necessary to display results that separately illustrate the effect of seafloor slope and trench water depth in affecting tsunami runup due to trench-breaching slip.

5.2.5.3. Effects of fault dip

In Figure 5.7, we show models that are modified from those in Figure 5.6a by uniformly tilting the subducting plate around a pivot point at the trench which is fixed at a constant water depth. The models are named after the average fault dip over the 0–50 km distance (see bottom panel of Figure 5.7a). With other parameters fixed, an increase $\Delta\beta$ in fault dip β has two effects that both lead to greater tsunami runup, and both are explained by the deformation mechanisms described in section 3 and Figures 3 and 4. First, it increases the thickness of the upper plate and hence the effect of elastic thickening (see section 3.2 and Figure 5.4). Second, with a negligibly small decrease in the horizontal rigid-body translation, roughly by a factor of $(1-\Delta\beta\cdot\beta)\approx1$, it increases the upward rigid-body translation roughly by a factor of $(1+\Delta\beta/\beta)$ and hence leads to greater seafloor uplift. Our model results indicate that, due to the combination of these two effects, a greater fault dip results in similar increase in seafloor uplift in all rupture models (Figure 5.7a) and hence an upward shift of the runup vs. trench slip curve (Figure 5.7b).

5.2.5.4. Effects of slip distribution in buried ruptures

The results presented in Figures 6 and 7 show that, given peak slip, the degree of trench-breaching has little impact on the tsunamigenic potential of megathrust ruptures. In particular, none of these models produces tsunami runup as high as in Ref2. Here we investigate what slip distribution makes a fully buried rupture more tsunamigenic. For this, we vary the skewness parameter q of the bell-shape slip distribution function (Wang et al., 2013) from 0.1 to 0.9 without altering the width of the rupture. This results in ruptures with shallower to deeper concentration of slip (Figure 5.8). We run the same tests for all the three near-trench seafloor slope angles in Figure 5.6 (Figure 5.8a). We also compare these models with those with the Ref2 rupture depth (Figure 5.8b).

The models in Figures 8a and 8b with the shallow (i.e., not Ref2) rupture depth demonstrate the importance of the shape of seafloor deformation in tsunami generation discussed in section 2.2. In these models, slip skewness very weakly affects the contribution to uplift from the sloping seafloor (e.g., shaded areas in Figure 5.8a) but strongly affects how elastic thickening is accomplished. Recall that elastic thickening (or thinning) is controlled by the gradient and depth of the slip (section 3.2). For these shallow ruptures, slip skewness not only slightly affects the peak slip depth but greatly affects the slip gradient. In seaward skewed models (e.g. q= 0.3), elastic thickening due to the sharp updip slip gradient at a shallow depth causes large but narrow uplift near the trench, but elastic thinning due to the smoother downdip gradient at a greater depth causes small but broad subsidence closer to the coast. This combination results in seafloor deformation with a gentle land-facing slope between the peak uplift and peak subsidence. The landward skewed models (e.g. q= 0.7) are just the opposite. Their seafloor deformation features a broader seafloor bulge and a steeper land-facing slope – deformation characteristics that are well known to increase tsunami runup (Figure 5.8c) (Tadepalli and Synolakis 1994; Geist 1998; Satake et al. 2013). We have done the same tests for the three fault dips in Figure 5.7 (with the same seafloor slope angle 6º), and the results show the same effect of slip skewness on tsunami runup (Figure 5.8c). Therefore, for this model set

up, no matter what geologically reasonable seafloor slope and fault dip we assume, a landward skewed rupture always produces greater tsunami runup. For the 10 m peak slip assumed in these models, the runup difference between the two end member skewness values q= 0.1 and 0.9 is around 1.5 m for any of our geometrical combinations (Figure 5.8c). In comparison, the influence of the degree of trench breaching is much smaller. For example, even with a very high seafloor slope of 10º, increasing the trench slip from 0 to 100% of the peak slip of 10 m increases runup by only 0.5 m (Figure 5.6c).

Comparison with models of the Ref2 rupture depth (Figure 5.8b) demonstrates the role of rupture depth in controlling elastic thickening. In general, given slip skewness, a deeper rupture leads to a higher seafloor bulge and greater tsunami runup (Figure 5.8c). Exceptions occur if the slip is extremely landward skewed such as q= 0.9. In this situation, contribution from the limited horizontal motion of the sloping seafloor is still appreciable in the shallow-rupture model but almost absent in the model of Ref2 rupture depth. As a result, for q= 0.9, the “Ref2 depth” model produces even lower tsunami runup than the shallow-rupture model with the same seafloor slope (6º) and fault dip (6.5º) (black curve in Figure 5.8c) – a subtle display of the trade-off between the two deformation components discussed in section 3. The “Ref2 depth” models in Figure 5.8b also illustrate the competing roles played by the size and shape of the seafloor deformation in tsunami generation. Here the symmetric slip (Ref2) leads to the highest runup (Figure 5.8c). Compared to Ref2, the seaward skewed models produce larger peak seafloor uplift, but the gentler land-facing slope of the seafloor bulge reduces its tsunamigenic potential. On the other hand, the landward skewed models produce a steeper land-facing slope of the seafloor bulge, but the smaller peak uplift reduces its tsunamigenic potential. For the landward skewed models, the propagation path effect discussed in section 2.2 further reduces the tsunamigenic potential: the leading wave is less amplified because deformation occurs mostly under very shallow water or on land (Geist et al. 2006; Carvajal et al. 2017b).

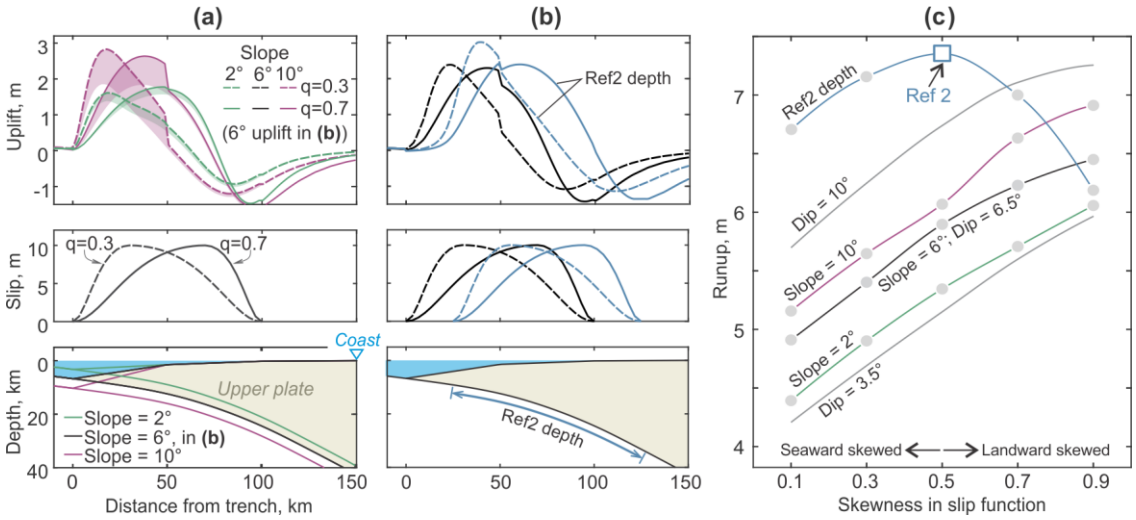

Figure 5.8. Test models to illustrate how tsunami runup due to buried rupture is affected by the skewness q of fault slip distribution. (a) Test models for different seafloor slope angles as in Figure 5.6. From bottom to top: model geometry, two slip distributions with $q = 0.3$ (dashed) and 0.7 (solid), and the resultant seafloor uplift with the shaded area indicating contribution from the horizontal motion of the sloping seafloor. (b) Models with the same seafloor slope (6º) but different rupture depths. One set of models (black) has the same shallow rupture depth as in (a), and the other set (blue) has the same rupture depth as Ref2 as shown in the bottom panel. (c) Runup as a function of slip skewness for the three seafloor slope angles in (a) and for the "Ref2 depth" models. Each circle represents a model test. The two gray lines with no circles show results for the 3.5º and 10º fault dips (see Figure 5.7). For each curve in this plot, if the seafloor slope or fault slip is not indicated, it means that the value is the same as for the black curve.

5.2.6. Discussion

5.2.6.1. Real-world complexities

To focus on the main objective of this work, our modeling studies assume that the upper and lower plates are homogeneously elastic in the deformation process, that slip occurs only along the megathrust, and that the trench is not filled by large amounts of sediment. Other complications in the real world certainly also affect tsunami runup. For example, near-trench seafloor uplift can be enhanced by inelastic deformation of wedge sediments (Tanioka and Seno, 2011; Ma and Nie, 2019) or by slip diverted to steeper faults off the megathrust such as splay faults or frontal thrusts (Wang and Tréhu, 2016; Gao et al., 2018; Felix et al., 2021).

Despite these real-world complexities, much of the main message we have learned regarding the effect of slip depth on tsunamigenic seafloor deformation is still valid. For example, let us consider a subduction zone with a 2- or 5-km-thick sediment layer burying the trench (Figure 5.9a). The 5-km case is similar to what has been reported in southern Sumatra (Gulick et al. 2011). In these scenarios, if a trench-breaching rupture does happen, slip will have to be diverted from the megathrust to one or multiple frontal thrusts. For simplicity, let us follow Gao et al. (2018) to assume that all the slip is diverted to a hypothetical single frontal thrust along the full strike length of the megathrust rupture so that it can be represented by a 2-D model (lower panel in Figure 5.9a). Slip along the steeply dipping frontal thrust results in a spike in near-trench uplift, of which the amplitude and width increase with trench slip and sediment thickness, respectively (Figure 5.9a). The higher and the wider this near-trench uplift spike is, the larger its contribution to runup. As a consequence, with 100% of the peak slip diverted to the frontal thrust, the model with a 5-km sediment layer produces higher tsunami runups than those with 0 or 2 km sediment and even exceeds that of the buried-rupture model Ref2 (Figure 5.9b). However, if less than 50% of the peak slip is diverted to the frontal thrust, the resultant runup is still less than in Ref2.

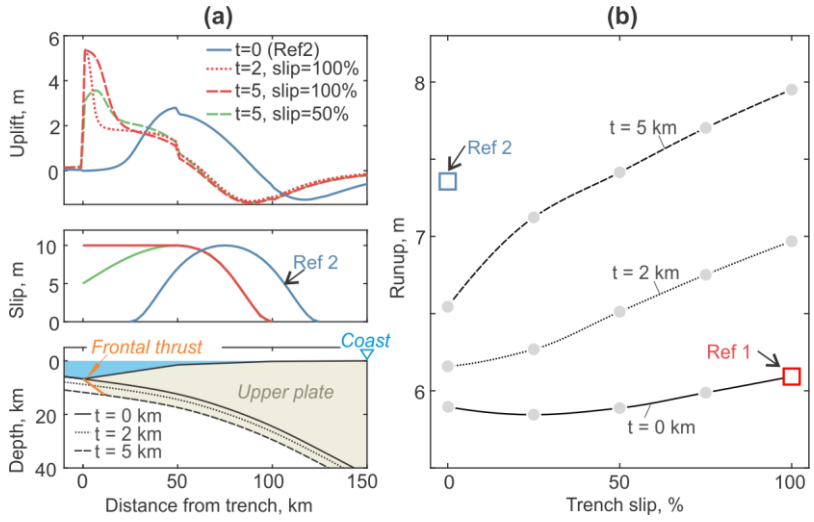

Figure 5.9. Test models to illustrate how trench-breaching rupture may occur to affect tsunami runup in the presence of thick sediment, in comparison with Ref2. (a) From bottom to top: model geometry, slip distribution, and seafloor uplift, coded by line color and style. In these models, the trench is assumed to be filled by a sediment layer of thickness t. Trench-breaching slip reaches the surface through a frontal thrust shown in orange in the lower panel. (b) Runup as a function of trench slip for the three different

t values in (b). Each circle represents a model test. The $t = 0$ curve is identical to the slope = 6° curve in Figure 5.6c and the dip = 6.5° curve in Figure 5.7b.

The potency of Ref2 in producing large runup owes to the broad bulge farther landward due to enhanced elastic thickening (Figures 3a and 5c). As can be deduced from the frontal thrust rupture examples (Figure 5.9), other rupture scenarios involving near-trench complexities (e.g., Ma and Nie, 2019) would mostly affect shorter-wavelength deformation near the trench (Felix et al., 2021) and therefore be unable to produce the large tsunamigenic bulge as in Ref2. Therefore, it still holds that moderately-buried ruptures such as Ref2 would usually be among the most effective in causing tsunami runups.

5.2.6.2. Re-examining the cause of the large tsunami in the Tohoku-oki earthquake

The results of our models motivate us to rethink about the role of the shallow depth and trench-breaching nature of the slip in the 2011 Mw=9 Tohoku-oki earthquake in generating the large tsunami runups along the adjacent coast. In this section, we compare runup predictions by slip distributions of different degrees of trench-breaching or different depths along the megathrust. Specifically, we evaluate whether the same slip not breaching the trench or buried to a greater depth would have produced smaller runups. It is well known that the largest runups in this event occurred north of 39°N, not in the region of main rupture (Figure S4) (Mori et al., 2011). The source for the largest runup in the north is still not fully understood (Kodaira et al., 2021), although some efforts have been made to explain it (e.g., Satake et al., 2013; Yamazaki et al., 2019; Du et al. 2021). We are not in a position to tackle this scientific mystery. To focus on the main theme of this paper, we pay attention only to the coastal area directly facing the main rupture zone, between 37.3 to 39°N (Figure 5.10e and Figure S4).

We take the average slip distribution of 44 slip models for this earthquake in the literature (Wang et al., 2018) as the “original” model (“Trench-breaching (original)” in Figure 5.10), and modify it to produce two hypothetical sets of slip models. In one set,

we modify the slip distribution seaward of the peak slip to let the slip breach the trench to different degrees, including 0% (“No trench-breaching” in Figure 5.10). In the other set, we systematically shift the original distribution downdip to greater depths to produce buried-rupture models with the same peak slip (e.g., “Moderately buried” in Figure 5.10). When doing the downdip shifting, we filled the originally non-existent part of the slip distribution seaward of the trench with slip values that smoothly taper to zero at or before reaching the trench (Figure S5). The slip distributions of all the 8 test models are shown in Figure S5 in map and cross-section views.

For the 3-D tsunami modeling, we use a computational domain that encompasses the Tohoku-oki rupture area, extending from 36.5°N to 40°N and 140.5°E to 144.7°E (Figure S4a). Because the experiment focuses on assessing the effect of the depth or trench-breaching nature of the slip on the overall tsunami size at the adjacent coast rather than assessing the details of the coastal hydrodynamics, it suffices to use the coarse bathymetry data from the GEBCO (2019) digital atlas which has a grid resolution of 15 arc-sec or ~500 m. We calculated tsunami propagation and runup using COMCOT with model parameters similar to those of the 2-D models described at the end of Section 2.2. Simulation time was 2 h, adequate for modeling runup along the adjacent coast associated with the leading wave. Despite the simplicity of the model setup and the low-resolution of the elevation data in the coastal region, our model predicted runup using the averaged slip model of Wang et al. (2018) compare reasonably well with both the values of and along-shore variations in the observed runups along the coast facing the main rupture zone (Figure 5.10c and S4b).

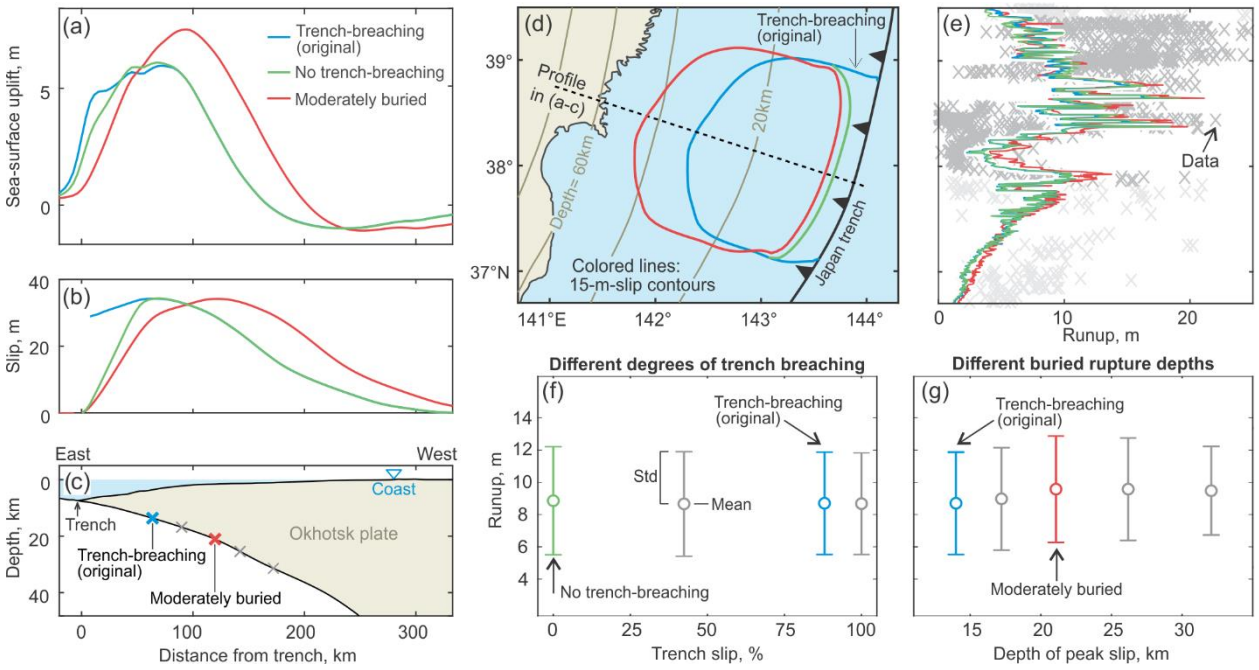

Figure 5.10. Numerical experiments to test the role of the depth and trench-breaching nature of the slip in the 2011 Tohoku-oki earthquake in generating tsunami runups along the coast facing the area of maximum fault slip. (a) Sea surface deformation along the profile shown in (d) predicted by 3 of the 8 slip models tested in these experiments. (b) Fault slip distributions for the 3 models in (a) along the same profile, coded by line color and style. The original "Trench-breaching" slip model is the average of 44 slip models in the literature (Wang et al., 2018). "No trench-breaching" is modified from the original model by forcing the slip to taper to zero at trench. "Moderately buried" is constructed by shifting the original model downdip while allowing the slip to taper to zero at trench. (c) Fault geometry along the same profile and tested depths of peak slip (crosses). (d) Map view of the three slip models in (b), represented by their (color coded) 15-m contours. (e) Tsunami runup predicted by the three (color coded) solid-line slip models in (d). The observed values (data) are from The 2011 Tohoku Earthquake Tsunami Joint Survey (TTJS) Group (2011) (http://www.coastal.jp/tsunami2011). (f) Runup predictions by models modified from the original model by forcing trench slip to be a fraction of the peak slip. (g) Runup predictions by models with the same value but different depths of peak slip. See (c) for peak slip depths.

The results in Figure 5.10f show that, for fixed peak slip, whether fault slip breaches the trench and by what degree have little impact on tsunami runup. If anything, the "No trench-breaching" model, which is similar to a severely seaward skewed rupture model in Figure 5.8, produces a slightly higher average runup than any of the trench-breaching models.

The results in Figure 5.10g indicate that, given the same peak slip, trench-breaching shallow slip does not lead to the largest average runup. Instead, higher tsunami runups would have been produced had the slip been buried to a greater depth. Models with peak slip occurring at moderate depths (20–25 km) such as the "Moderately buried" model predict the highest average runup owing to the enhanced effect of elastic thickening. These results further confirm what has been learned from our 2-D synthetic models discussed in sections 3 and 4.

The results in Figure 5.10 collectively show that whether or not the megathrust slip is very shallow or trench-breaching is not a major factor affecting tsunami runup. The Tohoku-oki earthquake generated a very large tsunami because its fault slip was very large, regardless of whether the slip was very shallow or breached the trench. Because of the above explained purpose of this modeling experiment, we have used the same peak slip for models of different rupture depths. Whether these hypothetical scenarios are geologically reasonable is a different matter that is not discussed here.

5.2.6.3. Implications for understanding tsunami earthquakes

Tsunami earthquakes produce larger tsunami runups than expected from their seismologically determined earthquake size (Kanamori 1972). Based on independent seismic and geodetic evidence, it is clear that tsunami earthquakes indeed feature very shallow, and possibly trench-breaching ruptures (e.g., Hill et al. 2012; Sallarès et al. 2021), but our 2-D models (Figs. 6-8) and Tohoku-oki experiment (Figure 5.10) make it clear that being shallow is not an adequate reason for the rupture to be anomalously tsunamigenic.

By inference, our results imply that the disproportionately large tsunamis in these events are more likely due to their fault slip being disproportionately large. Satake (1994), Sallarès and Ranero (2019), and many others have shown that failing to account for the very low rigidity of near-trench materials in the common practice of inferring fault slip from seismic records may greatly underestimate the magnitude of shallow slip. If the underestimated slip is enlarged by a factor of two or more to account for the low rigidity, it may be more compatible with the observed tsunami runup (e.g., Satake, 1994; Geist and Bilek 2001; Prada et al., 2021). However, the

cause for the very large slip is not fully understood because fault zone properties also play a vital role (see section 2.1.2). Besides, a self-consistent mechanism must also account for the long-term slip budget of the megathrust and the availability of elastic strain energy prior to the earthquake. There are also other attempts to explain the geology of tsunami earthquakes by resorting to unusual geometry and rupture style (e.g., Pelayo and Wiens 1992; Hill et al., 2012; Hananto et al. 2020). Explaining tsunami earthquakes is beyond the scope of this paper, but we think our results have clarified some important concepts and raised important questions for future studies of these events.

5.2.7. Conclusions

In this study, we investigate the mechanics of seafloor deformation in megathrust earthquakes and how it influences tsunami runup. To address the key question whether trench-breaching shallow rupture is more tsunamigenic than buried deeper rupture with the same maximum slip, we use a finite element model to simulate elastic crustal deformation and a shallow-water equation model to simulate the ensuing tsunami propagation and runup. Our main findings are summarized as follows.

1. In a megathrust earthquake, tsunamigenic deformation of the upper plate consists of two components: rigid-body translation and elastic thickening. Fundamental to tsunami generation is the trade-off between the two, that is, the enhancement of one component is often at the cost of the other. Deformation due to large slip at the trench is dominated by rigid-body translation, such that the horizontal motion of the sloping seafloor greatly enhances seafloor uplift near the trench, but it does not necessarily enhance tsunami runup, because seafloor uplift further landward due to elastic thickening is greatly reduced at the same time (Figures 5–8).

2. The importance of elastic thickening is commonly under-appreciated. For buried ruptures, the updip tapering of fault slip causes elastic shortening and hence bulging of the seafloor with size and shape dependent on the slip gradient and rupture depth (Figures 4). Given slip distribution, there is an “optimal rupture depth” that maximizes elastic thickening and hence the tsunamigenic potential of a buried rupture.

3. Given depth range of a buried rupture, its downdip slip distribution and the resultant variations in slip gradient greatly affect tsunami runup (Figure 5.8). For ruptures at a relatively shallow depth, greater seaward skewing of the slip distribution, that is, greater concentration of slip near the trench, results in a narrow seafloor bulge near the trench with a gentler land-facing slope which is less potent in causing tsunami runup. The accompanying enhancement of the seaward motion of the sloping seafloor is inadequate to offset this effect.

4. Our synthetic models covering a wide range of geometrical and slip parameters demonstrate that a rupture buried to an optimal depth produces larger seafloor uplift and tsunami runup than almost all the shallower and trench-breaching ruptures with the same peak slip (Ref2 in Figures 5-8). Exceptions occur only when very special rupture geometry is involved, such as a steep frontal thrust cutting through extremely thick trench sediment (Figure 5.9). Such exceptions are purely hypothetical, because no such special geometry in real subduction zones is expected to persist over a very long distance along strike as implied by 2-D models.

5. Geometrical factors generally do not strongly influence the relative tsunamigenic potential of trench-breaching vs. buried ruptures with the same peak slip, although a very steep near-trench seafloor makes the former a little more tsunamigenic by strengthening the rigid-body translation component (Figure 5.6). Greater fault dip strengthens elastic thickening and the vertical component of rigid-body translation to enhance seafloor uplift in both rupture types similarly.

6. The theoretical knowledge learned in this study enables us to reassess the reason for the large tsunami generated by the 2011 M=9 Tohoku-oki earthquake. We conclude that the tsunami was very large not because the rupture was very shallow and breached the trench but simply because the fault slip was very large. We have numerically demonstrated that, had the same large slip occurred 20 km deeper without breaching the trench, tsunami runup along the coast facing the area of maximum fault slip would have been similar or greater. The reason for the very large slip is an important research subject but is not addressed in this paper.

Chapter 6

Leveraging the past to reduce future tsunami surprises in Central Chile

This chapter consists of a manuscript still under preparation that shows how eyewitnesses' descriptions of a sequence of historical earthquakes in central Chile provide key constraints on past and future tsunami sources in Chile's most populated coast.

The manuscript information is provided in Section 6.1. and the manuscript itself is presented in Section 6.2.

6.1. Manuscript information

Title: Depth variation in megathrust rupture explains the tsunami gap in metropolitan Chile

The supplementary material is available in the Appendix B.

6.2. Manuscript: Depth variation in megathrust rupture explains the tsunami gap in metropolitan Chile

6.2.1. Abstract

"Seismic gaps" refer to those sections of the fault that are presumed to be locked and have not ruptured in a time period comparable with the recurrence intervals of past earthquakes, and can therefore rupture any time (McNally 1983). The underlying principle is the cyclic process of buildup and release of elastic strain energy in the rocks surrounding the fault (Savage 1983) and is typically assessed in the strike direction and ignored along dip. However, modern seismological records of subduction megathrust earthquakes have shown that rupture can occur at a variety of depths with depth-dependent seismic and tsunami hazards (Lay et al. 2012), but there is little information on whether great earthquakes (magnitude (M) > 8) can involve different depths of the megathrust in a given subduction zone segment due to the lack of downdip resolution in past earthquake ruptures. Here, we present

unambiguous historical evidence for successive rupture variations in the dip direction in the central Chile megathrust. By combining newly found first-hand accounts of coastal uplift and tsunamis with coupled deformation-tsunami models, we show that the distinct depth variations in four great earthquake ruptures of the past three centuries explain the gap of large tsunamis in the country's most populated coast since AD 1730 and imply that it could be filled with a large tsunami any time. We conclude that identifying seismic gaps in a one-dimensional fault in the strike direction may overlook hazardous tsunami gaps if faults also exhibit downdip variations of slip recurrence and size.

6.2.2. Main text

Along the Chile subduction zone, the Nazca plate subducts beneath South America at a rate of 6-7 meters per century (Angermann et al., 1999). Since the beginning of written history in 1541, central Chile (~30-37°S) has been affected by many great megathrust earthquakes and their tsunamis, with the two most recent ones being the 2010 M=8.8 Maule earthquake (Vigny et al., 2011) in the south and the 2015 M=8.3 Illapel earthquake (Tilmann et al., 2016) in the north (Figure 6.1b). The area between these two ruptures, known as metropolitan Chile because it hosts most of the country's population (Figure 6.1a), has been affected by great (M8+) earthquakes every ~85 years: in 1730 (M>9), 1822 (M8-8.5), 1906 (M8-8.5), and 1985 (M8) (Figure 6.1c), plus by a number of smaller (M7-8) events (e.g., 1575, 1580, 1971) (Lomnitz, 1970; Nishenko, 1985; Comte et al., 1986; Udías et al., 2012; Cisternas et al, 2012). Despite the high recurrence of great earthquakes, the coast of metropolitan Chile has been affected by a large tsunami only once in its history, in 1730, with flooding being reported as far as Japan (Tsuji 2013). Here, by combining historical evidence with numerical modeling, we explain this gap of large tsunamis by deep ruptures in the three post-1730 earthquakes of 1822, 1906 and 1985.

The source of the 1730 earthquake was previously studied by Carvajal et al. (2017), comparing modeled versus observed tsunami inundation in both the near- and far-field. Details of the 1730 earthquake source and effects are summarized in Figure 6.1c and Table S1.

We studied the 1822 and 1906 earthquakes by expanding previously published compilations of their effects (Montessus de Ballore, 1912; Lomnitz, 1970) through first-hand accounts from newly found original documents. We searched over a hundred sources including contemporaneous newspapers, magazines, and telegraphs. The search focused on evidence of coseismic land-level changes and tsunamis. The results, involving 19 and 13 new first-hand descriptions for the 1822 and 1906 earthquakes, respectively, are shown in Table S1. Documentary search was not extended to the 1985 earthquake, because it was recorded by modern instruments and its source was previously studied by inverting land-level changes derived from pre and post topographic surveys (Barrientos 1988). We expand this data with additional geodetic observations and jointly invert them with nearby tsunami waveforms from the original 1985 tide gauge records.

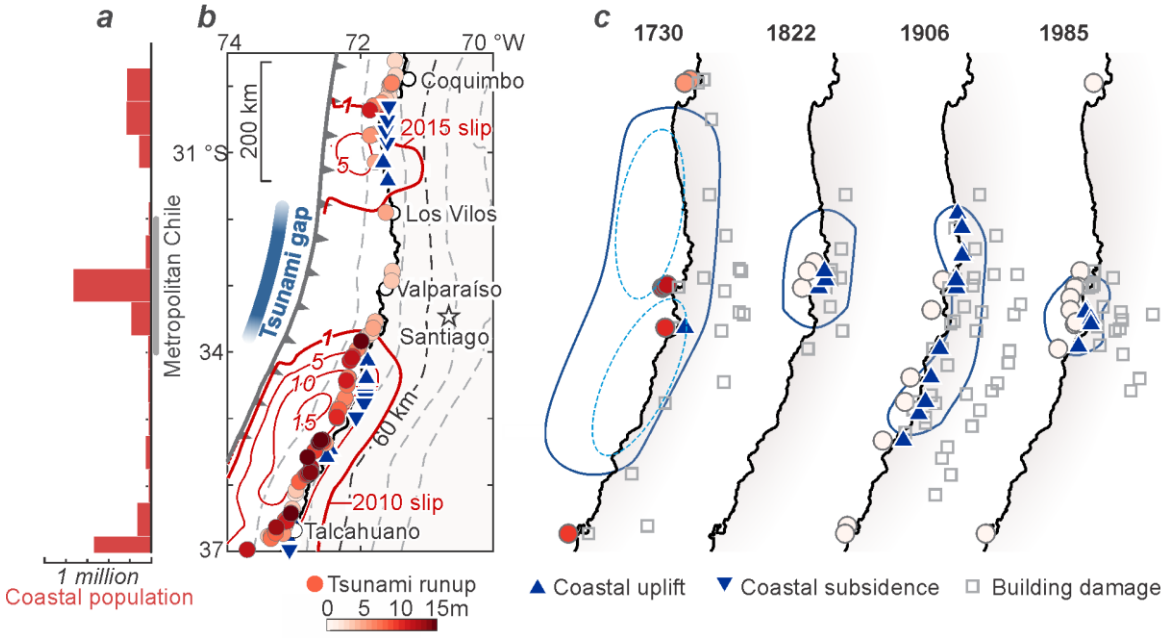

Figure 6.1. Tsunami gap area and earthquake and tsunami observations. (a) Population living in coastal areas (estimated from official 2017 census data of coastal cities). (b) The 2010 and 2015 fault slip (contours in m) (Moreno et al., 2012; Tilmann et al., 2016), observed coastal deformation (Farías et al., 2010; Zhang et al., 2016), and tsunami runup (Fritz et al., 2011; Aránguiz et al., 2016). (c) Approximated coastal deformation, tsunami runup and building damage due to historical megathrust earthquakes. Blue lines outline inferred rupture areas (see Figure S1 for slip distributions). Dashed ellipses within the 1730 rupture area indicate high-slip areas (Carvajal et al., 2017).

In contrast to the large, widely recognized 1730 tsunami (Carvajal et al. 2017), those triggered by the three post-1730 earthquakes were quite small. Eyewitnesses in 1822 and 1906, who initially had feared for the flooding of the city's lower parts when the earthquakes occurred, eventually saw only benign sea-level increase followed by a notorious sea withdraw that left the boats dry (Table S1). The 1985 event occurred in the instrumental era, and tide gauge records indicate tsunami amplitudes less than 1 m, about half of those produced at the same site by the more distant 2010 and 2015 earthquakes. In the many documents we reviewed (Table S1), we did not find a single report of tsunami damage associated with these three earthquakes.

Despite the small tsunamis, the three post-1730 earthquakes caused conspicuous coastal uplift. Seaward advance of the coastline and/or sudden exposure of previously submerged rocks were widely reported along the source areas of these events (Figure 6.1c) (Table S1). For example, by observing emerged rocks after the 1822 earthquake, British diarist and writer Mrs. Maria Graham reported in the Transactions of the Geological Society of London that *"the whole line of coast, from north to south, to the distance of one hundred miles, had been raised above its former level […]* by "*about 3* […] *or 4 feet*" (Graham, 1824) (Table S1). Her reports, first disputed by contemporaneous geologists until later confirmed by Charles Darwin and others, are the first published observation of crustal deformation caused by a subduction earthquake. Historical evidence indicates that the coastal uplift in 1906 was similarly large but observed over a greater distance along the coast (Figure 6.1c). Many of the eyewitness accounts in 1906 include specific uplift values, which indicate average uplift up to ~100 cm along various parts of the coast (Figure 6.3b) (Table S1). The coastal uplift in 1985 was inferred from dead intertidal organisms to be only 44-59 cm (Castilla, 1988) which was later confirmed by leveling data surveyed from the coast to 100 km inland (I.G.M., 1986).

The historical records summarized in Table S1 and highlighted above suggest that the 1822, 1906, and 1985 events differ from the 1730, 2010, and 2015 events for having their ruptures confined to the deeper part of the megathrust. For the instrumentally recorded 1985 event, this is quantitatively shown by direct inversion of

geodetic observations (Barrientos 1988) and confirmed by tide gauge records (not shown). To confirm and quantify the deep ruptures in the 1822 and 1906 events, we use the historical records of Table S1 in tandem with numerical models of surface deformation and tsunami propagation. The results confirming a deep rupture in the 1906 earthquake are summarized in Figure 6.2, which also illustrates the procedure. The 1822 results are similar but are not shown here.

The models shown in Figure 6.2 cover a wide range of assumed depths of the updip limit of the rupture but a fixed downdip limit of 60 km. Placing the downdip limit at depths greater than 40 km leads to similar conclusions but shallower than this cannot explain the coastal uplift observations (not shown). For deformation modeling, we assign a smooth slip distribution to the 3-D curved megathrust using the method of Wang et al. (2013), with an example shown in map view in Figure 6.2a. The depth of the rupture is represented by the average depth of the two identical peak slip values in the slip distribution north and south of the rupture. Ruptures with slip uniformly distributed in the strike direction cannot explain the uplift variations along the coast but leads to the same conclusion of a deep rupture (not shown). Because coastal uplift scales linearly with slip, for each rupture depth (defined with the updip limit) we search for the peak slip value that minimizes the Root Mean Square Error (RMSE) of model fit to coastal uplift reports (Figure 6.2d). Then we use this best fit slip to calculate coastal tsunamis heights and compare them with observations (Figure 6.2e).

Three rupture examples are shown in Figure 6.2a, and their predicted coastal uplift and tsunami heights are shown in Figures 6.2b and 6.2c, respectively, in comparison with witness reports. The coastal uplift reports are best explained by the preferred model, with a peak slip of 4.5 m at 38 km depths (Figures 6.2b and 6.2d). Although other models can explain the data reasonably well (not shown), the most important conclusion is that if the main slip zone is shallower than 30 km, the models very poorly fit both the uplift and tsunami observations (Figures 6.2d and 6.2e). Therefore, the 1906 rupture must have been restricted mostly to the deep part of the megathrust with limited slip extending offshore and with little if any slip shallower than 20 km

depths. The same is true for the 1822 earthquake with a peak slip of 6.5 m at 35 km depths (not shown), and for the 1985 earthquake with a peak slip of 3 m at 35 km depths (not shown). These characteristics sharply contrast those of the great 1730 earthquake rupture, whose tsunami effects in the near- and far-field are consistent with up to 20-30 m of slip peaking at depths shallower than 20 km (Carvajal et al. 2017; Figure 6.1c). Therefore, even in the same segment of a subduction zone, different great earthquakes can involve markedly different slip sizes at markedly different megathrust depths.

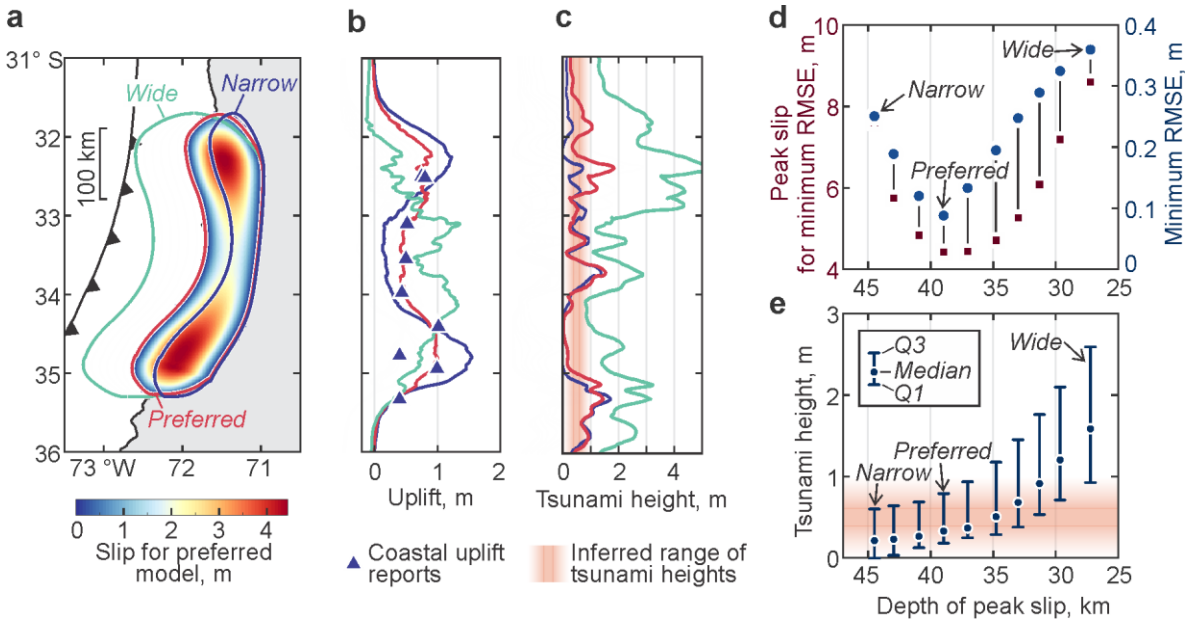

Figure 6.2. Results of model tests to show that the 1906 rupture must have been confined to a deep depth. (a) Three test models with different updip rupture limits including the preferred model. (b) Coastal uplift predicted with the three models in (a) (color coded) in comparison with historical reports. (c) Tsunami runup heights predicted with the three models in (a) (color coded) in comparison with actual heights in 1906 inferred from eye-witness reports shown in Table S1. (d) Results of systematic search for the depth of peak slip (northern and southern peaks are at similar depths). Peak slip (red square) assigned to each rupture geometry in order to minimize the Root Mean Square Error (RMSE) between model-predicted and observed coastal uplift (blue circle). Results in (b) and (c) are based on these peak slip values. (e) Model-predicted tsunami heights along the coast compared with the inferred range of the reported 1906 tsunami heights. Note that a peak slip shallower than 30 km very poorly fits the uplift and tsunami observations.

Downdip variation of slip in successive earthquakes reconciles the incompatible recurrence intervals between the historical great earthquakes and the large prehistoric tsunamis geologically inferred. If the historical sequence of great metropolitan Chile earthquakes is somewhat representative of the recent prehistory, then deep ruptures with moderate slip amounts interspersed by less frequent shallow rupture with higher slip amounts can explain why large prehistoric tsunamis in the region occurred only every 2 to 6 centuries (Dura et al. 2015) and not every century as the historical great earthquakes did. As for the historic 1730 tsunami, it is likely that the sources of such prehistoric tsunami inundation events were also large offshore slips that previous deep ruptures left unspent.

This fault behavior seems similar to those inferred at other subduction zones that have recently hosted highly tsunamigenic earthquakes as a result of large shallow slip. Well-studied examples include the Miyagi-oki megathrust section of the Japan Trench and the Mentawai section of the Sunda Trench, where the fault portions downdip of the most tsunamigenic earthquakes known in each region were repeatedly ruptured over the preceding centuries (Philibosian and Meltzner 2020). However, the post-1730 earthquakes of metropolitan Chile are different in that they ruptured much deeper than the deep Mentawai earthquakes and were much larger in magnitude and ruptured fault area than the deep Miyagi-oki earthquakes. Aside from these key differences, these three examples suggest much longer buildup times of shallow versus deeper slip deficit.

The unambiguous historical evidence for depth variation of megathrust rupture in successive great metropolitan Chile earthquakes adds a note of caution to the seismic gap concept, especially when it is used to assess the near-future tsunamigenic potential. The filling of a seismic gap in the strike direction by recent earthquakes does not necessarily mean the filling of a tsunami gap in a fault that also exhibits downdip variation of slip recurrence and size. Where tsunami size varies markedly among successive earthquakes on the same strike section of a fault, much of the shallow fault slip during the most tsunamigenic earthquakes may have thus accumulated over earlier earthquake cycles of deeper ruptures. Understanding the

reason for the different recurrence intervals of shallow versus deeper megathrust slip is key for improving our knowledge on plate boundary dynamics and assessing tsunami hazards and is thus an important direction of future research.

Given that the time elapsed since the last large tsunami in 1730 already surpassed the minimum recurrence interval among individual prehistoric tsunamis (Dura et al. 2015; Carvajal et al. 2017), the recognition of the depth variations in megathrust rupture has grim societal implications for the most populated coast of Chile. Cumulative slip of all the three post-1730 event fills only the deeper part of the fault between the 2010 and 2015 earthquake ruptures (Figure 6.3a). There is a possibility that the slip deficit in the shallow part of the megathrust has been aseismically consumed such as by afterslip of the three post-1730 events or ongoing megathrust creep. However, because it ruptured in 1730, and most likely every 2 or 6 centuries in the prehistoric past (Dura et al. 2015), we consider it much more likely that it is currently locked and will rupture again. Although its locking state cannot yet be reliably constrained for lack of seafloor geodetic observations (Moreno et al., 2010), the low level of modern (2014-2018) background microseismicity in this shallow region (Figure 6.3b) is consistent with locking (Sippl et al., 2021). Regional tsunami modeling warns that even partial ruptures of this unfilled part of the shallow fault can generate a tsunami in metropolitan Chile comparable to the one in 1730 and much larger than in 2010 and 2015 (Figure 6.3c). Given the increased population and infrastructure of this area today, the consequence of a large tsunami would be much worse than in 1730.

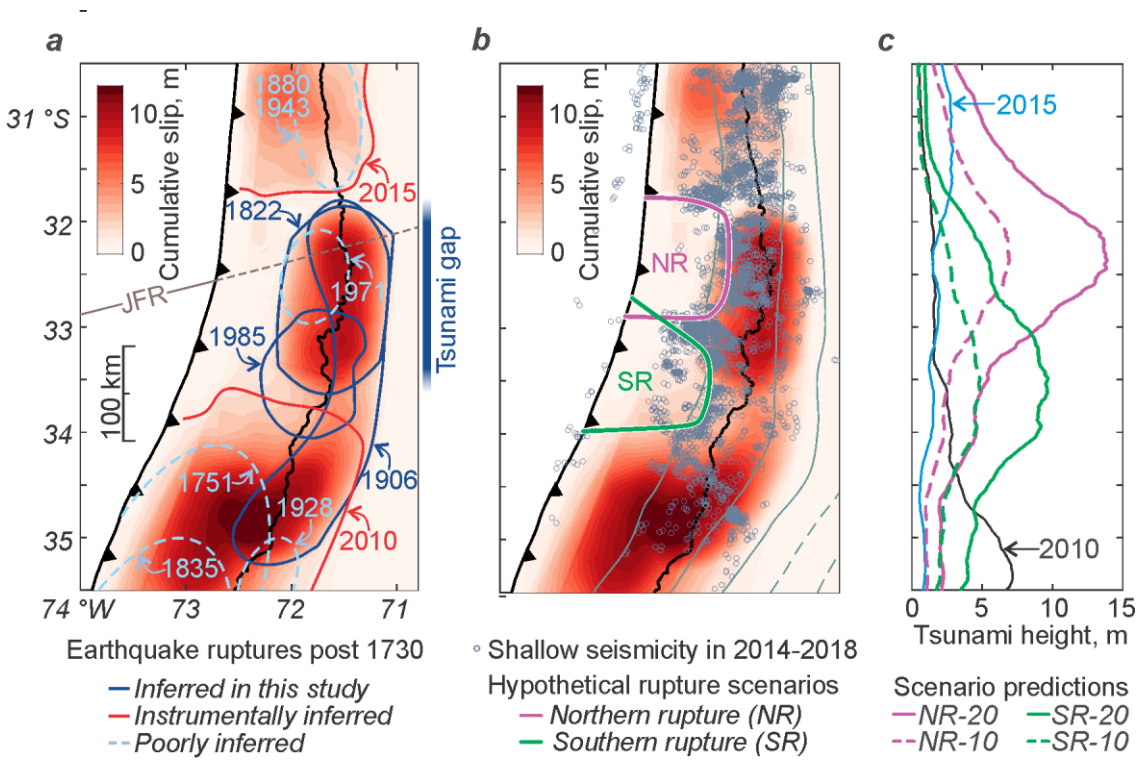

Figure 6.3. Mature fault patch and potential future rupture and tsunami scenarios. (a) Cumulative coseismic slip since 1730, estimated by the sum of the 1822, 1906, 1985, 2010 (average of 19 published models) and 2015 (average of 8 published models) slip distributions. Dashed ellipses indicate poorly constrained rupture areas which are not included in the cumulative slip estimation. (b) Shallow seismicity (mostly interpolate; Sippl et al. 2021) and two possible trench-breaching rupture scenarios filling the north (NR) and south (SR) half portions of the unruptured shallow fault patch. (c) Maximum tsunami heights along the coast predicted by the two hypothetical rupture scenarios shown in (b) assuming 10 or 20 m of peak slip at the trench compared to those in 2010 (based on Moreno et al., 2012) and 2015 (based on Tilmann et. al., 2016).

Chapter 7

Discussion and final remarks

This chapter discusses four interrelated points. In section 7.1, we show how the tsunami events studied here, individually, and all together, provide strong support for this thesis' hypothesis that the actual generation mechanisms of tsunamis are much more complex and diverse than those usually assumed in mitigation strategies. In section 7.2, we show how combining knowledge from different subduction zones helps to improve our scientific knowledge about poorly understood tsunami sources and provide fundamental insights into Earth Science. In section 7.3, we show why assessing hazards with reasonable accuracy is difficult and that model sophistication does not necessarily help too much when the purpose is saving lives. In section 7.4 we offer some final thoughts and lessons derived from the study of past events.

7.1 Complexities and diversity of actual tsunami sources

The cases of Palu (Chapter 2), Tonga (Chapter 3) and Rapa Nui (Chapter 4) expose our limited understanding of the tsunamigenic potential and complexities of non-traditional sources, and this is why we have been often taken by surprise. In the case of Palu, the tsunami warning issued by the Indonesian early warning system largely underestimated the tsunami heights in the bay of Palu mainly because the procedure only considered earthquakes as tsunami sources. However, our work using social media videos (see Chapter 2) concluded that although there was a contribution from the earthquake faulting beneath the bay, the 2018 Palu tsunamis were mainly caused by coastal and submarine landslides triggered by the shaking. Similarly, the tsunami warnings issued by different tsunami agencies of the Pacific Ocean after the 2022 Tonga eruption were untimely and inaccurate (Somerville et al. 2022). The reason, as revealed by hundreds of tide gauge records across the world (see Chapter 3), was that the main source of the tsunami was a moving atmospheric pressure wave originated in the volcanic blast that circled the earth multiple times at nearly the speed of sound, a tsunamigenic source that, although was reported in the literature (Press and Harkrider 1966), was not well known, and hence not considered by tsunami

agencies responsible for alerting the public. Finally, although the Chilean coastal warning system forecasted the large wind waves that affected Rapa Nui in 2020, the massive overtopping observed in social media videos could not be directly deduced from the warning system alerts alone. As concluded by our analysis of multiple datasets (see Chapter 4), coastal inundation at the island is largely controlled by other processes that make the sea level higher and hence the wind waves more hazardous. Among them, meteotsunamis, previously unrecognized at the island, play a major role in augmenting the sea level especially during specific wind conditions. The failure of warning systems in accurately forecasting the height of tsunamis in these events expose our incomplete understanding of non-traditional sources in generating tsunamis in different geologic settings. Alternatively, it may instead or also expose the insufficient transfer of scientific knowledge into mitigation strategies. From a different viewpoint, these examples also demonstrate the key role of the diverse type of evidence in identifying non-traditional tsunami source mechanisms.

Our results in Chapter 5 show that our lack of knowledge of tsunami generation from non-traditional sources extends also to traditional sources. The possibility of large tsunamigenic slip extending all the way to the trench recognized after the Tohoku-oki earthquake led to considerable efforts in the scientific community, including efforts to assess future near-trench tsunamigenic slip potential at subduction zones (Hirono et al. 2016), incorporate shallow slip detection methods in tsunami early warning systems (Lay et al. 2019), and reevaluate tsunami hazard by allowing rupture scenarios with near-trench slip (Lindsey et al. 2021). The underlying premise encouraging such efforts is that shallow slip is more tsunamigenic than deeper slip of the same size. However, our theoretical work in Chapter 5 questioned the premise by demonstrating that, for a fixed amount of slip placed fully offshore, tsunami generation is instead maximized when the rupture is buried to moderate depths, and that the 2011 tsunami was large mainly because the fault slip was large not because the slip was shallow. This conclusion indicates that our knowledge about tsunami generation from traditional tsunami sources is also incomplete.

7.2. Historical evidence provides fundamental insights into Earth science

As show in Chapter 5, the amount of offshore slip is more important to the production of a tsunami, than the depth of slip. This finding raises key scientific questions that have a direct impact on mitigation strategy. For example: Why was the amount of slip (~50 m) in the Tohoku-oki earthquake so large? The documentary evidence of a sequence of historical earthquakes in the Chile subduction zone on the other side of the Pacific, analyzed in Chapter 6, seems to provide possible insight into this issue. Using eyewitness reports of the effects of historical earthquakes and tsunamis in central Chile, we argued that the megathrust is segmented in the dip direction, enabling both infrequent shallow rupture with large offshore slip amounts and more frequent deeper rupture with smaller slip amounts beneath land. In agreement with the hypothesis of Satake and Fujii (2014), the megathrust rupture behavior in central Chile offers a promising mechanism for the large slip in the Tohoku-oki earthquake: Fault segmentation in the dip direction and hence downdip variations of both the recurrence intervals and size of seismogenic slip. So, much of the shallow fault slip in the 2011 northeast Japan and 1730 central Chile earthquakes may have thus accumulated over earlier earthquake cycles of deeper ruptures. Future research aimed at understanding the reason for the different recurrence intervals of shallow versus deeper megathrust slip will provide key insights for anticipating future tsunami sources in other subduction zones, designing better mitigation strategies and improving our knowledge on plate boundary dynamics.

7.3. The pitfalls of sophisticated modeling approaches for hazard assessments

The complexities and diversity of actual tsunami sources demonstrated in Chapters 2-6 add a note of caution when implementing sophisticated tsunami hazard assessments into evacuation planning, in the sense that we must be conscious of their limitations.

The increasing capacity of computer modeling in recent years has allowed assessing hazards with more spatiotemporal precision and resolution (Gibbons et al. 2020); sophisticated numerical models have therefore become popular for this purpose around the world (e.g., Sepúlveda et al. 2019; Zamora et al. 2021). However, as

demonstrated by the 21st century tsunami surprises studied here, the increasing capacity of computer modeling has not necessarily benefited the accuracy of hazard assessments because the accuracy is usually more dependent on the tsunami source assumptions than in the model sophistication. In this regard, the undeniable benefits of sophisticated numerical models should be handled with caution, especially when they are used for evacuation planning.

Probabilistic Tsunami Hazard Analysis (PTHA) is a clear example of sophisticated approaches used for hazard assessments. PTHA have become quite popular due to its advantage of estimating the likelihood that a tsunami at a particular location will exceed a given level within a certain period of time (Gibbons et al. 2020). This type of approach is of course encouraging and useful for engineering and urban purposes; however, it has a major limitation when used for evacuation planning: the estimated likelihood strongly depends on the preconceptions of the developer about the tsunami sources, which some times may ignore the natural complexities and diversity that actual tsunami sources have as revealed in this thesis. Let us use the case of the 2018 Palu tsunami discussed in Chapter 2 as an illustrative example. Four years before this event, Horspool et al. (2014) published the first national probabilistic tsunami hazard assessment for Indonesia providing forecasts of long-term tsunami hazard along most of the country's coastline. The hazard was calculated using thousands of tsunami sources and included epistemic and aleatory uncertainties based on logic trees and sampling probability density functions. The resulting hazard estimations were described in a set of maps showing the tsunami height at the coast for a range of return periods as well as the annual probability of exceeding prescribed threshold tsunami heights. For the bay of Palu, the results indicate that, on average, tsunami amplitudes are expected to exceed 2 m every 100 years, 4 m every 500 years, and 7 m every 2500 years. However, all these forecasts proved inaccurate in September 2018, when the coast of Palu bay was inundated by tsunami waves of >8 m above mean sea level (see Chapter 2), which together with other earthquake-related effects took >4,000 lives. According to Prasetya et al. (2001), the bay of Palu was also affected by large tsunamis in 1927 and 1968. The reason for the discrepancy between the PTHA of Horspool et al. (2014) and what actually happened

on 2018, and likely in 1927 and 1968, is obvious for most tsunami scientists and PTHA developers: the PTHA did not consider submarine landslides as tsunami sources. Although Horspool et al. explicitly acknowledged this limitation in their paper, the sophistication of the PTHA model and preciseness of the results may have misled potential users responsible for its implementation into the real world. Emphasizing the limitations of sophisticated approaches, such as PTHA, and properly communicating them to the public and authorities is essential for reducing future tsunami surprises.

7.4. Lessons from the past to reduce tsunami surprises in the future

The complexities of actual tsunami sources and our incomplete knowledge about them does not currently allow us to prevent future tsunami surprises from happening, or at least not within the near future. As systematically shown through history, and by the tsunami events studies here, nature always manages to find a way to surprise us (i.e., scientists, mitigation strategies, or both). However, the tsunami events studied here do provide some useful insights that can help reduce future surprises.

First, it is important that we admit that there are things about the source of tsunamis that we just don't know and can thus not be anticipated at this stage. Admitting this and properly communicating it to the public and authorities is important to reduce future surprises and hence save lives.

Second, the results of this thesis highlight the importance of using the past to reduce tsunami surprises in different geologic settings. The "past" here not only includes the local past but also the experience of other regions, especially if they have similar geologic and geomorphologic settings than our area of interest. This is especially important given the short observation period and long recurrence of tsunami events in a given area. For example, the tsunamigenic atmospheric pressure waves originated in the Tonga eruption were also reported for the 1883 volcanic eruption of the Krakatoa volcano in Indonesia (Press and Harkrider 1966). So, with the wisdom of hindsight, the worldwide reach and early-than-expected arrival of the Tonga tsunami need not have been a surprise to tsunami warning systems. Also in hindsight, the tsunamigenic delta failures triggered by the strong Palu earthquake shaking need not had been a surprise either. It is well known that deltas are very sensitive to failure by

seismic shaking (e.g., Hilbe and Anselmetti 2014), and that landslide failures within these deltas have the potential to generate tsunamis, such as occurred in the magnitude 7 Haiti strike slip earthquake (Hornbach et al., 2010). A timely identification and communication of the tsunami hazard posed by the noticeable presence of the multiple river deltas along the coast of Palu bay would have helped reduce the surprise factor of the deadly Palu tsunamis. The warning that a large tsunami could affect the metropolitan coast of Chile in the near future is essentially motivated by knowledge gained from other subduction zones (Chapter 6). Actually, it is only when the documentary evidence of central Chile earthquakes is viewed in a global context of recent highly tsunamigenic earthquakes as a result of large shallow offshore slip that the warning becomes more credible. Of course, the warning could be a false positive, but if not, we hope it can influence mitigation strategies so that the future rupture of the shallow megathrust off metropolitan Chile does not catch us by surprise.

The unanticipated complexities of actual tsunami sources make the task of assessing future hazards extremely delicate, especially for evacuation planning in which human lives are involved. No recipe has proven completely successful, and this thesis does not offer a perfect one either. However, the Palu experience provides some hope to compensate for this shortcoming. As clearly shown by multiple social media videos, the Palu tsunamis inundated widely separated coastal areas within a few minutes after the earthquake. However, some of the videos clearly showed how appropriate human behavior and appropriate evacuation routes were key to save lives and highlighted the effectiveness of vertical evacuation especially in situations when there was nothing else to do. Suitable and well publicized evacuation routes (both horizontal and vertical) and a community that is informed by science, and aware of its limitations and uncertainties, can be “prepared for the unexpected” (in Kanamori’s (1995) words). Together these strategies to facilitate and promote self-evacuation can reduce loss of life when existing hazard maps fail. This is the best way to compensate for the inevitably large uncertainties of future tsunamis hazards due to our poor knowledge of natural tsunami sources.

References

Adam, D. (2022). Tonga volcano eruption created puzzling ripples in Earth's atmosphere. Nature.

Allen, T., & Hayes, G. (2017). Alternative rupture-scaling relationships for subduction interface and other offshore environments. *Bulletin of the Seismological Society of America*, *107*(3), 1240–1253.

Angermann, D., Klotz, J., & Reigber, C. (1999). Space-geodetic estimation of the Nazca-South America Euler vector. *Earth and Planetary Science Letters*, *171*(3), 329-334.

Aránguiz, R., González, G., Cienfuegos, R., Yagi, Y., Okuwaki, R., Urra, L., ... & Rojas, C. (2017). The 16 September 2015 Chile tsunami from the post-tsunami survey and numerical modeling perspectives. In *The Chile-2015 (Illapel) earthquake and tsunami* (pp. 219-234). Birkhäuser, Cham.

Baker PE, Buckley F, Holland JG (1974) Petrology and geochemistry of Easter Island. Contrib Mineral Petrol 44: 85-100.

Bao, H., Ampuero, J. P., Meng, L., Fielding, E. J., Liang, C., Milliner, C. W., ... & Huang, H. (2019). Early and persistent supershear rupture of the 2018 magnitude 7.5 Palu earthquake. Nature Geoscience DOI, 10.

Barrientos, S. E. (1988). Slip distribution of the 1985 central Chile earthquake. *Tectonophysics*, *145*(3-4), 225-241.

Bellier, Olivier, Michel Sébrier, Thierry Beaudouin, Michel Villeneuve, Regis Braucher, Didier Bourles, Lionel Siame, Eka Putranto, and Indyo Pratomo. 2001. 'High slip rate for a low seismicity along the Palu-Koro active fault in central Sulawesi (Indonesia)', Terra Nova, 13: 463-70.

Bernard, E. N., Mofjeld, H. O., Titov, V., Synolakis, C. E., & González, F. I. (2006). Tsunami: scientific frontiers, mitigation, forecasting and policy implications. *Philosophical Transactions of the Royal Society A: Mathematical, Physical and Engineering Sciences*, *364*(1845), 1989-2007.

Beyá J, Álvarez M, Gallardo A, Hidalgo H, Winckler P (2017) Generation and validation of the Chilean Wave Atlas database. Ocean Modelling 116: 16-32.

Carvajal, M., & Gubler, A. (2016). The Effects on Tsunami Hazard Assessment in Chile of Assuming Earthquake Scenarios with Spatially Uniform Slip. *Pure and Applied Geophysics*, *173*(12).

Carvajal, M., Cisternas, M., & Catalán, P. A. (2017a). Source of the 1730 Chilean earthquake from historical records: Implications for the future tsunami hazard on the coast of

Metropolitan Chile. *Journal of Geophysical Research: Solid Earth*, *122*(5), 3648-3660.

Carvajal, M., Cisternas, M., Gubler, A., Catalán, P. A., Winckler, P., & Wesson, R. L. (2017b). Reexamination of the magnitudes for the 1906 and 1922 Chilean earthquakes using Japanese tsunami amplitudes: Implications for source depth constraints. *Journal of Geophysical Research: Solid Earth*, *122*(1), 4-17.
Castilla, J. C. (1988). Earthquake-caused coastal uplift and its effects on rocky intertidal kelp communities. *Science*, *242*(4877), 440-443.

Chagué-Goff, C., Szczuciński, W., & Shinozaki, T. (2017). Applications of geochemistry in tsunami research: A review. *Earth-Science Reviews*, *165*, 203-244.

Cienfuegos, Rodrigo, Patricio A Catalán, Alejandro Urrutia, Roberto Benavente, Rafael Aránguiz, and Gabriel González. 2018. 'What can we do to forecast tsunami hazards in the near field given large epistemic uncertainty in rapid seismic source inversions?', Geophysical Research Letters, 45: 4944-55.

Cisternas, M., Torrejón, F., & Gorigoitia, N. (2012). Amending and complicating Chile's seismic catalog with the Santiago earthquake of 7 August 1580. *Journal of South American Earth Sciences*, *33*(1), 102-109.

Comte, D., Eisenberg, A., Lorca, E., Pardo, M., Ponce, L., Saragoni, R., ... & Suárez, G. (1986). The 1985 central Chile earthquake: A repeat of previous great earthquakes in the region?. *Science*, *233*(4762), 449-453.

Dangendorf S, Hay C, Calafat FM, Marcos M, Piecuch CG, Berk K, Jensen J (2019) Persistent acceleration in global sea-level rise since the 1960s. Nat Clim Change 9: 705–710.

Day, S., & Fearnley, C. (2015). A classification of mitigation strategies for natural hazards: implications for the understanding of interactions between mitigation strategies. *Natural Hazards*, *79*(2), 1219-1238.

Dean RG, Bender CJ (2006) Static wave setup with emphasis on damping effects by vegetation and bottom friction. Coastal Engineering 53(2-3): 149-156.

Defant A (1961) Physical oceanography, vol. 2. London: Pergamon Press. 613pp.

Du, Y., Ma, S., Kubota, T., & Saito, T. (2021). Impulsive tsunami and large runup along the Sanriku coast of Japan produced by an inelastic wedge deformation model. *Journal of Geophysical Research: Solid Earth*, *126*(8), e2021JB022098.
Dura, T., Cisternas, M., Horton, B. P., Ely, L. L., Nelson, A. R., Wesson, R. L., & Pilarczyk, J. E. (2015). Coastal evidence for Holocene subduction-zone earthquakes and tsunamis in central Chile. *Quaternary Science Reviews*, *113*, 93-111.

Elbanna, A., Abdelmeguid, M., Ma, X., Amlani, F., Bhat, H. S., Synolakis, C., & Rosakis, A. J. (2021). Anatomy of strike-slip fault tsunami genesis. *Proceedings of the National Academy of Sciences*, *118*(19).

Espinoza V, Waliser DE, Guan B, Lavers DA, Ralph FM (2018) Global analysis of climate change projection effects on atmospheric rivers. Geophysical Research Letters 45(9): 4299-4308.

Farías, M., Vargas, G., Tassara, A., Carretier, S., Baize, S., Melnick, D., & Bataille, K. (2010). Land-level changes produced by the M w 8.8 2010 Chilean earthquake. *Science*, *329*(5994), 916-916.

Felix, R. P., Hubbard, J. A., Moore, J. D., & Switzer, A. D. (2021). The Role of Frontal Thrusts in Tsunami Earthquake Generation. *Bulletin of the Seismological Society of America.* XX, 1–15, doi: 10.1785/0120210154

Field, M. E., Gardner, J. V., Jennings, A. E., & Edwards, B. D. (1982). Earthquake-induced sediment failures on a 0.25° slope, Klamath River delta, California. *Geology*, *10*(10), 542-546.

Fountain, H. (2022). Here's What Scientists Know About the Tonga Volcano Eruption. Published in New York Times on January 19, 2022 and updated on January 21, 2022. https://www.nytimes.com/2022/01/19/climate/scientists-tonga-volcano-eruption-effects.html

Freund, L. B., & Barnett, D. M. (1976). A two-dimensional analysis of surface deformation due to dip-slip faulting. *Bulletin of the Seismological Society of America*, *66*(3), 667-675.

Fritz, H. M., Petroff, C. M., Catalán, P. A., Cienfuegos, R., Winckler, P., Kalligeris, N., ... & Synolakis, C. E. (2011). Field survey of the 27 February 2010 Chile tsunami. *Pure and Applied Geophysics*, *168*(11), 1989-2010.

Fritz, H., Synolakis, C., Kalligeris, N., Skanavis, V., Santoso, F., Rizal, M., Sapta, G. Prasetya, Liu, Y., and Liu, P. 2018. 'Field survey of the 28 September 2018 Sulawesi tsunami', Paper presented at the Fall Meeting, AGU, Washington DC, December 10-14, 2018.

Fujiwara, T., Kodaira, S., No, T., Kaiho, Y., Takahashi, N., & Kaneda, Y. (2011). The 2011 Tohoku-Oki earthquake: Displacement reaching the trench axis. *Science*, *334*(6060), 1240-1240.

Gao, D., Wang, K., Insua, T. L., Sypus, M., Riedel, M., & Sun, T. (2018). Defining megathrust tsunami source scenarios for northernmost Cascadia. *Natural Hazards*, *94*(1), 445-469.

GEBCO Bathymetric Compilation Group. (2019). The GEBCO_2019 Grid-a continuous terrain model of the global oceans and land. British Oceanographic Data Centre, National Oceanography Centre, NERC, UK.

Geist, E. L. (1998). Local tsunamis and earthquake source parameters. *Advances in Geophysics*, *39*, 117-209.

Geist, E. L., & Bilek, S. L. (2001). Effect of depth-dependent shear modulus on tsunami

generation along subduction zones. *Geophysical research letters*, *28*(7), 1315-1318.
Geist, E. L., & Dmowska, R. (1999). Local tsunamis and distributed slip at the source. In *Seismogenic and Tsunamigenic Processes in Shallow Subduction Zones* (pp. 485-512). Birkhäuser, Basel.

Geist, E. L., Bilek, S. L., Arcas, D., & Titov, V. V. (2006). Differences in tsunami generation between the December 26, 2004 and March 28, 2005 Sumatra earthquakes. *Earth, planets and space*, *58*(2), 185-193.

Geospasial, Badan Informasi. 2018a. 'Contour map of Palu Bay, Retrieved from https://cloud.big.go.id. Accessed 15 Oct 2018'.

Gibbons, S. J., Lorito, S., Macías, J., Løvholt, F., Selva, J., Volpe, M., ... & Vöge, M. (2020). Probabilistic tsunami hazard analysis: high performance computing for massive scale inundation simulations. *Frontiers in Earth Science*, *8*, 623.

Girardclos, S., Schmidt, O. T., Sturm, M., Ariztegui, D., Pugin, A., & Anselmetti, F. S. (2007). The 1996 AD delta collapse and large turbidite in Lake Brienz. *Marine Geology*, *241*(1-4), 137-154.

Globe, Digital. 2018. 'Open Data program, Indonesia earthquake and Tsunami. https://www.digitalglobe.com/opendata/indonesia-earthquake-tsunami/post-event'.

Graham, M. (1824). XXV.—An Account of some Effects of the late Earthquakes in Chili. Extracted from a letter to Henry Warburton, Esq. VPGS. *Transactions of the Geological Society of London*, *2*(2), 413-415.

Grezio, A., Babeyko, A., Baptista, M. A., Behrens, J., Costa, A., Davies, G., ... & Thio, H. K. (2017). Probabilistic tsunami hazard analysis: multiple sources and global applications. *Reviews of Geophysics*, *55*(4), 1158-1198.

Guan B, Waliser D (2015) Detection of atmospheric rivers: Evaluation and application of an algorithm for global studies. J Geophys Res Atmos 120(24): 12514–12535

Gulick, S. P., Austin, J. A., McNeill, L. C., Bangs, N. L., Martin, K. M., Henstock, T. J., ... & Permana, H. (2011). Updip rupture of the 2004 Sumatra earthquake extended by thick indurated sediments. *Nature Geoscience*, *4*(7), 453-456.

Hananto, N. D., Leclerc, F., Li, L., Etchebes, M., Carton, H., Tapponnier, P., ... & Wei, S. (2020). Tsunami earthquakes: Vertical pop-up expulsion at the forefront of subduction megathrust. *Earth and Planetary Science Letters*, *538*, 116197.

Hasiotis, T., Charalampakis, M., Stefatos, A., Papatheodorou, G., & Ferentinos, G. (2006). Fan delta development and processes offshore a seasonal river in a seismically active region, NW Gulf of Corinth. *Geo-Marine Letters*, *26*(4), 199-211.

Hayes, G. P. (2019). Modeling Tsunamis with Social Media. Retrieved from https://eos.org/editor-highlights/modeling-tsunamis-with-social-media

Heidarzadeh, M., Muhari, A., & Wijanarto, A. B. (2019). Insights on the source of the 28 September 2018 Sulawesi tsunami, Indonesia based on spectral analyses and numerical simulations. *Pure and Applied Geophysics*, *176*(1), 25-43.

Hersbach, H, de Rosnay P, Bell B, Schepers D, Simmons A, Soci C, Abdalla S, Alonso-Balmaseda M, Balsamo G, Bechtold P, Berrisford P, Bidlot J-R, de Boisséson E, Bonavita M, Browne P, Buizza R, Dahlgren P, Dee D, Dragani R, Diamantakis M, Flemming J, Forbes R, Geer AJ, Haiden T, Hólm E, Haimberger L, Hogan R, Horányi A, Janiskova M, Laloyaux P, Lopez P, Munoz-Sabater J, Peubey C, Radu R, Richardson D, Thépaut J-N, Vitart F, Yang X, Zsótér E, Zuo H (2018) Operational global reanalysis: Progress, future directions and synergies with NWP. European Centre for Medium Range Weather Forecasts. ERA Report Series No. 27. 63 pp.

Hilbe, M., & Anselmetti, F. S. (2014). Signatures of slope failures and river-delta collapses in a perialpine lake (Lake Lucerne, Switzerland). *Sedimentology*, *61*(7), 1883-1907.

Hill, E. M., Borrero, J. C., Huang, Z., Qiu, Q., Banerjee, P., Natawidjaja, D. H., ... & Sieh, K. (2012). The 2010 Mw 7.8 Mentawai earthquake: Very shallow source of a rare tsunami earthquake determined from tsunami field survey and near-field GPS data. *Journal of Geophysical Research: Solid Earth*, *117*(B6).

Hirono, T., Tsuda, K., Tanikawa, W., Ampuero, J. P., Shibazaki, B., Kinoshita, M., & Mori, J. J. (2016). Near-trench slip potential of megaquakes evaluated from fault properties and conditions. *Scientific reports*, *6*(1), 1-13.

Hoffmann, T. L., Triyono, R., Weniza, A., Heryandoko, N., Daniarsyad, G., Karyono, A., ... & Spahn, H. (2018, December). The 2018 Mw 7.5 Sulawesi Indonesia earthquake: The immediate response of the InaTEWS Warning Centre at BMKG and related operational issues. In *AGU Fall Meeting 2018*. AGU.

Hooper, A., Pietrzak, J., Simons, W., Cui, H., Riva, R., Naeije, M., ... & Socquet, A. (2013). Importance of horizontal seafloor motion on tsunami height for the 2011 Mw= 9.0 Tohoku-Oki earthquake. *Earth and Planetary Science Letters*, *361*, 469-479.
Horspool, N., Pranantyo, I., Griffin, J., Latief, H., Natawidjaja, D. H., Kongko, W., ... & Thio, H. K. (2014). A probabilistic tsunami hazard assessment for Indonesia. *Natural Hazards and Earth System Sciences*, *14*(11), 3105-3122.

Hu, Y., & Wang, K. (2008). Coseismic strengthening of the shallow portion of the subduction fault and its effects on wedge taper. *Journal of Geophysical Research: Solid Earth*, *113*, B12411.

Hu, Y., Wang, K., He, J., Klotz, J., & Khazaradze, G. (2004). Three-dimensional viscoelastic finite element model for postseismic deformation of the great 1960 Chile earthquake. *Journal of Geophysical Research: Solid Earth*, *109*(B12), B12403.

Hubbard, J., Barbot, S., Hill, E. M., & Tapponnier, P. (2015). Coseismic slip on shallow décollement megathrusts: Implications for seismic and tsunami hazard. *Earth-Science Reviews, 141*, 45-55.

Huppert, H. E., & Sparks, R. S. J. (2006). Extreme natural hazards: population growth, globalization and environmental change. *Philosophical Transactions of the Royal Society A: Mathematical, Physical and Engineering Sciences, 364*(1845), 1875-1888.

Imamura, F., Synolakis, C. E., Gica, E., Titov, V., Listanco, E., & Lee, H. J. (1995). Field survey of the 1994 Mindoro Island, Philippines tsunami. *Pure and applied geophysics, 144*(3), 875-890.

Kajiura, K. (1963). The leading wave of a tsunami. *Bulletin of the Earthquake Research Institute, University of Tokyo*, *41*(3), 535-571.

Kanamori, H. (1972). Mechanism of tsunami earthquakes. *Physics of the earth and planetary interiors*, *6*(5), 346-359.

Kanamori, H. (1995). Preparing for the Unexpected. *Seismological Research Letters, 66*(1), 7-8.

Kanoğlu, U., Titov, V., Bernard, E., & Synolakis, C. (2015). Tsunamis: bridging science, engineering and society. *Philosophical Transactions of the Royal Society A: Mathematical, Physical and Engineering Sciences, 373*(2053), 20140369.

Katili, J. A. (1970). Large transcurrent faults in Southeast Asia with special reference to Indonesia. *Geologische Rundschau, 59*(2), 581-600.

Kennedy AB, Westerink JJ, Smith JM, Hope ME, Hartman M, Taflanidis AA, Hamann M (2012) Tropical cyclone inundation potential on the Hawaiian Islands of Oahu and Kauai. Ocean Modelling 52-53: 54-68.

Khouakhi A, Villarini G (2016) On the relationship between atmospheric rivers and high sea water levels along the US West Coast. Geophysical Research Letters 43(16): 8815-8822.

Kodaira, S., No, T., Nakamura, Y., Fujiwara, T., Kaiho, Y., Miura, S., ... & Taira, A. (2012). Coseismic fault rupture at the trench axis during the 2011 Tohoku-oki earthquake. *Nature Geoscience, 5*(9), 646-650.

Kodaira, S., Iinuma, T., & Imai, K. (2021). Investigating a tsunamigenic megathrust earthquake in the Japan Trench. *Science*, *371*(6534).

Kotani, M., Imamura, F., & Shuto, N. (1998). New method of tsunami runup and estimation of damage using GIS data. *Proceedings of the Coastal Engineering, Japan Society of Civil Engineers, 45*, 356-360.

Kozdon, J. E., & Dunham, E. M. (2013). Rupture to the trench: Dynamic rupture simulations of the 11 March 2011 Tohoku earthquake. *Bulletin of the Seismological Society of America, 103*(2B), 1275-1289.

Lay, T., & Rhode, A. (2019). Evaluating the updip extent of large megathrust ruptures using Pcoda levels. *Geophysical Research Letters, 46*(10), 5198-5206.

Lay, T., Kanamori, H., Ammon, C. J., Koper, K. D., Hutko, A. R., Ye, L., ... & Rushing, T. M. (2012). Depth-varying rupture properties of subduction zone megathrust faults. *Journal of Geophysical Research: Solid Earth, 117*(B4).

Lay, T., Liu, C., & Kanamori, H. (2019). Enhancing tsunami warning using P wave coda. *Journal of Geophysical Research: Solid Earth, 124*(10), 10583-10609.

Leithold, E. L., Wegmann, K. W., Bohnenstiehl, D. R., Smith, S. G., Noren, A., & O'Grady, R. (2018). Slope failures within and upstream of Lake Quinault, Washington, as uneven responses to Holocene earthquakes along the Cascadia subduction zone. *Quaternary Research, 89*(1), 178-200.

Lindsey, E. O., Mallick, R., Hubbard, J. A., Bradley, K. E., Almeida, R. V., Moore, J. D., ... & Hill, E. M. (2021). Slip rate deficit and earthquake potential on shallow megathrusts. *Nature Geoscience, 14*(5), 321-326.

Liu Y, San Liang X, Weisberg RH (2007) Rectification of the bias in the wavelet power spectrum. Journal of Atmospheric and Oceanic Technology 24(12): 2093-2102.

Lomnitz, C. (1970). Major earthquakes and tsunamis in Chile during the period 1535 to 1955. *Geologische Rundschau, 59*(3), 938-960.

Luo, H., & Wang, K. (2021). Postseismic geodetic signature of cold forearc mantle in subduction zones. *Nature Geoscience, 14*(2), 104-109.

Ma, S., & Nie, S. (2019). Dynamic wedge failure and along-arc variations of tsunamigenesis in the Japan trench margin. *Geophysical Research Letters, 46*(15), 8782-8790.

Marshall, M. (2019). Mystery of deadly Indonesian tsunami cracked using social-media videos. *Nature, 569*(7755), 463-465.

Matsuyama, M., Walsh, J. P., & Yeh, H. (1999). The effect of bathymetry on tsunami characteristics at Sisano Lagoon, Papua New Guinea. *Geophysical Research Letters, 26*(23), 3513-3516.

McNally, K. C. (1983). Seismic gaps in space and time. *Annual Review of Earth and Planetary Sciences, 11*(1), 359-369.

Montessus de Ballore, F. D. (1912). Historia sísmica de los Andes Meridionales al sur del paralelo XVI. Cuarta parte. In *Anales de la Universidad de Chile* (pp. ág-773).

Monserrat S, Vilibić I, Rabinovich AB (2006) Meteotsunamis: atmospherically induced destructive ocean waves in the tsunami frequency band. Nat Hazards Earth Syst Sci 6: 1035–1051.

Moreno, M., Rosenau, M., & Oncken, O. (2010). 2010 Maule earthquake slip correlates with pre-seismic locking of Andean subduction zone. *Nature*, *467*(7312), 198-202.

Moreno, M., Melnick, D., Rosenau, M., Baez, J., Klotz, J., Oncken, O., ... & Hase, H. (2012). Toward understanding tectonic control on the Mw 8.8 2010 Maule Chile earthquake. *Earth and Planetary Science Letters*, *321*, 152-165.

Mori, N., Takahashi, T., Yasuda, T., & Yanagisawa, H. (2011). Survey of 2011 Tohoku earthquake tsunami inundation and run-up. *Geophysical research letters*, *38*(7).

Muhari, A., Imamura, F., Arikawa, T., Hakim, A. R., & Afriyanto, B. (2018). Solving the puzzle of the September 2018 Palu, Indonesia, tsunami mystery: clues from the tsunami waveform and the initial field survey data. *Journal of Disaster Research*, *13*(Scientific Communication), sc20181108.

Nishenko, S. P. (1985). Seismic potential for large and great interplate earthquakes along the Chilean and southern Peruvian margins of South America: a quantitative reappraisal. *Journal of Geophysical Research: Solid Earth*, *90*(B5), 3589-3615.

Okada, Y. (1985). Surface deformation due to shear and tensile faults in a half-space. *Bulletin of the seismological society of America*, *75*(4), 1135-1154.

Parsons, T., Geist, E. L., Ryan, H. F., Lee, H. J., Haeussler, P. J., Lynett, P., ... & Roland, E. (2014). Source and progression of a submarine landslide and tsunami: The 1964 Great Alaska earthquake at Valdez. *Journal of Geophysical Research: Solid Earth*, *119*(11), 8502-8516.

Pawlowicz, R., Beardsley, B., & Lentz, S. (2002). Classical tidal harmonic analysis including error estimates in MATLAB using T_TIDE. *Computers & Geosciences*, *28*(8), 929-937.

Pelayo, A. M., & Wiens, D. A. (1992). Tsunami earthquakes: Slow thrust-faulting events in the accretionary wedge. *Journal of Geophysical Research: Solid Earth*, *97*(B11), 15321-15337.

Petley, David. 2018. 'Giant landslides in Palu from the 2018 Sulawesi earthquake. https://blogs.agu.org/landslideblog/2018/10/02/palu-sulawesi-earthquake-2/'.

Philibosian, B., & Meltzner, A. J. (2020). Segmentation and supercycles: a catalog of earthquake rupture patterns from the Sumatran Sunda Megathrust and other well-studied faults worldwide. *Quaternary Science Reviews*, *241*, 106390.

Polet, J., & Kanamori, H. (2000). Shallow subduction zone earthquakes and their tsunamigenic potential. *Geophysical Journal International*, *142*(3), 684-702.

Prada, M., Galvez, P., Ampuero, J. P., Sallarès, V., Sánchez-Linares, C., Macías, J., & Peter, D. (2021). The Influence of Depth-Varying Elastic Properties of the Upper Plate on Megathrust Earthquake Rupture Dynamics and Tsunamigenesis. *Journal of Geophysical Research: Solid Earth, 126*(11), e2021JB022328.

Prasetya, G. S., De Lange, W. P., & Healy, T. R. (2001). The Makassar strait tsunamigenic region, Indonesia. *Natural Hazards, 24*(3), 295-307.

Press, Associated (2018). Indonesia Earthquake Ship. http://www.aparchive.com/metadata/youtube/abf7ff674bfc102aec5cdf7b7a959423'.

Press, F., & Harkrider, D. (1966). Air-sea waves from the explosion of Krakatoa. *Science, 154*(3754), 1325-1327.

Pugh D, Woodworth P (2014). Sea-Level Science: Understanding Tides, Surges, Tsunamis and Mean Sea Level Changes. Cambridge University Press. 407 pp.

Quilliam L, Cox R, Campbell P, Wright M (2011) Coastal climate change impacts for Easter Island in 2100. In Coasts and Ports 2011: Diverse and Developing: Proceedings of the 20th Australasian Coastal and Ocean Engineering Conference and the 13th Australasian Port and Harbour Conference, Engineers Australia, p. 617-622.

Quilliam L, Cox R, Campbell P, Wright M (2014) Coastal climate change impacts for Easter Island in 2100. Rapa Nui Journal 28(1): 60-67

Rabinovich A (2009) Seiches and Harbor Oscillations. Handbook of Coastal and Ocean Engineering (edited by Y.C. Kim), Chapter 9., World Scientific Publ, Singapore.

Rabinovich AB (2020) Twenty-seven years of progress in the science of meteorological tsunamis following the 1992 Daytona Beach event. Pure Appl Geophys 177: 1193–1230.

Ralph FM, Dettinger MD, Cairns MM, Galarneau TJ, Eylander J (2018) Defining "atmospheric river": How the Glossary of Meteorology helped resolve a debate. Bulletin of the American Meteorological Society 99(4): 837-839.

Rangel-Buitrago N, Contreras-López M, Martínez C & Williams A (2018) Can coastal scenery be managed? The Valparaíso region, Chile as a case study. Ocean & Coastal Management 163: 383 – 400.

Ramos, M. D., & Huang, Y. (2019). How the transition region along the Cascadia megathrust influences coseismic behavior: Insights from 2-D dynamic rupture simulations. *Geophysical Research Letters, 46*(4), 1973-1983.

Rappaport Y, Naar DF, Barton CC, Liu ZJ, Hey RN (1997) Morphology and distribution of seamounts surrounding Easter Island. Journal of Geophysical Research: Solid Earth 102(B11): 24713-24728.

Rudnicki, J. W., & Wu, M. (1995). Mechanics of dip-slip faulting in an elastic half-space. *Journal of Geophysical Research: Solid Earth*, *100*(B11), 22173-22186.

Sallarès, V., & Ranero, C. R. (2019). Upper-plate rigidity determines depth-varying rupture behaviour of megathrust earthquakes. *Nature*, *576*(7785), 96-101.

Sallarès, V., Prada, M., Riquelme, S., Meléndez, A., Calahorrano, A., Grevemeyer, I., & Ranero, C. R. (2021). Large slip, long duration, and moderate shaking of the Nicaragua 1992 tsunami earthquake caused by low near-trench rock rigidity. *Science Advances*, *7*(32), eabg8659.

Sassa, S., & Takagawa, T. (2019). Liquefied gravity flow-induced tsunami: first evidence and comparison from the 2018 Indonesia Sulawesi earthquake and tsunami disasters. *Landslides*, *16*(1), 195-200.

Satake, K. (1994). Mechanism of the 1992 Nicaragua tsunami earthquake. *Geophysical Research Letters*, *21*(23), 2519-2522.

Satake, K., & Atwater, B. F. (2007). Long-term perspectives on giant earthquakes and tsunamis at subduction zones. *Annu. Rev. Earth Planet. Sci.*, *35*, 349-374.

Satake, K., Fujii, Y., Harada, T., & Namegaya, Y. (2013). Time and space distribution of coseismic slip of the 2011 Tohoku earthquake as inferred from tsunami waveform data. *Bulletin of the seismological society of America*, *103*(2B), 1473-1492.

Satake, K., & Fujii, Y. (2014). source models of the 2011 Tohoku earthquake and long-term forecast of large earthquakes. *Journal of Disaster Research*, *9*(3), 272-280.

Satake, K. (2015). Geological and historical evidence of irregular recurrent earthquakes in Japan. *Philosophical Transactions of the Royal Society A: Mathematical, Physical and Engineering Sciences*, *373*(2053), 20140375.

Savage, J. C. (1983). A dislocation model of strain accumulation and release at a subduction zone. *Journal of Geophysical Research: Solid Earth*, *88*(B6), 4984-4996.

Sepúlveda, I., Liu, P. L. F., & Grigoriu, M. (2019). Probabilistic tsunami hazard assessment in South China Sea with consideration of uncertain earthquake characteristics. *Journal of Geophysical Research: Solid Earth*, *124*(1), 658-688.

Shinoda T, Zamudio L, Guo Y, Metzger EJ, Fairall CW (2019) Ocean variability and air-sea fluxes produced by atmospheric rivers. Scientific Reports 9: 2152.

Sippl, C., Moreno, M., & Benavente, R. (2021). Microseismicity appears to outline highly coupled regions on the Central Chile megathrust. *Journal of Geophysical Research: Solid Earth*, *126*(11), e2021JB022252.

Scholz, C. H. (1998). Earthquakes and friction laws. *Nature*, *391*(6662), 37-42.

Socquet, A., Simons, W., Vigny, C., McCaffrey, R., Subarya, C., Sarsito, D., ... & Spakman, W. (2006). Microblock rotations and fault coupling in SE Asia triple junction (Sulawesi, Indonesia) from GPS and earthquake slip vector data. *Journal of Geophysical Research: Solid Earth*, *111*(B8).

Socquet, A., Hollingsworth, J., Pathier, E., & Bouchon, M. (2019). Evidence of supershear during the 2018 magnitude 7.5 Palu earthquake from space geodesy. *Nature Geoscience*, *12*(3), 192-199.

Soloviev, S. L., & Go, C. N. (1974). Catalog of tsunamis on the western shore of the Pacific.

Somerville, P., Blong, R., and Gissing, A. (2022). Why the Tonga tsunami arrived much earlier and much larger than expected. Retrieved from https://riskfrontiers.com/insights/why-the-tonga-tsunami-arrived-much-earlier-and-much-larger-than-expected/

Stein, S., Geller, R. J., & Liu, M. (2012). Why earthquake hazard maps often fail and what to do about it. *Tectonophysics*, *562*, 1-25.

Sun, T., Wang, K., Iinuma, T., Hino, R., He, J., Fujimoto, H., ... & Hu, Y. (2014). Prevalence of viscoelastic relaxation after the 2011 Tohoku-oki earthquake. *Nature*, *514*(7520), 84-87.

Sun, T., Wang, K., Fujiwara, T., Kodaira, S., & He, J. (2017). Large fault slip peaking at trench in the 2011 Tohoku-oki earthquake. *Nature communications*, *8*(1), 1-8.

Sun, T., Wang, K., & He, J. (2018). Crustal deformation following great subduction earthquakes controlled by earthquake size and mantle rheology. *Journal of Geophysical Research: Solid Earth*, *123*(6), 5323-5345.

Tadepalli, S., & Synolakis, C. E. (1994). The run-up of N-waves on sloping beaches. *Proceedings of the Royal Society of London. Series A: Mathematical and Physical Sciences*, *445*(1923), 99-112.

Tanioka, Y., & Satake, K. (1996). Tsunami generation by horizontal displacement of ocean bottom. *Geophysical research letters*, *23*(8), 861-864.

Tanioka, Y., & Seno, T. (2001). Sediment effect on tsunami generation of the 1896 Sanriku tsunami earthquake. *Geophysical Research Letters*, *28*(17), 3389-3392.

Tappin, D. R. (2021). Submarine landslides and their tsunami hazard. *Annual Review of Earth and Planetary Sciences*, *49*, 551-578.

The 2011 Tohoku Earthquake Tsunami Joint Survey Group (2011). Nationwide Field Survey of the 2011 Off the Pacific Coast of Tohoku Earthquake Tsunami, Journal of Japan Society of Civil Engineers, Series B, Vol. 67 (2011) , No.1 pp.63-66.

Tilmann, F., Zhang, Y., Moreno, M., Saul, J., Eckelmann, F., Palo, M., ... & Dahm, T. (2016). The 2015 Illapel earthquake, central Chile: A type case for a characteristic earthquake?. *Geophysical Research Letters*, *43*(2), 574-583.

Titov, V., Cronin, M. F., Dziak, R., Wei, Y., Arcas, D., Moore, C., et al. (2022). Understanding a unique tsunami event caused by the Tonga volcano eruption. Retrieved from https://www.pmel.noaa.gov/news-story/understanding-unique-tsunami-event-caused-tonga-volcano-eruption

Tolman H (2014) User Manual and System Documentation of WaveWatch III, Version 4.18. Environmental Modeling Center Marine Modeling and Analysis Branch. 361pp.

Torrence, C., & Compo, G. P. (1998). A practical guide to wavelet analysis. *Bulletin of the American Meteorological society*, *79*(1), 61-78.

Tribune, Chicago (2018) Crew members recount terror of tsunami that dumped 208-foot ferry in Indonesian village. https://www.chicagotribune.com/news/nationworld/ct-indonesia-tsunami-ferry-ashore-20181004-story.html'.

Tsuji, Y. (2013). Catalog of distant tsunamis reaching Japan from Chile and Peru. *Rep. Tsunami Eng*, *30*, 61-68.

Tsuji, T., Kawamura, K., Kanamatsu, T., Kasaya, T., Fujikura, K., Ito, Y., ... & Kinoshita, M. (2013). Extension of continental crust by anelastic deformation during the 2011 Tohoku-oki earthquake: The role of extensional faulting in the generation of a great tsunami. *Earth and Planetary Science Letters*, 364, 44-58.

Udías, A., Madariaga, R., Buforn, E., Muñoz, D., & Ros, M. (2012). The large Chilean historical earthquakes of 1647, 1657, 1730, and 1751 from contemporary documents. *Bulletin of the Seismological Society of America*, *102*(4), 1639-1653.

U.S. Geological Survey (2018). "M 7.5 - 70km N of Palu, Indonesia, https://earthquake.usgs.gov/earthquakes/eventpage/us1000h3p4/finite-fault."

U.S. Geological Survey (2022). M 5.8 Volcanic Eruption - 68 km NNW of Nukuʻalofa, Tonga, https://earthquake.usgs.gov/earthquakes/eventpage/pt22015050/executive

Vanneste, K., Wils, K., & Van Daele, M. (2018). Probabilistic evaluation of fault sources based on Paleoseismic evidence from mass-transport deposits: The example of Aysén Fjord, Chile. *Journal of Geophysical Research: Solid Earth*, *123*(11), 9842-9865.

Viale M, Valenzuela R, Garreaud R, Ralph M (2018) Impacts of Atmospheric Rivers on Precipitation in Southern South America. J Hydrometeor 19: 1671-1686.

Vigny, C., Socquet, A., Peyrat, S., Ruegg, J. C., Métois, M., Madariaga, R., ... & Kendrick, E. (2011). The 2010 M w 8.8 Maule megathrust earthquake of central Chile, monitored by GPS. *Science*, *332*(6036), 1417-1421.

Walpersdorf, A., Vigny, C., Manurung, P., Subarya, C., & Sutisna, S. (1998). Determining the Sula block kinematics in the triple junction area in Indonesia by GPS. *Geophysical Journal International*, *135*(2), 351-361.

Wang, K., & He, J. (2008). Effects of frictional behavior and geometry of subduction fault on coseismic seafloor deformation. *Bulletin of the Seismological Society of America*, *98*(2), 571-579.

Wang, K., Hu, Y., & He, J. (2012). Deformation cycles of subduction earthquakes in a viscoelastic Earth. *Nature*, *484*(7394), 327-332.

Wang, K., & Tréhu, A. M. (2016). Invited review paper: Some outstanding issues in the study of great megathrust earthquakes—The Cascadia example. *Journal of Geodynamics*, *98*, 1-18.

Wang, K., Sun, T., Brown, L., Hino, R., Tomita, F., Kido, M., ... & Fujiwara, T. (2018). Learning from crustal deformation associated with the M9 2011 Tohoku-oki earthquake. *Geosphere*, *14*(2), 552-571.

Wang, P. L., Engelhart, S. E., Wang, K., Hawkes, A. D., Horton, B. P., Nelson, A. R., & Witter, R. C. (2013). Heterogeneous rupture in the great Cascadia earthquake of 1700 inferred from coastal subsidence estimates. *Journal of Geophysical Research: Solid Earth*, *118*(5), 2460-2473.

Wang, X., & Power, W. L. (2011). *COMCOT: a tsunami generation propagation and run-up model*. GNS Science.

Ward, S.N. (2011). Tsunami. in, Encyclopedia of solid earth geophysics (Springer).

Ward, S. N. (1980). Relationships of tsunami generation and an earthquake source. *Journal of Physics of the Earth*, *28*(5), 441-474.

Watkinson, I. M., & Hall, R. (2017). Fault systems of the eastern Indonesian triple junction: evaluation of Quaternary activity and implications for seismic hazards. *Geological Society, London, Special Publications*, *441*(1), 71-120.

Watkinson, I. M., Hall, R., Cottam, M. A., Sevastjanova, I., Suggate, S., Gunawan, I., ... & Advocaat, E. (2012). New insights into the geological evolution of Eastern Indonesia from recent research projects by the SE Asia Research Group. *Berita Sedimentologi*, *23*(1), 21-27.

Watts, P., Grilli, S. T., Tappin, D. R., & Fryer, G. J. (2005). Tsunami generation by submarine mass failure. II: Predictive equations and case studies. *Journal of waterway, port, coastal, and ocean engineering*, *131*(6), 298-310.

Wunsch C, Stammer D (1997) Atmospheric loading and the oceanic “inverted barometer” effect. Reviews of Geophysics 35(1): 79-107.

Yamazaki, Y., Cheung, K. F., & Kowalik, Z. (2011). Depth-integrated, non-hydrostatic model with grid nesting for tsunami generation, propagation, and run-up. *International Journal for Numerical Methods in Fluids*, *67*(12), 2081-2107.

Zamora, N., Catalán, P. A., Gubler, A., & Carvajal, M. (2021). Microzoning tsunami hazard by combining flow depths and arrival times. *Frontiers in Earth Science*, *8*, 747.

Zhang, Y., Zhang, G., Hetland, E. A., Shan, X., Wen, S., & Zuo, R. (2016). Coseismic fault slip of the September 16, 2015 Mw 8.3 Illapel, Chile earthquake estimated from InSAR data. *Pure and Applied Geophysics*, *173*(4), 1029-1038.

Appendix A

Supporting material for Article in Chapter 5

Text S1: Comparison of runup values predicted by COMCOT and NEOWAVE

Compared to COMCOT (Wang and Power, 2011), NEOWAVE (Yamazaki et al. 2013) has two main advantages. First, it better describes dispersive waves and nonhydrostatic flows over steep bathymetric slopes by including non-hydrostatic pressure and vertical velocity terms in the Shallow Water Equations. Second, it adopts a shock-capturing scheme that ensures conservation of momentum across flow discontinuities, such as those that could develop during the runup process. To check the validity of our runup results based on COMCOT, we compared a selected representative subset of these results, including Ref1 and Ref2, with those predicted by NEOWAVE (Figure S3a). It can be seen that the two tsunami codes predict similar runup values. The difference is typically less than 20 cm (inset in Figure S3a). In this paper, two 100% trench-breaching rupture models may push the theoretical performance limits of COMCOT. The first one, denoted M1 in Figure S3b, has a 10.3 km deep trench (also shown in Figure 6b). The large water depths near the trench gives rise to a large value of the dispersion parameter $\mu = d/l$, where d is the characteristic water depth and l the characteristic wavelength of the ensuing tsunami waves. The other one, denoted M2 in Figure S3b, has a steep frontal thrust through a 5-km-thick sediment layer (also shown in Figure 5.9), and the resultant narrow sea surface elevation spike leads to a large dispersion parameter value. Even for these two models, the two tsunami modelling codes yield rather similar results (Figure S3a).

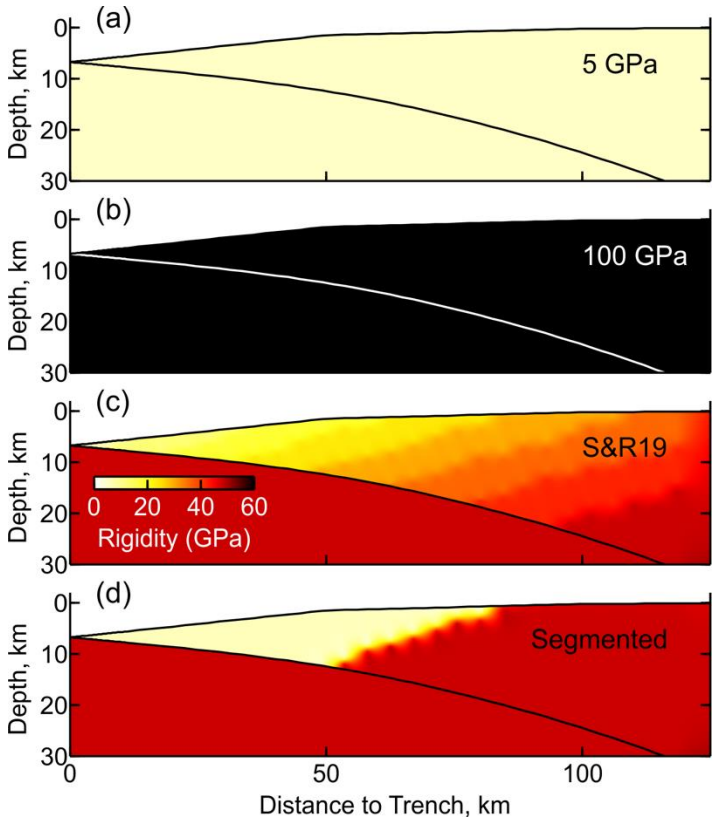

Figure S1. Rigidity distributions used for model tests in Figure S2. (a) and (b) Uniform rigidity with very low (5 GPa) and very high (100 GPa) values, respectively. (c) Gradual spatial variations in upper-plate rigidity. Variations along the base of the upper plate follows Sallarès & Ranero (2019) (S&R19). (d) An abrupt change in upper-plate rigidity.

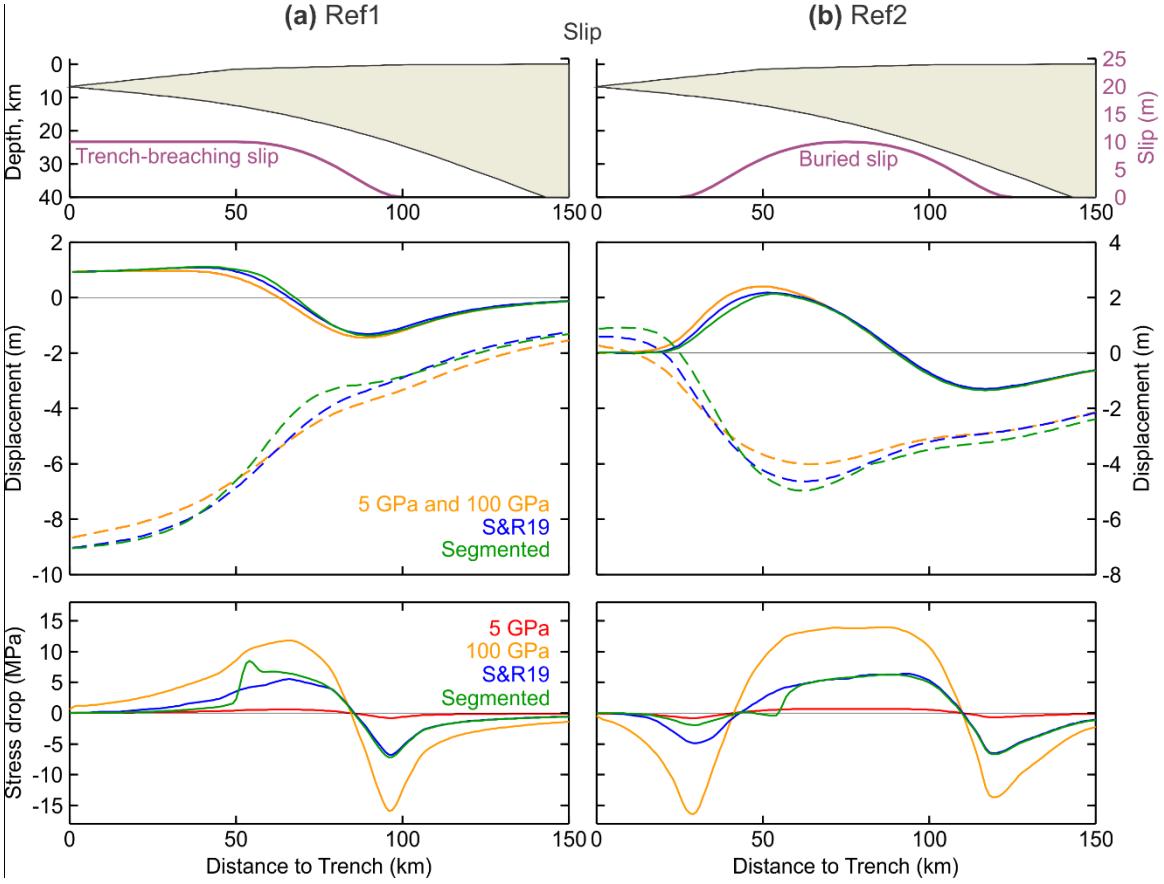

Figure S2. Model results for the four rigidity models shown in Figure S1 (color coding defined in (a)) using the slip distributions of Ref1 or Ref2 (top panel). For this demonstration, the effect of gravity is neglected. All the four models yield similar surface deformation patterns (middle panel) although rather different stress drop distributions along the megathrust (lower panel). Note that the 5 GPa and 100 GPa (or any other uniform rigidity value) models yield identical displacements; including gravity would very slightly modify the low-rigidity results.

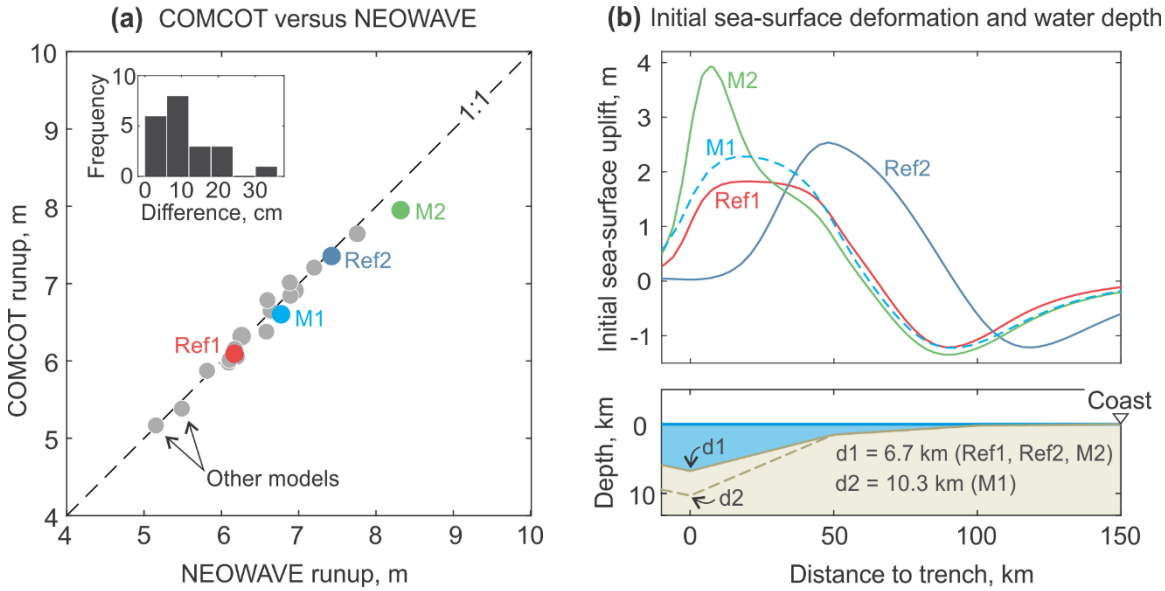

Figure S3. Comparison of runup results predicted by the tsunami modeling codes COMCOT (used in this study) and NEOWAVE. The generic model setup is as shown in Figure 5.2. (a) Summary of results for all the 21 models used for the comparison. The inset shows a histogram of the runup differences between the two codes (NEOWAVE -COMCOT). (b) Four of the 21 models. Upper panel shows the initial sea-surface deformation. See Figures 5.3 and 5.5 for details of Ref1 and Ref2. See Text S1 for discussion of M1 and M2. The lower panel shows a cross-section bathymetry profile for these models, indicating their respective trench depths.

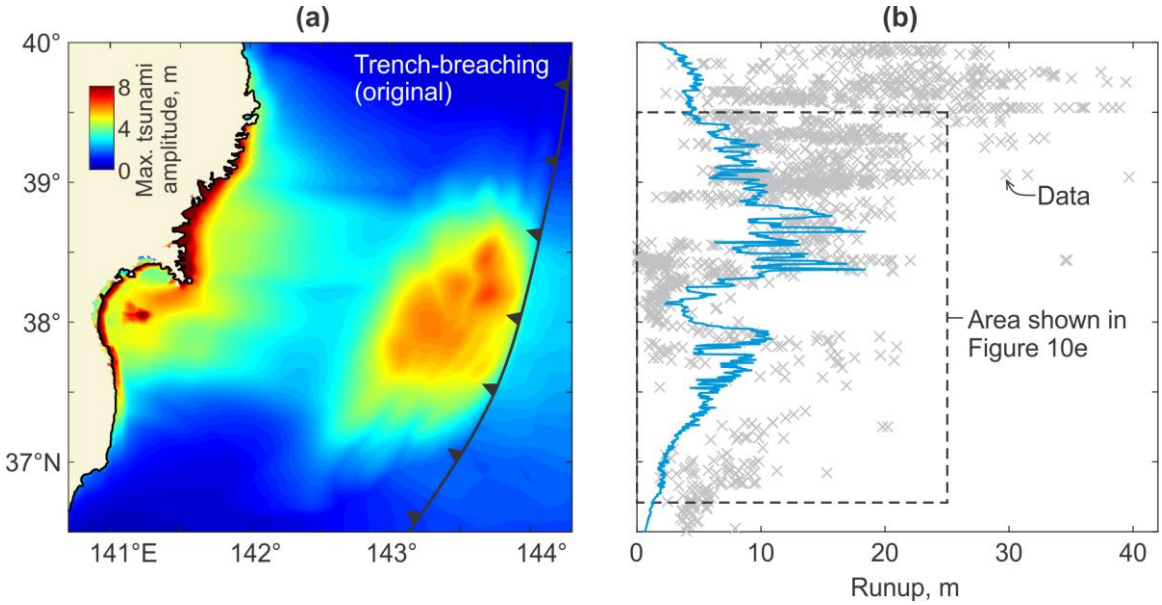

Figure S4. Tsunami results for the Trench-breaching (original) model and runup measurements along the northeast Japan coast. (a) Maximum tsunami amplitude predicted by the Trench-breaching (original) model (see Figure S5a for slip distribution). (b) Same as Figure 5.10e but displayed for a longer stretch of the coastline. The source for the large runups north of 39°N is outside of the maximum fault slip area. The nature of that source, still under investigation (Kodaira et al. 2021), is beyond the scope of this study.

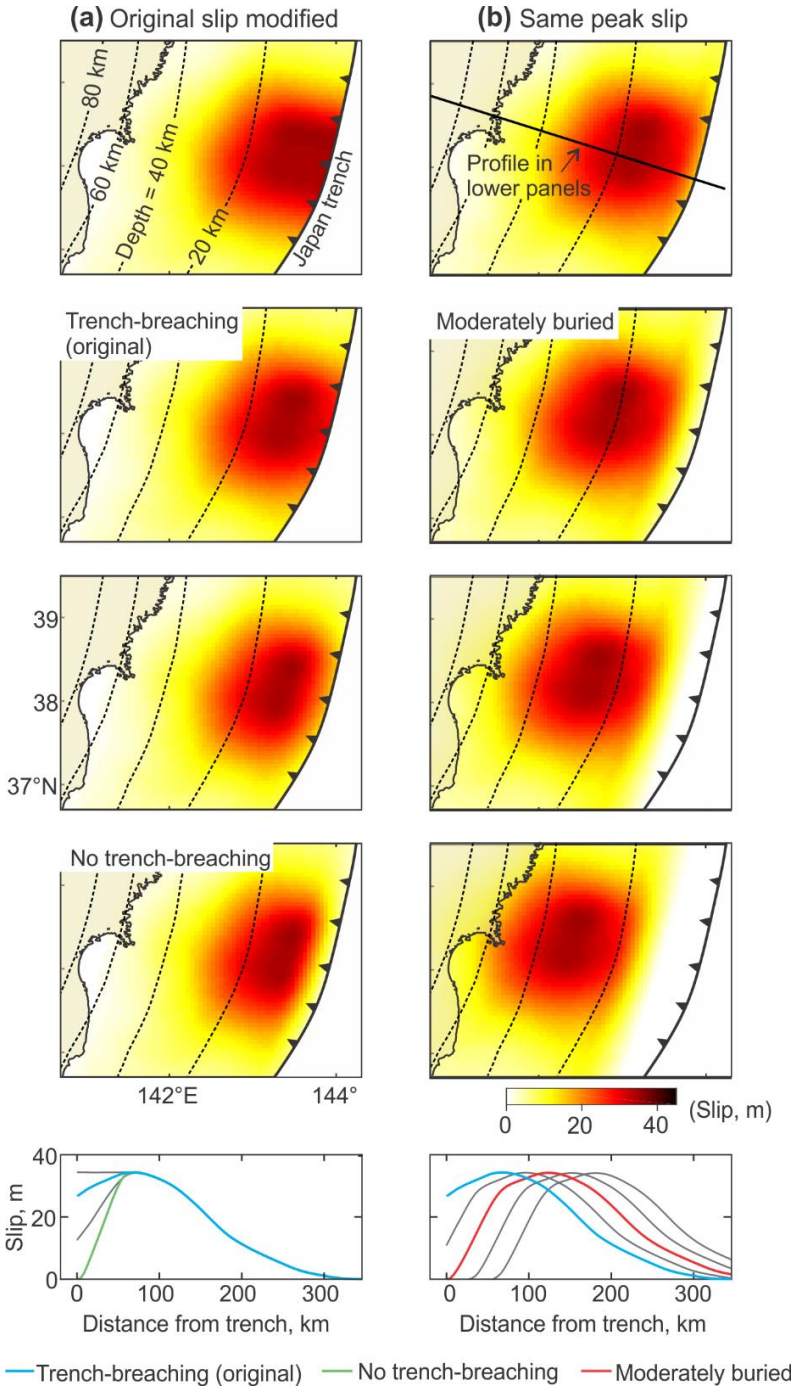

Figure S5. Slip distributions of the original Tohoku-oki earthquake (i.e., Trench-breaching (original)) model and other test models. (a) Hypothetical rupture models in which the slip distribution seaward of the peak slip is modified from the original model to let the slip breach the trench with different fractions of the peak slip value. (b) Hypothetical rupture models in which the slip distribution of the original model is systematically shifted downdip to greater depths to produce buried-rupture models with the same peak slip. In both (a) and (b), the lower panel shows slip distributions of the shown rupture models along the profile in the top panel of (b).

Appendix B

Supporting material for Article in Chapter 6

Table S1. Written records of the 1822 and 1906 Metropolitan Chile earthquakes and tsunamis

Presentation

This supplementary table presents written descriptions of effects of previously poorly documented earthquakes that struck Metropolitan Chile in 1822 and 1906. The reported effects are key for our argument of associated deeper ruptures, inferred from described land level changes and tsunamis. Some accounts were previously compiled by Montessus de Ballore (1912, 1915) and summarized by Lomnitz (1970). Here we complement their work by presenting 32 first-hand accounts, nineteen pertain to the 1822 event (**records 1-19**), and 13 to 1906 (**20-32**). With 12 exceptions the originals were written in Spanish, which we reproduce beside a fairly literal translation into English. The excerpts describe the 1822 and 1906 earthquakes in order of their recorded or estimated dates of composition.

We begin with an overview of the region´s seismic history. Then, we preface each of the two earthquakes with a description based on the accounts themselves. We then introduce each specific account with additional historical background and highpoints provided by the account. Additionally, for each account we include a map locating the mentioned places. We conclude the record by giving its bibliographic source. References cited elsewhere in the table are on pages 60 and 61.

Seismic history of Metropolitan Chile

Owing to the early and continuous Spanish settlement in Metropolitan Chile since 1541, the region has a 480-year-long seismic historical record; the country´s longest. It has been struck by large earthquakes in 1575, 1580, 1647, 1730, 1822, 1906 and 1985 (Lomnitz, 1970; Cisternas et al., 2012). However, the 1575 and 1580 earthquakes may have been too small to be included in this list (Cisternas et al., 2012), and the 1647 event may differ from the rest in having an intraplate source (Cisternas, 2012). The last four of the sequence, although differing from one another in size, were certainly large interplate, underthrusting earthquakes as marked along the coast by strong shaking, land-level changes and tsunamis (Cisternas, 2012; Carvajal et al., 2017a; Carvajal et al. 2017b).

The July 8, 1730 earthquake has long been known as the largest event in Metropolitan Chile (Montessus de Ballore, 1912). It broke a quiescence period of at least 189 years without this kind of very large events, at least since 1541. The 1730 mainshock damaged buildings along 1,000 km, between northern Copiapó and southern Concepción, and as far east as Mendoza, in Argentina, beyond the Andes (Urbina et al., 2016). The waves of the ensuing tsunami were very destructive in the two main coastal cities at that time in Chile, reaching heights of ~11 m in Valparaíso and ~9 m at Concepción (Carvajal et al., 2017a). The tsunami also crossed the Pacific to Japan, being reported in six localities along northeast coast of Sendai, where it flooded rice fields and destroyed salt works, reaching a height of 2 m (Tsuji, 2013). These effects point to an earthquake of magnitude 9.1-9.3, with a rupture 600-800 km long, and up to 20 m of shallow slip offshore Metropolitan Chile (Carvajal et al., 2017a).

The three events following the 1730 earthquake (1822, 1906, and 1985) share some common features, including a similar recurrence interval, averaging 85 years, strong shaking on the coast, coastal uplift, and moderate tsunamis. These effects, which suggest their ruptures took place deep in the megathrust, occurred mostly between, or with modest extension into, the rupture zones of the latest large earthquakes in 2010 and 2015. Yet, the 1822, 1906 and 1985 earthquakes differ from one another in the details of their latitudinal extent and the location of their results. The effects of the 1906 event, which of the four earthquakes seems to be second in size to the 1730 earthquake, extended southward through the northern third of the 2010 rupture area. In contrast, the 1822 and 1985 events were likely smaller, similar in size, and with effects centered in Metropolitan Chile, but with the effects extending slightly to the north in 1822 and to the south in 1985.

Because the effects of the 1730 event are well documented (Urbina et al., 2016), and those of 1985 were recorded by modern instruments, published surveys, and papers (e.g. IGM, 1985; Plafker, 1985; Kausel, 1986; Comte et al., 1986; Barrientos 1988, 1995, 1997; Mendoza et al., 1994), this supplementary table focuses on the lesser studied earthquakes of 1822 and 1906.

Earthquake and Tsunami of November 19, 1822

On November 19, 1822, a large earthquake struck central Chile. The mainshock occurred between 10:30 and 11:00 PM, local time (**records 1, 2, 3, 4, 5, 6, 8, 10, 13, 15**) and lasted between 2 and 3 minutes (**1, 2, 4, 5, 6**). Shaking produced severe building damage in a region 260 km long, extending from Illapel in the north (**3**) to Rapel in the south (**12**). Shaking, damage and casualties were conspicuously larger in the coastal localities (**2, 4, 5, 6, 10, 12, 13**). The focus of shaking was located in an area including Valparaíso itself (**12**), or locations "somewhat" to the south (**13**), or 24 km northeast of this city (**12**). Coastal shaking generated ground cracks, landslides, and liquefaction features (**8, 9, 10, 13, 14)**. A very strong seaquake was felt on the ships anchored in Valparaíso bay (**8, 15**).

The coast of central Chile was evidently and suddenly raised as a consequence of the earthquake (**8, 10, 11, 12, 13, 15, 16, 17**). Uplift estimates made by the eyewitnesses, based on changes in the levels of tides and exposed and displaced sessile marine organisms attached to the rocks, agree well among them. Reports of uplift at Valparaíso bay include five estimates of around 0.9 m (**8, 10, 11, 12, 13**), and one ranging between 0.6 to 1.8 m (**17**). The coast of Quintero was uplifted even higher, about 1.2 m (**10, 11, 15**). Broad estimates for the whole raised coast also fall in this range, between 0.6 m and 1.2 m (**10, 11, 12**). In contrast, reports on the extension of such uplift along the coast differ. They range from 70-80 km (**8, 13**), through 160 km (**11**), to 220 km (**15**). One of the sources reports that the larger uplift occurred at the same locations as the most severe shaking was suffered (**12**). Subsequent observations of the dry remains of rocky intertidal organisms above their living range, made nine years after the 1822 earthquake, suggest the persistence of the uplift (**16**). A gradual uplift may have continued after the earthquake for as much as 22 years (**18**). The latter would agree with Charles Darwin's inference in 1834 (**19**) that coastal uplift at Valparaíso had been a long-term, gradual process, and being just interrupted and enhanced by sudden uplift during the earthquake.

Despite all these conspicuous results, the 1822 earthquake triggered only a moderate, non-destructive tsunami, with effects smaller than expected by the eyewitnesses (**10, 12**). One testimony describes it just as "The sea has not made a greater demonstration; it withdrew a little and filled back again the part it had emptied" (**9**). The tsunami consisted of three strong sea advances and retreats (**8**). While the first sudden rise of water level accompanied the mainshock (**8, 12, 13**), a subsequent and higher rise reached about 3.6 m over the ordinary sea level (**1, 8, 12**). This wave left a landing boat "higher than any boat had been before" (**10, 12**). The subsequent retreat was described as "frightful" (**10**) and left moored boats abruptly dry (**10, 11, 15**). Some eyewitnesses "fully expected a return, and the probable drowning of the town; but the water came back no more" (**10**). Another opined that none of the waves were "as violent as might have been expected" (**12**). Soundings of the water depth were made onboard ships during the sequence of waves. One report indicated a shoaling of at least 4 ½ m (**7**), and another described a variation in depth as much as 9 m (**9**). Afterwards, the sea moved in and out five or six times more, pushing the large anchored ships to move landward and seaward (**7**). The tsunami lasted the rest of the night (**9**). Notwithstanding these reports, no source describing actual damage by the tsunami has been found so far.

Record 1

1822

Bernardo O'Higgins, the primary leader of the independence movement that freed Chile from Spanish rule, and who is considered the country's founding father, reported from Valparaíso in his role of Supreme Director (1817-1823) to his government ministers in Santiago. As an eyewitness and wounded victim of the 1822 earthquake, O'Higgins wrote the earliest known document describing the earthquake's effects in Valparaíso. The letter, written 24 hours after the earthquake, gives the first account of damage, movements of sea, and casualties.

Yesterday, at three quarters past ten at night this town [Valparaiso] was plagued by an extraordinary earthquake that in a matter of two or three minutes, […] collapsing or ruining all the buildings, excepting neither temple nor house, either public or private; meantime the sea swung by a distance of 12 feet of elevation; […] although the earthquake [shaking] declined, the movement didn't stop at any moment […] until half past four in the morning, since then, until now, the moment when I am writing, the quakes repeat […] at intervals between five and seven minutes, […], fifteen or twenty people […] we know were buried by the ruins; however, confusion impedes [the effort] to fix the number of victims that, very likely, is much larger.

Ayer a las diez y tres cuartos de la noche fue plagado este pueblo [Valparaíso] de un terremoto tan extraordinario que en obra de dos o tres minutos, […] se desplomaron o quedaron ruinosos todos sus edificios, sin exceptuarse templo ni casa alguna pública o particular; el mar entretanto se balanceó por la distancia de más de doce pies de elevación; […] fue declinado el terremoto pero no cesó un solo instante el movimiento […], hasta las cuatro y media de la mañana, desde cuya hora […] hasta el momento en que escribe, que se repiten los temblores […] por intervalos de cinco a siete minutos, […] quince o veinte personas […] que sabemos haber sepultado las ruinas; bien en que la confusión impide fijar el número de las víctimas que, con grande probabilidad, es mucho mayor.

Source: "Oficio a los Delegados Supremos de Gobierno de Hacienda y Guerra". *Dated:* November 20, 1822 in Valparaíso. *Collected in:* Gazeta Ministerial de Chile, Tomo III, 1822-1823.

Bernardo O'Higgins (1778-1842), was caught by the 1822 earthquake in Valparaíso when facing serious political problems. During the earthquake he was wounded by a falling wall in the back.

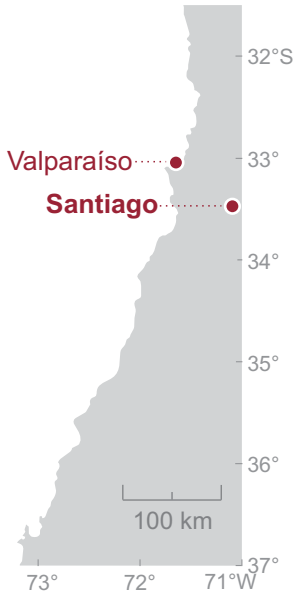

Record 2 1822

*Answering the letter sent by Bernardo O´Higgins on the 1822 earthquake's effects in coastal Valparaíso (**record 1**), the government ministers, Joaquín de Echeverría and José Antonio Rodríguez, replied two days later, on November 22 from Santiago, describing the consequences inland, in the country's capital. This reply makes clear that the effects in that city were not as severe as those observed in coastal Valparaíso as described by the Supreme Director.*

When at this date we received the honorable note of HE [His Excellency] of the current [month] 20, we were giving active remits […] because the earthquake of the night of 19, […] gathering data and observations to inform HE about the event and its results […]. The Capital didn't experience such a terrible catastrophe that HE has witnessed in Valparaíso, […]. On Tuesday 19 of the current at ten to eleven at night, […] a horrid noise announced and preceded by few seconds an earthquake that hadn't been experienced since 1730. Its explosion manifested by two strong shakes, which lasted between two and a half and three minutes; […]. It was believed the total ruin of the city. The concern was general, but happily there were not more disgraces than some people injured by fragments, falling from the buildings, or by the flying roof tiles.

Cuando en esta fecha recibimos la honorable nota de V. E. S. [Vuestra Excelencia Suprema] 20 del corriente, nos hallábamos dando activas providencias, […] por el terremoto de la noche del 19, […] reuniendo datos y observaciones para continuar a V. E. S. el suceso y sus resultados […]. No experimentó la capital esa terrible catástrofe que V. E. S. ha presenciado en Valparaíso, […]. El martes 19 del corriente a las diez horas 50 minutos de la noche, […] un ruido horrendo anunció y precedió de algunos segundos el terremoto que no se había experimentado desde el 1730. Su explosión se manifestó por dos fuertes concusiones, que durarían de dos y medio a tres minutos; […]. Se creyó la ruina total de la ciudad. La consternación fue general, pero felizmente no ha habido más desgracias que las de algunas personas heridas por los fragmentos, que caían de los edificios, o por las tejas que volaban.

Source: "Contestación-Contéstese con lo observado-Echeverría-Rodríguez-Muxica, Subsecretario". *Dated:* November 22, 1822 in Santiago. *Collected in:* Gazeta Ministerial de Chile, Tomo III, 1822-1823.

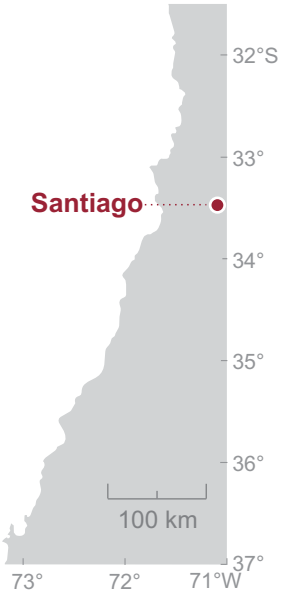

Record 3 1822

On November 22, three days after the 1822 earthquake, José del Solar, mayor of the inland mining town of Illapel, located 210 km north of Santiago, reported to the central government in Santiago about the effects of the earthquake. This record is significant because it identifies the northernmost known place where the earthquake produced significant building damage.

Announcing to HE [His Excellency] the sad catastrophe this town has experienced. On 19 of the current [month], between ten and eleven o'clock at night came a very strong earthquake that shaking the land with a strange movement it demolished all the buildings overthrowing most of them, leaving the town almost ruined, and its ill-fated inhabitants covered by panic concern […]. In middle of so much confusion nothing worries us more than the unhappy state to which the only two churches in our compound were reduced, […].

Al anunciar a V.E. [Vuestra Excelencia] la lamentable catástrofe que ha experimentado esta Población […]. El 19 del corriente entre diez u once de la noche sobre vino un fuertísimo terremoto que estremeciéndose la tierra con un extraño movimiento demolió todos los edificios derribando los más de ellos, dejando al Pueblo cuasi arruinado, y a sus infelices habitantes cubiertos de una pánica consternación […]. En medio de tanta confusión nada nos aflige más que el estado infeliz que han quedado reducidas las dos Iglesias únicas que teníamos en el recinto de la Población, […].

Source: "José del Solar Informa de los perjuicios ocasionados por el terremoto del día 19 de noviembre de 1822". *Dated:* November 22, 1822 in Illapel. *Collected in:* Archivo Nacional, CG, Vol. 813, Fjs. 257-258.

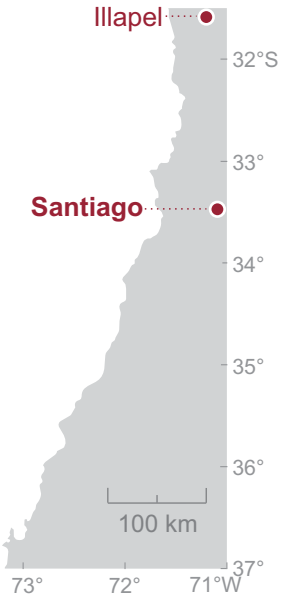

Record 4 1822

One of the only two regular contemporary periodicals in Santiago, El Cosmopolita, published on November 23, three days after the 1822 earthquake, an article highlighting the building damage in Santiago. The article reports, by hearsay, damage outside Santiago, including in the two seaward towns of Casablanca and Melipilla and in Aconcagua to the north, where larger destruction seems to have happened.

Dreadful earthquake in Chile. On November 19 […] at forty-five past ten at night […]. preceded by a formidable rumble; […] two violent shocks that would last about three minutes, suggesting the total ruin of the Capital […]. The taller buildings have received considerable damage, particularly the Cathedral, La Merced [church], S. Agustín [church], the Director's Palace, the towers of the Cajas and Jail, the Mint, etc. […]. According to the news received so far, the greatest damage has been experienced in Valparaíso, the ruin of the churches and houses being almost total […]. Casa Blanca [town] is levelled […]. The ruin of Melipilla, Aconcagua and other places is variously described.

Terremoto espantoso en Chile. El 19 de noviembre […] A las diez y tres cuartos de la noche […], precedido de un estruendo formidable; […] dos violentísimas conmociones que durarían como unos tres minutos, amagando la total ruina de la Capital […]. Los edificios de más elevación han recibido bastante daño, particularmente la Catedral, la Merced, S. Agustín, el Palacio Directoral, torres de las Cajas y Cárcel, Casa de Moneda, etc […]. Según las noticias recibidas hasta ahora, los mayores estragos se han experimentado en Valparaíso, siendo casi total la ruina de las Iglesias y casas […]. Casa Blanca [pueblo] está por tierra […]. Se habla con variedad de la ruina de Melipilla, Aconcagua y otros puntos…

Source: "Terremoto espantoso en Chile". *Collected in:* El Cosmopolita, Santiago. *Dated:* November 23, 1822, N°15, p. 9-10.

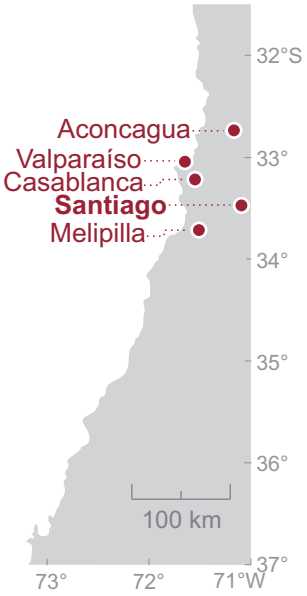

Record 5

1822

A little more than a month after the 1822 earthquake, El Mercurio de Chile, the other monthly periodic published in Santiago, included an article on the effects of the earthquake outside the capital. It reports that Santiago didn't suffer as much as did the cities located to the northwest, included Valparaíso, which were completely ruined.

At 10 hours and 54 minutes in the evening a terrible tremor was felt that lasted two and a half minutes. In the capital, it did not cause any damage worthy of consideration, but outside the capital the havoc and losses were lamentable. Valparaíso, Quillota, la Ligua, Casablanca, were entirely ruined. The houses and fences of a large number of haciendas and farms fell. It seems that the number of dead will not exceed two hundred. We still do not know to how many millions will mount losses, and we do not yet know the extent of the harm and ruins. The earthquake was not preceded by any subterranean noise [...] For now it is desirable [...] that the towers, both ruined and unruined, be demolished, for they are always menacing: that the displaced tiles be taken out; that the roads be repaired; and that the unhappy people of Valparaiso be helped.

A las 10 horas y 54 minutos de la noche se sintió un temblor espantoso que duró dos minutos y medio. En la capital no causó daño alguno digno de consideración, pero fuera de ella los estragos y pérdidas fueron lamentables. Valparaíso, Quillota, la Ligua, Casablanca, fueron enteramente arruinados. Han caído las casas y cercas de un gran número de haciendas y chácaras. Parece que el número de muertos no pasará de doscientos. Aun no sabemos a cuantos millones montarán las pérdidas, y no conocemos aún la extensión de los males y ruinas. El terremoto no fue precedido de ruido alguno subterráneo […]. Por ahora es de desear […] se derriben las torres tanto ruinosas como las no ruinosas pues son siempre amenazantes: que se separen las tejas movidas; que los caminos se reparen; y que los infelices de Valparaíso sean auxiliados.

Source: "19 de Noviembre de 1822". *Collected in*: El Mercurio de Chile, Santiago.
Dated: December 2, 1822, N°16, p. 323-324.

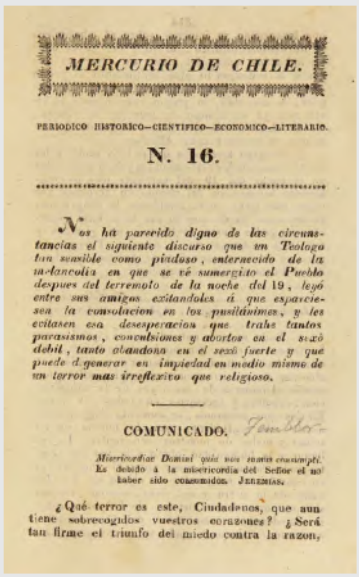

MERCURIO DE CHILE.

PERIODICO HISTORICO—CIENTIFICO—ECONOMICO—LITERARIO.

N. 16.

No ha parecido digno de las circunstancias el siguiente discurso que un Teologo tan sensible como piadoso, enternecido de la melancolia en que se vé sumergido el Pueblo despues del terremoto de la noche del 19, leyó entre sus amigos exitandoles á que esparciesen la consolacion en los pusilánimes, y les evitasen esa desesperacion que trahe tantos paraxismos, convulsiones y abortos en el sexô debil, tanto olvidados en el sexô fuerte y qué puede degenerar en impiedad en medio mismo de un terror mas irreflexivo que religioso.

COMUNICADO.

Misericordiæ Domini quia non sumus consumpti. Es debido á la misericordia del señor el no haber sido consumidos. JEREMIAS.

¿Qué terror es este, Ciudadanos, que aun tiene sobrecogidos vuestros corazones? ¿Será tan firme el triunfo del miedo contra la razon,

El Mercurio de Chile (1822-1823), was a monthly periodic founded by the Chilean Friar Camilo Henriquez (above), a priest, author, and politician. He is considered a pioneer intellectual, strongly influenced by French Enlightenment philosophy, and founding father of the Republic for his passionate leadership and influential writings. The Mercurio was focused on history, social and administrative sciences, political economy, and literature.

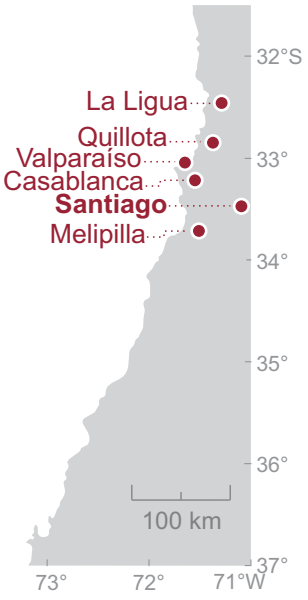

Record 6 1822

The national magazine Niles' Weekly Register, issued in Baltimore, USA, published in May 17, 1823 a letter from a "Bostonian, residing at Valparaiso, to a gentleman in Boston". The letter, dated November 26, 1822 at Valparaíso, describes the effects of the 1822 earthquake. The Bostonian emphasizes that inland Santiago suffered comparatively lesser damage than coastal Valparaíso. Reinforcing this difference between the effects in coastal towns from those inland, the writer tells that a captain just arrived in Valparaíso informed him that in coastal San Antonio, south of Valparaíso, the shock was "most terrible".

The present is principally to acquaint you of the effects of a most tremendous and terrible earthquake, which was experienced here on the evening of the 18th. It took place between 10 and 11 o'clock, and the first shock, which was probably of two or three minutes duration, laid the greater part of Valparaiso in ruins, […]. Many lives were lost by the fall of buildings, but the number has not been ascertained; and nearly 200 are known to have perished and others are missing; many too were wounded severely, among whom was the supreme director, […]. The churches are, some of them, levelled to the ground […]. Some of the neighboring towns and villages are entirely ruined, and there was the most painful apprehensions respecting the fate of the capital, (Santiago), but fortunately that city has escaped with comparative trifling injury. […]. Capt. Scott, of the Ida, who has since arrived here, was that evening on shore at St. Antonia [sic], a little port about 30 miles to the S. where the shock was most terrible […].

Source: "Earthquakes at Valparaiso". *Dated:* November 26, 1822 in Valparaiso. *Collected in:* Nile's Weekly Register, Baltimore. May 17, 1823. N° *11, Vol. XXIV, pp 171-172.*

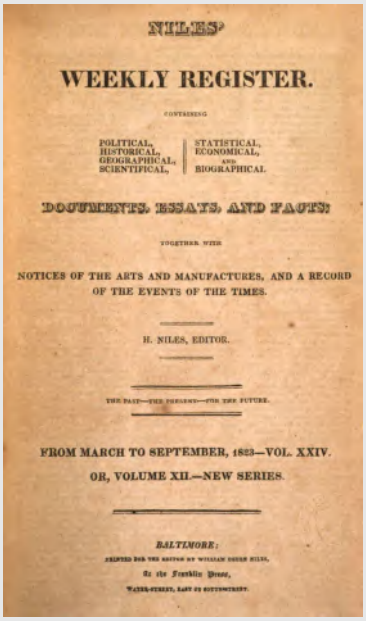
NILES'

WEEKLY REGISTER.

CONTAINING

POLITICAL, HISTORICAL, GEOGRAPHICAL, SCIENTIFICAL, | STATISTICAL, ECONOMICAL, AND BIOGRAPHICAL.

DOCUMENTS, ESSAYS, AND FACTS;

TOGETHER WITH

NOTICES OF THE ARTS AND MANUFACTURES, AND A RECORD OF THE EVENTS OF THE TIMES.

H. NILES, EDITOR.

THE PAST—THE PRESENT—OUR FUTURE.

FROM MARCH TO SEPTEMBER, 1823—VOL. XXIV.

OR, VOLUME XII.—NEW SERIES.

BALTIMORE:

PRINTED FOR THE EDITOR BY WILLIAM OSBORN NILES,

At the Franklin Press,

Calvert-street, East of Gay-street.

Niles' Weekly Register (1811-1848), was a national magazine published in Baltimore, Maryland by Hezekiah Niles. In issue N° 11, Vol. XXIV, May 17, 1823, (left) it printed a letter from a Bostonian living in Valparaíso describing the 1822 earthquake's effects. Although the article's heading states the letter was "dated November 26th, 1823", it must be a typo, because the magazine issue was released in May 17, 1823. From the reading of the letter, it seems clear that the eyewitness describes a recent event, including basic information still unknown for him. Thus, we infer the letter was actually dated November 26th, 1822, one week after the earthquake.

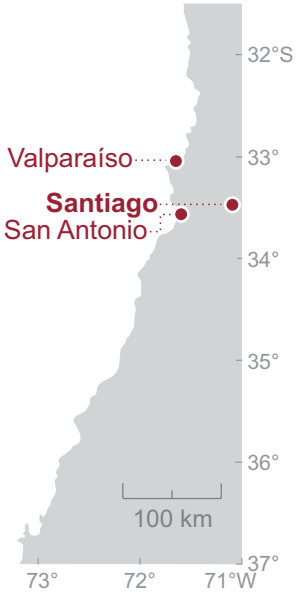

Record 7 1822

*Nearly a month after the 1822 earthquake, Mr. I. Robinson, "a gentleman of Virginia", who was in Valparaíso when the earthquake happened, sent a letter to the editor of the Nantucket Inquirer of Massachusetts. After describing the effects of shaking, Mr. Robinson focuses on the ensuing sea movements reported by seamen onboard a ship anchored in Valparaíso bay. Remarkably, they sounded the water depth with a lead during the sea movements. The water shoaled 2½ fathoms, probably about 4 ½ m using the most common, but not universal, contemporary definition of the fathom as 6 feet in the early 19th century. Such a great retreat agrees well with the effects reported by other accounts: "[the sea] retire[d] frightfully, and [left] many of the launches and other small vessels dry" (**record 10**), and "The launches, [...], which were moored about a hundred yards from the landing place, were suddenly left dry" (**15**). More valuable information on the sea movements is that large anchored ships swung landward and seaward five or six times, and that those movements involved strong currents as deduced from the "extraordinary vibration" of the sounding led.*

The catastrophe occurred in the night of the 19th of Nov., 1822. […] at half past 10 o´clock, P.M., appalling shocks of an earthquake began; every thing on the surface was in motion; the hills near at hand, oscillated; the ground rose and fell; houses reeled, like ships on the ocean; trees waved as if bent by a blast of wind […], the sea retired, and the tremendous convulsion seemed to threaten universal dissolution. […] On board ships, it was observed by sounding, that the water shoaled two and a half fathoms; vessels of war at their moorings, swung five or six times inshore and out again; as there was no wind and as it was low water with a smooth sea. When the lead was thrown; it seemed to catch, as if pinched in a fissure, first made and then closed by the earthquake; it sometimes required two persons to draw it up, and it was observed to swing with an extraordinary vibration.

Source: Letter extracted from "Earthquake and rising of the sea coast of Chili, in November, 1822". *Collected in:* The American Journal of Science and Arts, Vol. XXX, July, 1836. pp. 110-113. *Dated:* December 15, 1822 in Valparaíso.

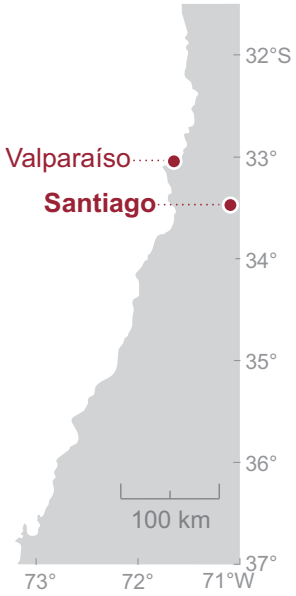

Record 8 1822

*After the 1822 earthquake the governor of Valparaíso, General José Ignacio Zenteno, requested a report on the earthquake's effects from engineer Carlos Thurn. Although the account, released five weeks after the earthquake, mainly deals with damage and casualties, it also highlights natural effects on the coast, including sea movements and land level changes. However, Thurn's report is a bit ambiguous, without clearly differentiating between vertical and horizontal estimates. First, he describes the tsunami as "the water raised to the height of 12 feet over its ordinary level" but then he reports "more striking has been that since then the sea was left retreated 8 to 10 feet from land." The latter might possibly be interpreted as a permanent land uplift of 8 to 10 feet, but it seems much more likely that here he is describing a horizontal displacement of the strandline owing to the uplift of the land that he describes elsewhere of about "3 feet". Such ambiguity casts doubt on the reported tsunami height of 12 feet; however, two other accounts mention the same elevation using different wording: "the sea swung by a distance of 12 feet of elevation" (**record 1**), and "a man-of-war's boat [...], landed at the door of the Custom-house, which is twelve feet above the usual high-water mark" (**12**). The engineer also provides the approximate extension of the level changes along the coast, which "have been observed up to the distance of 7 to 8 leagues windward and leeward". Since southerly wind prevails in Valparaíso, he must refer to land level changes along ~70-80 km along the coast, counting ~35-40 km southward and ~35-40 km northward of the destroyed city.*

At 10 and 50 minutes at that night […] the land was suddenly shaken with so extraordinary violence that it scarcely gave time to escape from […] the falling buildings, […], it lasted […] 40 seconds, […] 66 people among the death and missing, […] 110 […] injured and battered. The governor's house, forts, and jail were completely levelled. The customs house, […] post office, warehouses […], and hospitals […] were left useless, […]. La Matriz church was left mistreated, […] The one of Santo Domingo was lost […]; the same for the one of San Francisco and its convent; [and] the one of Merced and its convent […]. The ruined private houses are about 700 […]. During the violence of the earthquake three advances and retreats were observed in the sea, in the higher of them the water raised to the height of 12 feet over its ordinary level; but the more striking has been that since then the sea was left retreated 8 to 10 feet from land […], such phenomenon is seen in the harbor, and all nearby beaches that have been observed up to the distance of 7 to 8 leagues [~35-40 km] windward and leeward; thus, it is believed that a large part of this coast was raised at least 3 feet over the water level […]. [In] the moment of the great quake […] it was observed in the war [ships] that the cannons jumped vertically, […]. In many streets […] cracks were made four inches wide [,] many steps long, and diverse feet deep, […].

A las 10 y 50 minutos de esa noche […] se conmovió súbitamente la tierra con tan extraordinaria violencia que apenas dio tiempo al vecindario para huir de […] los edificios que se desplomaban, […], duró […] 40 segundos, […] entre las personas muertas y que se echan menos 66 individuos, […] heridos y contusos […] 110 […]. La casa de gobierno, cuarteles y cárcel vinieron enteramente abajo. La aduana, […] correos, almacenes […], y hospitales […] quedaron […] inútiles, […]. La Iglesia Matriz quedó bien maltratada, […]. La de Santo Domingo fue perdida […]; lo mismo la de San Francisco y su convento; [y] la de la Merced y su convento […]. Las casas particulares arruinadas se aproximan a 700 […]. Durante la violencia del terremoto se observaron en el mar tres fuertes accesos y recesos, elevándose las aguas en el mayor de ellos a la altura de 12 pies sobre su nivel ordinario; pero lo más notable ha sido que desde entonces ha quedado retirado el mar 8 a 10 pies de la tierra […], cuyo fenómeno se ve en la bahía, y en todas las playas inmediatas que han sido observadas hasta la distancia de 7 a 8 leguas [~35-40 km] a barlovento y sotavento; de suerte que se cree que una gran parte de esta costa se ha elevado 3 pies a lo menos sobre el nivel de las aguas. [En] los momentos del gran temblor […] se observó en los [buques] de guerra que los cañones saltaban verticalmente, […]. En muchas calles […] se hicieron hendiduras de una hasta cuatro pulgadas de ancho [,] de muchos pasos de largo, y de diversos pies de profundidad, […].

Source: "Descripción de los estragos que causó en Valparaíso el terremoto del 19 de noviembre de 1822, con las posteriores observaciones que se han hecho. Informe dirigido al señor Brigadier y Gobernador de la Plaza de Valparaíso, don José Ignacio Zenteno, por don Carlos Thurn*". Dated:* December 30, 1822 at Valparaíso. *Collected in:* Revista de Historia y Geografía, 1919. Tomo XXI, p. 189-193.

José Ignacio Zenteno (1786-1847), was a soldier, politician and hero of the Chilean War of Independence. He was entrusted with the formation of the First Chilean Navy Squadron, and laid the foundation of the Chilean Navy. By 1822, after retiring from the ministry of war, he was appointed political and military governor of Valparaíso.

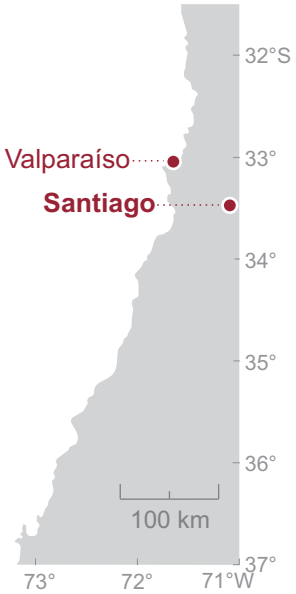

Record 9 1822

Nearly two months after the 1822 earthquake, in January 15, 1823, the Argentinian periodical La Abeja Argentina published an article on the 1822 Chilean earthquake. The narrative style suggests that the unidentified author intended the article as a compilation of letters sent by eyewitnesses. Two aspects highlighted by the compilation are significant to characterize the event. First, it divided the area affected by the earthquake in two large parts; while most damage occurred north of Santiago, much lesser was to the south. This point is supported by identifying the specific affected localities and the effects on them. Second, it describes the resulting tsunami in Valparaíso as a long-lasting sequence ("it remained all night") of sea advances and retreats, but without causing damage on the coast. As remarkably as that reported in ***record 7****, an eyewitness onboard a ship also sounded the water depth with a lead during the tsunami. When gauging, the water level oscillated five fathoms, about 9 m. Such a great change agrees well with the effects reported by other accounts (****7, 10, 12, 13, 15****).*

Happily the first movements [in Santiago] were by undulation and so all the main damage has been experienced on the roofs that started throwing tiles. There isn't a building in the city that hasn't suffered, mainly the temples. […]. In the countryside it was generally ruinous, particularly to the north. The hacienda of Polpaico [...] was destroyed in all of its buildings: the ground opened up in many places, and it is assured that water came out of some of them. The [houses] of Colina were included in the total. The city of San Felipe [...] was almost entirely demolished, [...]. The village of Los Andes suffered the same fate. Putaendo and Quillota the same.

To the south, nothing of consequence is heard; it seems that it was more benign there. In Melipilla they suffered quite a lot. […]. In Rancagua they have not experienced significant damage, as only the roofs had suffered. […]. I have several letters from Valparaíso [...]. One of them [...] reads as follows […]. The sea has not made a greater demonstration; it withdrew a little and filled back again the part it had emptied. Don Onofre Bunster, who was in Valparaíso on the night of the earthquake, told me that after he was caught walking on the beach in front of his house, he wanted to climb the near hill, but that he could not make it [...], for which reason he returned to the resguardo [custom office's landing place] to take a boat, to embark [...]. So he saw himself on board his ship [,] he set out to observe the movements of the sea, and to that end he threw his sounding lead and found 13 fathoms of water; soon after he did the same operation and there were only eight fathoms, in this alternative of access and retreat it remained all night without causing the least damage on land.

Felizmente los primeros movimientos [in Santiago] fueron por ondulación y así es que todo el daño principal se ha experimentado en los techos que empezaron a despedir tejas. No hay un edificio en la ciudad que no esté sentido, principalmente los templos. […]. En la campaña fue generalmente ruinoso en todo el lado norte con particularidad. La hacienda de Polpaico […] fue destruida en todos sus edificios: la tierra se abrió en muchas partes, y se asegura que de algunas salió agua. Las [casas] de Colina se incluyeron en el número. La ciudad de San Felipe […] fue casi demolida enteramente, […]. La villa de Los Andes corrió la misma suerte. Putaendo y Quillota por el tenor. De los lados del sur no se oye decir cosa de consecuencia; parece que allí fue más benigno. En Melipilla sufrieron bastante. […]. En Rancagua no se han experimentado daños de consideración, pues sólo han padecido los tejados. […]. Tengo varias cartas de Valparaíso […]. La una de ellas […] dice a la letra como sigue: […]. La mar no ha hecho mayor demostración; se retiró muy poco y volvió a llenar la parte que había vaciado. Don Onofre Bunster que se hallaba en Valparaíso en la noche del temblor, me ha dicho que habiéndole tomado paseándose en la playa al frente de su casa, quiso subir al cerro inmediato, pero que no pudo conseguirlo […], por cuyo motivo se volvió al resguardo [área de desembarco de la aduana] a tomar bote, para embarcarse, […]. Así que se vio a bordo de su buque [,] se propuso observar los movimientos del mar, y al efecto tiró la sondaleza y encontró 13 brazas de agua; al poco rato hizo la misma operación y solo había ocho brazas, en esta alternativa de acceso y retroceso permaneció toda la noche sin causar en tierra el menor daño".

Source: "Temblor en Chile". *Dated:* January 15, 1823 in Buenos Aires. *Collected in:* La Abeja Argentina, N° 10, pp 35-40.

LA

ABEJA ARGENTINA.

NUM. 14.

15 DE JUNIO DE 1823.

Este periódico saldrá el 15 de cada mes: se vende en la vereda ancha tienda de Ochagavia á 4 reales cada número: tambien se admiten subscripciones á 3. pesos cada semestre.

Apes favos struunt melicos, nectare florum
melle, fructibus dulcibus vicitantes.
Linne. sist. nat. 248.
Buenos Aires año de 1823.

IMPRENTA DE LA INDEPENDENCIA

La Abeja Argentina (1822-1823), was a monthly Argentinian periodical published by the Literary Society of Buenos Aires. Although the main focus of the publication was the political news of the new Republic, it had a section of varieties that included discoveries, tales, biographies, and meteorological observations.

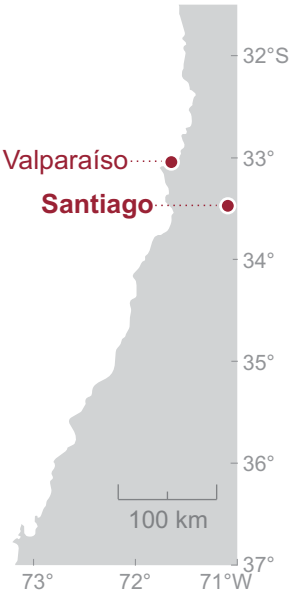

Record 10 1822

*Likely the most complete, detailed and famous account on the 1822 earthquake was written by Maria Graham, a well-known 19th century British writer, in her personal journal (published in 1824). She was caught by the earthquake when living in Chile, in a house high on a hill facing Quintero bay, 30 km north of Valparaíso. With almost scientific devotion, she wrote daily entries on the aftershocks and earthquake's results during the two following months. This was accomplished using both her own observations and the testimonies of other survivors. She made purposeful post-earthquake observations on horseback and boat trips between Quintero and Valparaíso. Some trips were made together with Lord Cochrane, the then expatriate former British admiral who at the time was completing a stint as admiral in the Chilean Navy. She wrote, for example: "we went chiefly for the purpose of tracing the effects of the earthquake along the rocks." The territory she surveyed also included the intermediate coastal localities of Concon and Viña del Mar; and those landward of Quillota, Casablanca, and Valle Alegre. Her account of land level changes, far ahead of its time, was judged so significant that it found its way into the Transactions of the Geological Society of London (1824) and into one of the most important geology book ever written: Principles of Geology by Charles Lyell (1830) (**record 11**). Her account is key for our case of a deep rupture in 1822; first, because it offers strong evidence for uplift, including dead sessile organisms still attached to rocks and man-made structures out of place, both tied to changes in sea level. Second, Graham gives details on the tsunami, particularly an extraordinary recession of the sea. Both these observations suggest a rupture largely inland from the coast and down dip.*

[...] at a quarter past ten, the house received a violent shock, […] the chimneys fell, and I saw the walls of the house open. […]. The shock lasted three minutes […]. At day light I went out of the tent to look at the earth. […] here and there cracks of various sizes appeared in various parts of the hill. At the roots of the trees, […], the earth appeared separate, so that I could put my hand in; […]. In […] the gardens, the earth has cracked, and water and sand have been forced up through the surface […] great fissures are made on the banks of the lake […]. At Concon the whole house in unroofed, the walls cracked, the iron supporters broken, the mill a ruin, and the banks of the mill-stream fallen in […], during the night the sea seems to have receded in an extraordinary manner, and specially in Quintero bay. I see from the hill, rocks above water that never were exposed before; and the wreck of the Aquila appears […] to be approachable dry-shod, […] that was not the case in the lowest tides […]. We heard reports that the large and populous town of Quillota, is a heap of ruins, and Valparaíso is little better. […]. Casa Blanca is totally ruined. […] we learnt that Santiago is less damaged that we expected. […] during the great shock, the sea in Valparaíso bay rose suddenly, and as suddenly retired in an extraordinary manner, and in about a quarter of an hour seemed to recover its equilibrium; but the whole shore is more exposed, and the rocks are four feet higher out of the water than before. […] between la Herradura [Quintero bay] and Concon some rocks and stones that the lowest tides never left dry, have now a passage between them […]. As I approached the river [Aconcagua], the cracks and rents in the alluvial soil almost assumed the appearance of chasms, […] as in Valle Allegri, water and sand have been forced up through the rents. […]. The church of Concon is overthrown, […]. At Viña a la Mar […] the ruin has been complete; […]. The whole of the little plain is covered with small cones from one to four feet high […] from which sand and water had been thrown out. […]. The road between Viña de la Mar and the port is very much injured by the falling of the rocks from above […]. The Almendral presents a sad spectacle: not a house remains habitable; […]. It appears that where the veins of granite rock ran under the foundations, the buildings have stood tolerably well; but wherever any thing was erected on the sand or clay it has been damaged. […]. Mr. C. […] has just arrived from Conception, a distance of 170 leagues, […]. He had passed through Talca and San Fernando; at both of which places, as well as Conception, the earthquake […] had been felt, but not severely. […]. I went to the admiral's ship […] the officers […] told me, that feeling the shock […] Lord Cochrane and others threw themselves immediately into a boat, to go to the assistance […] of the suffers. The rushing wave landed them higher than any boat had been before; and they then saw it retire frightfully, and leave many of the launches and other small vessels dry. They fully expected a return, and the probable drowning of the town; but the water came back no more […]. I had a pleasant walk to the [Quintero] beach […]; we went chiefly for the purpose of tracing the effects of the earthquake along the rocks. At Valparaíso, the beach is raised about three feet, and some rocks are exposed, which allows the fishermen to collect the clam, or scallop, shell-fish […]. Although it was high water, many rocks, with bed of muscles, remain dry, and the fish are dead; which proves that the beach is raised about four feet at [Quintero]. […] we found a long strip or bed of sea-weed, and another of muscles, dead and very offensive; they had never been within reach of the tide since the 19th November.

Source: Graham, M., 1824. Journal of a residence in Chile during the year 1822 and a Voyage from Chile to Brazil in 1823. Longman, Hurst, Rees, Orme, Brown, and Green (Eds.), London. p. 305-347.

Maria Graham (1785-1842), was a British writer of travel and children's books. Born as Maria Dundas she married in 1809 Thomas Graham, a Scottish naval officer. In 1821 she accompanied him, when as the captain of a HMS frigate, he commanded the vessel on an official voyage to Chile. In April 1822, after the ship rounded Cape Horn, her husband died of a fever. When she arrived in Valparaíso she decided to remain in Chile. She spent almost a year in the country witnessing at first hand the political issues of the new Republic and the largest 19th century earthquake of central Chile.

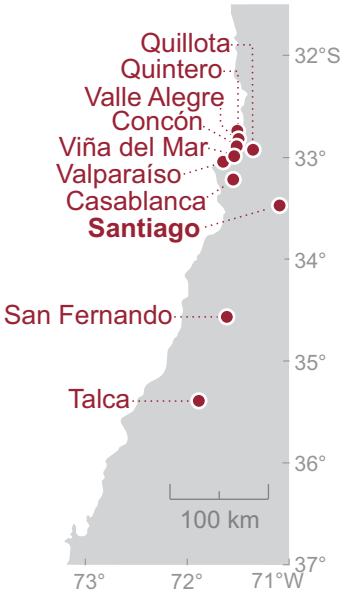

Record 11 1822

*In a more targeted way, Maria Graham (**record 10**) describes her main observations on the effects of the 1822 earthquake in a letter to Henry Warburton, fellow of the Geological Society of London. The letter, written in 1824, was published in the society's transactions as "An account of some effects of the late Earthquake in Chili". Six years later, in 1830, Charles Lyell included this account in Principles of Geology for his case of mountain building (Lyell, 1830, 1832, 1833). The account summarizes the observations formerly recorded in her journal and complements it giving the extension of the raised coast to "one hundred miles", about 160 km. Additionally, she clarifies that after the tsunami in Valparaíso the water did not come back to its "original level", and that the old wreck used as a level reference was not "shifted" horizontally. Finally, she reaffirms that Valparaíso was uplifted "about three feet" and Quintero "about four feet".*

On the first shock, on the night of the 19th of November, the sea, in Valparaiso harbor, rose to a great height, and then receded, so as to leave the small vessels, that were before afloat [,] dry on the beach; it then returned again, but, as compared with the level of the land, not to its original level. All this is stated to have happened in a quarter of an hour. It appeared […], that the whole line of coast, from north to south, to the distance of one hundred miles, had been raised above its former level. I perceived, from a small hill near Quintero, that an old wreck of a ship, which before could not be approached, was now accessible from the land, although its place on the shore had not been shifted. The alteration of the level at Valparaiso was about three feet, and some rocks were thus newly exposed […]. At Quintero, the elevation was about four feet. When I went to examine the coast, […], although it was high water, I found the ancient bed of the sea laid bare, and dry, with beds of oysters, muscles, and other shells adhering to the rocks on which they grew, the fish being all dead, and exhaling most offensive effluvia.

Source: "An account of some effects of the late Earthquake in Chili. Extracted from a Letter to Henry Warburton, Esq. v.p.g.s.*". Dated:* March 4, 1824 in London. *Collected in:* Transactions of the Geological Society of London, Second Series, V.1, pp. 413-415.

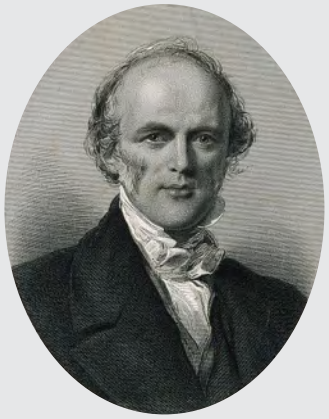

Charles Lyell (1797-1875), was a British geologist who proposed that Earth was shaped by the same natural processes that are operating today. He presented this idea in *Principles of Geology* (1830-1833). When explaining the role of the earthquakes on mountain building he used, among others, the account of Maria Graham on the 1822 Chile earthquake.

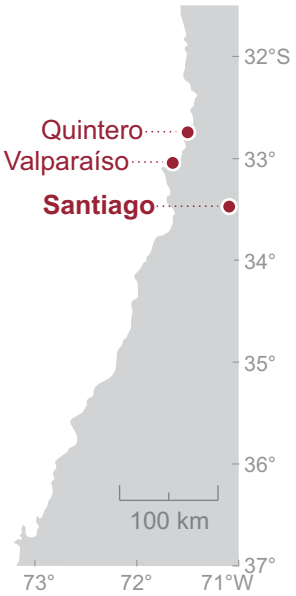

Record 12 1822

*In 1824, well-known English social reformer Francis Place published in The Quarterly Journal of Science the article "Account of the earthquake in Chili, in November, 1822, from observations made by several Englishmen residing in that Country." Although he never visited Chile, he received and compiled letters from residing countrymen. Unfortunately, Place didn't identify the authors of different reports, simply placing their words in quotes. One of them was most likely his son-in-law, John Miers, who published his own experiences two years later (**record 13**). The observations in Place's compilation are important for several reasons. First, they set Rapel (Mapel) as a southern limit for the severe building damage in 1822, focus shaking in Valparaíso, and stress that shaking in Santiago was much less severe than in Valparaíso. Second, they report 0.6 to 1.2 m of coastal uplift, identifying the places, Valparaíso, Concón and Quintero, where submerged rocks were now exposed, adding that the high-water mark is now about 0.9 m lower. Other remarkable observations on level changes are: i) where the most severe shaking occurred, the highest uplift was seen, and ii) in an axis perpendicular to the coast, at the latitude of Concón, the highest estimated uplift (1.5 to 1.8 m) occurred 1.2 to 1.9 km inland, diminishing both landward and seaward. Third, witnesses report that after the earthquake the sea withdrew and returned several times but without the expected violence, and that a boat going onshore in Valparaíso was left stranded at the door of the custom-house, which was about 3.6 m above the usual high-water mark.*

The great earthquake on the night of the 19th of November, 1822, was felt over the whole surface of the country, from the mountains to the sea […]. Its force seems to have diminished in a pretty exact proportion to its distance from Valparaiso. […]. Its effects are thus described by an English man, residing at Concon, […]. "The surface of the country has been raised all along the coast, as far as my information extends. It seems to have been raised highest at the distance of from two to three miles from the shore, diminishing both ways. The rise of the coast is from two to four feet; at the distance of a mile inland, the rise must have been from five to six or seven feet; for in the cut for the tail water course of a mill, at the distance of about a mile from the sea, a fall of fourteen inches has been gained in little more than a hundred yards. "At Valparaiso, near the mouth of the Concon, and along the coast northward to Quintero, rocks have appeared in many places, where none before were visible. The high-water mark along shore is about three feet above the place the tide now reaches, and a vessel, which had been wrecked on this coast, and which could only be approached at low water in a boat, is now accessible on dry land at a half tide. "At Santiago […], the earthquake was less severe; no houses were thrown down, […] no lives were lost. […] but at Casa Blanca, not a single house or wall of any kind was left standing. At Mapel (sic), the shocks were very severe, great part of the village was destroyed, and a pool of water was formed in the market-place. Quillota also suffered to a considerable extent, many houses were destroyed […]. "The greatest force of the earthquake appears to have been felt at the distance of about fifteen miles N.E. of Valparaiso; the whole country, from the foot of the Andes to far out at sea, has been raised; the raise has, however, been very unequal. […]. "[…]. Where the shocks were most severe, the earth has been raised the highest, and its not subsiding again to its former level […]. "During the earthquakethe sea, for a considerable distance along the coast, receded and return several times. […] At Valparaiso, a man-of-war's boat, going ashore, landed at the door of the Custom-house, which is twelve feet above the usual high-water mark. Neither the recussion (sic), nor the retrocession of the sea, were as violent as might have been expected.

Source: Place, F., 1824. Account of the earthquake in Chili, in November, 1822, from observations made by several Englishmen residing in that Country. *Collected in:* The Quarterly Journal of Science, Literature, and the Arts, Vol. XVII, pp. 38-46.

Francis Place (1771-1854) was a noted English social reformer. As a self-educated man, he was involved in a movement for public education as a way to eradicate the working class' problems. He developed diverse projects, including political operations, educational programs and even the first birth control campaign. Since 1818, along with radical politics and utilitarians, he paid attention to the newly independent South America. They saw the region as a political and social laboratory for experimenting with their ideas. They wanted to convince the new governments on the benefits of public education and industrialization. Place went even farther. Violating a British law that prohibited exporting machinery, he smuggled 100 tons of machinery to Chile. He entrusted his son-in-law, John Miers, in this venture; however, the 1822 earthquake hampered their industrialization project (**record 13**).

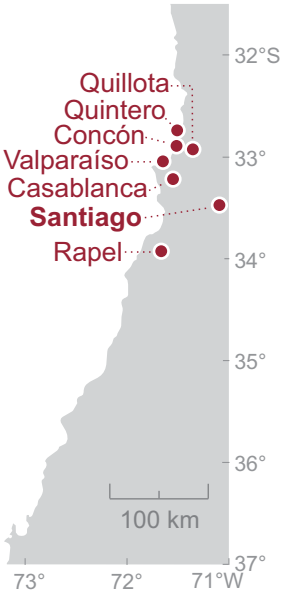

Record 13

1822

*British naturalist John Miers, fellow of the Royal and Linnean societies of London, and son-in-law of Francis Place (**record 12**), was living in Concon, between Valparaíso and Quintero at the Aconcagua river mouth, when the 1822 earthquake struck. He had attempted to develop a business with a modern flour mill moved by the river waters. However, the 1822 earthquake prevented him to reach this goal. Once back in England, he published a book in 1826 about his experiences in Chile and Argentina, which included the traumatic effects of the 1822 earthquake. The same night of the earthquake he was told that the water level at a ford across the Mantagua, a coastal lagoon 5 km north of Concón, had risen by a "great rise of the sea which accompanied the first and most violent shock". Besides indicating a large flood in Mantagua, this assertion is interesting because the rise seems to accompany the mainshock. The same hint appears in the reports of his Quintero neighbor and countrywoman, Maria Graham, "during the great shock, the sea in Valparaíso bay rose suddenly" (**10**), and "On the first shock, […], the sea, in Valparaiso harbor, rose to a great height" (**11**). Miers also agrees with Graham when neatly describing the ground liquefaction effects, the dissimilar shaking results between coastal and inland towns, and the rise of the coast, including its amounts. However, their accounts disagree when reporting the extension along the coast of such land rise; while Graham states "one hundred miles" (**11**), Miers reports just "fifty miles".*

At half-past ten o'clock on the night of Tuesday, the 19th November, 1822 […]. The earth was violently convulsed, heaving up and down in a manner hardly conceivable […]. [It] seemed not only to consist of horizontal oscillations, but also of violent uplifting concussions […] my mills, which were on the edge of the river […] had been thrown down. […] In the course of the night, a friend came from […] Quintero […] he informed us that the ground over which he had passed was much altered, and torn in many places in wide rents. The sand-hills had been thrown into the Quintero lake, and the ford […] was greatly swelled so that the water rose above his saddle. This appears to have been caused by an influx of salt water into the lake, during the great rise of the sea which accompanied the first and most violent shock. […] the morning dawned […]. The ground […] was cracked in all directions. […] clefts above a foot wide […]. On many spots were numerous hillocks of sand and mud, which had been forced through the crevices. They appeared like mud volcanoes in miniature. […] On the Saturday […] I visited Valparaiso […] I was astonished at the extent of the ruin […]. It appears that the centre of the shock was out at sea, somewhat to the south of Valparaiso […] the more inland towns, such as Santiago, Aconcagua, and Rancagua, though shaken severely, and much damaged, were not overthrown like Valparaiso […]. Remarkable as was the extent of this earthquake, […], for all the line of coast of the extent of fifty miles was raised nearly three feet above its former level; in some places the rocks on the shore were raised four feet.

Source: Miers, J., 1826. Travels in Chile and La Plata, including accounts respecting the Geography, Geology, Statistics, Government, Finances, Agriculture, Manners and Customs and the Mining Operations in Chile. Baldwin, Cradock, and Joy (Eds.), London. Vol. 1. p. 388-394.

John Miers (1789-1879), was a British botanist and engineer best known for his later work on plants of Chile and Argentina. He traveled to Chile in 1819 interested in developing industrial businesses in the new Republic. Bringing smuggled machinery from England (**record 12**), he established a modern flour mill in Concón, on the northern bank of the Aconcagua river. Unfortunately, the 1822 earthquake flattened the new venture. After trying other businesses without success, he left Chile in 1825.

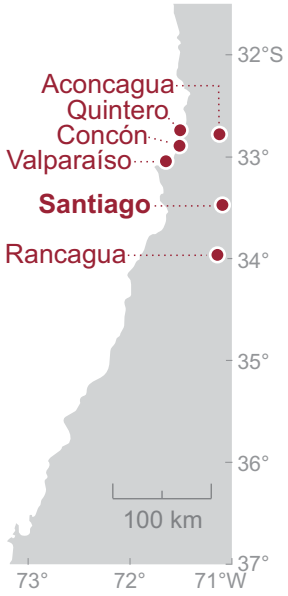

Record 14

1822

*After serving as an officer in the Corps of Engineers of the British Army, between 1811 and 1825, British engineer Francis Head attempted to set up a gold and silver mining company in Argentina. To supervise "certain mines" he traveled, between 1825 and 1826, through the Pampas, crossed the Andes and visited central Chile. Besides his notes on mining, he took a "few rough notes", on "anything which interested or amused me". One of those things were the still visible effects of the earthquake that struck Chile three years earlier, in 1822. Once back in England, Head included these notes in a book published in 1826. His account is one of the few that reports 1822 damage in places other than Santiago and Valparaíso. Petorca, Aconcagua and El Bronce are all located north of Valparaíso and south of Illapel, where the northernmost known destructive effects were reported (**record 3)**.*

[…] we reached the village of Petorca, […]. The church, like that at Aconcagua, was overturned by the earthquake of 1822, and the walls of the houses were cracked and rent from top to bottom. […] we set off […] to visit some trapiches and mills which had existed before the earthquake. We found the roofs shaken from two of the huts, and the rest tottering. The two mills were so completely annihilated, that it was difficult to trace the foundation on which they had stood. […], the following morning […] we started to inspect the gold mines of El Bronce […]. I visited this mine accompanied by a very intelligent Chilean miner, who […] was in a mine on this lode a hundred fathoms deep, when the great earthquake of the 19th of November 1822, […], took place. He told me that several of his comrades were killed, and nothing could equal the horror of their situation. He said that the mountain shook so that he could scarcely ascend; large pieces of the lode were falling down, and every instant they expected the walls of the lode would come together, and either crush them or shut them up in prison from which no human power could liberate them. He added, that when he got to the mouth of the mine […]; large masses of rock were rolling down the side of the mountain […], and he heard them coming and rushing past him without being able to see how to avoid them, and he therefore stood his ground, afraid to move.

Source: Head, F. B., 1826. Rough notes taken during some rapid journeys across The Pampas and among The Andes by Captain F. B. Head. John Murray (Ed.), 1826, London. p. 199-209.

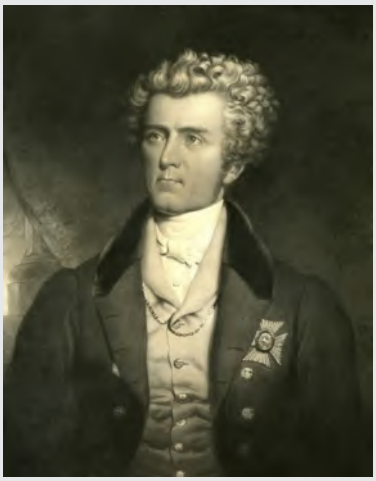

Francis B. Head (1793-1875), was a British officer in the corps of Royal Engineers of the British Army. In 1825 he left the army and accepted a post supervising the mines of the Rio Plata Mining Association. The "Rough Notes" chronicled his travels as a supervisor. One decade later, he become the Lieutenant-Governor of Upper Canada.

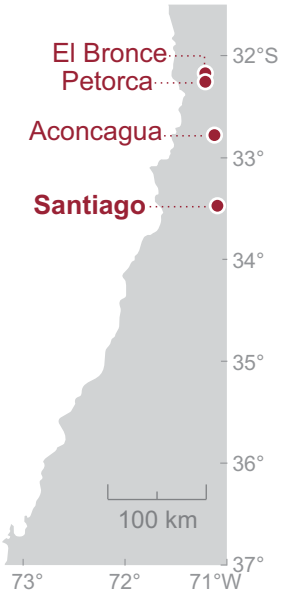

Record 15

1822

*British mercenary Richard Longeville Vowell, a marine infantry officer, joined the Chilean Navy Squadron in November, 1821. Precisely one year later, he was onboard the corvette Independencia, anchored in Valparaíso bay, when the 1822 earthquake struck. Once back in England, he published a book in 1831 in which he tells what he saw and learned about the earthquake. Resembling Maria Graham's accounts (**records 10, 11**), Vowell reports floating boats suddenly left dry during the sea movements, and that the coast of Valparaíso and Quintero bays was raised. Perhaps both compatriots exchanged information at some point; however, for the case of Valparaíso, Vowell is a first-hand eyewitness. A key piece of information, of which perhaps only a seaman would take into account, is what the coasters reported when arrived back to Valparaíso after the earthquake: level changes extended "two degrees along the coast". Such extension, around 220 km at the latitude of Valparaíso, is the largest reported compared with those of Thurn, 70-80 km (**8**), Miers, 80 km, (**13**), and Graham, 160 km (**11**).*

A few months after our arrival in Chile, on the 19th of November, 1822 an earthquake was felt […]. This was by far the most severe that had been experienced, within the memory of the oldest inhabitants […]. At half-past ten at night, the first shock was felt […]; and continued with such violence, that, in a few seconds, every church in Valparaiso was reduced to a heap of ruins. The houses in the Almendral, in particular, which is a sandy soil, were so instantaneously overthrown, that many of the inhabitants perished in the ruins. […]. On board the ships in the bay, the earthquake was felt in a greater degree than could have been supposed possible. […]. The sea boiled up in a succession of short waves, like a ripple caused by the meeting of two strong currents. The launches, used in the harbor for loading and unloading vessels, which were moored about a hundred yards from the landing place, were suddenly left dry. […]. Several sand-banks were raised, and the soundings materially altered, in Valparaiso bay. The little harbor of Quintero, where vessels used previously to anchor in 21/2 to 3 fathoms, was ruined as a port; for the bottom was permanently raised four feet on the night of the 22d. […]. The coasters, which arrived at Valparaiso subsequently to the earthquake, reported that a very considerable alteration in sounding had taken place, near the land and in the little harbours which they frequented, for two degrees along the coast.

Source: Vowel, R. L., 1831. Campaigns and Cruises, in Venezuela and New Grenada, and in the Pacific Ocean; from 1817 to 1830. Longman and Co. (Ed.), London. Vol. 1. p. 290-295.

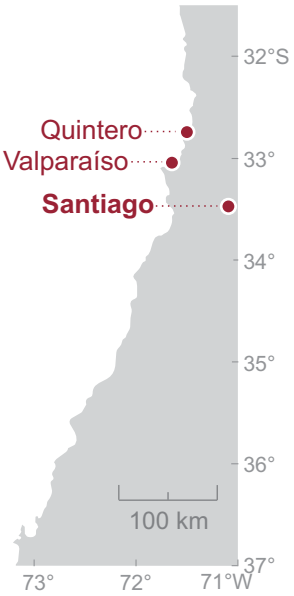

Record 16

1822

Nine years after the 1822 earthquake, Prussian naturalist Franz Meyen visited Valparaíso as a part of a scientific expedition to South America and China on board the royal ship Prinzess Louise. In his double capacity of surgeon and naturalist, he had to collect natural history specimens and make scientific observations during the two-year long world cruise. Meyen spent more than two months, between January and March 1831, in Valparaíso and Santiago taking notes of his observations. When studying the intertidal organisms on the rocky coast of Valparaíso Bay, including algae, which he calls "plants", and animals, he found the same species dead on the rocks uplifted by the 1822 earthquake. He stresses that those rocks are no longer covered by the water and that the organisms died by the resulting sea retreat. This observation is interesting because it suggests that almost a decade after the 1822 uplift, the coast of Valparaíso was still higher.

One afternoon, when the sea breeze was not very strong, we took a trip to the cliffs that are located at the northernmost part of the port, far away from Almendral; we were pleasantly surprised by the extraordinary richness and the diversity of plants and animals, which were covering these syenite blocks lying half under water. They were also among the rocks that were raised 3 to 4 feet above the surface of the sea following the last major earthquake in 1822. Here, on these blocks, some of which are no longer covered by water, all the masses of plants and animals that once inhabited the surface have died; millions and millions of individuals have found their death here, through the retreat of the water.

Eines Nachmittags, als der Seewind gerade nicht sehr bedeutend war, machten wir eine Fahrt nach den Klippen, die am nördlichsten Theile des Hafens, weit oberhalb Almendral hinaus liegen; wir wurden auf das angenehmste überrascht durch den ausserordentlichen Reichthum und dureh die Verschiedenheit der Gewächse und Thiere, welche diese, halb unter Wasser liegenden Sienitblöcke bedecken. Auch sie gehören zu den Felsen, welche in Folge des letzten grossen Erdbebens von 1822, um eine Höhe von 3 bis 4 Fuss über die Oberfläche des Meeres emporgehoben worden sind. Hier auf diesen Blöcken, die jetzt zum Theil nicht mehr vom Wasser gedeckt werden, sind alle die Massen von Pflanzen und Thieren, welche einst die Fläche derselben belebten, abgestorben; Millionen und aber Millionen von Individuen haben hier, durch das Zurücktreten des Wassers, ihren Tod gefunden.

Source: Meyen, F., 1834. Reise um die Erde. Sander'schen Buchhandlung (Ed.), Berlin. Vol. 1. p. 221.

Franz Meyen (1804-1840) was a renowned Prussian physician and botanist. After publishing a pioneer book on plant anatomy (Phytotomie), he took part of the scientific expedition that brought him to visit South America and describe new species such as the Humboldt penguin.

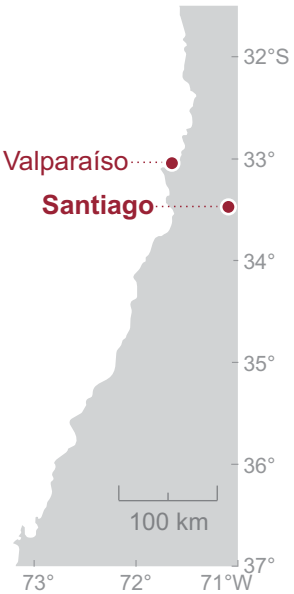

Record 17 1822

*One decade after Maria Graham sent her letter on the 1822 earthquake to the Geological Society (**record 11**); its president, George Greenough, launched a public attack against her during his presidential address to the Geological Society, refuting her account of the rising of the coast by earthquakes (Greenough, 1834). Greenough's attack spurred a broad scientific debate as casting doubt on the validity of Charles Lyell's conclusions (**11**). Amidst the debate, Benjamin Silliman, editor of the American Journal of Science, asked Robert Joy, a Nantucket whaling master who had visited Valparaíso eleven days after the earthquake, to share his testimony. In his letter of reply, dated September 23, 1835, Joy makes clear that the whole coast of Valparaíso bay was obviously raised, a fact evident for others too. He estimates the rocks were between 0.6 and 1.8 m above the "usual tide water mark".*

I find by referring to my journal, that I arrived at Valparaiso on the thirtieth of Nov. ten days after the earthquake [of 1822], and that I left it on the seventeenth of Dec. for the United States […]. The rising of the shore above the usual tide was visible on the whole margin of the bay; it was the cause and the subject of daily remark, among many of my acquaintances, and frequent visits were made to the shores to observe the effects and alterations made by the earthquake upon them. They were most visible on the rocky parts where we found the rocks from two to six feet above the usual tide water mark: […].

Source: Letter extracted from "Earthquake and rising of the sea coast of Chili, in November, 1822". *Collected in:* The American Journal of Science and Arts, Vol. XXX, July, 1836. p. 113. *Dated:* September 23, 1835 in Nantucket.

Robert M. Joy (1793-1862) was a well-known whaling master from Nantucket, MA. In command of the whaling ship Atlas he departed Nantucket in July 16, 1820 and returned in April 4, 1823. Returning home, he stopped on Valparaíso Bay in November 30, 1822, eleven days after the 1822 Chile earthquake.

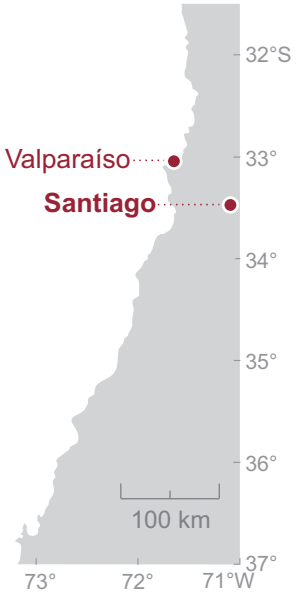

Record 18

1822

*María del Tránsito Cruz de Rosales, an elder neighbor of Valparaíso and owner of several properties on the town´s coast, writes in 1844 a letter to the national Congress' president, in Santiago, demanding her property rights on the neighboring new land left dry by the receding sea. The letter, included in the Congress proceedings, spurred a heated debate among the senators about the property rights on the land abandoned by the sea. One senator states: "It is known that the sea withdraws every day, not only in Valparaiso but also in Coquimbo and in other points of the coast; and if this is true it is convenient to make a general law that includes all these cases". Interestingly, María reports that since 1822 the sea "has slowly withdrawn". She uses the walls of her buildings as a reference for such change, adding that a street and a shed for public supply were built by the Municipality in the land that now is dry. This allusion to a slow withdrawal, in addition to the sudden retreat as a consequence of the 1822 uplift, is remarkable because it fits well with similar inferences made independently by Charles Darwin in 1834 (**record 19**).*

Sovereign Sir: María del Tránsito Cruz de Rosales, before Your Sovereignty I respectfully state: that I have a house and a warehouse in Valparaíso [...], which I inherited from my late father Don Juan Manuel Cruz. Until 1822, the sea bathed the walls of my buildings; but since then it has slowly withdrawn, leaving a portion of the land dry. [...], it was arbitrarily appropriated by the Municipality, having a shed built there for public supply with the condition of provisional [...]. However, despite the fact that the new market building was built later, it did not want to vacate the land on my property [...], where, in accordance with the Congress [...], it declared the land left by the sea to belong to the public, with the new street formed behind the backs of the former owners as its boundary. Therefore, I respectfully request that you declare the aforementioned decree to be of no value or effect [...] insofar as it adversely affects my rights [...] or that the land adjacent to my property, abandoned by the sea and which it will henceforth abandon, belongs to me.

Soberano señor: María del Tránsito Cruz de Rosales, ante Vuestra Soberanía respetuosamente espongo: que tengo una casa i bodega en Valparaíso […], que heredé de mi finado padre don Juan Manuel Cruz. Hasta el año de 1822, el mar bañaba las murallas de mis edificios; pero desde esa época ha ido retirándose lentamente, i dejado en seco una porción de terreno. […], se lo apropió arbitrariamente la Municipalidad, haciendo construir en él un galpon para el abasto público con la calidad de provisional […]. Mas, a pesar de haberse construido después la nueva recova, no ha querido desocupar dicho terreno de mi propiedad, […], en que de acuerdo con el Congreso […] declaró pertenecer al público el terreno dejado por el mar, fijándose por lindero la nueva calle formada a espaldas de los antiguos propietarios. Por tanto, A Vuestra Soberanía, reverentemente suplico, se sirva declarar sin ningún valor ni efecto el referido decreto […] en la parte que perjudica a mis derechos, […], o que me pertenece el terreno adyacente a mi propiedad, abandonado por el mar i que en lo sucesivo abandone.

Source: "Anexos Núm. 76". *Collected in:* Cámara de senadores (Proceedings), Santiago. July 29, 1844, Fourteen session. p. 160.

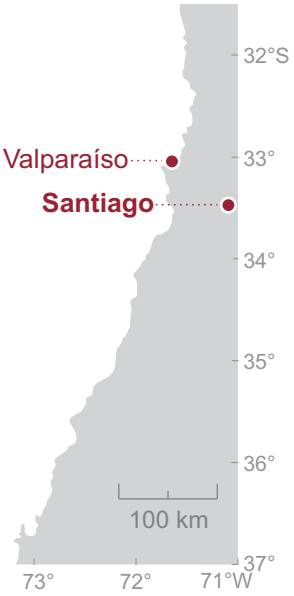

1844

1823

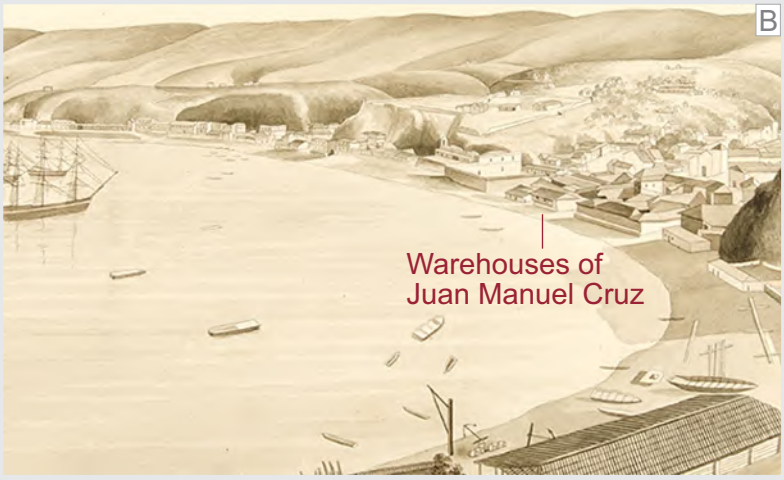

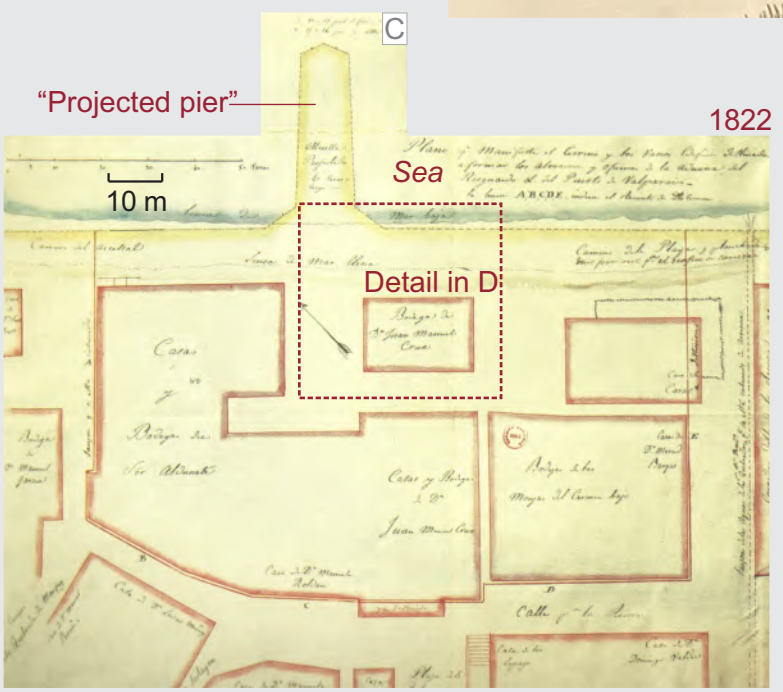

María del Tránsito Cruz de Rosales (1807-) (A), inherited from her father, Juan Manuel Cruz, warehouses located on the very coast of Valparaíso (B). A site plan of these buildings, made likely shortly before the November 19, 1822 earthquake, identifies its owner (C). According to this plan, in 1822 the warehouses were just 5 m horizontally from the high tide line, and 13 m from the low (D). The view of the city taken after the earthquake (B), in 1823, shows Maria's father's warehouses still close to the beach. Nevertheless, in her request to the Congress, written two decades later, she tells that since that time the sea "has slowly withdrawn" and that a large shed for public supply and a new street were made on the land "abandoned by the sea", between her buildings and the new coastline.

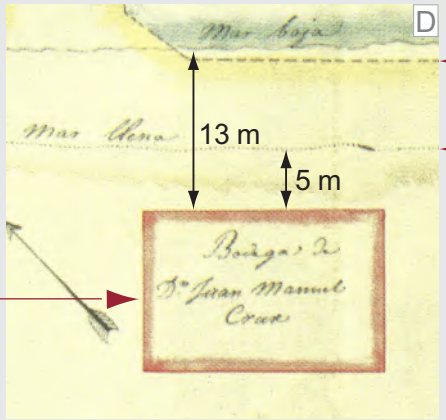

Record 19 1822

The famed second survey expedition of HMS Beagle, from December 27, 1831 to October 2, 1836, intended to conduct a hydrographic survey of the coast of the southern part of South America. Its commander, Robert FitzRoy, decided to include in the expedition a naturalist with knowledge in geology. A 22-year-old Charles Darwin was chosen. The Beagle arrived in Valparaíso on July 23, 1834 and remained in port until November 10, 1834. During this time Darwin visited the surroundings towns and returning back to Valparaíso. On November 10, the Beagle set sail with Darwin on board, returning to continue surveys in the south of Chile. When the expedition was working its way back north, was caught around Valdivia by the February 20, 1835 earthquake. After witnessing the effects of this earthquake, including conspicuous coastal uplift around Concepción, the Beagle returned to Valparaíso on March 11, 1835. Three days later, Darwin left for Santiago to begin his loop over the Andes and back, arriving in Valparaíso on April 15. He finally left Valparaíso on land for Copiapó on April 27, 1835. During this central Chile stage, one of his main concerns was the long-term uplift of the coast. He wrote in his notebook: "As every one has heard of the upheaval of the coast of Chili, I took particular pains to see if any signs of former beaches were to be discovered". Besides studying raised beaches and shells, he interviewed "elder inhabitants" and English residents in Valparaíso to rebuild the recent elevation history of the town´s coast. In his Geological observations, Darwin highlights two interesting inferences related to the 1822 earthquake obtained from interviews. First, 1822 coastal uplift was not homogenous in the east-west direction, only the eastern coast of the bay had been uplifted in 1822. Second, Darwin infers that coastal uplift in Valparaíso had been a gradual process that started soon before the 1822 earthquake, and by the time he was there (1834) the process would still be operating. For him, the 1822 uplift would have only partially contributed to the long-term uprising. For us, as a minimum, the coast in 1834 was as high as it was left in 1822.

During two successive years I carefully examined, […], into all the facts connected with the recent elevation of this neighbourhood [Valparaiso]. […]. I can add nothing to the accounts already published of the elevation of the land at Valparaiso [referring to **record 16**], which accompanied the earthquake of 1822: but I heard it confidently asserted, that a sentinel on duty, immediately after the shock, saw a part of a fort, which previously was not within the line of his vision, and this would indicate that the uplifting was not horizontal: it would even appear from some facts collected by Mr. Alison, that only the eastern half of the bay was then elevated. […], I am able to give an interesting account of the changes of level, which have supervened here within historical periods: about the year 1680 a long sea-wall (or Prefil) was built, of which only a few fragments now remain; up to the year 1817, the sea often broke over it, and washed the houses on the opposite side of the road […]; and even in 1819, Mr. J. Martin remembers walking at the foot of this wall, and being often obliged to climb over it to escape the waves. There now stands (1834) on the sea-ward side of this wall, and between it and the beach, in one part a single row of houses, and in another part two rows with a street between them. This great extension of the beach in so short a time cannot be attributed simply to the accumulation of detritus; for a resident engineer measured for me the height between the lowest part of the wall visible, and the present beach-line at spring-tides, and the difference was eleven feet six inches. […]. From the facts given with respect to the sea-wall, and from the testimony of the elder inhabitants, it appears certain that the change in level began to be manifest about the year 1817. The only sudden elevation of which there is any record occurred in 1822, and this seems to have been less than three feet. Since that year, I was assured by several competent observers, that part of an old wreck, which is firmly embedded near the beach, has sensibly emerged; hence here, as at Chiloe, a slow rise of the land appears to be now in progress.

Source: Darwin, Ch., 1846. Geological observations on South America. Being the third part of the geology of the voyage of the Beagle, under the command of Capt. Fitzroy, R.N. during the years 1832 to 1836. Smith Elder and Co. (Eds.), London. p. 31-35.

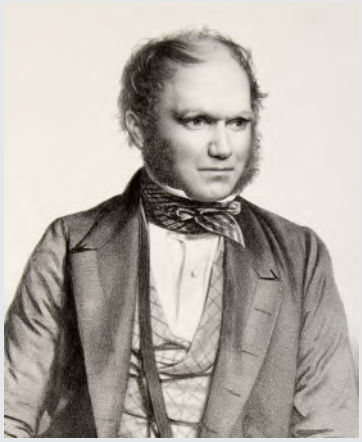

Charles R. Darwin (1809-1882) was an English naturalist, geologist and biologist, best known for his contributions to the science of evolution. His work as a naturalist of the second expedition of the HMS Beagle (1831-1836) set him as a well-recognized geologist whose observations and inferences supported Charles Lyell's ideas (**record 11**).

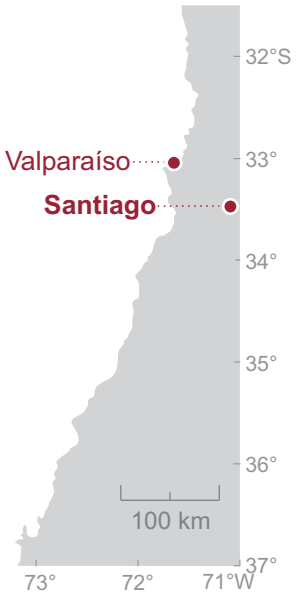

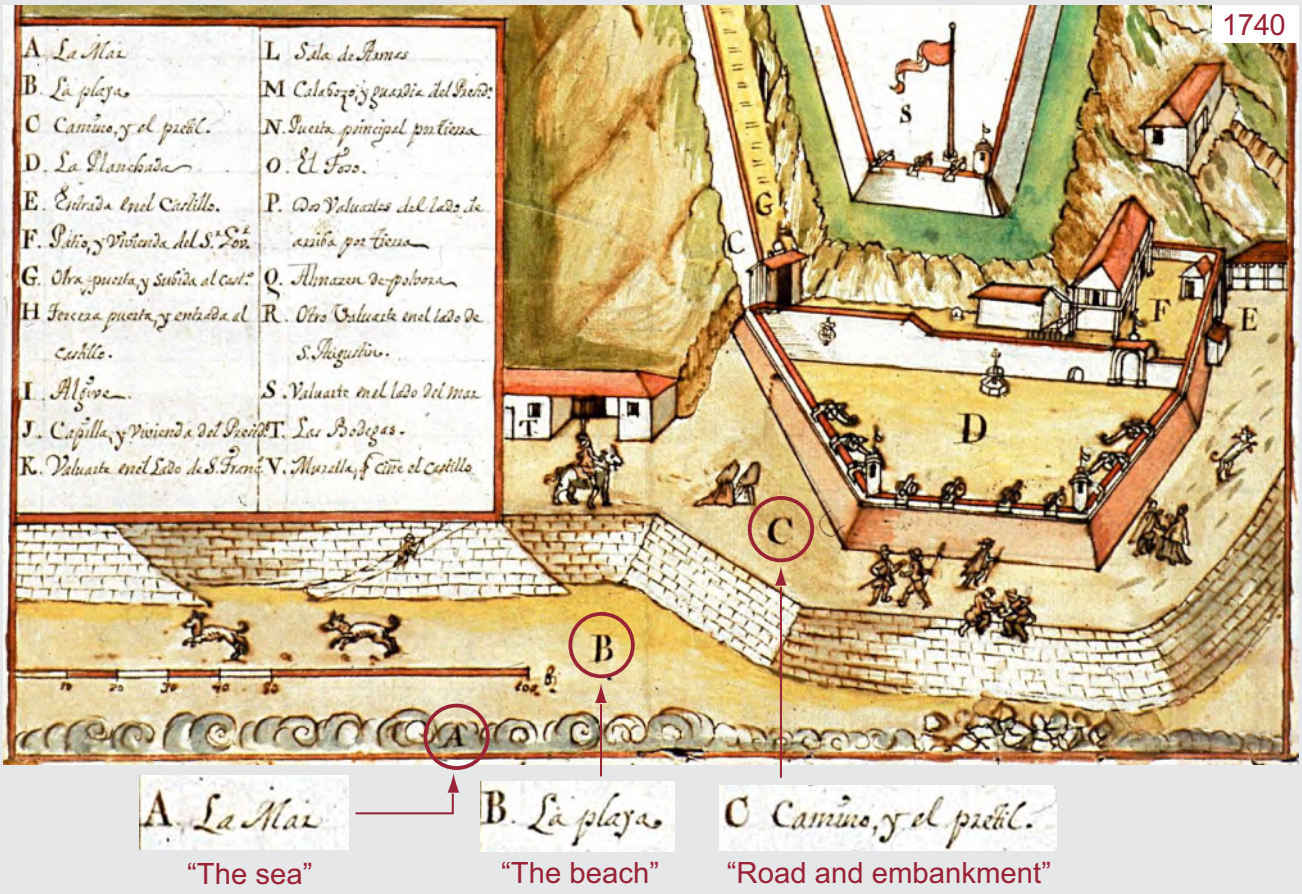

A 1740 view of the coast of Valparaíso shows the "Prefil" (sic) or sea-wall used by Darwin to estimate the long-term uplift of the coast. It likely shows a condition similar to that described before 1817 by Mr. Martin, who was "often obliged to climb over it to escape the waves". The view depicts the sea waves (A), the beach (B), and the road and the embankment slope (C).

Earthquake and Tsunami of August 16, 1906

Compared with the 1822 earthquake, the 1906 earthquake is a well-documented event. By then, modern seismology was dawning in Chile and a series of early scientific reports on the earthquake were issued soon after (**records 23**, **24**, **26**, **27**, **28**, **29**). Likewise, mass media, including widely distributed newspapers, magazines and books (**20**, **22**, **25**, **30**), and the telegraph (**24**) had become a source of profuse, although disperse, information. The most systematic work compiling primary information on the 1906 earthquake was made by the commission, appointed just one week later by the Chilean government, to study the earthquake aftermaths (hereinafter the Commission). Led by astronomer Alberto Obrecht, the Commission was composed by scientists already working on natural sciences in Chile, including among others geographer Hans Steffen (**26-28**) and geologists Lars Sundt **(27)** and Miguel Machado (**29**).

The Commission sent 2,500 questionnaires to the local authorities and public servants all over the country. Unfortunately, only 155 were properly answered and returned. Additionally, 120 reports from the Meteorological Agency local branches and other 17 from the Maritime authorities were received. Soon after the formation of the Commission, on August 23, 1906, the commissioners began a first field survey to Valparaíso. Afterwards, they divided themselves into four groups, one heading to the north of the affected area through the country's central valley, another to the south, and the other two groups to the north and south along the coast. The results of the Commission's work, summarized by Steffen (1907) (**26-28**), were the basis for the chapters reporting effects outside Valparaíso in the book by Rodriguez and Gajardo (1906) (**25**), and also support most of the significant volume on the 1906 earthquake by Montessus de Ballore (1915) (**31**, **32**). Because we did not have access to the original Commission's raw data, we used Steffen's summary book, his handwritten notes, and the volume of Montessus de Ballore, who evidently had such data available.

Based on the above information, the following pages compile significant primary sources to offer a description of the effects, mainly shaking, uplift and tsunami, of the penultimate large earthquake that struck Metropolitan Chile.

The central Chile earthquake of 16 August 1906 appears to be the second largest historical event of this region after the 1730 earthquake. However, it shares most of the features reported for the smaller 1822 earthquake (**1-19**), including strong coastal shaking, uplift of the coast and a moderate tsunami. The difference between them is mainly in the latitudinal extent of their effects. The 1906 earthquake effects extended over a much larger north-south area than those in 1822, perhaps twice as large. Alternatively, some of the effects, mostly intensity and coastal uplift, extended over two separated patches, one between Los Vilos and Valparaíso to the north, and another between Matanzas and Constitución to the south.

The 1906 mainshock occurred at 19:59 and lasted about 4 minutes according to the Astronomic Observatory of Santiago (**20**). Eyewitnesses felt the mainshock as composed of two large shaking pulses separated by “an interval of relative calm” (**23**, **26**). While the first pulse was the longest, lasting 4 to 5 minutes, the second “of equal or perhaps greater strength than the first”, lasted “only 1 minute or a little less” (**26**). These two pulses were only perceived inside the area of stronger shaking, outside it, to its northern and southern ends, the mainshock was felt as a single quake (**26**). There was a large aftershock at 20:15, which lasted 20 seconds (**20**).

A contemporaneous analysis of building damage and reported shaking shows that higher intensities (>VII) were entirely confined in the east-west direction between the Andes and the sea. In the north-south direction, they extended along 430 km, between 31.5° and 36° latitude South. The highest intensities (IX-X) where located on the coast, along 390 km, between Los Vilos and Constitución (**26**). Shaking, damage, and casualties were conspicuously larger on the coast, around Valparaíso, than in inland Santiago (**23**). Coastal shaking generated ground cracks, landslides, and liquefaction (**21**, **23**).

As in 1822, the coast of central Chile was suddenly and evidently raised as a consequence of the 1906 earthquake (**27**, **29**, **30**, **31**). Uplift estimates were mainly made using changes in the levels of tides and exposed and displaced sessile marine organisms attached to the rocks (**27**, **30**). The uplifted coast extended between Los Vilos (**27**) and Constitución (**29**), along 390 km. The amount of noticed uplift ranged between 0.4 m in Llico and 0.8 m in Zapallar (**27**). Based on these two well supported uplift amounts, it was suggested a trend of larger uplift in the north of the affected area and lesser in the south (**27**). Despite of all the conspicuous evidence for uplift, there

was an intermediate stretch of coast, between Valparaíso and Matanzas, along ~100 km, where the evidence was not as clear (**27**, **31**). Along this stretch, including Algarrobo, Cartagena and San Antonio, reports are confusing or even refute any land or sea level change. Thus, the resulting contemporaneous mapping of coastal uplift shows two separated sections, the northern one, the largest, between Los Vilos and Valparaíso, and a southern one, between Matanzas and Llico (map in **27**).

Despite the large north-south extension of shaking and associated coastal level changes, the 1906 earthquake triggered a moderate, non-destructive tsunami (**22**, **25**, **28**, **32**). Although unusual seas were reported all along the coast of the 1906-earthquake area, the more evident effects were observed in its southern reaches, between Pichilemu and Concepción Bay (**28**, **32**)*. From this stretch of coast, the effects progressively diminished both northward and southward. In the peripheral locations the tsunami was observed as "rough seas", and ebbs and flows that did not surpass the usual high tide level, which is around 1 m above mean sea level. On the contrary, between Pichilemu and Concepción Bay the tsunami surpassed the high-tide level and its large ebbs and flows retreated and advanced, by tens of meters, beyond the horizontal positions of the low- and high-tide lines (**28**, **32**)[1]. Bores, around 1 m high, were reported running up the main streams of the region, including the Aconcagua, Maipo, and Maule rivers (**25, 28, 32**). As a whole, according to the timing given by different reports, the unusual seas lasted for more than three hours, starting soon after the mainshock, around 15 minutes later in Constitución and Tomé (**28**, **32**), while the lowest sea level reached during an ebb was recorded in Penco at 23:30, three and a half hours after the mainshock. The 1906 tsunami crossed the Pacific reaching the Hawaiian Islands, with maximum amplitudes of 1.5 m at Hilo (**24**). It was also detected, with decimetric amplitudes, on tidal gauges in California and Japan (Soloviev and Go, 1984; Okal, 2005).

*A possible exception to this trend, based on contradictory reports, occurred in Valparaíso, which, although located in the earthquake´s northern reaches, experienced at least one sequence of a large ebb and flow. This possibility is stated by one report, seemingly well supported: "In reality there was movement in the sea, according to many sailors, both from war and merchant ships, the guards of the fiscal pier and various other people who witnessed the phenomenon: the sea retreated and left the beach at the foot of the seawall dry, and it was calculated that the descent of the waters was four meters more or less below the level of that hour; then the sea returned towards land, but the seawalls stopped it and prevented the flooding, as the water was seen splashing, through the mouth of the drainage canals [...]" (**25**). The other available report for Valparaíso, based on the Commission´s compilation, challenges the occurrence of such ebb and flow: "in the bay of Valparaiso itself, the sea was very calm at the precise moments of the catastrophe, although it later broke up until it reached a state of "rough sea", but without unusual ebbs and flows" (**28**). So far, no other well-supported report has been found to resolve this contradiction. Based on the large-scale geographical trend of the 1906 tsunami, which points to more evident effects in the southern reaches of the 1906 earthquake area, we prefer, if the large ebb and flow actually occurred in Valparaíso, to explain it through another source, like an underwater landslide. Such a landslide could also explain the cutting of the submarine Valparaíso-La Serena cable which occurred during the earthquake 3.5 km north of Valparaíso (Soloviev and Go, 1985).

Record 20 1906

The first available, written report of the 1906 earthquake was published in the newspaper El Mercurio of Santiago just several hours after the event. It gives the time of the mainshock, "at 7:59 P.M.", and its approximate duration, "three to four minutes". Another large shock occurred fifteen minutes later, "at 8:15", lasting only "20 seconds". Two subsequent, large aftershocks are reported at "12:10 and 2:02 [A.M.]". Building damage and fires are reported in Santiago. Unfortunately, the seismograph at Santiago did not record the earthquake. It is not clear whether the instrument was broken down before the earthquake or damaged by the shaking.

Last night's earthquake. At 7:59 P.M. there was an earthquake lasting three to four minutes. Immense and indescribable panic in the city. [...]. Collapse and cracking of buildings. Fires and threat of fires occur at various points. [...]. As of 5 A.M. no news from Valparaíso and southern provinces. [...]. Seismic movements are repeated frequently, but with less intensity. [...]. The earthquake occurred in a violent manner from its beginning [...]. The two- or three-story buildings [...] swayed like a ship at sea. The shaking was so strong that many people believed that the earth was going to open up in deep and long furrows. [...]. Fires broke out in various quarters of the city as a result of gas escaping or lamps shattering [...]. The telegraph and telephone lines were on the ground [...]. [...] after nine o'clock last night and during the early hours of this morning, tremors continued to be repeated, but with little force and very short duration. The main ones occurred at 12:10 and 2:02 [A.M.]. [...]. [At the Astronomical Observatory of Santiago] they gave us the following information: The first quake was felt at 7:59 and lasted about four minutes. The second one at 8:15 with a duration of 20 seconds and with quite a lot of oscillation. [...] unfortunately, there was no data on the phenomenon in the establishment, because at the beginning of the event, the seismograph had broken down [...].

El terremoto de anoche. A las 7.59 P.M. se produce un terremoto que dura de tres a cuatro minutos. Inmenso e indescriptible pánico en la ciudad. […]. Derrumbes y agrietamientos en edificios. Ocurren incendios y amagos en varios puntos. […]. Hasta las 5 A.M. sin noticias de Valparaíso y provincias del sur. […]. Los movimientos sísmicos se repiten con frecuencia, pero con menos intensidad. […]. El terremoto se produjo de una manera violenta desde su iniciación […]. Los edificios de dos o tres pisos […] se balanceaban como un buque en alta mar. Los sacudimientos eran tan fuertes que muchas personas creían que la tierra se iba a abrir en hondos y largos surcos. […]. En diversos barrios de la ciudad se produjeron incendios con motivo del escape de gas o del choque de las lámparas […]. Las líneas telegráficas y telefónicas estaban en tierra. […] después de las nueve de anoche y durante la madrugada de hoy, han continuado repitiéndose los temblores, pero con poca fuerza y muy corta duración. Los principales han ocurrido a las 12.10 y a las 2.02 [A.M.]. […]. [En el observatorio Astronómico de Santiago] nos dieron las siguientes informaciones: El primer temblor se sintió a las 7 h. 59 m. y duró alrededor de cuatro minutos. El segundo a las 8.15 con una duración de 20 segundos y con bastante oscilación. […] desgraciadamente en el establecimiento no había datos del fenómeno, pues al comienzo de este, el sismógrafo se había descompuesto […].

Source: "El Terremoto de Anoche". *Collected in*: El Mercurio, Santiago.
Dated: August 17, 1906, N°2.260, p. 1.

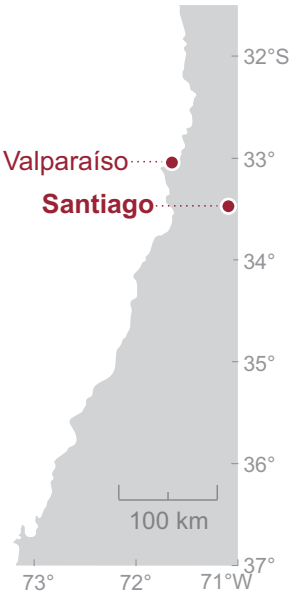

Record 21

1906

Two days after the 1906 earthquake, on August 18, the Intendente (provincial governor) of the Valparaíso province, Enrique Larraín, sent a dispatch to the President of Chile, Germán Riesco. The Intendente reports that Valparaíso is mostly destroyed and that it has been uncommunicated because roads and railways are cut. Larraín gives the first details that will be known in Santiago about the Valparaíso's fate, including a preliminary number of victims, the aftershocks, the lack of drinking water supply, and the fires. Additionally, he gives the first news about the surrounding towns of Viña del Mar, Casablanca, Limache, Quillota and Layllay, all of them destroyed as Valparaíso was. Finally, he reports changes in the depths of the main mooring of Valparaíso bay. Although he doesn't specify the sense of the changes, the fact that he states that a "rectification of soundings" will be necessary, it likely implies the soundings diminished.

I have the sorrow of communicating to you that on the 16th of the present [month], at 7:55 P.M., a great earthquake occurred in this city, causing the almost total loss of this town and surroundings. [...]. Up to the present time, the dead exceed 300 and the wounded 800; [...]. [...] the constant repetition of the tremors [...] has caused [...] panic [...]. Drinking water is scarce, due to the partial destruction of the water supply main pipe. [...]. In the city there is no lighting other than that of the fires, [...]. The towns of Viña del Mar, Casablanca, Limache, Quillota and Llay-Llay have suffered more or less the [same] destruction. Railroad communication with them is almost impossible [...]; the line is removed in great extensions, there are large landslides and some bridges are in a bad state. [...]. In the bay some changes have been noted in the depths near the fiscal dock, which will require, [...], a rectification of soundings.

Tengo el sentimiento de comunicar a US. que el 16 del presente, a las 7:55 P.M., se produjo en esta ciudad un gran terremoto, causando la pérdida casi total de esta población y sus alrededores. […]. Hasta el momento, los muertos pasan de 300 y los heridos de 800; […]. […] la constante repetición de los temblores […] ha causado […] pánico […]. El agua potable escasea, debido a la destrucción en parte de la cañería matriz. […]. En la ciudad no hay más luz que la de los incendios, […]. Las poblaciones de Viña del Mar, Casablanca, Limache, Quillota y Llay-Llay han sufrido más o menos los [mismos] destrozos. La comunicación del ferrocarril con ellas se hace casi imposible […]; la línea está removida en grandes extensiones hay derrumbes enormes y algunos puentes en mal estado. […]. En la bahía se han notado algunos cambios en las profundidades cercanas al muelle fiscal, lo que exigirá, […], una rectificación de sondajes.

Source: Carta del Intendente de Valparaíso Enrique Larraín a Germán Riesco. *Dated*: August 18, 1906 in Valparaíso. *Collected in*: Rodriguez, A. and C. Gajardo, 1906. La catástrofe del 16 de Agosto de 1906 en la República de Chile. Imprenta, Litografía y Encuadernación Barcelona, 1906, Santiago de Chile. p. 180-183.

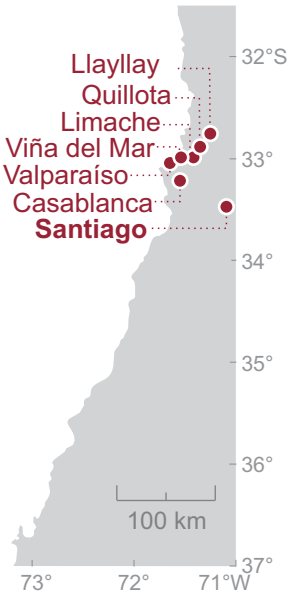

Record 22

1906

*Nine days after the 1906 earthquake, El Diario Ilustrado, a newspaper from Santiago, includes an undated note taken from a "newspaper of Concepción" telling of a delayed and "extremely rapid" high tide at Talcahuano harbor. Considering the reference to the ship in dry dock threatened by the shaking from the earthquake and the near simultaneity of the sea movements described here with those of other reports in the same bay (**records 28, 32**), it most likely refers to the 1906 tsunami. The observer reports that high tide occurred much later than the expected, at 11 P.M. This report is important because it makes one of the three different locations within Concepción Bay (Talcahuano, Penco, and Tomé) from where large ebbs and flows were reported taking place two to three hours after the 1906 mainshock (**28, 32**). It is striking that the vertical values of sea level changes, "a flow of 70 cm and an ebb of 80 cm", are given with such precision, perhaps implying that some method of measurement in "the docks" was used.*

In Talcahuano. A newspaper of Concepción says: "In Talcahuano we are informed that the high tide, which should have taken place last night at 1 P.M., was considerably delayed, taking place at 11 o'clock, after the sea had receded to the end of the docks. It was extremely rapid, rising up to 70 centimeters. Shortly afterwards it descended almost abruptly by 80 centimeters. The steamer "Mexico", which was in the dry dock, lost with the movement many of its [supporting] wedges, being in the dangerous situation of lying down if another quake like the first one had come later".

Source: "En Talcahuano". El Diario Ilustrado, N° 1581, August 25, 1906. Santiago Chile. p. 3.

En Talcahuano. Dice un diario de Concepción: "En Talcahuano se nos informa, la pleamar, que debía verificarse antenoche a la 1 P.M., se retrasó considerablemente, verificándose a las 11, después de retirarse el mar hasta el extremo de los muelles. Se produjo sumamente rápida, subiendo hasta 70 centímetros. Poco después descendió casi bruscamente 80 centímetros. El vapor "México", que se encontraba en el dique, perdió con el movimiento muchas de sus cuñas [de soporte], quedando en la peligrosa situación de tumbarse si hubiera venido posteriormente otro temblor como el primero".

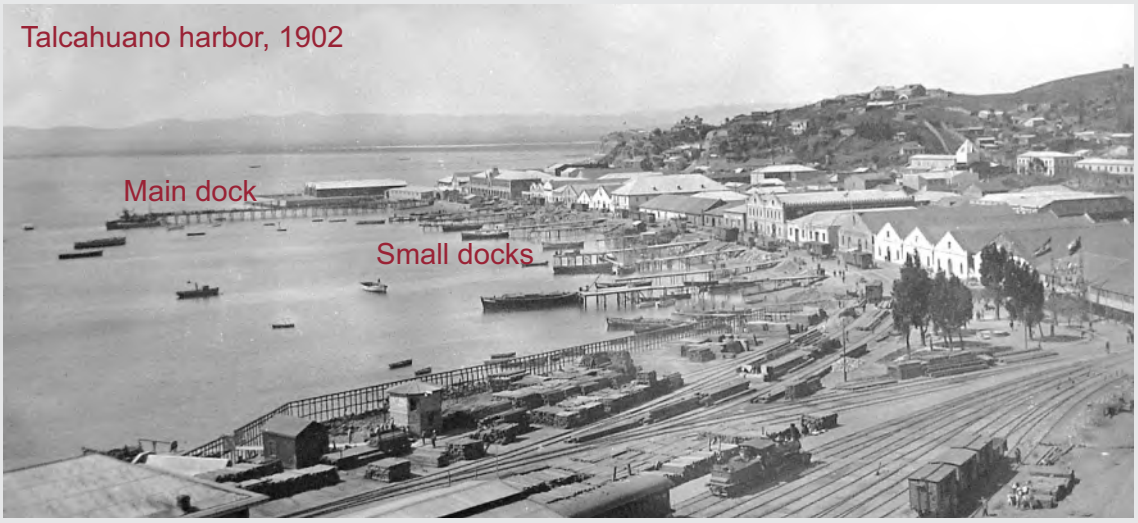

Docks at Talcahuano Harbor used as 1906 tsunami gauges. A photo of the Talcahuano harbor, taken four years before the 1906 earthquake, shows the docks from where unusual seas were seen and quantified after the earthquake. A "delayed" and "extremely rapid", 70-cm "high tide" occurred after "the sea had receded to the end of the docks". Afterwards, the sea descended "abruptly" again 80 cm. Most likely, the reference to the "docks" denotes the small docks depicted in this 1902 photo.

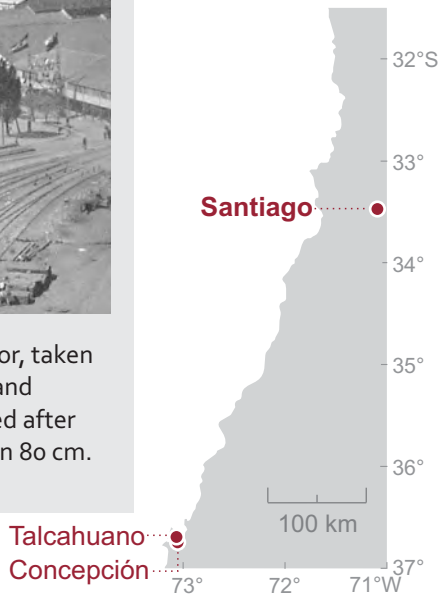

Record 23 1906

One month after the 1906 earthquake, on September 20, 1906, Luis Zegers, a professor at the Faculty of Physics and Mathematics Sciences at Universidad de Chile, published a short essay on the earthquake. Zegers gave a detailed description of the mainshock sequence at Santiago during the earthquake, which included two large shocks separated by "3 minutes". He concludes that although Santiago was affected by the earthquake it was not the focus of the earthquake but it was on the coast, in an area surrounding Valparaíso, between Puchuncaví to the north and Casablanca to the south. Zegers bases this conclusion on the reported damage of the railroad from Valparaíso to Santiago that loops to the north before heading south to Santiago. The railroad itself and the buildings of the railroad's neighboring towns suffered much more damage along half of the route closest to Valparaíso, up to Laillai. In this segment more ground cracks were also observed. At Puchuncaví, in the northern end of his suggested focus area, Zegers reports profuse vented ground water. He ends the report asserting that no subsequent unusual seas were seen on the coast and that shaking was felt by sailing ships 300 km offshore but not in Juan Fernández islands, which are 650 km farther west from the Valparaíso coast.

Minutes before 8 P.M., a dull noise was felt in Santiago and a few minutes later the ground began to vibrate, transforming the tremor into a large and prolonged earthquake, moments later [...], without ceasing to tremble, [after 3 minutes] a new shock, as intense as the first, indicated if not the conclusion of the earthquake, at least the end of the period of more energetic tremors. [...]. Santiago has suffered the effects of a great quake, but it has not been the center or focus [...]. The effects [...] were much more destructive on the coast than in the center, and much less towards the Andes Mountains. [...]. The focus was Valparaíso and its surroundings. From Valparaíso to Llaillai, a town located in the middle of the railway line that connects Santiago to that port, the quake literally razed the houses, rendering the railway useless in many parts, [...] while, from Llaillai to the capital, the railway did not experience serious damage [...]. Between El Salto and Quilpué and in Llallai, mainly, the ground cracked during the earthquake [...]; this phenomenon occurred with great intensity in [...] Puchuncaví [...], where there were great disturbances in the ground and the boiling water gushed abundantly in great stretches. [...]. [...] in Valparaíso and in all the other coast of the country, there were no abnormal phenomena, nor were there any swells [...]. The sea remained calm [...]. Judging by the information [from] sailing vessels [...], the earthquake was felt up to 300 km from the coast; but its action was null in the Juan Fernández islands, located [...] in the parallel of Valparaíso and about 650 km from this point.

Minutos antes de las 8 P.M. se sintió en Santiago un ruido sordo i a los pocos minutos empezó a vibrar el suelo, transformándose el temblor en un grande i prolongado terremoto, momentos después […], sin cesar de temblar, [después de 3 minutos] un nuevo choque, tan intenso como el primero, señaló sino la conclusión del terremoto, al menos la terminación del periodo de sacudimientos más enérgicos. […]. Santiago ha sufrido los efectos de un gran temblor, pero no ha sido el centro o foco […]. Los efectos […] fueron mucho más destructivos en la costa que en el centro, i mucho menores hacia la Cordillera de los Andes. […]. El foco fue Valparaíso i sus alrededores. Desde Valparaíso a Llaillai, pueblo situado en la medianía de la línea férrea que une Santiago a ese puerto, el temblor arrasó literalmente las habitaciones, inutilizó en muchas partes la línea férrea, […] mientras que, desde Llaillai a la capital, la línea férrea no experimentó graves desperfectos […]. Entre el Salto i Quilpue i en Llaillai, principalmente, el suelo se agrietó, durante el terremoto […]; este fenómeno se produjo con mucha intensidad en […] Puchuncaví […], en donde hubo grandes trastornos en el suelo i el agua hirviente brotó abundantemente en grandes estensiones. […]. […] en Valparaíso i en toda la demás costa del país, no se han presentado fenómenos anormales, ni se levantaron marejadas […]. El mar se mantuvo en calma […]. A juzgar por los datos [de] embarcaciones que navegaban […], el terremoto se sintió hasta unos 300 km de la costa; pero su acción fue nula en las islas de Juan Fernández, situadas […] en el paralelo de Valparaíso i a unos 650 km de este punto.

Source: Zegers, L., 1906. El terremoto del 16 de Agosto de 1906. Imprenta Cervantes, 1906, Santiago de Chile. p. 29-34.

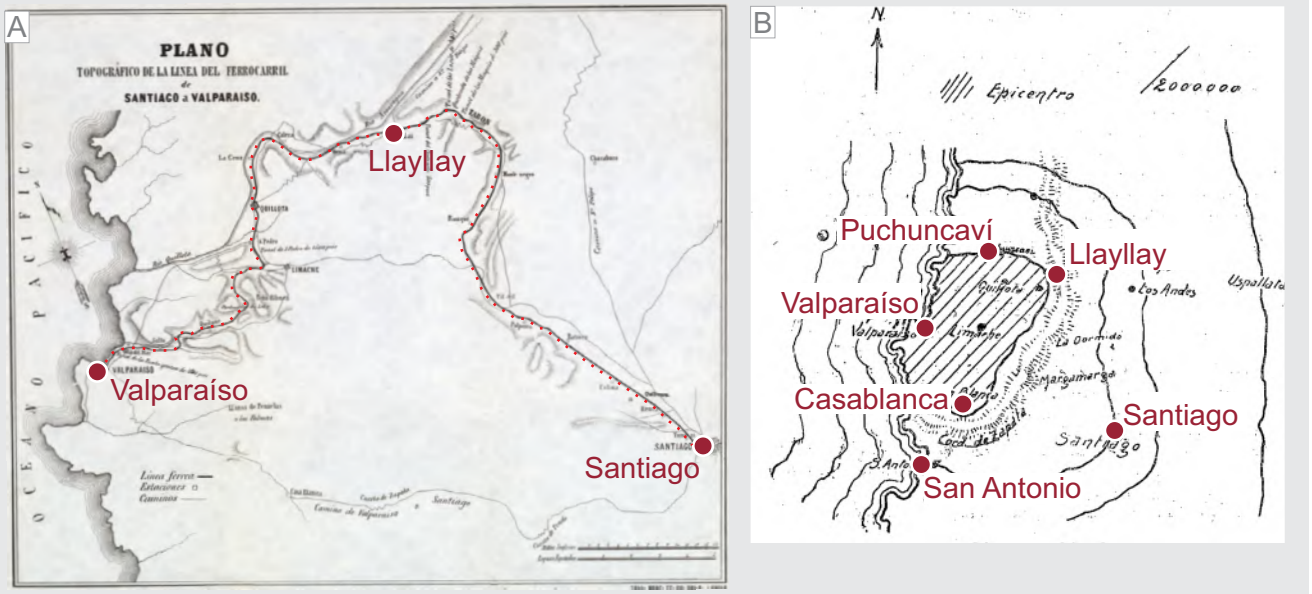

First proposed epicentral area of the 1906 earthquake. Based on building damage, ground disturbances, such as cracks and vented water, together with the reported damage on the railroad between Santiago and Valparaíso, depicted in A on a contemporaneous railroad map, Luis Zegers published just one month later a proposed focal area (B). Zegers was not only a pioneer in early publishing about the 1906 earthquake but also in his work on x-rays. He published a report on the first radiograph obtained in Chile, and only the second in the Americas, on March 27, 1896, just three months after the world's first report by Wilhelm Röntgen.

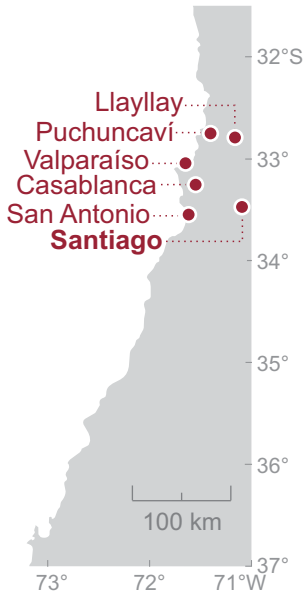

Record 24 1906

*Just two months after the 1906 earthquake, on October 1906, the Geographical Journal of the Royal Geographical Society of London, published a short article about the earthquake and its effects in the Pacific Ocean. Based on telegraphic information, the journal reports damage and casualties between Illapel and Talca, and an "absence" of "any sea-wave on the American coast", but "sea-waves" in Hawaii. The reference to the "American coast" is a bit confusing as to whether it is intended to imply the entire coast of North and South America or something else. Certainly, the absence of waves along the Chilean coast is challenged by local reports compiled by the Commission, which show that a moderate tsunami struck the coast of Central Chile (**records 22**, **25**, **28**, **32**). The 1906 tsunami had reached ~10 cm in Mahui and ~1.5 m in Hilo. The much larger figure of ~3.7 m at Maalea Bay, in Mahui, has been called into question by Okal (2005), arguing that the time of flood doesn't fit with the time of the earthquake, suggesting a local underwater landslide as a source. Questioning whether the earthquake was accompanied by "any permanent change in the relative level of land and sea", the article mentions that earlier reports describe some "alteration in the shore-line after the earthquake" but that later ones, based on soundings made in Valparaíso Bay, "showed that there had been no important change in the bottom of the bay". The latter deduction is also challenged by local reports, which show that a large stretch of the central Chile coast was uplifted (**27, 29, 30, 31**). Even more contradictory to the sounding results is the drastic testimony included in record **31**, which states that: "The lowering of the sea is a fact. How much the drop is, it is difficult to know, but the fact is so visible and so notorious, that everybody knows it except the person that the government sent to do the soundings.".*

The earthquake which laid Valparaiso in ruins at about quarter-past seven on the evening of August 16 […]. […]. So far as can be gathered from the telegraphic reports, the shock was even greater one than that destroyed San Francisco […]. […] it seems certain that the shock was of destructive violence, accompanied by widespread ruin and loss of life from Illapel on the north to Talca on the south […]. […] It is to be feared that this earthquake will not receive the same thorough investigation […], as it seems to present problems of great interest. One of these is the explanation of the absence, so far as reports go, of any sea-wave on the American coast, though sea-waves were recorded on the tide-gauge at Honolulu, and observed on the coast of Sandwich Islands. At Honolulu the oscillation is reported to have been only 3 or 4 inches [~8-10 cm], but at Mani (sic) and Hilo the waves were 5 feet [~1.5 m] high, and in the enclosed Bay of Maalea reached 12 feet [~3.7 m]. The time at which these waves were recorded shows that they were originated by the earthquake; they were, however, small in comparison with the sea-waves of the Peruvian earthquake of May 9, 1877, which had a height of 58 inches [~147 cm] at Honolulu and 36 feet [~11 m] at Hilo. These sea-waves point to a submarine origin of the earthquake, while the distribution of the damage done shows that the line of fissure, along which the earthquake must have originated, passed inland somewhat to the north of Valparaiso, running in an approximately north-to-south line, with a slight easterly trend. We are still uncertain whether the disturbance of the sea-bottom, which gave rise to the sea-waves, was accompanied by any permanent change in the relative level of land and sea. Some of the earlier accounts made specific mention of alteration in the shore-line after the earthquake, but, according to a later account, soundings taken at sixty-four places in the Bay of Valparaiso showed that there had been no important change in the bottom of the bay. This does not, however, prove that no change has taken place, for it would not require an important change in the depth of water to account for the earthquake and its sea-wave, nor is it impossible that there may have been important changes further north, though not at Valparaiso. […].

Source: "The Valparaiso Earthquake". The Geographical Journal, 28(2): 386-387 (1906).


San Francisco
Hawaiian Islands
Sandwich Islands
Honolulu
Mahui
Hilo
Maalaea
Chile
Detail at right

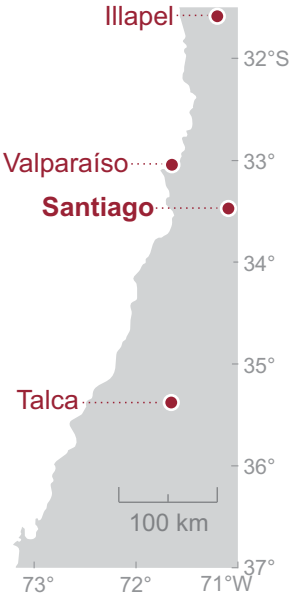
Illapel
32°S
Valparaíso
33°
Santiago
34°
35°
Talca
36°
100 km
37°
73°
72°
71°W

Record 25

1906

*Alfredo Rodriguez and Carlos Gajardo argue forcefully in their book on the earthquake that the sea did indeed retreat, then rise again, at Valparaíso after the earthquake. They used the testimonies of sailors on ships and guards at the fiscal dock to conclude that the sea first receded, leaving the beach at the base of the seawall dry falling the level about 4 m, then rose again, but without overtopping the seawall. This record is important because it challenges the two other records stating there were no ebbs and flows in Valparaíso (**23**, **28**), and it also challenges the purported trend of the most noticeable tsunami effects being focused along the coast at the southern reaches of the 1906 earthquake (**32**). Unfortunately, Rodriguez and Gajardo do not give further details of the time when the ebb and flow occurred or if this sequence was repeated. Ebbs and flows were indeed reported in Concepción Bay, where their maximum expression occurred two to three hours after the mainshock (**28**, **32**). The last part of the entry increases the puzzle even more. It states that in Concón, at the mouth of Aconcagua river, the largest river in the Valparaíso region and located 20 km north of that city, there was an ebb followed by a flow going into the river and reaching up to where the highest tides "had never reached before." Perhaps the ebb and flow at Valparaíso and Concón did occur, but alternatively they accompanied the shaking itself or resulted from another source, like a submarine landslide. The lack of the timing for the phenomenon limits any further conclusion.*

In reality there was movement in the sea, according to many sailors, both from war and merchant ships, the guards of the fiscal pier and various other people who witnessed the phenomenon: the sea retreated and left the beach at the foot of the seawall dry, and it was calculated that the descent of the waters was four meters more or less below the level of that hour; then the sea returned towards land, but the seawalls stopped it and prevented the flooding, as the water was seen splashing, through the mouth of the drainage canals [...]. […]. In Concón [...]. The sea retreated and after a moment it went up the Aconcagua River, which debouches at this point, to where the highest tides had never reached before.

En realidad hubo movimiento en el mar, según exponen muchos marinos, tanto de naves de guerra como mercantes, los guardas del muelle fiscal y diversas otras personas que presenciaron el fenómeno: el mar se retiró y dejó en seco la playa al pie del malecón, y se calculó que el descenso de las aguas fue de cuatro metros más o menos bajo el nivel de esa hora; después el mar volvió hacia tierra, pero los malecones lo detuvieron e impidieron la inundación, como que se vio saltar el agua, por la boca de los cauces […]. […]. En Concón […]. El mar se retiró y después de un momento subió por el río Aconcagua que desemboca en este punto, hasta donde jamás habían llegado las más altas mareas.

Source: Rodriguez, A. and C. Gajardo, 1906. La catástrofe del 16 de Agosto de 1906 en la República de Chile. Imprenta, Litografía y Encuadernación Barcelona, 1906, Santiago de Chile. p. 54, 282.

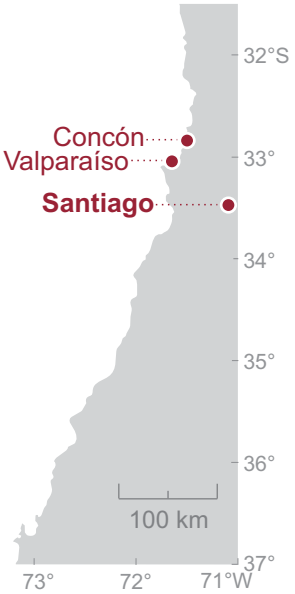

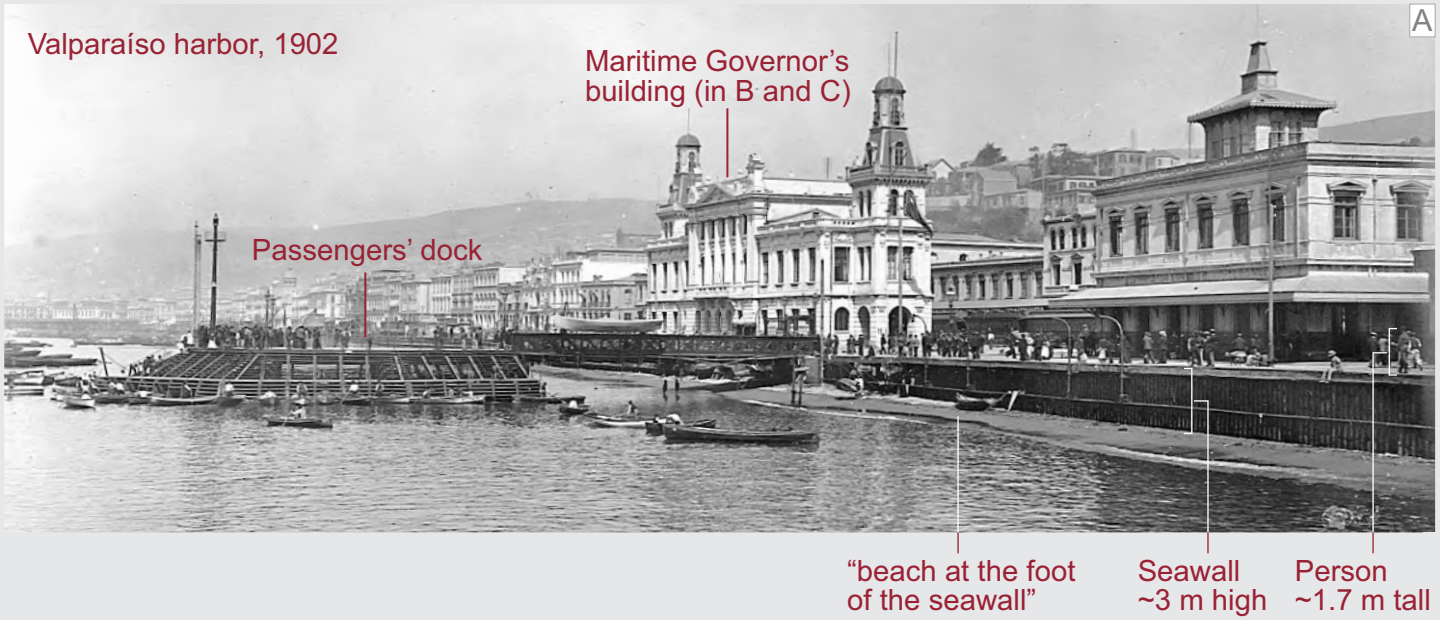

The seawall that was not overtopped by the 1906 tsunami. Unlike most of the records discarding unusual seas at Valparaíso after the 1906 earthquake, Rodriguez and Gajardo report that such seas did in fact occur. The authors collected testimonies at the "fiscal dock," from where the upper, pre-earthquake photograph was taken (A). It shows the Maritime Governor´s building and the Passengers' dock, both important landmarks of the harbor. Additionally, the photo shows the seawall, which "stopped" the flow and "prevented the flooding". By scaling the height of the person in the photo, the seawall is estimated to be ~3 m high, suggesting that the flow was not above that height. The beach seen at the base of the seawall was mentioned when describing the first retreat of the sea, of about 4 m: it "left the beach at the foot of the seawall dry". The lower photos, all taken from the Passengers' dock, show close-ups of the Maritime Governor´s building and the seawall before (B) and after the earthquake (C). One of the drainage channels outlets mentioned by Rodriguez and Gajardo, is seen in the sea wall: although the flow did not overtop the seawall, "the water was seen splashing, through the mouth of the drainage canals". Partial caving of the seawall, most likely produced by the earthquake, can be seen in C.

Record 26

1906

*Hans Steffen, a German geographer working for the Chilean government between 1889 and 1914, witnessed the 1906 earthquake in Santiago. One week after the earthquake, on August 23, 1906, he was appointed by the government to the Commission to study the earthquake's effects. Nine months later, in May 1907, Steffen published a full report in Spanish summarizing the accounts collected by the Commission and his own field observations. The same year he published an abridged version in German in Petermanns Geographische Mitteilungen, the oldest German journal of geography. At the beginning of the full report, Steffen highlights that the earthquake was composed by two, well-defined shocks separated by a period of relative calm. While the first pulse, the longest, spanned 4 to 5 minutes, the second was only 1-minute long. This seismic sequence agrees well with the one reported by Zegers (**record 23**). Steffen delimits the area where the mainshock was felt as two pulses, between 28° and 39° S, and where it was felt as a single long pulse, in the southern and northern peripheral regions. The report includes a fine isoseismal map that he describes as showing half, concentric ellipses, whose longer axes align with the coastline and higher intensities occur along the coast between Matanzas to the south and Zapallar to the north.*

[...] the general way in which the earthquake has manifested itself in the central part of the macroseismic region [...] [between 28° and 39° S] has been of two series of oscillations, separated by an interval of relative calm, well distinguishable, but appreciated in very different ways in their duration [...]. The first strong shock [...] was exceptionally long, lasting 4 to 5 minutes, while the second, of equal or perhaps greater strength than the first, lasted only 1 minute or a little less. In the southern and northern peripheral regions the distinction of the two series is blurred [...] [felt] as only one [...]. [...]. [Only] the isoseismals [...] VII and higher [...] remain entirely to the west of the Andes Mountains, extending [...] in the form of concentric and elongated half ellipses across the region [...] between parallels 36° and 31½° approximately. The major axis of the ellipses coincides [...] with the coastline [...]. Within this region [...] grades IX to X predominate [...], along the stretch of the coast from Matanzas to Zapallar [...].

[…] la forma general en que el terremoto se ha manifestado en la parte central de la región macrosísmica […] [entre 28° y 39° S] ha sido de dos series de oscilaciones, separadas por un intervalo de calma relativa, bien distinguible, pero apreciado de muy diversa manera respecto de su duración […]. El primer sacudimiento fuerte […] fue excepcionalmente largo, de 4 a 5 m [minutos] de duración, mientras que el segundo, de igual o talvez mayor fuerza que el primero, duró solamente 1 m o poco menos. En las regiones periféricas del sur y norte se borra la distinción de las dos series […] [sintiéndose] como uno solo […]. […]. [Sólo] las isosistas […] VII y superiores […] quedan enteramente al occidente de la Cordillera de los Andes, extendiéndose […] en forma de medios elipses concéntricos y alargados a través de la región […] entre los paralelos 36° y 31½° aproximadamente. El eje mayor de las elipses coincide […] con la línea de costa […]. Dentro de esta región […] predominan los grados de IX a X […], en el trecho de la costa desde Matanzas hasta Zapallar […].

Source: Steffen, H., 1907a. Contribuciones para un estudio científico del Terremoto del 16 de Agosto de 1906. Imprenta Cervantes, Santiago de Chile. p. 23.

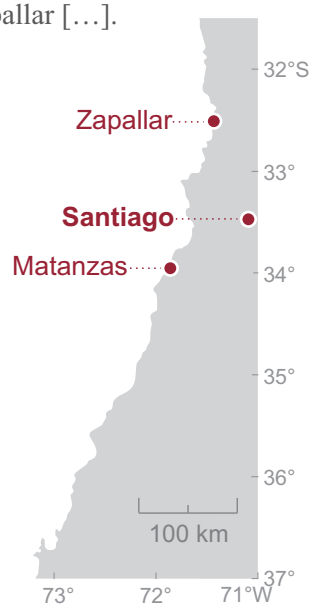

Geographer Hans Steffen (1865-1936), is well known in Chile for his boundary surveyor work in the rugged Aysén region in northern Patagonia, an area disputed between Chile and Argentina when interpreting the 1881 Boundary Treaty. Between 1893 and 1899, Steffen mapped the main river basins and discovered important geographic landmarks, some of which are named after him. In the photograph above Steffens poses, sitting and wearing a bowler hat, along with his 1894 Palena River expedition group. At the turn of the century Steffen resumed his work at the university in Santiago, where he was caught by the 1906 earthquake. As a renowned geographer, the Chilean government appointed him to the Commission to study the earthquake's aftermaths. The results of the Commission's work, summarized and published by him, included his isoseismal map at left.

Record 27 1906

*Just as happened after the 1822 earthquake (**records 10**, **11**, **12**, **13**), after the 1906 earthquake, eyewitnesses reported evident and conspicuous evidence for coastal uplift (**27**, **30**, **31**). Similarly, their testimonies and estimates were based on changes in the levels of tides and exposed and displaced sessile marine organisms attached to the rocks. Using the local reports collected by the Commission (**26**), Hans Steffen compiled those testimonies about uplift from south to north. The southernmost evidence comes from Llico, a town located on the southern bank of a long drainage channel of a coastal lagoon. The testimony, based on water level changes in sedimentary environments, such as the channel bed and sandbanks, reports ~40 cm of uplift. Further north, Steffen found stronger evidence in rocky places along the coast between Cahuil and Pichilemu. There, shellfish gatherers found that rocks, previously submerged, were "above the surface of the water to a height of one meter". According to one of the reports, waters of the Cahuil lagoon accumulated at the lagoon's head as a result of the tilting produced by the coastal uplift. Further north, reports on level changes along the coast between the mouth of the Maipo river and Valparaiso, through ~65 km, become uncertain. In Valparaíso evidence for uplift is obvious again and well-marked by a white, ~50-cm wide fringe of dead shellfish still attached to the rocks. North of Valparaiso, along 125 km of coast, including Horcón, Zapallar, Papudo, and Pichidangui, evidence for uplift (~70 cm) becomes persistent up to Los Vilos. In sum, Steffen concludes: i) that there is no doubt that there were level changes on the coast associated to the 1906 earthquake between Mataquito and Choapa rivers, along 380 km; ii) such extension coincides with the region of the largest shaking intensity; and iii) uplift was larger in the north than in the south of the affected area.*

[The] problem of the abrupt uplifts […], of the coast […] is related to the earthquakes that strike, from time to time, the Chilean coast. The southernmost point from which news of definite modifications [...], is Llico, [...]. We owe the information [...] to Mr. [...] Bunster [...]: "[...] the following facts give me the impression that there has been uplift: 1. The fords in the channel have all become less than half the depth they were the day before the earthquake, a difference that I estimate at 40 centimeters. 2. Several sandbanks, both at the mouth of the lagoon and in the channel, in the sea and in the lagoon itself, which used to be at the surface of the water at low tide, appeared to be out about 40 centimeters today. 3. A launch of mine that sunk two years ago [...] and that at low tide could only be seen about 10 centimeters from the gunwale, today, at low tide, it can also be seen no less than 25 centimeters and the surrounding sand bank is very dry [...]". In the stretch of coast that continues further north, especially between Cahuil and Pichilemu, there were also signs of modifications [...]. The [...] customs office of Pichilemu reports [...] that [...] "the shellfish gatherers state that a rock [...] that has always remained under the water, today rises above the surface of the water to a height of one meter, allowing [...] a large quantity of shellfish [...] to be extracted [...]". We add to this some extracts [...]: "The most noteworthy of the effects produced by the earthquake are [...] the changes that occurred on the coast and especially in the Cahuil lagoon. The sea receded as never before at low tides [...], women could safely enter [...] to collect sea urchins up to

Con los terremotos que agitan, de vez en cuando, el litoral chileno, se relaciona […] [el] problema de los solevantamientos bruscos, […], de la costa […]. El punto más meridional de donde provienen noticias acerca de ciertas modificaciones […], es Llico, […]. Debemos las informaciones […] al señor […] Bunster […]: "[…] los siguientes hechos me dan la impresión de que ha habido solevantamiento: 1. Los vados que tiene el canal han quedado todos a menos de la mitad de la hondura que tenían el día antes del terremoto, diferencia que calculo en 40 centímetros. 2. Varios bancos de arena, tanto en la boca de la laguna como en el canal, en el mar mismo y en la laguna misma, que antes quedaban a flor de agua en baja marea, aparecieron fuera unos 40 centímetros al día. 3. Una lancha que hace dos años se me fue a pique […] y que en baja marea sólo se veía unos 10 centímetros de la borda, hoy, en baja marea, también se la divisa no menos de 25 centímetros y el banco de arena que la rodea queda bien seco […]". En el trecho de costa que sigue más al norte, especialmente entre Cahuil y Pichilemu, se presentaron también indicios de modificaciones […]. La […] aduana de Pichilemu informa […] que […] "los mariscadores exponen que una piedra […] que siempre ha permanecido debajo de las aguas, hoy se eleva sobre la superficie de estas hasta una altura de un metro, permitiendo […] extraer gran cantidad de mariscos […]". Agregamos a esto algunos extractos […]: "Lo más digno de notarse entre los efectos producidos por el terremoto, son, […] los cambios habidos en la costa y especialmente en la laguna de Cahuil. El mar se retiró como nunca en

some rocks beyond the "Piedras de los Lobos", which ordinarily do not appear at the surface of the water. […]. For the region [...] north of the Maipo River mouth we have only uncertain data. The maritime authorities of San Antonio are doubtful [...]. In Algarrobo, the fishermen [...] at first answered negatively, but in [...] the conversation they said that the sea was now perhaps a little lower than before [...]. In Cartagena there are also no sure indications of changes in the level of the shore. Conversely, in [...] the bay of Valparaíso there are several points where knowledgeable people
[...] believe they have noticed alterations in the water level since the date of the earthquake. [...] Julio Fonck sent the Commission a communication [...] and Mr. Sundt, on his second trip to the coast, was able to verify, accompanied by [...] Fonck, that some 200 meters west of the Matadero or Portales wharf, a white strip is now visible on the rocks, made up of [...] barnacles (Balanus) and a seaweed of the Corallinaceae family, forming a very visible natural mark that at [...] low tide is exposed up to two feet below, while before the earthquake it was not visible, as confirmed by [...] the pier administrator and the head of the warehouse [...]. The latter [...], who has been observing the coastline for 18 years, also pointed out a rock that now shows with its peak at the lowest tides, being invisible before the earthquake. The same white strip [...], with a width of a foot or so, is also noted in the cove of Membrillo and in other points of the bay [...]. [On] the coast of [...] La Ligua we again find signs of alterations [...]. The maritime sub-delegate of Zapallar says [...]: "[...] from the mouth of the Ligua River in the north to the Horcón Bay in the south, all of us who know this coast agree that the earthquake [...] has caused an uplift of no less than 80 centimeters." [...]. One of the best connoisseurs of the [...] Papudo Bay, Mr. Otto Harnecker, has reported [complete first-hand testimony from Otto Harnecker in **record 30**]. […]. Once past the Ligua River mouth to the north, the obvious vestiges become rarer [...]. According to the [...] maritime sub-delegate of Pichidangui, since August 17th "the low tides are much greater than before [...]". [...], the Customs lieutenant of Los Vilos reports that "after the earthquake of the 16th the sea is lower and further away from the beach. The fishermen here confirm this at one voice". The data as a whole [...] can scarcely leave any doubt as to the effectiveness of a change in level along the entire [...] coast from the mouth of the Mataquito River to that of the Choapa, that is, in a stretch that corresponds more or less to the region [...] [with] the highest degrees (VII to

las bajas mareas […], las mujeres podían entrar sin peligro […] a recoger erizos hasta unas rocas que hay más allá de las "Piedras de los Lobos", las cuales ordinariamente no aparecen a flor de agua. […] Para la región […] al norte de la desembocadura del río Maipo no tenemos sino datos inseguros. Las autoridades marítimas de San Antonio se expresan dudosas […]. En Algarrobo, los pescadores […] contestaron al principio negativamente, pero en […] la conversación dijeron que el mar estaba ahora talvez un poco más bajo que antes […]. En Cartagena no hay tampoco indicios seguros de cambios de nivel en la orilla. En cambio existen en […] la bahía de Valparaíso varios puntos donde los conocedores […] creen haber notado alteraciones del nivel de las aguas desde la fecha del terremoto. […] Julio Fonck envió a la Comisión una comunicación […] y el señor Sundt, en su segundo viaje a la costa, pudo comprobar, acompañado por […] Fonck, que unos 200 metros al Oeste del muelle del Matadero o Portales, se ve ahora sobre las rocas una faja blanca, compuesta de […] picos (Balanus) y de un alga de la familia de las Corallinaceas, formando una marca natural muy visible que en […] baja marea queda en descubierto hasta unos dos pies más abajo, mientras que antes del terremoto no se divisaba, lo que confirman […] el administrador del muelle y el jefe del Resguardo […]. Este último […], que observa la línea de costa desde 18 años, señaló además una roca que ahora asoma con su cúspide en las mareas más bajas, siendo invisible antes del terremoto. La misma faja blanca […], con un ancho de un pie más o menos, se nota también en la caleta de Membrillo y en otros puntos de la bahía […]. [En] la costa de […] La Ligua volvemos a encontrar indicios de alteraciones […]. El subdelegado marítimo de Zapallar dice […]: "[…] desde la desembocadura del rio Ligua por el norte hasta la bahía de Horcón por el Sur, todos los que conocemos esta costa estamos de acuerdo que ha habido con el terremoto […] un levantamiento en toda ella no menor de 80 centímetros." […]. Uno de los mejores conocedores de la […] bahía de Papudo, don Otto Harnecker, ha publicado [testimonio completo, de primera fuente de Otto Harnecker en **record 30**]. […] Pasada la desembocadura del rio Ligua hacia al Norte, se hacen más raros los vestigios manifiestos […]. Según el […] subdelegado marítimo de Pichidangui, se nota desde el 17 de Agosto "las bajas mareas son mucho mayores que antes […]". […], el teniente de Aduana de Los Vilos comunica que "después del terremoto del 16 el mar se encuentra más abajo y más retirado de la playa. Los pescadores de aquí a una voz lo confirman". El conjunto de los datos […]

X) of intensity. [It is] difficult to determine exactly the difference in level produced [...], however, [...], the oscillation has been greater [in the North] than in the South. [...] this would result from a comparison of the two most reliable [...] indications [...], which refer to Llico (40 cm) and Zapallar (70 to 80 cm), [...].

apenas puede dejar duda alguna acerca de la efectividad de un cambio de nivel habido en toda […] la costa desde la desembocadura del río Mataquito hasta la del Choapa, o sea en un trecho que corresponde más o menos a la región […] [con] los grados más altos (VII a X) de intensidad. [Es] difícil determinar con exactitud la diferencia de nivel producida […], sin embargo, […], la oscilación ha sido mayor [en el Norte] que en la parte Sur. […] resultaría eso de una comparación de las dos indicaciones […] más fidedignas […], que se refieren a Llico (40 cm) y a Zapallar (70 a 80 cm), […].

Source: Steffen, H., 1907a. Contribuciones para un estudio científico del Terremoto del 16 de Agosto de 1906. Imprenta Cervantes, Santiago de Chile. p. 72-83.

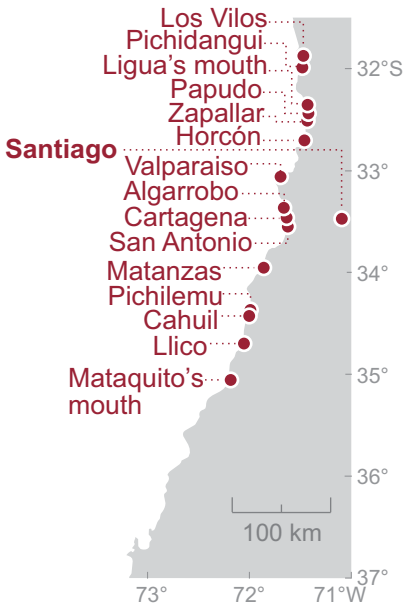

Unharmed Valparaíso

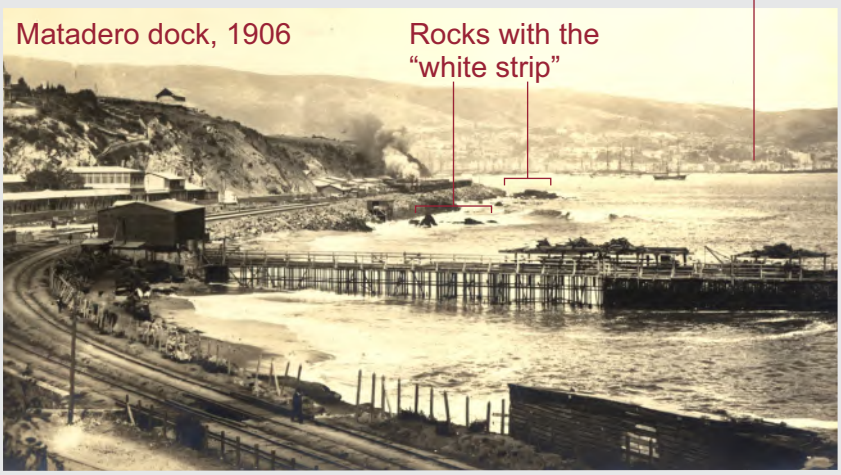

Erklärungen: Explanations:

Anzeichen von Hebung der Küste im Gefolge d. Erdbebens. Reports of coastal uplift during the earthquake

Mapped coastal uplift associated with the 1906 earthquake (A). Hans Steffen (**record 26**), wearing white hat and shoes in the above 1898 photograph (B), compiled tens of first-hand reports of coastal uplift resulting from the 1906 earthquake. He carefully mapped those reports defining areas of coastal uplift (A) (Steffen, 1907b). At least two more or less independent large areas of uplift can be recognized; a northern one between Los Vilos and Valparaíso and another in the south, roughly between Pichilemu and Llico. One definite and obvious type of gathered evidence were white fringes of dead shellfish attached to the rocks. They are largely produced by the bleaching of the Lithothamnium coralline algae. This crustose, low-intertidal algae, usually pale-pink in color, cannot survive long periods of desiccation, therefore is killed by co-seismic coastal uplift, leaving a bleached fringe the width of which is approximately proportional to the uplift amount. This approach was taken to its maximum by Robert Fitz-Roy to estimate uplift in Santa María Island soon after the 1835 south-central Chile earthquake (Fitz-Roy, 1839; Wesson et al., 2015). It has been more recently used after the 1995 northern Chile earthquake (Ortlieb et al., 1996) and the 2010 south-central Chile earthquake (Farías et al., 2010; Melnick et al., 2012). Some of the most definite evidence of coastal uplift in 1906 came from white strips seen in the rocks west of the Matadero dock at the Valparaíso Bay (C). Steffen reports that Mr. Julio Fonck, a "knowledgeable" person, sent a communication to the Commission describing such a fringe. Later, a commissioner, Norwegian geologist Lars Sundt, visited the dock to confirm this fact. Sundt found that west of the wharf "a white strip is now visible on the rocks, made up of [...] barnacles (Balanus) and a seaweed of the Corallinaceae family, forming a very visible natural mark that at [...] low tide is exposed up to two feet below, while before the earthquake it was not visible [...].". This photo of the dock, taken in 1906, but likely before the earthquake (Valparaíso appears unharmed in the background), shows the rocks that will be uplifted on the following 16 August.

Record 28

1906

*Although no damage from the tsunami following the 1906 earthquake were testified, Hans Steffen (**record 26**) devotes a section of his report to the unusual seas observed after the mainshock. Reviewing, from south to north, the reports sent by the local maritime authorities and eyewitnesses, Steffen found the first unambiguous evidence of unusual seas in Talcahuano Bay (also known as Concepción Bay). About 15 minutes after the mainshock a series of sea ebbs and flows were observed in Tomé, at the mouth of the bay. These horizontal movements reached 50-60 m. A similar description was reported for Penco, at the head of the bay and 14 km south of Tomé. There, the ebbs and flows were comparable to those in Tomé, but began later (or extended longer), perhaps 2 hours after the mainshock. The advances of the sea reached, but did not overtop, the railroad embankment that runs parallel to the coast, between ~40 and ~100 m inland. In contrast to what happened in 1906, this embankment, which still exists today, was overtopped by the 2010 tsunami. Further to the north, reports from Constitución describe ebbs and flows along the "entire coast", reaching more than 1 m high. At least two bores, 0.8-1 m high, were seen running up the Maule River one and a half hour after the mainshock. At Llico, 70 km north of Constitución, the sea seemed boiling, a phenomenon that lasted one hour and a half. Along the portion of the coast that suffered the stronger shaking, including Valparaíso and further north, the unusual seas were much less evident, lacking the ebbs and flows described to the south, and were only described just as "rough seas". The latter observation conflicts with **record 25**, which describes at least one ebb, of about 4 m, and one flow at Valparaíso.*

[...] in [...] Talcahuano Bay we found [...] unequivocal data about the ebb and flow of an extraordinary tide [...] after [...] the earthquake. From all the reports sent [...] [from] Tomé, it appears that, at the moment of the quake itself, the sea remained calm; but at 8:15 [20:15] [...] it began to withdraw for about fifty meters to immediately return to its place with complete smoothness. "These retreats were repeated under the same conditions three or four times, the last ones being the greatest, for they reached sixty meters." [...] an outflow of the sea was observed in Penco, which began some time (according to [...] the press about two hours) after the quake, with the ebbs and flows reaching more or less the same proportions as those observed in Tomé. The wave reached the neighboring embankment of the railway line and passed through the drainage canals further inland; but in general the phenomenon, although it caused alarm among the neighbors who began to take refuge in the hills; it was brief, since, according to an informant, the sea returned to its normal state "in less than ten minutes". On the coast of the Maule, Talca and Curicó provinces, there have also been some phenomena that suggest an extraordinary agitation of the sea, [...]. The maritime governor of Constitución states that, after the third of the seismic shocks felt in that port, that is, "at 8:07 P.M., there was an ebb and flow of the sea along the entire coast [...] of this governorate which [...] reached a height of more than one meter [...]". This waters movement also produced a considerable disturbance in the current of the Maule River, [...] the principal of the high school [...] reports [...]: "At half past nine on the night of the 16th a

[…] en […] la bahía de Talcahuano nos encontramos con […] datos inequívocos acerca del flujo y reflujo de una marea extraordinaria […] después […] del terremoto. Del conjunto de los informes remitidos […] [desde] Tomé, resulta que, en el momento del temblor mismo, el mar se mantuvo en tranquilidad; pero a las 8h 15m [20:15] […] principió a retirarse por unos cincuenta metros para volver a ocupar en seguida su lugar con toda suavidad. "Estas retiradas se repetían en las mismas condiciones tres o cuatro veces, siendo las últimas las mayores, pues alcanzaron a sesenta metros". […] se comprobó una salida de mar en Penco, que comenzó algún tiempo (según […] la prensa unas dos horas) después del temblor, alcanzando los flujos y reflujos más o menos las mismas proporciones que las observadas en Tomé. La ola llegó hasta el vecino terraplén de la línea férrea y pasó por las alcantarillas [de drenaje] más al interior; pero en general el fenómeno, aunque produjo alarma entre los vecinos que empezaron a refugiarse en los cerros; fue pasajero, pues, según afirma un informante, el mar volvió a su estado normal "en menos de diez minutos". En el litoral de las provincias de Maule, Talca y Curicó, se han presentado también algunos fenómenos que hacen presumir una agitación extraordinaria del mar, […]. El gobernador marítimo de Constitución afirma que, después del tercero de los choques sísmicos percibidos en aquel puerto, o sea "a las 8h 7m P.M., se produjo en toda la costa […] de esta gobernación un flujo y reflujo de mar que […] llegó a una altura mayor de un metro […]". Dicho movimiento de las aguas produjo también una perturbación considerable en la corriente del río Maule,

large wave or undertow was noted in the Maule River that raised the level of the current a *vara* [80 cm] or so, and minutes later another that reached [...] a meter in height [...]". [...]. Mr. Leigh Bunster, who observed the state of the sea in the port of Llico, says: "During the earthquake the sea seemed to boil [...]". Another informant also states that "in the sea the waves were paralyzed and the movement of the water was a boiling in the form of a gush, for an hour and a half or so". On the coasts [...] [of] Colchagua, Santiago, Valparaiso and Aconcagua, where [...] the earthquake displayed its greatest intensity, the sea has not been affected by extraordinary upheavals. On the contrary, at various points along this coast, such as in the bay of Valparaiso itself, the sea was very calm at the precise moments of the catastrophe, although it later broke up until it reached a state of "rough sea", but without unusual ebbs and flows. More or less the same can be said about the state of the sea along the entire [...] coast from here to the north [...].

[…] el rector del liceo […] informa […]: "A las nueve y media de la noche del 16 se notó en el río Maule una gran ola o resaca que levantó el nivel de la corriente una vara [80 cm] más o menos, y minutos después otra que llegó […] a un metro de altura […]". […]. El señor Leigh Bunster que observó el estado del mar en el puerto de Llico, dice: "Durante el terremoto el mar parecía que hervía […]. Otro informante afirma también que "en el mar se paralizaron las olas y el movimiento del agua fue un hervidero en forma de borbollón, durante una hora y media más o menos". En las costas […] [de] Colchagua, Santiago, Valparaiso y Aconcagua, donde […] el terremoto desplegó su mayor intensidad, el mar no ha sido afectado por agitaciones extraordinarias. Por el contrario, en varios puntos de ese litoral, como en la misma bahía de Valparaiso, llamó la atención la gran tranquilidad del mar en los momentos precisos de la catástrofe, si bien se descompuso después, hasta llegar al estado de "braveza", pero sin flujos y reflujos inusitados. Más o menos lo mismo se puede decir respecto del estado del mar en toda la […] costa que sigue de aquí al Norte […].

Source: Steffen, H., 1907a. Contribuciones para un estudio científico del Terremoto del 16 de Agosto de 1906. Imprenta Cervantes, Santiago de Chile. p. 65-72.

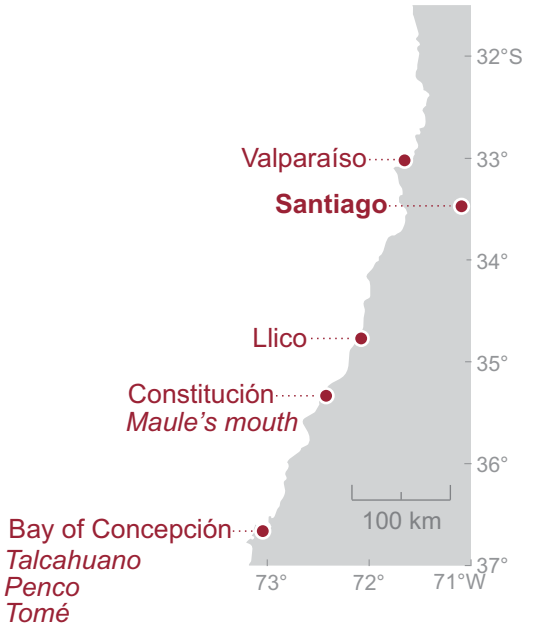

Although the 1906 tsunami did not overtop the Penco railroad embankment, it did pass through the drainage canals that intersect it. The railway embankment that runs parallel to the coast in Penco was built 15 years before the 1906 earthquake, in 1891, and still exists today (A and B). The structure, which still exhibits characteristics of old construction, extends 1.2 km parallel to the coast. In some sections of the embankment, the slope facing the sea is formed by a seawall (C) intersected by old drainage canals outlets (D and E). According to our dGPS leveling, made in 2019, the top of the embankment along the railway, is about 3-4 m above mean sea level and the bases of three crossing drainage canals were 1 m above mean sea level. The broad shape of the embankment is seen in a coast-perpendicular topographic profile (F), made midway along the railway ridge (A). If the relative sea level has not changed significantly at Penco since 1906, Steffen's report would imply that the 1906 tsunami reached a height between 1 and 3 m above mean sea level there.

Record 29 1906

*This record, written by commissioner Miguel Machado, a geologist at the Museo Nacional, is important because it extends 70 km southward, the stretch of coast reported by Steffen´s summary as uplifted during the 1906 earthquake (**record 27**). Although it is known that Machado visited Constitución and made interviews, unfortunately he does not specify how uplift was recognized and assessed. Machado simply states "It has been calculated that the rocks on the beaches rose about forty centimeters above the average sea level". These rocks on the beach at Constitución are conspicuous and well-known landmarks. Additionally, Machado reported building damage in Constitución and three large waves going up the Maule river, which flooded the adjacent part of that town. The latter testimony coincides with the report given by the principal of the Constitución high school that was compiled by Steffen (**28**). The principal estimated the height of the waves at about 1 m.*

This city [Constitución] is located to the west of Talca [...]. This beautiful beach resort is on the south side of the Maule River [...]. On the same beach there is a series of high rocks, 10 to 25 meters high [...]. The tremor knocked down some very old houses in this town and others only cracked in their walls; but in general the roofs tiles [...] fell to the ground. The Governor [...], told us that some days before the earthquake, it was noticed that the speed of the current of the Maule River increased from hour to hour and that there came a time when the captain of a steamer [...] was barely able to prevent, by moorings, his ship from being swept away by the river. […]. Once the earthquake had passed, not only was it noted that the water slowed down its rapid rush, but a few moments later three enormous waves from the sea came up the river and flooded the town near the Maule [river]. It has been calculated that the rocks on the beaches rose about forty centimeters above the average sea level. This phenomenon gave rise to a change that came to be noticed very well about two years after the earthquake; thus the part of the beach where the vacationers bathed was frequently lashed by big waves that made it difficult to swim safely; but the rising of land in this region completely modified the bad conditions of this bathing and today it is one of the best in Chile.

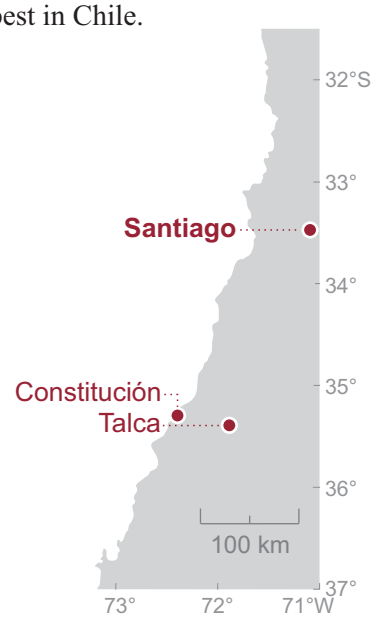

Esta ciudad [Constitución] está situada al poniente de Talca […]. Este hermoso balneario está al lado sur del rio Maule […]. En la misma playa existe una serie de altas rocas, de 10 a 25 metros de elevación, […]. El temblor derribó en este pueblo algunas casas muy antiguas y otras sólo se agrietaron en sus muros; pero en general los tejados […] se vinieron al suelo. El Gobernador […], nos contó que algunos días antes del terremoto, se notó que la velocidad de la corriente del río Maule aumentaba de hora en hora y que llegó un momento en que el capitán de un vapor […] a duras penas pudo impedir, por medio de amarras, que su buque fuese arrastrado por el río. […]. Una vez pasado el terremoto no sólo se notó que el agua disminuyó su rápida carrera, sino que algunos instantes después tres enormes olas venidas desde el mar remontaron el río e inundaron el pueblo en su parte cercana al Maule. Se ha calculado que las rocas de las playas subieron sobre el nivel medio del mar unos cuarenta centímetros. Este fenómeno dio lugar a un cambio que se vino a notar muy bien unos dos años después del terremoto; así la parte de la playa en que los veraneantes se bañaban se encontraba frecuentemente azotada por grandes olas que dificultaban el nadar con seguridad; pero el solevantamiento de tierra en esta región modificó completamente las malas condiciones de este baño y hoy es uno de los mejores de Chile.

Source: Machado, M., 1909. Los temblores en Chile; su causa inmediata y el porqué de sus efectos. Boletín del Museo Nacional de Chile, 1(6): 75-86.

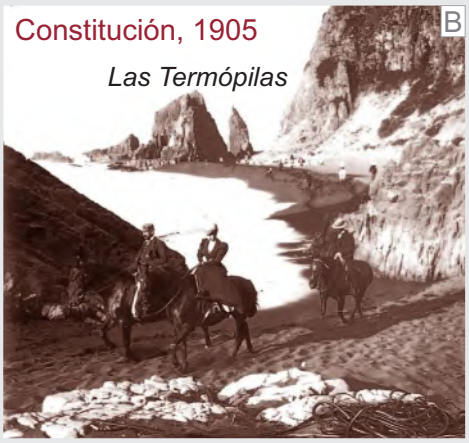

Well-known rocks uplifted in 1906. When commissioner Miguel Machado visited Constitución after the 1906 earthquake, he was told that the large rocks on the beach "rose about forty centimeters above the average sea level". This report is noteworthy because those rocks are, at least since the mid-19th century, well-known landmarks and highly visited touristic attractions, so much so that each large rock has its own name (A-D). In 2007 these rocks were eventually proclaimed National monument. It is very likely that any change that they underwent in 1906 would have been quickly noticed by the inhabitants of Constitución. The satellite image above shows the location of those rocks (profusely photographed at the beginning of the 20th century, A-D), the mouth of the Maule River, where three large waves were seen going upstream after the earthquake, and the adjacent part of the town that was flooded. Also shown is the street crossing mentioned by the boatmen that indicated to the commissioners where boats were left high and dry after the tsunami receded (red dot; **record 32**). The commissioners estimated the elevation of this landing place to be 1.5 m above the pre-earthquake level of the river.

Record 30 1906

Otto Harnecker was a Germany-born mining engineer and well-known industrialist involved with saltpeter and copper. He arrived in Chile as a child and completed his university studies in Santiago. As a survivor of the great 1877 northern Chile earthquake and tsunami, he became interested in earthquakes as an avocation. In 1895 he published the essay "Terremotos i Temblores" (Earthquakes and Tremors), in which he describes the 1877 earthquake, criticizes a previous earthquake theory based on magma tides, and proposes his own, suggesting that earthquakes are caused by the crystallization of Earth's inner magma, and finally argues in favor of the influences of the sun and moon. He lived and worked in his copper smelter facilities at La Ligua, a town located 20 km inland from Papudo and Zapallar, a coastal stretch which he used to visit regularly for sport fishing from the shore, his other hobby. Eight years after the 1906 earthquake he published a note in El Progreso, a newspaper in Cabildo, a neighboring town to the east, describing the coastal level changes produced by the earthquake in Papudo and Zapallar. First, Harnecker gives the opinion of the local fishermen and inhabitants, and then he reports his own observations, made two months after the earthquake. Both lines of argument point to an evident and conspicuous uplift. His statement "The coastline appears as if it were in continuous low tide" offers a broad estimate of the experienced change. If he considered the previous mean sea level as a reference, the uplift was at least 45 cm, because that is the difference between mean sea level and mean low tide at Papudo and Zapallar.

Two months after the earthquake [of 1906] we visited the coast of Papudo and Zapallar with great interest. There is no doubt that it rose up. I have known it for 23 years as because of my love of fishing, I have vivid memories of every rock and every inlet. The first impression was already decisive. The coastline appears as if it were in continuous low tide. [...]. Let's start with the "vox populi". Both the fishermen and the other inhabitants of the coast agree "that the sea has receded". "The sea no longer fills as it used to". "To shellfish you have to go further in the sea". "On a very low tide, the keel of a ship wrecked 30 years ago shows up and was not seen before". We continue with our own observations. Rocky peaks and rocks that used to be good for fishing to regular depths, at all hours, do not have those depths anymore. Others that were only accessible at low tide are now reachable at all hours. In spite of the frequent cloudy weather and the continuous rough seas since August 16, the kelp and seaweed have dried up all along the coast, in the area no longer bathed by the sea. This vegetation that used to exist between the heights of the high and low tide, is now dry, the sea is no longer able to wet it. Thus, and for the same reason, the small mollusks that inhabit this area have dried up. Enclosed in their small white shroud, they make the rocks look as if they were painted with lime. Next to the headland at Papudo there existed for a long time a small fresh water lagoon populated by small fish, and separated by 30 or 40 meters of distance from the high tide. This lagoon has disappeared; the water has infiltrated now with the "retreat of the sea" there would no longer be any back pressure from the salt water. The southern part of the Papudo port is occupied

Con mucho interés visitamos dos meses después del terremoto [de 1906] la costa de Papudo y Zapallar. No cabe duda de que ella se levantó. La conozco desde 23 años y con motivo de la afición a la pesca, tengo recuerdos vivos de cada roca y de cada ensenada. La primera impresión ya fue decisiva. La costa figura como si estuviera de continua baja marea. […]. Principiemos con la "vox populi". Tanto los pescadores como los demás habitantes de la costa están de acuerdo "que el mar se ha retirado". "El mar ya no llena como antes". "Para mariscar hay que entrarse más adentro". "En una muy baja marea asoma la quilla de un buque que naufragó 30 años atrás y que antes no se veía". Seguimos con nuestras propias observaciones. Peñas y rocas que antes a toda hora se presentaban para pescar a regular hondura, ya no la tienen. Otras que sólo eran accesibles en baja marea, están ahora al alcance a cualquier hora. A pesar del frecuente nublado y de las continuas bravezas del mar desde el 16 de Agosto, se ha secado el huiro y el luche en toda la costa, en la zona ya no bañada por el mar. Esta vegetación que antes existía entre las alturas de la alta y baja marea, actualmente está seca, el mar ya no alcanza a humedecer. Así, y por el mismo motivo, se han secado los pequeños moluscos que habitan esta zona. Encerrados en su mortajita blanca, hacen el efecto de haberse blanqueado con cal las rocas. Junto al morro de Papudo existía una pequeña laguna de agua dulce de largo tiempo atrás poblada por pequeños peces, y separada por 30 o 40 metros de distancia de la alta marea. Esta laguna ha desaparecido; el agua se infiltró ahora que con "retirarse el mar" no habrá ya contrapresión del agua salada. La parte sur del puerto de Papudo lo ocupa la pintoresca isla

by the picturesque "Pike" island [...], separated from the mainland by a channel 30 to 60 meters wide. The large waves raised by the south wind formerly crossed this channel from south to north, which no longer happens since the earthquake, because even the largest swells at high tide crash at the entrance of the south side and the channel now looks more like a lagoon for its calm waters. I repeat, therefore, that there is no doubt about the rise of the coast.

de "Pike" […], separada del continente por un canal de 30 a 60 metros de ancho. Las grandes olas levantadas por el viento sur atravesaban anteriormente de sur a norte este canal, lo que no sucede ya desde el terremoto, pues aun las marejadas más grandes y en alta marea se estrellan a la entrada del lado sur y el canal de antes más parece ahora laguna por sus tranquilas aguas. Repito, por tanto, que no cabe duda del solevantamiento de la costa.

Source: "Levantamiento de la costa de Papudo y Zapallar". Diario el Progreso de Cabildo. *Dated:* January 14, 1914. *Collected in:* Montessus de Ballore (19015), p. 296-297.

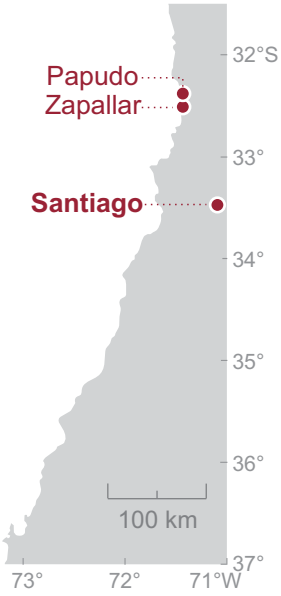

The rocks of Zapallar reported as uplifted by Otto Harnecker and photographed by Hans Steffen. Otto Harnecker, above in a late 19th century portrait, visited Zapallar two months after the 1906 earthquake. He reported that rocks with which he was quite familiar had evidently been raised. Their attached *huiro*, Chilean kelp, and *luche*, a sea lettuce, "have dried up all along the coast, in the area no longer bathed by the sea". Perhaps coincidentally, the famed geographer Hans Steffen (**records 26-28**), was also interested in these rocks and photographed them, making close-ups of the attached *huiro*, *luche* and barnacles. Three photos of the sequence are shown here (A-C). We found the series in the archive of the Ibero-Amerikanisches Institute (https://digital.iai.spk-berlin.de/viewer/collections/nachlass-hans-steffen/).

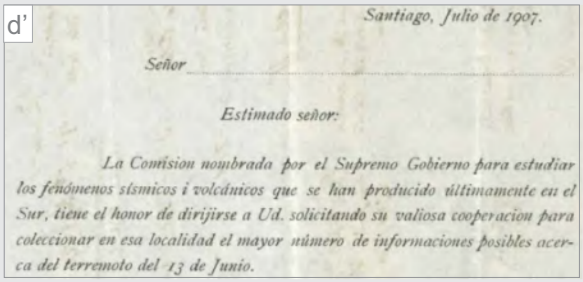
d'

Santiago, Julio de 1907.

Señor

Estimado señor:

La Comision nombrada por el Supremo Gobierno para estudiar los fenómenos sísmicos i volcánicos que se han producido últimamente en el Sur, tiene el honor de dirijirse a Ud. solicitando su valiosa cooperacion para coleccionar en esa localidad el mayor número de informaciones posibles acerca del terremoto del 13 de Junio.

Santiago, July 1907 – Mister:.. – Dear Sir:

The commission appointed by the supreme government to study the seismic and volcanic phenomena that have occurred lately in the South, has the honor to address you requesting your valuable cooperation to collect as much information as possible about the earthquake of June 13th.

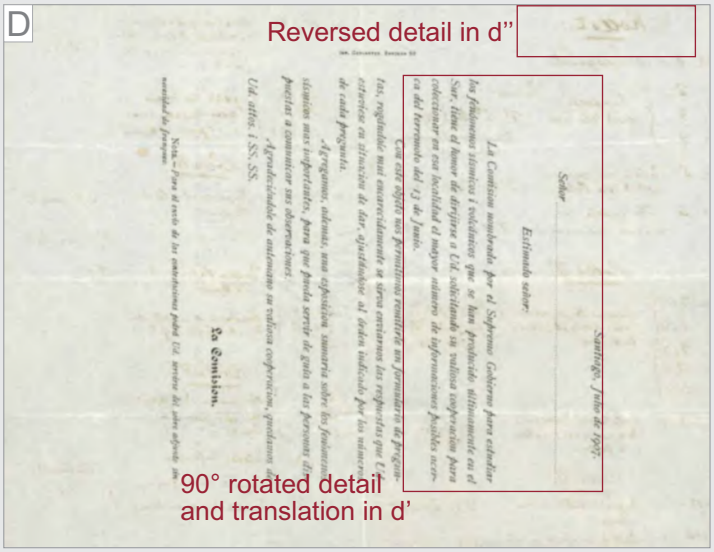
D

Reversed detail in d''

90° rotated detail and translation in d'


d''

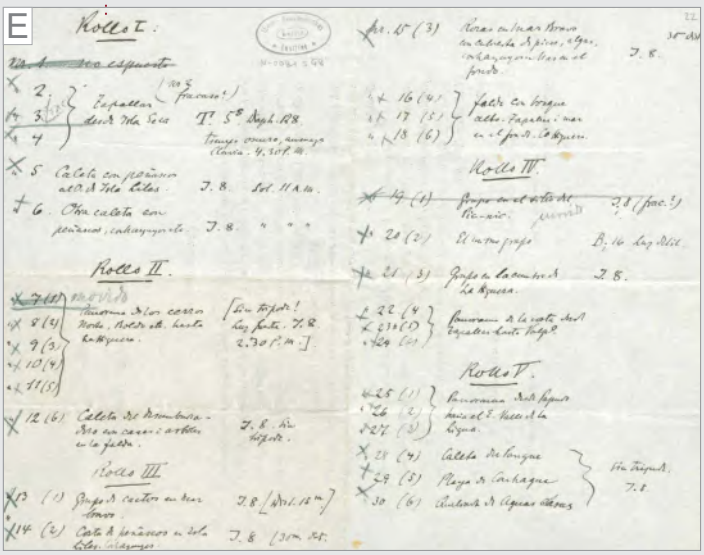
E

Rolle I.

Rolle II.

Rolle III.

Rolle IV.

Rolle V.

Steffen's photos of the rocks at Zapallar probably postdate the 1906 earthquake. Although the photos of the rocks at Zapallar (A-C) are not dated, we infer they were taken after July 1907 because the Steffen's handwritten notes, describing the subject and exposure details of each photo (E), are written on the back side of a printed letter introducing a questionnaire requesting information about the southern Chile earthquake of June 13, 1907 (D, d', d''). For the photo in A, Steffen noted "Coast of Liles Island, Zapallar – Another cove with rocks, kelp, sun 11AM. For the photo in B, he wrote "Rocks of Mar Bravo, Zapallar – Rocks in Mar Bravo covered with barnacles, algae, kelp – sea in the background". We do not know the context of the Steffen's visit to Zapallar; however, we speculate he likely went there to see with his own eyes the uplift evidence reported previously by eyewitnesses, including Harnecker, and compiled in his report of the Commission's work (**26** and **27**). In any case, it seems most likely that Steffen's visit occurred after July 1907, the date of the questionnaire and almost a year after the 1906 earthquake, when the evidence of uplift based on dry algae was likely gone.

Record 31 1906

*One year after the 1906 earthquake, the Chilean government appointed French seismologist Fernand Montessus de Ballore to found the Chilean Seismological Service. One of his first tasks was to make a comprehensive compilation of primary historical sources of the Chilean earthquakes since the 16th century. The effort eventually resulted in the publication of six volumes between 1911 and 1916. The 1906 earthquake, as the most recent large event of the seismic sequence by that time, deserved a full volume. It collects testimonies retrieved from the responses to questionnaires and field surveys of the Commission to study the earthquake (**record 26**). From that volume, here we extract significant testimonies on coastal uplift gathered by the Commission but that were not included in Hans Steffen's summary (**27**). Unlike what was done by Steffen, Montessus de Ballore, a non-believer in the idea of vertical changes generated by earthquakes, ordered the testimonies from north to south, heading each with the location name (here in bold type). From the testimonies, some of them provided by people closely related to the coast including fishermen, it was evident the coast was uplifted between Los Vilos and Valparaíso, ranging the vertical change between 60 and 80 cm. However, south of Valparaíso, including Algarrobo and San Antonio, uplift was less evident or perhaps did not occur. The coastal uplift was again evident in Matanzas, where 45 cm of uplift was estimated. These two sections of the coast where uplift was obvious, with a gap in between where uplift is unclear, agree with the Steffen's conclusions and mapping (**27**).*

Los Vilos.
[...] just yesterday we questioned several old inhabitants and fishermen here, and in one voice they confirmed that after the earthquake of last August 16, the sea was lower or further away from the beach.
Pichidangui.
Since August 17, it is noticed that the low tides are much larger than before, which leads one to believe that there was some raise in the land, although it is normalizing.
Zapallar.
[...] from the mouth of the Ligua river in the north to the Horcón bay in the south, all of us who know this coast, agree that there has been a lifting with the earthquake of August 16, a raise of all of it, no less than eighty centimeters.
Valparaíso.
[Passengers dock] Several boat charterers assured me that after the earthquake the sea is at least half a meter lower than before [...]. [The] chief of fishermen [...] declares that now the highest tide in a storm, which had occurred after the earthquake, was about two feet lower than the former high tides [...], from his fishermen he had learned that a similar difference in sea level is noticeable as far as Concon. [On the coast of Valparaíso the] lowering of the sea is a fact. How much the drop is it is difficult to know, but the fact is so visible and so notorious, that everybody knows it except the person that the government sent to do the soundings. The fishermen of Caleta Cochoa [...] say it, the sea no longer fills so much, the same at the dock of the Vergara quarter [...]. At the dock of Mr. Murphy's factory, one pier is now dry. Likewise, any boat charterer at the dock [...] Prat also confirms the same. I observed

Los Vilos.
[…] ayer mismo interrogamos a varios antiguos y a los pescadores de aquí, y a una voz nos confirmaron que después del terremoto del 16 de agosto último, se encontraba el mar más abajo o más retirado de la playa.
Pichidangui.
Desde el 17 de agosto se nota que las bajas mareas son mucho mayores que antes, lo que hace creer que hubo cierto levantamiento en la tierra, aunque se va normalizando.
Zapallar.
[…] de la desembocadura del río Ligua por el norte hasta la bahía de Horcón por el sur, todos los que conocemos esta costa, estamos de acuerdo que ha habido un levantamiento con el terremoto del 16 de agosto, un levantamiento de toda ella, no menos de ochenta centímetros.
Valparaíso.
[Muelle de pasajeros] Varios fleteros me aseguraron que después del terremoto el mar está a lo menos medio metro más bajo que antes […]. [El] jefe de pescadores […] declara que ahora la más alta marea en un temporal, que había habido después del terremoto, quedaba como a dos pies más abajo que las antiguas altas mareas […], por sus pescadores había sabido que una diferencia parecida en el nivel del mar se nota hasta Concon. [En la costa de Valparaíso el] descenso del mar es un hecho. Cuanto sea el descenso es difícil de apreciar, pero el hecho es tan visible y tan notorio, que lo conoce todo el mundo con excepción de la persona que el gobierno mando a hacer los sondajes. Los pescadores de la Caleta Cochoa […] lo dicen, el mar ya no llena tanto, ídem en el muelle de la

that the rocks on the beach from the Recreo to the Baron were showing a white ribbon (more pronounced every day) that I did not see before, not even at the lowest tide. These are certain mollusks [...] that live attached to the rock at shallow depths. With the average sea level now withdrawn, these shellfish die and form a line or mark that is very noticeable for its visibility [...].

Algarrobo.

On asking the fishermen if the sea is presently lower than before the earthquake, they first replied no. After almost confused with questions they said that perhaps it is lower.

San Antonio.

The sea retains the same level as before the earthquake. [...].

Matanzas.

The sea retreated about 45 centimeters, according to what I observed by the putrefied waste, marine vegetations and incrustations in rocks that are left out of the water in the high tides.

Población Vergara […]. En el muellecito de la fábrica del señor Murphy, un machón ahora queda en seco. Igualmente cualquier fletero del muelle […] Prat confirma también lo mismo. Observé que las rocas en la playa desde el Recreo al Barón iban manifestando una cinta blanca (más pronunciada cada día) que antes yo no veía ni en la más baja marea. Se trata de ciertos moluscos […] que habitan pegados a la roca a poca profundidad. Retirado ahora el promedio del nivel del mar, estos mariscos mueren y forman una línea o marca muy notable por su visibilidad […].

Algarrobo.

Al preguntar a los pescadores si el mar está actualmente más abajo que antes del terremoto, contestaron primero que no. Después de casi confundidos con preguntas dijeron que quizá está más bajo.

San Antonio.

El mar conserva el mismo nivel que antes del terremoto. […].

Matanzas.

El mar se retiró unos 45 centímetros, según lo observé por los desperdicios putrefactos, las vegetaciones marinas e incrustaciones en rocas que quedan fuera del agua en las altas mareas.

Source: Montessus de Ballore, F., 1915. Historia Sísmica de los Andes Meridionales al Sur del paralelo XVI. Quinta Parte. El Terremoto del 16 de Agosto de 1906. Sociedad Imprenta-Litografía "Barcelona", Santiago-Valparaíso, Chile. p. 291-304.

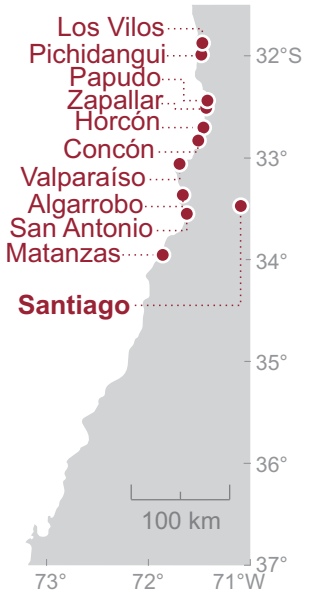

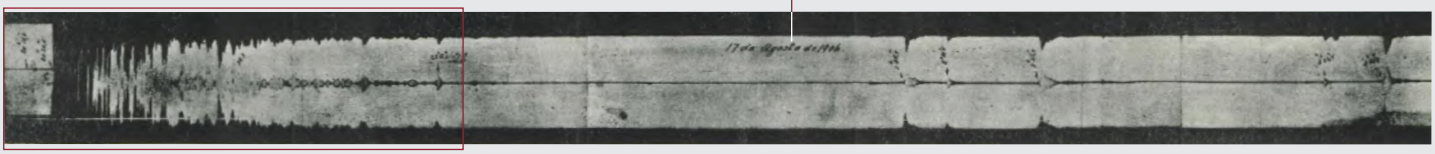

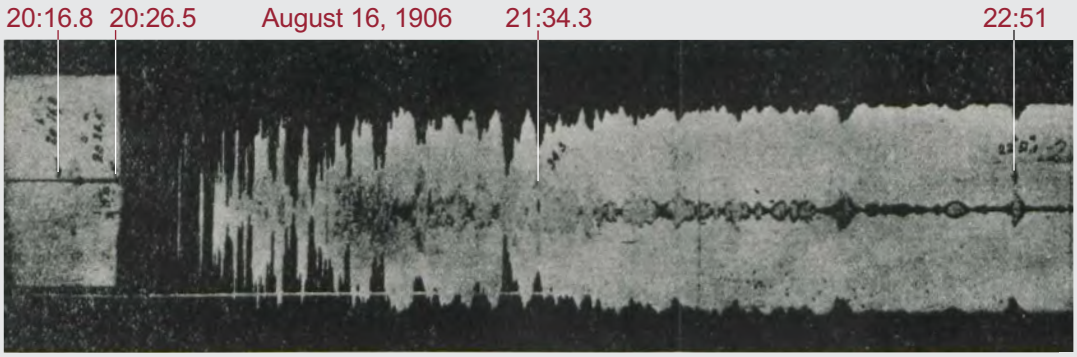

Córdoba local time, noted in hours, minutes and tenths of minutes. At the time of the 1906 earthquake, Argentina operated on the meridional time at Córdoba, 4 hours, 16 minutes, and 48 seconds behind UTC.

Fernand Montessus de Ballore (1851-1923), the first modern seismologist in Chile, and a puzzling seismogram of the 1906 earthquake. Between 1911 and 1916 Montessus de Ballore, above along with an early seismograph and the first modern Chilean seismological station in Santiago, published the *Historia Sísmica de los Andes Meridionales al Sur del paralelo XVI* [Seismic History of the Southern Andes South of the 16th Parallel]. Its six volumes make up the most comprehensive compilation of primary historical sources of Chilean earthquakes since the Spaniards arrival. He benefited from his era's excellence in Chilean historiography, compiling and analyzing primary sources found previously by historians in archives of Chile, Perú and Spain. The fifth volume of the work (above), published in 1915, compiles the information about the 1906 earthquake, which he collected after his arrival in Chile in 1907. At the time of the 1906 earthquake, before his arrival, there were no continuous, operational seismographs in the country. Hence, the closest seismogram from this earthquake (above) was recorded by a Milne seismograph at the Pilar Magnetic Observatory in Córdoba, Argentina, 740 km ENE of Valparaíso (Steffen, 1907, p. 13-14). Hans Steffen (**record 26**) believed, on the advice of the Argentinians, that the oscillations recorded at 20:16.8 (see blue box above) were the first arrivals from the Valparaíso earthquake. Actually these oscillations were seismic waves from a large earthquake with magnitude Mw 8.2 near the Aleutian Islands, Alaska, that occurred 29 minutes before the one near Valparaíso. The waves arriving from the Aleutians continued for several minutes, then either merged with, or were overwhelmed by, the first arrivals from the Valparaíso at 20:26.5, when the amplitudes increased dramatically, exceeding the recording width of the photographic paper (40 mm). The main oscillations extended for 12 minutes, decreasing but with intermittent, strong shaking until 21:34.3. The arrival at 22:51 is likely a large aftershock. The observatory reported to Steffen that a great number of large aftershocks continued through August 19th.

Record 32 1906

*As in **record 31** for the coastal uplift, here we extract from Montessus de Ballore's volume significant testimonies on the 1906 tsunami originally gathered by the Commission but that were not included in Hans Steffen's summary (**28**). Although Montesssus de Ballore states that "the effects of the earthquake on the Pacific waters have been almost null, in other words, it was not accompanied by a maremoto, or sunami (sic)" (Montessus de Ballore, 2015, p.283), his compilation actually did support that a moderate tsunami occurred. After showing his point for the region north of Valparaíso, where the tsunami was hardly evident, Montessus de Ballore reproduces the testimonies for the southern localities, stretching from Algarrobo to Puerto Saavedra, the latter located 660 km south of Valparaíso. At least three pieces of significant information can be mined from this compilation: i) the most noticeable tsunami effects along this stretch of coast were focused between Pichilemu and Concepción Bay (Tomé, Penco), at the southern reaches of the 1906 earthquake. From there the effects progressively diminished both northward and southward. While in the outermost localities to the north and to the south, the tsunami was perceived as ebbs and flows that did not surpass the high tide level or as "rough seas," by contrast between Pichilemu and Concepción Bay the tsunami surpassed the high-tide level and its large ebbs and flows exceeded the usual horizontal limits of the sea by tens of meters (see a possible exception to this trend in **record 25**); ii) the reports of waves going up the rivers Maipo and Maule adds to a similar report given for the Aconcagua river (**25**) supporting, along with others for Maule river (**28**) that the 1906 tsunami generated noticeable bores in the main rivers of the region; iii) the first effects of the 1906 tsunami were evident soon after the earthquake and continued for at least three hours. The first ebbs and flows were observed at Constitución eight minutes after the mainshock, although the time reference "After the third quake", could be actually pointing to the large aftershock at 20:15 (**20**), meaning that the first unusual seas were seen 16 minutes after the mainshock. This time agrees with that of the first evident recede at Tomé, in the Concepción Bay: "At 20:15 [the sea] retreated about 50 meters and gently resumed its place". One of the bores in the Maule river was observed one and a half hour after the mainshock, "at half past nine". Finally, at Penco on Concepción Bay, the lowest sea level during an ebb was recorded at 23:30, three and a half hours after the mainshock. The latter timing could be linked to **record 22** that describes a large ebb followed by a rapid flow at 23:00 in Talcahuano, on the same bay.*

Algarrobo.
Several times the sea receded and rose again to the height of the high tide.
San Antonio.
The sea was rough during the earthquake, but neither came in nor went out. One person saw a wave going up by the Maipo River.
Pichilemu.
The sea, from its main or highest level, rose about 2 meters [...].
Constitución.
[...]. After the third quake, that is at XX.7 [20:07] there was an ebb and flow of the sea along the entire coast [...] of this governorate, which, according to rough estimates, reached a height of more than a meter higher than that observed up to that date [...]. At half past nine on the night of the 16th (the earthquake was at XIX.55 [19:55]) a large wave, or undertow, was noted in the Maule River that raised the level of the current a *vara* [80 cm] or so, and minutes later, another one that reached about a meter in height and made the inhabitants fear a flood of the sea. [...]. According to information taken from the boatmen,

Algarrobo.
El mar se recogió y subió otra vez a la altura de la alta marea varias veces.
San Antonio.
El mar estaba bravo durante el terremoto, pero ni se recogió, ni salió. Una persona vio una ola subir por el río Maipo.
Pichilemu.
El mar, de su mayor o más alto nivel, subió cerca de 2 metros […].
Constitución.
[…]. Después del tercer temblor, o sea a las XX.7 [20:07] se produjo en toda la costa […] de esta gobernación, un flujo y reflujo de mar que, según cálculos aproximados, llegó a una altura mayor de un metro a lo observado hasta esa fecha […]. A las nueve y media de la noche del 16 (el terremoto fue a las XIX.55 [19:55]) se notó en el Río Maule una gran ola, o resaca que levantó el nivel de la corriente una vara [80 cm] más o menos, y minutos después, otra que llegó como hasta un metro de altura y que hizo temer a los habitantes una salida de mar. […]. Según informaciones tomadas entre los boteros, media

half an hour after the earthquake, the level of the river [Maule] suddenly rose, and the boats were then left dry at a point that was indicated to us, as we were also shown how far the river reached before the tremor. The difference in level that we obtained is 1 m.50 [1.5 m]. This data refers to the crossing of Echeverría and Montt streets.

Penco.

The sea went out about 60 meters further out than its usual level, immediately ebbing another 60 or 70 meters, returning to its normal state in less than 10' [10 minutes]. The lowest tide took place at XXIII ½ [23:30] on the 16th.

Tomé.

It was stated that the sea had receded a few fathoms without causing any outflow worthy of consideration; but it must be borne in mind that at that hour the tide was very low. [...]. At XX.15 [20:15] [...] [the sea] retreated about 50 meters and gently resumed its place. These withdrawals were repeated under the same conditions three or four times, the last two being the greatest, as they reached about 60 meters.

Coronel.

After the quake, [there were] high waves without wind. As for the phenomena observed after the quake, I can note a very curious one, for the night being so calm, without the slightest breeze blowing, the sea became so agitated, raising such enormous waves that they produced a deafening roar. We were able to notice this very well, as our house is situated near the sea, on flat, sandy ground.

Baja Imperial [Puerto Saavedra].

The sea went out, like a high tide.

hora después del terremoto subió el nivel del río [Maule] de repente, quedando después los botes en seco en un punto que nos fue indicado, como también se nos mostró hasta donde llegaba el río antes del temblor. La diferencia de nivel que obtuvimos es de 1 m.50 [1.5 m]. Este dato se refiere al crucero de las calles Echeverría y Montt.

Penco.

El mar salió como 60 metros más afuera de su nivel habitual, recogiéndose en seguida otros 60 o 70 metros, volviendo enseguida a su estado normal en menos de 10' [10 minutos]. La más baja marea tuvo lugar a las XXIII ½ [23:30] del 16. […].

Tomé.

Se habló de que el mar se había retirado algunas brazas sin ocasionar salida digna de consideración; pero hay que tomar en cuenta que a esa hora la marea era muy baja. […]. A las XX.15 [20:25] […] [el mar] se retiró como 50 metros y volvió a ocupar su sitio con toda suavidad. Estas retiradas se repitieron en las mismas condiciones tres o cuatro veces, siendo las dos últimas las mayores, pues alcanzaron como a 60 metros.

Coronel.

Después del temblor, [hubo] oleaje alto sin viento. En cuanto a los fenómenos observados después del temblor, puedo anotar uno muy curioso, pues estando la noche tan apacible, sin que soplara la más suave brisa, el mar se agitó tanto, levantándose olas tan enormes que producían un estruendo ensordecedor. Pudimos notar esto muy bien, pues nuestra casa está situada cerca del mar, en un terreno plano y arenoso.

Baja Imperial [Puerto Saavedra].

Salió el mar, como una alta marea.

Source: Montessus de Ballore, F., 1915. Historia Sísmica de los Andes Meridionales al Sur del paralelo XVI. Quinta Parte. El Terremoto del 16 de Agosto de 1906. Sociedad Imprenta-Litografía "Barcelona", Santiago-Valparaíso, Chile. p. 283-289.

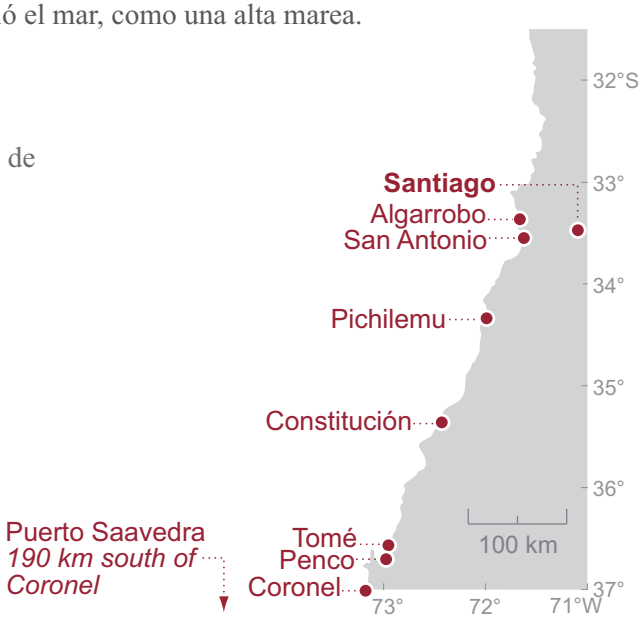

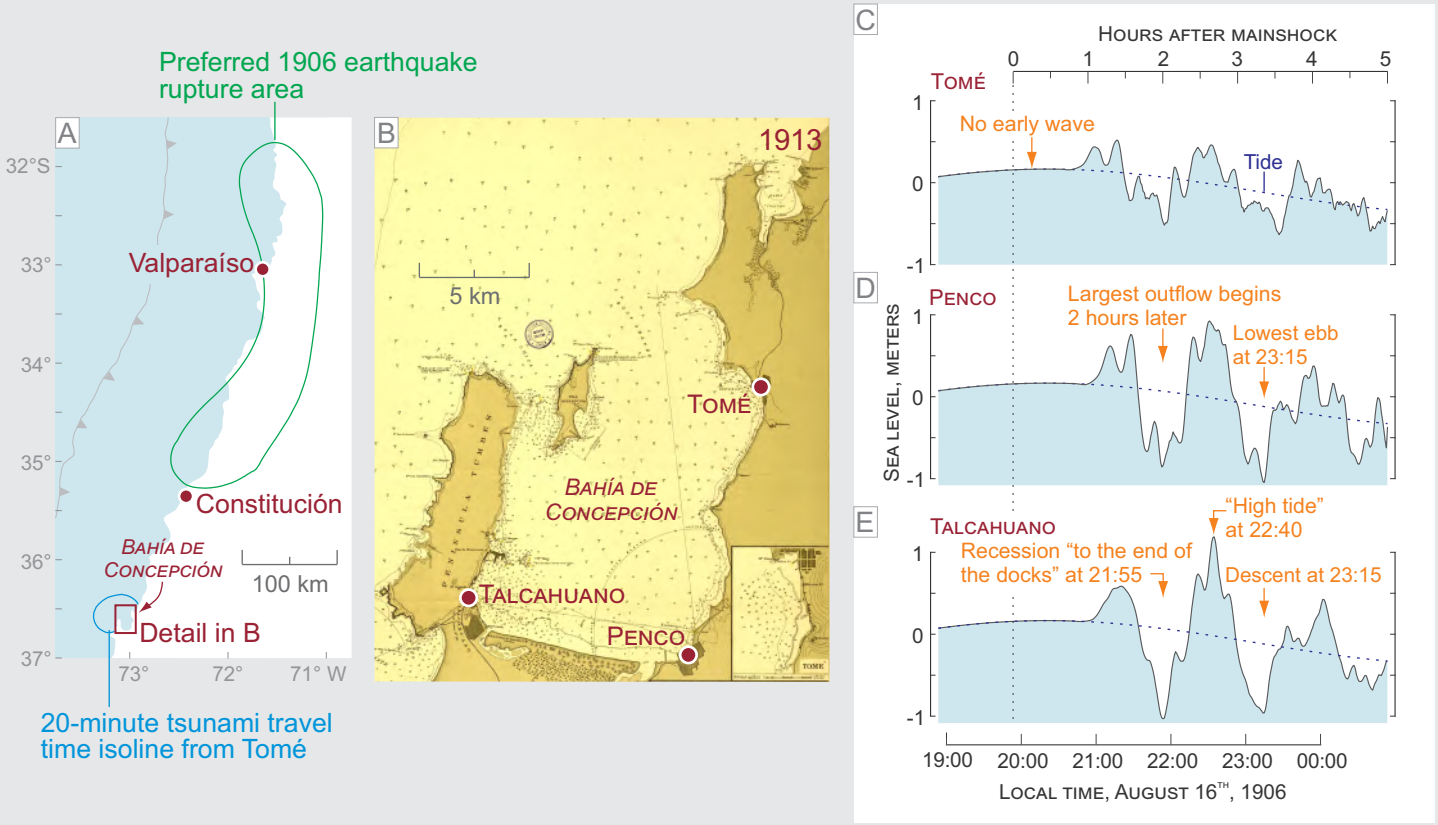

The 1906 tsunami in Bahía Concepción. The 1906 tsunami reports, compiled by Montessus de Ballore (**this record**) along with those by Hans Steffen (**28**) and the Diario Ilustrado (**22**), show that the 1906 tsunami had its greatest manifestation, with a series of ebbs and flows, in Bahía Concepción (A and B). The observations within the bay, at Tomé, Penco and Talcahuano (B), compared with the results of tsunami modelling for the same locations (C-E) allow to test our preferred 1906 earthquake rupture area (A).

Tomé—The first comparison, using the reported tsunami arrival time in Tomé, presents a puzzle. The observations, which probably share a common source, tell that "at the moment of the quake itself, the sea remained calm; but at 8:15 [20:15] [...] it began to withdraw for about fifty meters to immediately return to its place with complete smoothness" (**28**), and "At XX.15 [20:15] [...] [the sea] retreated about 50 meters and gently resumed its place" (**this record**). If the earthquake was at 19:59 (**20**), it took only 16 minutes for the tsunami to get from its source to Tomé. The 20-minute tsunami travel isoline from Tomé, resulting from backward tsunami ray tracing, encompasses the source area for any wave that would take less than 20 minutes to arrive in Tomé (A). Such a source location, if tectonic, is not consistent with the spatial distribution of the 1906 earthquake intensities (**26**) and land level changes (**27**), which suggest a rupture located much farther north. Thus, this early wave is not predicted by our modeling (C). Alternatively, if not an error in the reported time, that initial wave at 20:15 could have resulted from a subaerial or submarine landslide within the area bounded by the 20-minute isoline (A).

Penco—The observations collected in Penco are more consistent and fit the results of the modeling much better (D). One report states that "an outflow of the sea was observed in Penco, which began some time (according to [...] the press about two hours) after the quake, with the ebbs and flows [...]" (**28**). If "the press" missed the first 40-cm-high flow, predicted ~1 hour after the mainshock, they likely refer to the more conspicuous 1.5-m outflow that followed the first large ebb and that began "about two hours" after the earthquake, i.e. around 22:00 (D). A second report states that "The sea went out about 60 meters further out than its usual level, immediately ebbing another 60 or 70 meters, [...]. The lowest tide took place at XXIII ½ [23:30] on the 16th." (**this record**). This agrees well with the tsunami modeling for Penco, which predicts the lowest ebb at 23:15, just 15 minutes before the reported 23:30 (D). The amplitude of the observed lowest ebb also agrees reasonable well with the prediction (D).

Talcahuano—The tsunami observation made in Talcahuano is relevant because in addition to giving the time of the highest flow it also gives vertical heights. The report says "In Talcahuano [...] the high tide, [...], was considerably delayed, taking place at 11 o'clock, after the sea had receded to the end of the docks. It was extremely rapid, rising up to 70 centimeters. Shortly afterwards it descended almost abruptly by 80 centimeters" (**22**). It appears from the wording, that the observer thought that the rise at 23:00, which followed a first recession of the sea, was a "high tide" and not necessarily related to the earthquake. If so, it is feasible that the eyewitness used the mark of a rough mean sea level at the dock as a vertical reference to estimate the "70 centimeters" of the "high tide", and the "80 centimeters" of the following abrupt descent. As a whole, this reported sequence and heights would agree well with the predictions of ~1-m ebb at 21:55, the ~1-m flow at 22:40, and the ~1-m ebb at 23:15 (E).

References cited

Barrientos, S., 1988. Slip distribution of the 1985 central Chile earthquake. *Tectonophysics*, 145: 225-241.

Barrientos, S., 1995. Dual seismogenic behavior: The 1985 central Chile earthquake. *Geophysical Research Letters*, 22: 3541-3544.

Barrientos, S., 1997. Central Chile: an example of quasi-static crustal behavior. *Island Arc*, 6: 281-287.

Carvajal. M., M. Cisternas and P. Catalán, 2017a. Source of the 1730 Chilean earthquake from historical records: Implications for the future tsunami hazard on the coast of Metropolitan Chile. *Journal of Geophysical Research*, Solid Earth, 122: 3648–3660.

Carvajal, M., M. Cisternas, A. Gubler, P. Catalán, P. Winckler and R. Wesson, 2017. Reexamination of the magnitudes for the 1906 and 1922 Chilean earthquakes using Japanese tsunami amplitudes: implications for source depth constraints. *Journal of Geophysical Research*, Solid Earth, 122: 4-17.

Cisternas, M., F. Torrejón and N. Gorigoitia, 2012. Amending and complicating Chile's seismic catalog with the Santiago earthquake of 7 August 1580. *Journal of South American Earth Sciences*, 33: 102-109.

Cisternas, M., 2012. El terremoto de 1647 de Chile central como un evento intraplaca: ¿otra amenaza para Chile metropolitano? *Revista de Geografía Norte Grande*, 53:23-33.

Comte, D., A. Eisemberg, E. Lorca, M. Pardo, L. Ponce, R. Saragoni, S.K. Singh and G. Suárez, 1986. The 1985 central Chile earthquake: a repeat of previous great earthquakes in the region? *Science*, 233: 449-453.

Greenough, G. B., 1834. Address delivered at the Anniversary Meeting of the Geological Society, on the 21st of February 1834. *Proceedings of the Geological Society London*, v. II, 1833-1834, 35:42-70.

Instituto Geográfico Militar (IGM), 1985. El terremoto del 3 de Marzo de 1985 y los desplazamientos de la corteza terrestre. *Terra Australis*, 28: 7-12.

Kausel, E., 1986. Proceso sísmico, parámetros focales y réplicas del sismo del 3 de Marzo, 1985. In: El sismo del 3 de Marzo 1985, Chile. J. Monge (Ed.). Facultad de Ciencias Físicas y Matemáticas, Universidad de Chile. Santiago. 264 pp.

Lomnitz, C., 1970. Major earthquakes and tsunamis in Chile during the period 1535 to 1955. *Geol. Rundschau*, 59: 938-960.

Lyell, Ch., 1830. Principles of geology, being an attempt to explain the former changes of the Earth's surface, by reference to causes now in operation. John Murray (Ed.), London. Volume 1, 511 pp.

Lyell, Ch., 1832. Principles of geology, being an attempt to explain the former changes of the Earth's surface, by reference to causes now in operation. John Murray (Ed.), London. Volume 2, 332 pp.

Lyell, Ch., 1833. Principles of geology, being an attempt to explain the former changes of the Earth's surface, by reference to causes now in operation. John Murray (Ed.), London. Volume 3, 398 pp.

Machado, M., 1909. Los temblores en Chile; su causa inmediata y el porqué de sus efectos. *Boletín del Museo Nacional de Chile*, 1(6): 75-86.

Mendoza, C., Hartzell, S., Monfret, T., 1994. Wide-band analysis of the 3 March 1985 central Chile earthquake: Overall source process and rupture history. *Bull. Seism. Soc. Am.*, 84: 269-283.

References cited, *continued*

Montessus de Ballore, F., 1912. Historia Sísmica de los Andes Meridionales al Sur del paralelo XVI. Cuarta Parte. Chile central. Imprenta Cervantes, Santiago, Chile, 213 pp.

Montessus de Ballore, F., 1915. Historia Sísmica de los Andes Meridionales al Sur del paralelo XVI. Quinta Parte. El Terremoto del 16 de Agosto de 1906. Sociedad Imprenta-Litografía "Barcelona", Santiago-Valparaíso, Chile, 407 pp.

Okal, E., 2005. A re-evaluation of the great Aleutian and Chilean earthquakes of 1906 August 17. *Geophys. J. Int.*, 161: 268–282.

Plafker, G., 1985. Geologic reconnaissance of the March 3, 1985, Chile earthquake. In: Preliminary report of investigations of the central Chile Earthquake of March 3, 1985. S.T. Algermissen (Ed.) U.S. Geological Survey, Open file Report 85-542. Denver, Colorado. 180 pp.

Rodríguez, A. and C. Gajardo, 1906. La catástrofe del 16 de Agosto de 1906 en la República de Chile. Imprenta, Litografía y Encuadernación Barcelona, Santiago de Chile, 356 pp.

Soloviev, S. L. and Ch. N. Go, 1984. Catalogue of tsunamis on the eastern shore of the Pacific Ocean. Canadian Translation of Fisheries and Aquatic Sciences No. 5078, Canada Institute for Scientific and Technical Information, National Research Council, Ottawa, 293 pp.

Steffen, H., 1907a. Contribuciones para un estudio científico del Terremoto del 16 de Agosto de 1906. Imprenta Cervantes, Santiago de Chile, 83 pp.

Steffen, H., 1907b. Einige Ergebnisse der Untersuchungen über das mittelchilenische Erdbeben vom 16. August 1906. *Petermanns Geographische Mitteilungen*, 6: 1-7.

Tsuji, Y., 2013. Catalog of distant tsunamis reaching Japan from Chile and Peru (in Japanese), *Tsunami Eng.*, 30: 61-68.

Urbina, M., N. Gorigoitía, M. Cisternas, 2016. Aportes a la historia sísmica de Chile: el caso del gran terremoto de 1730. *Anuario de Estudios Americanos*, 73: 657-687.

Zegers, L., 1906. El terremoto del 16 de Agosto de 1906. Imprenta Cervantes, Santiago de Chile, 34 pp.